Reproductive Life Histories of Mammoths

by

Joseph Jameel El Adli

A dissertation submitted in partial fulfillment
of the requirements for the degree of
Doctor of Philosophy
(Earth and Environmental Sciences)
in the University of Michigan
2018

Doctoral Committee:

      Professor Daniel C. Fisher, Chair
      Professor Catherine Badgley
      Professor Emeritus Philip D. Gingerich
      Professor Kyger C Lohmann
      Associate Professor Jeffery A. Wilson

Joseph J. El Adli

jeladli@umich.edu

ORCID iD: 0000-0002-3989-5409

DEDICATION

To all those I've met along the way.

ACKNOWLEDGEMENTS

still to come for us. Finally, I would like to thank Karley for always being a fat little dog with occasionally good intentions.

TABLE OF CONTENTS

LIST OF TABLES

LIST OF FIGURES

ABSTRACT

  The end of the Pleistocene saw the extinction of many large vertebrate species, including mammoths (genus *Mammuthus*). Despite many decades of work by various researchers, the cause(s) of mammoth extinction are still heavily debated, with climate change and human hunting being the two primary hypothesized agents of extinction. One major problem with identifying the cause of this extinction is the fact that changing climates and movement of human hunters into ecosystems containing mammoths are both broadly associated with the time of extinction, making it difficult to decouple one potential cause from the other using only temporal data.

  This study bypasses the strictly chronological approach of many previous studies and instead investigates the cause of the end-Pleistocene extinction using information about reproductive life history. The age of first conception and the average time between conceptions are both expected to change predictably and divergently under the hypotheses of climate-driven extinction and hunting-driven extinction, so assessment of changes in these aspects of life history approaching the time of extinction could provide a test for cause of extinction.

  I use the record of growth within tusk dentin to identify patterns associated with reproductive life history in mammoths. Thin sections and serial isotope analyses document the periodicity of X-ray density features observed in microCT sections of tusks. These attenuation features form annually in both Columbian and woolly

mammoths (*Mammuthus columbi* and *Mammuthus primigenius*, respectively), but form semiannually in a gomphothere from South America.

MicroCT scans of entire tusks are employed to provide a record of multiple decades of growth for ten Siberian woolly mammoths. In eight of these specimens, all of them adult females, we observe a repeated 3- to 6-year-long cyclical pattern of regularly varying growth rate. This pattern was absent in both adult males and juveniles. We interpret this pattern as a record of calving in females, and its onset is observed in several individuals to occur at an age approximating that of sexual maturation in extant elephants. Our dataset shows a minor decrease in age of maturation and average calving interval near the end of the Pleistocene. This is predicted by a hunting-driven model of extinction but is not expected for extinction driven by climate change. This work contributes to our knowledge of the reproductive life history of mammoths, which we argue is key to understanding the cause of their extinction.

CHAPTER 1

Introduction

THE END

The end of the Pleistocene saw the disappearance of a multitude of species from across the globe. This mostly-mammalian extinction is notable in its bias toward removal of large-bodied animals (Alroy, 1999), including mammoths, mastodons, woolly rhinos, ground sloths, and giant beavers. These extinctions occurred in broad conjunction with the dispersal of *Homo sapiens* and with shifts in climate toward the conditions of the Holocene. The rough concurrence of changing climates and appearance of human hunters with the disappearance of Pleistocene megafauna has led many authors to hypothesize that one of these factors (or some combination of both) is responsible for the end-Pleistocene extinction (Martin, 1967, 1989; Grayson, 1991; Stuart, 1991; Beck, 1996; Barnosky et al., 2004; Koch and Barnosky, 2006; Faith and Surovell, 2009; Araujo et al., 2017). However, these arguments, often involving the timing of one or more potential cause relative to a presumed effect, are unable to distinguish either agent of extinction as preferable to the other on a strictly temporal basis. Fisher (1996) proposed a test that could fingerprint the cause of the Pleistocene megafaunal extinction among these two most prominent hypotheses using aspects of life history. He postulated that both climate change and human hunting would have predictable and often antithetic effects on the timing and duration of different aspects of

life history, especially reproductive life history. Thus if one could document life history through the last portion of the Pleistocene and note changes approaching the time of extinction, it should be possible to identify the dominant cause of extinction. It may seem surprising that such detailed paleoecological information could be obtained for extinct taxa, but an extensive record of life history does exist: within the tusks of proboscideans.

PROBOSCIDEA

Proboscideans are a group of afrotherian mammals characterized by large body size, prehensile trunks, and tusks. Today the group is solely represented by the elephantid genera *Loxodonta* and *Elephas.* However, the group has a diverse and deep paleontological history that goes back to the Paleocene (Shoshani and Tassy, 2005; Gheerbrant, 2009). Even as recently as the late Pleistocene, the clade Proboscidea was represented globally by at least four families (Elephantidae, Gomphotheriidae, Mammutidae, and Stegodontidae), with at least some species within each family disappearing during the end-Pleistocene extinction and three of the families being lost completely. Among these recently extinguished taxa, perhaps the most well-known are the mammoths (genus *Mammuthus*), a now-extinct member of the Elephantidae.

Mammoths

The genus *Mammuthus* likely originated in southern Africa at the beginning of the Pliocene, with *M. subplanifrons* being the oldest species currently known (Maglio, 1973;

Shoshani et al., 1998). By the Late Pliocene, some mammoth taxa had emigrated out of Africa into Europe and Asia, and during the Pleistocene at least two species reached North America (Lister et al., 2005; Rabinovich and Lister, 2017). Of particular importance for this study is the Pleistocene steppe mammoth (*M. trogontherii*), as this taxon is the likely progenitor of both the Columbian mammoth (*M. columbi*) and the woolly mammoth (*M. primigenius*), which is discussed in Chapters 2, 4, and 5.

Between 1.5 and 1.3 million years ago, a population of *M. trogontherii* invaded North America via Asia (Agenbroad, 2005; MacFadden and Hulbert, 2009). This population gave rise to *M. columbi*, which would occupy the warmer southern and middle latitudes of North America (Lister and Sher, 2015). In Eurasia, a separate population of *M. trogontherii* diverged to become *M. primigenius*. The time of this split is somewhat contentious with the oldest clear examples of *M. primigenius* dating to approximately 200 ka and specimens of more dubious identification known from up to 800 ka (Lister and Sher, 2001; Lister et al., 2005). *Mammuthus primigenius* made its way into North America via the Bering land bridge in the late Pleistocene where it occupied the northern latitudes of the continent with some overlap and occasional hybridization with endemic *M. columbi* (Lister, 1993; Enk et al., 2011).

On the continents both the woolly mammoth and Columbian mammoth survived until the end of the Pleistocene, with some radiocarbon dates from specimens of *M. primigenius* indicating survival of the species into the beginning of the Holocene on the Taymyr Peninsula (Sulerzhitsky, 1997; Stuart et al., 2002). Small populations of woolly mammoths trapped on islands off the coast of Alaska and Siberia would survive the end-Pleistocene extinction, but met with eventual demise. The last population of woolly

mammoths persisted on Wrangel Island in the Chukchi Sea until being wiped out

around 4,000 years before present (Vartanyan et al., 1993).

TUSKS

Tusks are a hallmark feature of elephants and are widespread throughout the

proboscidean clade. Although no empirical analysis of the functional role of tusks has

been conducted to date, observations of modern proboscideans show that tusks have

wide utility for sexual selection, defense, and manipulation of the environment (Chelliah

and Sukumar, 2013). Tusks themselves are enlarged, ever-growing incisor teeth

composed of the same dental tissues that are present in other mammal teeth: enamel,

cementum, and dentin. Each tusk is capped at the tip by enamel (although this is often

worn away during life) and is sheathed in cementum. The portion inside of the tusk

underlying the cementum is composed of dentin, which forms the greatest volume and

mass of the tooth. Dentin is formed via apposition at the pulp cavity by odontoblasts,

which lay down conical layers comprised of hydroxylapatite ($Ca_5[PO_4]_3[OH]$) and a

collagen matrix (Sisca and Provenza, 1972).

In proboscidean tusks there is a nested hierarchy of periodically-forming dentin

increments. Annually-forming (first-order) increments and daily-forming (third-order)

increments have been observed across multiple proboscidean taxa (Fisher, 2001; also

see Chapters 2-5). Second-order increments have been consistently shown to form on

a weekly basis in elephantids (including mammoths) and gomphotheres, but are

fortnightly-forming in *Mammut* (it is unclear if this is a feature of mammutids as a group).

4

These first-, second-, and third-order features form continuously from birth until death, which means that tusks contain a detailed and time-calibrated record of growth over an individual's life. Furthermore, Fisher (1996) suggested that the amount of dentin laid down for a given increment reflects the nutritional status of the individual at the time that the increment formed. Uno (2012) also documented isotopic changes in tusks of *Loxodonta* corresponding to known changes in floral composition, suggesting that tusks are indeed a sensitive recorder of activities during life. Given this, aspects of environment and life history should modify the composition and dimensions of dentin increments, leaving a signature within the tusk record that can then be interpreted. Such analyses of life history have been conducted by multiple authors, but there is still much to learn about the paleobiology of these organisms (Fisher, 2009).

CHAPTER OVERVIEWS

General Overview

This dissertation continues a long line of inquiry started by Daniel C. Fisher and taken on by many of his students. I do not (and would not) claim to be writing the final statement of this line of inquiry, but I do hope to 1) expand our understanding of available tools useful for analyses of life history (microCT), 2) identify patterns of tusk growth that represent distinct aspects of life history (especially patterns related to reproduction), and 3) provide preliminary data that may prove crucial in determining the cause of the end-Pleistocene extinction.

Chapters within this dissertation can be divided based on two main themes. The first theme is the scale of study. Chapters 2–4 deal mostly with intra-annual patterns of growth and identification of the periodicity and, to a lesser degree, the taxonomic distribution of density features inside of proboscidean tusks. Chapter 5 utilizes the information on annually-forming density features (documented in the previous three chapters) to assess inter-annual patterns of growth over multiple decades of life in several individuals. The second theme is patterns of reproductive life history recorded in proboscidean tusks. Chapters 2 and 3 discuss patterns of growth related to male reproductive life history that recur quasi-annually (musth), while Chapters 4 and 5 delve into multi-year patterns related to female reproductive life history (calving intervals).

Chapter 2

The second chapter serves as an introduction to the methods and analyses that are explored throughout the dissertation. This chapter focuses on documenting and interpreting internal features of the tusk of an adult male Columbian mammoth (*Mammuthus columbi*) from southern California using a combination of thin section, isotope, and CT analyses. This study provides one of the first published records documenting the recurrence of annual density bands in tusks, which I recognize as marked by an abrupt reduction in X-ray attenuation coinciding with the seasonal change from winter to spring. Once annual boundaries are established, I discuss intra-annual aspects of growth, which allow for identification of several musth intervals within the final years of life, as well as season of death.

Chapter 3

The third chapter of the dissertation revisits the techniques and methods established in Chapter 2 and calls into question the ubiquity of annually-forming density features in tusks. The study focuses on an adult male gomphothere (identified as *Stegomastodon platensis*) from central Chile and is the first analysis of its kind for a South American proboscidean. Density features in this individual formed twice per annum, once at the boundary between winter and spring and again in mid-summer. It is not yet clear whether the pattern of density feature formation is taxonomically constrained or is a product of geography or environment. These results suggest that boundaries between years need to be verified using multiple lines of evidence in order to assess the seasonal identity of density features in individuals from different regions or in different taxonomic groups. Other results of this study include identification of musth intervals in years prior to death (including the final year of life), growth rate, and season of death.

Chapter 4

The fourth chapter furthers the inquiry into intra-annual variation in tusks and the identification of boundaries between years (especially as they relate to density features observed in microCT). This study also provides the inspiration and basis for the study of inter-annual variation in tusks documented in Chapter 5. In Chapter 4, I utilize thin section and microCT analyses of partial tusks from five female woolly mammoths (*Mammuthus primigenius*) from Siberia to understand inter- and intra-annual variations in the final years of each animal's life. Within this study sample, density features

observed in microCT are formed on a yearly basis with distinct transitions from high- to low-attenuation marking the boundaries between the winter and spring of each year. This suggests that these density features are reliable for identifying annual growth increments (at least in woolly mammoths from Siberia) and therefore can be used in non-destructive studies of tusks to access potentially multi-decadal records of growth history. All female tusks studied, with the exception of one specimen representing a sub-adult individual, showed a pattern of sinusoidal change in annual appositional thickness over an interval of approximately four to five years. The presence of this pattern in older females, apparent lack of the pattern in the younger female, and absence of the pattern in the male individuals studied in Chapters 2 and 3, suggest that this pattern of growth represents an aspect of reproductive life history.

Chapter 5

The fifth chapter of the dissertation marks a shift from the mostly intra-annually-focused studies of the previous chapters to considerations of inter-annual variation over multiple decades of an individual's life. This study continues the inquiry into the several-years-long pattern of decrease and increase in annual increment thickness documented in Chapter 4 and tests the hypothesis that this pattern represents the signature for calving intervals in female mammoth tusks. In this study, several complete or nearly-complete tusks of adult and sub-adult woolly mammoths from northern Siberia were imaged using an industrial microCT scanner in order to measure annual increment areas, appositional thicknesses, and extensional lengths for all available years. All adult female tusks recorded a pattern of decrease and then increase in all types of

measurement over periods of three to five years. In younger individuals, this pattern was found to begin around the expected age of sexual maturation (based on observations of modern elephants), with earlier years of life showing an altogether different pattern. The three- to five-year pattern was also absent in tusks of male individuals. The appearance of this pattern only in adult females, and not in males or young individuals of either sex, suggests that it reflects some aspect of female reproductive life history. Given the similarity in periodicity of this pattern to that of calving intervals in modern elephants, it seems reasonable to interpret these cycles of change in annual increment area as representing calving intervals.

Chapter 6

The final chapter of the dissertation summarizes the results of the previous four chapters and provides insight into the importance of these types of studies. In Chapter 6, I discuss future directions for research and put the results of my dissertation into the context of broader studies of proboscidean paleobiology and megafaunal extinction.

REFERENCES

Agenbroad, L.D., 2005. North American proboscideans: Mammoths: The state of knowledge, 2003. Quaternary International 126, 73-92.

Alroy, J., 1999. Putting North America's end-Pleistocene megafaunal extinction in context, Extinctions in near time. Springer, pp. 105-143.

Araujo, B.B., Oliveira-Santos, L.G.R., Lima-Ribeiro, M.S., Diniz-Filho, J.A.F., Fernandez, F.A., 2017. Bigger kill than chill: The uneven roles of humans and climate on late Quaternary megafaunal extinctions. Quaternary International 431, 216-222.

Barnosky, A.D., Koch, P.L., Feranec, R.S., Wing, S.L., Shabel, A.B., 2004. Assessing the causes of Late Pleistocene extinctions on the continents. Science 306, 70-75.

Beck, M.W., 1996. On discerning the cause of late Pleistocene megafaunal extinctions. Paleobiology 22, 91-103.

Chelliah, K., Sukumar, R., 2013. The role of tusks, musth and body size in male–male competition among Asian elephants, *Elephas maximus*. Animal behaviour 86, 1207-1214.

Enk, J., Devault, A., Debruyne, R., King, C.E., Treangen, T., O'Rourke, D., Salzberg, S.L., Fisher, D., MacPhee, R., Poinar, H., 2011. Complete Columbian mammoth mitogenome suggests interbreeding with woolly mammoths. Genome biology 12, R51.

Faith, J.T., Surovell, T.A., 2009. Synchronous extinction of North America's Pleistocene mammals. Proceedings of the National Academy of Sciences 106, 20641-20645.

Fisher, D.C., 1996. Extinction of proboscideans in North America. In: Shoshani, J., Tassy, P. (Eds.), The Proboscidea: Evolution and palaeoecology of elephants and their relatives. Oxford University Press, Oxford, pp 296–315.

Fisher, D.C., 2001. Season of death, growth rates, and life history of North American mammoths. In: West, D.L. (Ed.), Mammoth site studies: Proceedings of the first international conference on mammoth site studies. Publications in Anthropology vol. 22, University of Kansas, Lawrence, pp. 121–135.

Fisher, D.C., 2009. Paleobiology and extinction of proboscideans in the Great Lakes region of North America. In: Haynes, G. (Ed.), American megafaunal extinctions at the end of the Pleistocene, Springer, New York, pp. 55–75.

Gheerbrant, E., 2009. Paleocene emergence of elephant relatives and the rapid radiation of African ungulates. Proceedings of the National Academy of Sciences 106, 10717-10721.

Grayson, D.K., 1991. Late Pleistocene mammalian extinctions in North America: taxonomy, chronology, and explanations. Journal of World Prehistory 5, 193-231.

Koch, P.L., Barnosky, A.D., 2006. Late Quaternary Extinctions: State of the Debate. Annual Review of Ecology, Evolution, and Systematics 37, 215-250.

Lister, A., 1993. Evolution of mammoths and moose: the Holarctic perspective. Quaternary mammals of North America. Cambridge University Press, Cambridge, UK, 178-204.

Lister, A., Sher, A., 2015. Evolution and dispersal of mammoths across the Northern Hemisphere. Science 350, 805-809.

Lister, A.M., Sher, A.V., 2001. The origin and evolution of the woolly mammoth. Science

294, 1094-1097.

Lister, A.M., Sher, A.V., van Essen, H., Wei, G., 2005. The pattern and process of mammoth evolution in Eurasia. Quaternary International 126, 49-64.

MacFadden, B.J., Hulbert, R.C., 2009. Calibration of mammoth (*Mammuthus*) dispersal into North America using rare earth elements of Plio-Pleistocene mammals from Florida. Quaternary Research 71, 41-48.

Maglio, V.J., 1973. Origin and evolution of the Elephantidae. Transactions of the American Philosophical Society 63, 1-149.

Martin, P.S., Klein, R.G., 1989. Quaternary extinctions: a prehistoric revolution. University of Arizona Press.

Martin, P.S., Wright, H.E., 1967. Pleistocene extinctions; the search for a cause.

Rabinovich, R., Lister, A.M., 2017. The earliest elephants out of Africa: Taxonomy and taphonomy of proboscidean remains from Bethlehem. Quaternary International 445, 23-42.

Shoshani, J., Golenberg, E.M., Yang, H., 1998. Elephantidae phylogeny: morphological versus molecular results. Acta Theriologica 43, 89-122.

Shoshani, J., Tassy, P., 2005. Advances in proboscidean taxonomy & classification, anatomy & physiology, and ecology & behavior. Quaternary International 126, 5-20.

Sisca, R., Provenza, D., 1972. Initial dentin formation in human deciduous teeth. Calcified Tissue International 9, 1-16.

Stuart, A.J., 1991. Mammalian extinctions in the Late Pleistocene of northern Eurasia and North America. Biological Reviews 66, 453-562.

Stuart, A.J., Sulerzhitsky, L.D., Orlova, L.A., Kuzmin, Y.V., Lister, A.M., 2002. The latest woolly mammoths (*Mammuthus primigenius* Blumenbach) in Europe and Asia: a review of the current evidence. Quaternary Science Reviews 21, 1559-1569.

Sulerzhitsky, L., 1997. Patterns of the radiocarbon chronology of mammoths in Siberia and northern Eastern Europe (as sub-stratum for human dispersal). Humans settle the Planet Earth, 184-202.

Uno, K.T., 2012. Advances in terrestrial paleoecology from intratooth stable isotope profiles in tooth enamel and tusk dentin. The University of Utah.

Vartanyan, S., Garutt, V., Sher, A.V., 1993. Holocene dwarf mammoths from Wrangel Island in the Siberian Arctic. Nature 362, 337-340.

CHAPTER 2

Last years of life and season of death of a Columbian mammoth from Rancho La Brea[1]

ABSTRACT

Excavations near the Los Angeles County Museum of Art in 2006 uncovered

Pleistocene-age fluvial deposits containing the disarticulated skeleton of an adult

Columbian mammoth (*Mammuthus columbi*). The skeleton is about 80% complete, with

osteological and dental features suggesting a male with a Laws' Age Class of XXVI,

representing an adult of prime reproductive age. A sample was excised from near the

proximal end of the left tusk to evaluate the last years of life and assess season of

death. This sample was scanned by microCT and then thin-sectioned. Viewing microCT

data in transverse section, the dentin is organized in concentric zones paralleling the

pulp cavity surface. Between the dentin-cementum interface and the pulp surface, there

are somewhat regularly spaced, abrupt transitions (inward, in the direction of dentin

apposition) from higher to lower x-ray attenuation, suggesting shifts from higher to lower

density. Similar transitions have been interpreted previously as reflecting winter-spring

boundaries. These same loci are associated consistently with periradicular topographic

features on the external surface of the alveolar portion of the tusk. Analysis of

---

[1] El Adli, J.J., Cherney, M.D., Fisher, D.C., Harris, J.M., Farrell, A.B., Cox, S.M., 2015. Last years of life and season of death of a Columbian mammoth from Rancho La Brea. In: Harris, J.M. (Ed.), La Brea and beyond: The paleontology of asphalt-preserved biotas. Natural History Museum of Los Angeles County, Science Series vol 42, pp. 65-80

approximately weekly incremental features in a transverse thin section shows little

systematic seasonal variation in rates of dentin apposition – not surprising for southern

California – but shorter-term patterns of rate variation do help confirm some of our

identifications of year boundaries. Daily dentin increments are visible in parts of the

sequence, but not consistently. Judging from rates of tusk growth in the last years of

life, death appears to have come in early summer, the season identified in prior work as

normal for musth, the period of heightened aggression and sexual activity in which

mating and male-male conflict would be expected to occur. We suspect that this male

died as a result of soft-tissue injuries sustained in a musth conflict.

INTRODUCTION

In 2006, construction of an underground parking structure by the Los Angeles

County Museum of Art in southern California exposed abundant fossil vertebrate

specimens from the Rancholabrean North American Land Mammal Age. This

assemblage was preserved in fluvial deposits that had been post-depositionally

permeated by asphalt (Harris et al., 2013), and it contained a nearly complete but

mostly disarticulated skeleton of a large Columbian mammoth, *Mammuthus columbi*

(Falconer, 1857). Approximately eighty percent of the skeleton was recovered.

This mammoth, nicknamed "Zed", is the largest and most complete proboscidean

collected from Rancho La Brea. An uncalibrated radiocarbon date on Zed's second

thoracic vertebra (P23-1316) returned an age of 36,770±750 RCYBP (Fuller et al., in

press). The left tusk (Los Angeles County Museum P23 10910) of this individual is 318

cm long, measured along its outer curve, and has a maximum diameter of 24 cm at a

position 90 cm from the proximal margin (Fig. 1). Tusk dimensions, especially length and circumference, confirm that this individual is a male (Smith and Fisher, 2011, 2013). Furthermore, the stage of molar replacement and wear suggests a Laws' Age Class (1966) of XXVI, representing an adult of prime reproductive age (Fig. 2).

As in other proboscideans, the tusks of Columbian mammoths record a remarkable diversity of information on life history. This information can be extracted from structural and compositional variation within annual (first-order), weekly (second-order), and daily (third-order) growth increments observable in tusks (Fisher, 2001). First-order dentin increments can also be observed in microCT data (Fisher et al., in review). Because incremental features form periodically, increment thickness can be used to assess growth rates, which are in turn related to nutrition and health of the individual (Fisher, 1996). By comparing rates of dentin apposition (thickness increase) and extension (length increase) with compositional changes and with external growth features of the tusk, it is often possible to recover information on specific life history events, including season of death.

MATERIALS AND METHODS

The left tusk of Zed was prepared at the George C. Page Museum. This tusk is largely intact, with only minor fracturing along its proximal margin. A sample block approximately 5 cm long and 2.5 cm wide, extending from the outermost cementum, inward to the pulp cavity surface, was removed from the tusk using a Dremel hand-held grinder and a carbide bit. Given the conical geometry of the pulp cavity, the sample block was 46 mm thick (along a tusk radius) at its distal end and 36 mm thick at its

proximal end. The sample site was located along the outer curve of the tusk (to maximize increment thickness), about 23 cm from the broken proximal margin, within a sequence of relatively well-defined periradicular topographic features (Fig. 1).

During removal of the sample block, the dentin sequence separated along a parting that followed a former position of the appositional surface. The outer block of dentin, with attached cementum, was set aside, and we continued cutting on the remainder of the sample block. This was removed intact, and the two parts were assembled with quick-setting epoxy. Inspection of the block revealed that the dentin was somewhat chalky (suggesting degradation of much of its original collagen matrix), but still structurally sound.

Following repair of the sample block, a region near its distal end was imaged in the MicroCT Core Facility at the University of Michigan School of Dentistry, using a SCANCO Medical μCT100 operating at 90kV, 78μA, and 500 ms, yielding uniform cubic voxels 60 μm on a side. To observe patterns of variation in x-ray attenuation within the tusk cross section, the CT scan was processed using Amira 5.4.1. Zones of high and low x-ray attenuation were noted by eye (Fig. 3A) and quantified by luminance measurements. Time-dependent luminance variation was documented using the "Measure" tool in ImageJ (Rasband, 1997) on a swath of pixels extending along a transect in the direction of dentin apposition (normal to appositional features). Grayscale values of ten neighboring pixels (the swath width) paralleling appositional features were averaged (in Adobe Photoshop CS5) for each position along the transect to reduce the influence of more highly localized factors (e.g., CT artifacts, vacuities, dentinal tubules).

For additional analyses, two adjacent 5-mm thick slabs were cut from the sample

block along transverse planes normal to the appositional surface, using a Buehler Isomet saw with a diamond wafering blade. Ethanol was used as a lubricant during cutting. Unlike cutting oils, ethanol evaporates quickly from the sample, leaving no residue. We avoid using water or aqueous solutions because the collagen in dentin is hygroscopic and expands in the presence of water, fracturing adjacent dentin that has not yet absorbed comparable amounts of water. A transverse thin section was made from one of the slabs, using ethanol for cutting and polishing (Fisher and Fox, 2003). This thin section was examined initially at 25x with a stereomicroscope (Wild) and then at 40x with a petrographic microscope (Leitz). Sixteen photomicrographs (e.g., Fig. 3B) were taken along a transect from the cementum to the pulp cavity surface, using plane-polarized light, with kerosene added to the slide to reduce scattering of light and enhance contrast. Thicknesses of second-order (approximately weekly) increments were measured from these micrographs using the ImageJ plug-in Inc Meas 1.3c (Rountrey, 2009).

The second slab cut from the sample block was used as a source for a time-series of samples for analyzing stable isotope changes in the tusk during the last years of life. Mill-paths for individual samples were laid out on a high-resolution scan of the polished slab surface, which was also aligned with a virtual section from the microCT scan. Comparing both records allowed us to limit samples to areas bounded by growth lines (time-dependent appositional discontinuities). Mill-paths were later transferred to the slab surface, and dentin powders from thirty samples of equal thickness (0.7 mm) were collected using a carbide bit and a manual drilling stage under a stereomicroscope (Fig. 4).

Samples were pretreated for isotope analysis of structural carbonate following methods described in Rountrey (2009). About 6.25 mg of each powder sample was vortexed in 0.5 mL of 30% H_2O_2 and then left for twenty-four hours in a fume hood. Samples were subsequently rinsed in five separate washes of 1.0 mL ultrapure water with vortexing, followed by centrifugation (five minutes at 6,000 rpm), and then by removal of supernatant between each wash. The rinsed samples were then vortexed in 0.5 mL of a 1M acetic acid-calcium acetate buffer solution and left in a fume hood for an additional twenty-four hours. Following this, the samples were again rinsed five times in ultrapure water, as described above. Samples were then freeze-dried overnight to remove all water. Using a microbalance, we measured 0.75 mg of each sample, loaded samples into boats, and then analyzed carbon and oxygen isotope ratios using a Finnigan MAT Kiel IV preparation device coupled directly to the inlet of a Finnigan MAT 253 triple collector isotope ratio mass spectrometer.

RESULTS

External features of the tusk

About 55 cm from the proximal end of the tusk, we note a discontinuity in surface texture characterized by a greater degree of abrasion and polish evident distally and more surface roughness (consistent with original attachment of periodontal ligament) preserved proximally. This shift marks the gingival (or alveolar) margin, separating the erupted part of the tusk that was subjected to use-wear during life (creating the smoother surface), from the proximal portion that was surrounded by and attached to periodontal ligament within the tusk alveolus. The external surface of the alveolar

17

portion of the tusk displays a series of circumferential, undulatory topographic features

referred to as "periradicular bands" (Dean, 1995; Fisher, 2008), where a single "band" is

one cycle of proximodistal variability in surface-relief. Complicating this picture, many

tusks (and other teeth), including this one, show two (or even three) different scales of

periradicular features in the form of finer-scale features with short wavelengths and only

subtle relief that co-occur with coarser-scale features with much longer wavelengths

and more pronounced relief. Descriptions of this system of features confront several

terminological issues (discussed below), but our usage follows Fisher (2008), where

"periradicular features" include any of the circumferential topographic elements on tooth

roots that represent structural increments of root extension. Such elements include

sinuous, but locally linear topographic features, both positive ("ridges") and negative

("grooves"), which roughly parallel the proximal, growing margin of the root. They also

include areas that are bounded by such linear elements, though for clarity, we always

distinguish between *increments* (the entirety of mass or surface added to an

appositional system during an interval of time) and *boundaries* (features that demarcate

increments and generally approximate a delimiting edge or interface of the appositional

system at a point in its history).

Periradicular features originate as primary (original) relief on the dentin-

cementum interface and therefore are usually most easily observed near the proximal

margin of roots, where the cementum layer is thinnest. Farther from the proximal

margin, where a greater accumulation of cementum mantles the topography of the

dentin-cementum interface, periradicular features are often more difficult to distinguish

(Laws, 1952). In addition, when viewing periradicular features through the cover of

cementum, some of the subtler features in a sequence may be obscured.

Periradicular features have a structural aspect in addition to their topographic expression, and this corresponds directly to elements of the hierarchy of incremental features documented in dentin cross sections (transverse or longitudinal; Fisher, 1984, 1987) or volumes (as in CT analyses; Fisher et al., in press). We refer to the largest-scale periradicular features as "first-order", and these reflect the same units of internal dentin structure that we describe as "first-order" and that have been demonstrated to recur with periods of about one year (Fisher, 1987, 1996, 2001; Koch et al., 1989). The next-largest-scale features are "second-order", corresponding to the second-order increments normally studied in dentin thin sections, and in mammoth tusks, these typically recur with periods of about one week (Fisher, 2001). On the external surface of Zed's tusk, there is generally a most-accentuated (within the local sequence) second-order negative periradicular feature, or groove, located within a broader, deeper trough separating successive positive first-order elements (ridges). We treat these grooves within troughs as bounding successive first-order periradicular bands and use their spacing along the outside curve of the tusk for quantifying the extensional magnitude of first-order periradicular bands. These features are shown in Figure 1, where low-angle lighting emphasizes the topography of first-order periradicular bands, and white arrows mark the boundaries of the last eight first-order features for which both distal and proximal boundaries are observed. Two additional first-order periradicular bands, distal to the last eight, were discerned during direct inspection but are not clear under the illumination used for Figure 1.

Extensional lengths of first-order periradicular bands on Zed's tusk are presented

19

in Table 1. This series of measurements starts near the gingival margin simply because, distal to this position, boundaries of periradicular features cannot be clearly distinguished on the external surface. There is no direct concordance between periradicular bands and the gingival (alveolar) margin because they represent separate aspects of anatomy – the first controlled by the geometry of the proximal margin of the tusk and the second by the geometry of the tusk "lip line." The measurements in Table 1 end with a year that is incomplete in two respects: (1) if we correctly interpret a short groove (marked by the proximal-most white arrow in Fig. 1, offset from the others, near the proximal margin of the tusk) as a last boundary between first-order periradicular bands, death appears to have befallen this individual before the expected end of this last year of life, Year X, leaving it narrower than preceding years; and (2) the proximal margin of the tusk is broken all around its circumference, so that Year X is nowhere seen with the extensional magnitude that was in fact realized in life.

The pattern of variation in extensional length of first-order periradicular bands is shown in Figure 5. In this graph, we do not show Year X because it is incomplete and thus not directly comparable to the preceding ten years. We provisionally accept the location of the periradicular feature marking the boundary between Years X and X-1, despite its preservation on only a small portion of the tusk margin. The average extensional length over Years X-1 through X-10 is then 5.4 cm, with a general pattern of declining values, except for the unusually long Year X-4.

Stage of dental development and sex

Close spatial association, lack of duplication of elements, and consistent sizes

and stages of development provide compelling evidence that the dental and skeletal elements discussed here are associated remains of a single individual. Only one molar is present within each quadrant of the dentition, and in each case, dimensions and loph counts (Tab. 2) confirm identification as a third molar. Dental traits are consistent with other reports for *Mammuthus columbi*, although the lamellar frequency is low in comparison to other material attributed to this species in current taxonomic practice (e.g., Saunders, 1970; Agenbroad, 1994).

An occlusal view of Zed's mandible with lower molars is shown in Figure 2. Upper molars are in a similar, but slightly less advanced stage of wear, especially in regard to attrition of the anterior margin. Similar differences in wear between uppers and lowers are reported for *Loxodonta africana* (Laws, 1966). Stages of molar eruption and wear in Columbian mammoths and African elephants are not identical, but the best approximation to the configuration seen in Zed is to Laws' Age Class XXVI (Laws, 1966). Although there has been no formal calibration of the dental eruption and wear schedule of *M. columbi*, most investigators accept the working hypothesis that ages assigned to *Loxodonta* at comparable stages of eruption and wear are a reasonable estimate of Columbian mammoth ages (e.g., Graham, 1986; Agenbroad, 1994). This would place Zed at about 49±2 years old.

Zed's tusk length and diameter are consistent with an age estimate of this magnitude. Accepting that first-order periradicular bands recur with approximately annual periodicity, the fact that ten such periradicular bands occur within barely more than the proximal one-sixth of tusk length could be taken to imply an even greater age. However, years prior to the last ten were likely characterized by greater extension rates

than were realized during the last decade (judging from the life-long pattern of variation in extension rate documented for mastodons; Fisher, 2008). Zed's tusk diameter declines from 24 cm at a position 90 cm from the proximal margin to a value of 19.5 cm at the proximal margin, a pattern typical of fully mature individuals. Asphalt and sediment were not completely removed from the pulp cavity at the time of sampling, but the pulp cavity is clearly not as shallow as would be expected for a very old individual. Without further sampling and analysis, knowledge of Zed's age will remain imprecise, but we have no reason to reject the Laws' age estimate.

Zed was originally identified as male on the basis of molar width (male molars being appreciably wider than those of females). Zed's tusk length and circumference also support identifying him as a male. One of the best-studied assemblages of *M. columbi* is from the Hot Springs Mammoth Site of South Dakota, and most of the individuals preserved there are interpreted as sexually mature, but still young males (Agenbroad, 1994; Lister and Agenbroad, 1994). Zed's tusk is longer than published values for Hot Springs *M. columbi*, but his tusk circumference is near the mean for their distribution (fig. 77 in Agenbroad, 1994). Given normal patterns of sexual dimorphism in proboscidean tusks (Fisher, 2008; Smith and Fisher, 2013) these measures are too great to consider this specimen female. Zed's pelvic aperture is not sufficiently intact to use its dimensions to evaluate sex (following Lister and Agenbroad, 1994), but the posterior aspect of his ischial tuberosities shows the relatively narrow V-shaped profile characteristic of males (text-fig. 12C in Fisher, 2008). The size and advanced state of epiphysis fusion on Zed's postcranial skeletal elements likewise corroborate his age and sex.

Computed tomographic features

X-ray computed microtomography was used to assess density features within the sample block removed from the tusk. Within this 3D dataset, the pulp cavity surface is a clear interface inclined relative to the outer surface of the block. The dentin-cementum interface is marked as a sharp transition in attenuation values (from higher values within cementum to generally lower values in dentin) that parallels the outer surface. Within the dentin sequence, smaller-scale transitions in attenuation value, some gradual and some abrupt, broadly parallel the pulp cavity surface and represent time-dependent variation in the attenuation value of coevally deposited dentin. We digitally extracted a slice oriented as a transverse section, perpendicular to the pulp cavity surface and to the transitions in attenuation value that parallel it. This slice was located near (and parallel to) the sample slabs that would later yield the thin section (dashed white line crossing the sample location footprint in Fig. 1). Viewing this virtual slice perpendicular to its principal plane and averaging attenuation through a thickness of 1 mm, we generated the image shown in Figure 3A. Luminance values in this image are a summation of attenuation values throughout the slice thickness, analogous to the optical summation of density that occurs in light microscopy.

Some luminance features in Figure 3A have nothing to do with time-dependent variation in properties of dentin. Air- or epoxy-filled cracks are much darker than average dentin values. The bright, ring-shaped feature in the upper part of the image is an artifact of the density reconstruction algorithm, and some of the vertically oriented (radially, in the tusk) bright swaths represent so-called "dead tracts" (Avery, 1988),

where the lumina of dentinal tubules have been partially filled with mineral, often as a response to some inflammatory process. The zone of high luminance adjacent to the pulp cavity could indicate early-diagenetic (postmortem) precipitation of carbonate within dentin pores most directly exposed to groundwater following burial. Globular loci of high luminance within the pulp cavity represent clastic sediments, surrounded by asphalt, that were left in place to protect the integrity of the pulp cavity surface.

Shifting to the more clearly zonal patterns of variation that parallel the pulp cavity surface, brighter zones (higher attenuation) suggest higher density of mineralization of the dentin, and darker zones suggest lower density, but the causes of these contrasting values are not self-evident. Without some external frame of reference, the concentric patterns of density variation in Figure 3A, clear as they are, might still be difficult to interpret in terms of first-order features. However, prior work on premaxillary and mandibular tusks of mastodons and molar roots of mammoths (Fisher, 1987; Fisher et al., in review) suggests that dentin is often more highly mineralized in late winter and less mineralized in spring, with relatively abrupt transitions between these conditions. Low-density dentin often continues to form into the summer, and the rest of the year may be characterized either by a gradual or step-wise increase in dentin density. We thus interpret abrupt transitions from higher to lower dentin luminance as suggestive of some approximation of a winter-spring boundary. Based on this search image, we placed white arrows along the right margin of Figure 3A, demarcating putative first-order dentin increments.

In this fashion, we provisionally identify four complete years in the intermediate portion of this dentin sequence and two partial years, one at the beginning of the

24

sequence and one at the end. Starting near the pulp cavity, we interpret the dentin that formed subsequent to the last winter-spring boundary as the initial portion of a final year of life that is thinner than other years and even at this scale of analysis appears to be incomplete. We propose that this year corresponds to the incomplete final year inferred from the record of tusk extension and identify it in Figure 3A as Year X. Extending attributions backward in time, the incomplete year recorded just inside the dentin-cementum interface would be Year X-5, and its incompleteness in this plane is simply a function of the proximodistal location of this slice of the data. Year X-4, just inside of Year X-5, has the greatest appositional thickness of any of these last years of life, matching its unusually great extensional length (Fig. 5). The luminance transitions noted above are also documented quantitatively in Figure 6B for the part of the sequence sampled isotopically. Provisionally accepting the winter-spring boundaries proposed in Figure 3A, annual appositional thickness averaged 6.4 mm in the last four complete years of life.

Second-order increment profile

When high-speed polishing of the thin section was complete, we examined it in reflected light under a stereomicroscope. Most of the zones of high x-ray attenuation in the microCT record, immediately preceding transitions to lower attenuation that we interpreted as associated with a winter-spring boundary, displayed slightly elevated topography of the section surface and a higher degree of polish than adjoining areas—implying greater hardness and confirming our inference of greater density. These observations confirmed placement of all of the first-order increment boundaries except

25

for the one between Years X-1 and X-2, which offered little corroboration of its placement.

Examination of the thin section in plane-polarized transmitted light reveals moderately distinct second-order dentin increments presenting typically as dark-light couplets whose thickness can be measured from one dark zone to the next. These couplets generally represent approximately weekly growth intervals and sometimes contain about seven third-order (daily) increments between them, although third-order increments are not always visible within each second-order increment in this specimen. In ideal conditions, second-order increments are distinguished from third-order increments by broader and often darker dark zones within their dark-light couplets. However, in intervals where third-order increments are not consistently developed, an anomalously dark third-order increment could be mistaken for a second-order increment. In this way, or worse, if there were aperiodic structural features mixed in with and indistinguishable from periodic increments, increment counts and thickness profiles could be subject to large errors. When increment numbers and thicknesses match expected patterns, they combine to yield a well-corroborated history of apposition, with growth rates documented by thickness variation of periodically formed increments. However, when expected patterns fail to emerge, it can be difficult to assess what aspect of the system has been misinterpreted.

Thicknesses of second-order increments in thin section were measured perpendicular to the appositional surface from the pulp cavity nearly to the dentin-cementum interface. These increments were fairly regular throughout the last few years of the animal's life and averaged 0.14 mm in thickness with a standard deviation of 0.04

mm. Both the raw data and a summary provided by a five-point moving average reveal weak annual fluctuations in apposition rate, with slight increases in what we interpret (based on x-ray attenuation features discussed above) as late winter-early spring and slower apposition in the summer. We do not see a strong pattern of sinusoidal seasonal variation comparable to patterns documented for specimens from temperate latitudes (Fisher, 1987; Koch et al., 1989). One exception to the generally smooth trend is a series of seven second-order increments that record low rates of apposition (averaging 0.087 mm per increment) at the very end of life (Figure 6D). This series begins about 16 increments after the last inferred winter-spring boundary and extends to the last increment, marking the time of death, about 23 increments into the last year of life. Several other intervals of low growth rate are observed in the tusk and are displaced comparably from a marked transition in x-ray attenuation. However, none of these is sustained for as long as at the end of life.

Isotope data

Thirty serial samples from Zed's last approximately four years of life were analyzed for the carbon and oxygen isotope compositions of structural carbonate in tusk dentin. Measured $\delta^{18}O$ values from Zed's tusk show little seasonal variation, with fluctuations of ~1‰ around an average of ~26.75‰ SMOW (Tab. 3; Fig. 6A). Thus, no clear evidence of season is available from this time series.

The time series of carbon values from the tusk shows relatively pronounced variation on an approximately annual scale, with fluctuations of up to ~5‰ VPDB within a given year (Tab. 3; Fig. 6A). Within interpreted years, winters usually have lower, but

still positive $\delta^{13}C$ values, while summers have higher (more enriched in ^{13}C) values. However, the $\delta^{13}C$ values recovered from the tusk are all abnormally high (averaging 6.4‰ VPDB), even for herbivores with a strictly C_4 diet, living in dry conditions (Koch et al., 1994). One final observation is that the series of $\delta^{13}C$ values appears to be inversely correlated with attenuation value of the dentin, measured as luminance in the microCT slice near the isotope sampling site (Fig. 3A, 6B).

DISCUSSION

Taken individually, each data series from Zed's left tusk, with the possible exception of periradicular bands, might be considered as offering only weak evidence of season of formation. The microCT features are somewhat faint, and the pattern of variation in attenuation within years is variable. Second-order growth increments show only hints of seasonal variation in thickness. Oxygen isotope values vary about a mean that is not unexpected, but the range of variation is so limited that this time series is uninformative with respect to season. Carbon isotope values show the only conspicuous pattern of variation on the timescale of years, but the actual values are unlike any observed previously in a proboscidean tusk. However, further probing of each data source and associations between them reveals greater cohesion.

The periradicular bands on the alveolar portion of Zed's tusk at least represent a clearly repeating pattern with a prior history of study. They were first described in proboscideans by Osborn (1936), who referred to them as "annulations", a generic noun referring to their ring-like configuration relative to the tusk axis, although he also proposed that their period of recurrence might approximate one year, opening the door

28

to some risk of confusion of "annular" features and "annual" features. Lest this seem unlikely, in another application of dental histology, "cementum annuli" – incremental features of cementum apposition that can indeed be seen as "annuli" when viewed in transverse sections of roots (although their three-dimensional geometry would be better described as quasi-cylindrical) – are routinely treated as annual and used in determinations of age and season of death. As evidence of the potential for confusion, Keiss (1969, p. 175), discussing cementum annuli in elk, cites Scheffer (1950) as the earliest report of "annular rings in the dental cementum", but "annular rings" would seem to be redundant, suggesting he may have meant "[annual] rings". Furthermore, Scheffer (1950) does not in fact address cementum annuli at all, describing instead features that are, in our terminology, first-order periradicular bands. Keiss (1969) also cites Laws (1952), but this paper deals with what we would call first-order dentin increments seen in transverse cross sections of tooth roots and is mainly concerned with demonstrating their annual nature, making no reference whatsoever to cementum annuli. Because of this potential for misunderstanding, Fisher (1987) cited Osborn's "annulations", illustrated and described first- and second-order "undulations" of the dentin-cementum interface traced in longitudinal section, and related them to first- and second-order features of dentin structure, but did not adopt Osborn's term.

Use of the phrase "periradicular bands" is generally traced to Komai and Miyauti (1938), but Smith and Reid (2009) suggest that the features Komai and Miyauti illustrated are not identical to what Dean (1995) describes as the basis for most recent applications of the concept. Dean's periradicular bands are manifestations at the dentin-cementum interface of what are called in the primate literature "long-period lines",

equivalent to our second-order increments (except for the focus on the "line" rather than the whole increment). Still, Smith and Reid (2009) cite and appear to accept the usage of Rinaldi and Cole (2004), who describe periradicular bands that are manifestations of daily (third-order) dentin increments (although in their usage, the "band" is the "line" or "groove"). Smith and Reid (2009) likewise cite Scheffer's (1950) annual (first-order) features, although they describe his topographic features as "regular concentric lines on mammalian root surfaces" (p. 90). On balance, we accept that periradicular features occur on a range of different scales, requiring only an appropriate modifier and description of details of expression to clarify usage. We prefer to treat "bands" as having measurable width on the dentin-cementum interface, rather than being infinitesimally narrow boundaries, but bands cannot be adequately described without stipulating how their boundaries are defined. The "short-period"/ "long-period" dichotomy used for increments of different scale in the primate literature works well there, where annual-scale features are not usually evident, but for a dental system with at least three clear hierarchical levels, our reference to first-order, second-order, and third-order features seems preferable.

One aspect of the periradicular pattern that we have not seen before is variation in surface color, which seems to be correlated with first-order periradicular topography (with darker shades just proximal to first-order periradicular band boundaries; Fig. 1). Cementum can vary in color seasonally, with darker shades usually associated with winter (Fisher, 1996), but the entire outer surface of cementum on the alveolar portion of a tusk is usually represented as forming at approximately the same time and is therefore expected to have about the same color. It is possible that cementum

apposition is conditioned by some factor related to periradicular topography, but characterizing this further will require additional investigation.

The causal basis for first- and second-order periradicular features is not well resolved, but as explained elsewhere (Fisher, 1987, 2001), third-order periradicular bands appear to reflect a shifting balance (one cycle per year) between appositional and extensional growth of the tusk. When extension is suppressed relative to apposition, tusk circumference is reduced. Since Zed's second-order increment profile shows little seasonal variation in rate of apposition, we suspect that the changing "balance" was mainly due to a reduction and later increase in extension rate. When extension rate regains its relative magnitude, its trajectory (more or less aligned with the pulp cavity surface) generally increases tusk circumference again. Rate of dentin apposition is probably a function of access to nutrients for both formation of organic matrix and mineralization, but rate of tusk extension is fundamentally constrained by tusk eruption, which requires extensive remodeling of the periodontal ligament, a process that is probably protein-limited. Where the seasonal pattern of these interactions has been worked out in most detail, for a Great Lakes region adult male mastodon (Fisher, 2008), we suspect that protein limitation is most pronounced during the winter and is relieved with access to new plant growth in the spring. We suspect that Zed's well-defined periradicular bands originated in a similar fashion and imply at least moderate seasonality in diet quality (emphasizing protein content) even if the quantity of apposition-limiting nutrients was not markedly variable.

The rates of extensional growth implied by the pattern of first-order periradicular bands on Zed's tusk correspond to values that would be expected for an adult male

31

(Fisher, 2001, fig. 13.6A). In addition, the trend toward lower values approaching the

proximal end of the tusk is closely comparable to the pattern of tusk growth in a mature

male American mastodon in his prime reproductive years, experiencing musth regularly

(Fisher, 2008, text-fig. 24). If there is anything surprising about Zed's values, it is that

his tusk is growing as rapidly at an inferred age on the order of fifty as was the tusk of

the mastodon Fisher studied, in its mid-thirties. Of course, differences in local climate,

among other factors, could be responsible for Zed's relative vigor.

Zones of abrupt transition from high to low x-ray attenuation in microCT of tusk

dentin, proposed here as part of the annually-recurring syndrome of traits marking first-

order features, are not as clearly defined as the year-long gradients in attenuation value

observed in tusks from the high-elevation Ziegler Reservoir site in Colorado (Fisher et

al., in review). This can be explained in terms of the much greater seasonality to which

proboscideans high in the Colorado Rockies would have been exposed. Still, the

general nature of these features is similar, and the *number* of microCT features

recognized in Zed's sample block between the cementum and the pulp surface

corresponds to the *number* of periradicular bands between the location of the sample

block and the proximal margin of the tusk. This match is highlighted by the consistent

numbering of years in Figures 1 and 3A.

Rates of appositional growth implied by the microCT features we recognize in the

sample block also match expectations for a mature male (Fisher, 2001, fig. 13.6B). For

this variable, no great diminution is expected with advancing age (Fisher, 2008, Text-fig.

24), nor is any seen in this short sequence.

Focusing even more closely on comparing the appositional record contained in

the sample block with the extensional record visible as periradicular bands on the tusk surface, we have compared appositional thicknesses of successive years with their extensional lengths. Year X-4 is both the thickest and the longest, with subsequent years being more or less similar in thickness and length. The correlation between thickness and length for the four years X-1 through X-4 (the only complete years for which we have both values) is moderate (R^2 = 0.70), but not significant (p = 0.16), primarily because we only have data for four years. As explained above, apposition and extension are probably controlled by different factors. The topographic relief associated with first-order periradicular bands itself implies a decoupling of these two processes on an intra-annual time scale, and even modest decoupling extending beyond the bounds of a single year would lead to some lack of strict proportionality between these two variables. Without further work, we cannot even be certain that the microCT features that we use to mark boundaries of first-order dentin increments meet the dentin-cementum interface at precisely the position of the features we recognize as boundaries of first-order periradicular bands. Our best opportunity to check this on Zed's tusks was to compare the distance between the last microCT feature and the pulp cavity surface in the sample block (2.66 mm, measured on our photomicrographs using Inc Meas 1.3c) to the tusk thickness along the broken proximal margin, near the boundary separating periradicular Year X and Year X-1. This latter value was 2.95 mm, and it must include some cementum as well as the dentin thickness associated with Year X. This close correspondence means that at least this last microCT feature must match the last periradicular year boundary very closely.

Another approach to evaluating the degree to which microCT features can be

confirmed as annual involves shifting to the record of appositional growth provided by second-order dentin increments. In mammoth tusks these are understood as generally having a periodicity of about one week (Fisher, 2001; confirmed following documentation of a similar periodicity in *Gomphotherium* by Fox, 2000). We were able to count third-order (daily) increments in some parts of our thin section, confirming a periodicity close to weekly for parts of the record. Nevertheless, the tally of weeks recognized in Years X-4 through X-1, the only complete years for which we have data, is 69, 42, 31, and 49, respectively, compared to an expected value near 52. At first, this variation seemed large enough to cast doubt on the supposition that these increments were strictly periodic. However, as argued by Fisher et al. (2008), the factors that influence the timing of the changes in dentin structure and composition that we use to recognize boundaries of first-order increments likely involve elements of local weather, behavior, and food resources that vary from season to season and year to year. Although these are influenced by astronomical patterns, they need not show strict regularity, especially in environments of low overall seasonality. In any case, the tally of weeks above implies a mean of 47.8 – close enough to 52 to re-awaken interest. In fact, we are not concerned at all about small departures from documented periodicities because the physiological rhythms that appear to control second- and third-order increments (or long-period and short-period features of other authors; Dean and Scandrett, 1996) display individual and species-level variation like any other aspect of the phenotype. We therefore consider the annual nature of Zed's microCT features as reasonably secure.

Despite the lack of any strong pattern of seasonal (intra-annual) variation in rate

of dentin apposition, we observe scattered occurrences of thicker-than-normal second-order increments in the weeks shortly before and after most of the winter-spring boundaries. This suggests that climate and dietary amelioration from whatever set of conditions is here recognized as "winter" (no doubt different from this season at temperate latitudes), typically began before the winter-spring boundary and continued into early spring. Lower rates of dentin apposition in summer could reflect drier conditions and/or lower forage quality, but we offer another interpretation below. Overall, this pattern of apposition is consistent with a relatively mild climate and adequate nutritional resources during most of the year. This degree of evenness is not surprising, given the relatively moderate climate reconstructions for southern California during the late Pleistocene (Spaulding, 1990; Minnich, 2007).

An alternative interpretation of the low rates of dentin apposition during a portion of the inferred summer is that this was Zed's season of musth, the period of hormonally-induced aggression and mate-seeking known also in extant elephants (e.g., Poole and Moss, 1981). Musth in elephants can last up to three months. In dominant adult males, it normally recurs annually and is associated with fasting behavior that would be expected to reduce rates of dentin apposition. Even in environments of relatively low seasonality, a season with elevated chance of rainfall, such as late winter and spring, judging from Zed's record of tusk growth, could be an optimal season for birth (e.g., based on food availability for a nursing mother), and given an elephant-like gestation period of about 22 months, summer would be an optimal mating season. In elephants, dominant males are especially likely to mate according to this optimal schedule (Poole, 1996).

Less is known for mammoths, but observations on the development of the deciduous dentition in woolly mammoths suggest birth in the spring and a gestation period similar to that of extant elephants (based on the duration of intrauterine development in dp2; Rountrey et al., 2012). Late spring to early summer has also been proposed as the normal musth season for Columbian mammoths from the North American Great Plains (Fisher, 2004), for woolly mammoths in northern Yakutia (Fisher, 2007), and for American mastodons in temperate North America (Fisher, 2008; Fisher and Fox, 2007).

Numerically, the $\delta^{18}O$ values we observe in Zed's tusk are similar to those recorded for *Bison* and *Equus* from Rancho La Brea (Feranec et al., 2009, reporting values relative to PDB rather than VSMOW), but Zed's intra-annual range of variation is only about 1‰, and his profile shows little repeated pattern from year to year. In contrast, Feranec et al. (2009) report annual ranges of ~1.5-5‰ per year in *Equus* and ~1-5‰ in *Bison*, with some patterns looking more like seasonal cycles than what we see in Zed. Either Zed experienced a lower level of variation in oxygen isotope ratio and less seasonally structured variation than did bison or horses, or his values could have been to some degree homogenized by diagenetic alteration, as dentin is generally understood to be less stable diagenetically than enamel (Ayliffe et al., 1994).

Zed's $\delta^{13}C$ profile stands in marked contrast to his $\delta^{18}O$ profile in that it shows conspicuous variation of ~3-5‰ within years and an intra-annual pattern that is at least somewhat consistent among years. However, the numerical values are much more positive than expected. Even herbivores with diets dominated by C_4 vegetation would not normally show values above about 2‰ (Koch et al., 1994). In this light, only the last

δ^{13}C value measured for Zed, adjacent to the pulp cavity, seem plausible as a primary value, although even this may be questionable given that both Coltrain et al. (2004) and Feranec et al. (2009) found no evidence of C_4 vegetation in the diets of Rancho La Brea herbivores they analyzed (although neither included mammoths). Analysis of Zed's molar enamel could clarify this discrepancy.

We have considered factors beyond diet that might elevate δ^{13}C values, such as severe water stress, but it seems difficult, not to mention inconsistent with the absence of seasonal enrichment in the δ^{18}O profile and with characterizations of contemporary climate as cool and mesic (Heusser, 1998), to explain the values observed here as unaltered, primary indicators of diet and climate. We do, however, note an apparent inverse association between dentin density, measured as luminance in the microCT record (Fig. 6B), and the δ^{13}C record. One possible explanation of this is that the structural carbonate of Zed's dentin may have been diagenetically altered, shifting values in a positive direction, and to a greater degree in zones of lower density, where greater permeability may have increased the effective volume of pore-water interacting with the dentin. Higher-density zones might thus retain less altered values. Most of these higher-density zones are primary features of dentin structure, but the *highest-*density dentin, adjacent to the pulp cavity, was interpreted above as having been altered postmortem by deposition of exogenous carbonate within dentin pores. This would have reduced the potential for further interaction with groundwater and could explain why it is only in this zone that we find a plausibly primary δ^{13}C value. The sample pretreatment methods for analysis of structural carbonate in bioapatites are designed precisely to remove this type of secondary carbonate (Koch et al., 1997), so

37

ironically, we may be seeing original isotope values only where dentin was "sequestered" within early-postmortem secondary carbonate. If the carbon isotope ratio of this last sample before death is intact, perhaps the oxygen isotope ratio is as well, but unfortunately, there is little we can do with a single value. We recognize that this explanation of our isotope results is incomplete, but it suggests that some scrap of meaning may yet remain in a record that otherwise failed to yield the quality of data we had hoped would be recovered.

For most of his last years of life, Zed's tusk growth record, most notably his rate of tusk extension, suggests excellent health, especially given his probable age. The first significant interruption of this pattern occurs near the end of life where the terminal series of seven second-order increments records a marked drop in weekly rate of apposition (Fig. 6D). As this pattern is sustained for nearly two months, we interpret it as a significant deterioration of condition.

Placing this terminal interval of low growth rate into context, it is immediately preceded by two thin, but not so dramatically thin increments, that occur 15 increments after the final inferred winter-spring boundary, or about a month into what might be considered summer (in the absence of more detailed information, we treat seasons as lasting about three months). Looking to previous years, we see similar intervals of low growth rates at about this same time of year, indicated in Figure 6D by bars labeled "M" or "M?" (depending on how clearly they stand out), alluding to our suggestion above that these intervals reflect musth periods. The duration of these periods ranges from about 6 increments in Year X-3 to about 16 increments in Year X-1, and although this last value seems high (relative to a maximum musth duration of about three months in African

38

elephants; Poole, 1996), low rates of apposition could in some cases continue beyond the musth interval itself into a "recovery period." When introduced above, considering only year-to-year comparisons, our interpretation of these intervals as musth episodes was admittedly speculative. However, with recognition of the last instance of this phenomenon as a preface to even lower rates of apposition, followed by death, this interpretation gains explanatory power.

Musth conflict between males is known to cause death in extant elephants (e.g., Buss, 1990) and has been interpreted as a cause of death in adult male Columbian mammoths (Fisher, 2004) and American mastodons (Fisher and Fox, 2007; Fisher, 2008). Zed's tusk does not show cementum defects like those that record musth battles in mastodons (Fisher, 2008), but with the more helical tusk geometry of mammoths, tusks might have been used less for "stabbing", and the peak stresses of tusk use may have been associated with rotation about the tusk axis rather than impingement of the proximal margin against the back of the tusk alveolus. We thus do not consider absence of cementum defects as evidence against musth battles.

We observe no damage on Zed's skeleton that is clearly perimortem, but there are multiple examples (healed rib fractures and vertebral damage) of injuries that occurred earlier in life and could have been sustained in musth battles. Without a clear record of perimortem skeletal damage, we suspect his death may have been caused by soft-tissue injuries. We suspect his final, nearly two-month interval of low tusk growth rate represents a period of decline during which he may have been capable of limited feeding and drinking, but from which he never managed to recover.

CONCLUSION

Zed's left tusk shows a pattern of variation in external topography and internal structure that corresponds closely to other proboscidean tusks that have been studied in even greater detail. Only our analysis of stable isotope values ($\delta^{18}O$ and $\delta^{13}C$) of structural carbonate of tusk dentin failed to reveal a periodic pattern that was independent of other variables. Accepting the largest-scale features of topographic and structural modulation as recurring on an annual basis, we have evidence of relatively steady and high tusk growth rates that suggest Zed was in good condition during most of the last decade of his life. Based on the association of first-order (annual) periradicular bands, microCT features, and patterns of variation in rate of dentin apposition in the last 4-5 years of life, death appears to have come in mid-summer, shortly after the start of a musth episode that was not sustained for the normal duration. Instead, it devolved quickly into an interval characterized by rates of dentin apposition as low as any observed in the last five years of life. This interval lasted for almost two months and ended with Zed's death. We suspect that this terminal interval was initiated by musth conflict, during which Zed sustained a serious soft-tissue injury. Following this injury, locomotion and feeding were probably difficult, but Zed would not have lasted as long as he did without some access to food and water.

Although our view of Zed's life covers only his last decade and offers interesting temporal resolution only for the last five years, it suggests that local weather conditions 37,000 years ago presented few extremes, with only low to moderate seasonality. In this environment, Columbian mammoths thrived to the degree that their sometimes tumultuous lives permitted. Zed's tusk record is important not only for the view it offers

40

of his life and times, but as a basis for comparison with mammoth life histories of other regions and times, especially closer to the last phases of mammoth history, just prior to extinction.

REFERNCES

Agenbroad, L.D. 1994. Taxonomy of North American *Mammuthus* and biometrics of the Hot Springs mammoths. In *The Hot Springs mammoth site: A decade of field and laboratory research in paleontology, geology, and paleoecology*, ed. L.D. Agenbroad and J.I. Mead, 158-207. Hot Springs: The Mammoth Site of Hot Springs, South Dakota.

Avery, J.K. 1988. *Oral development and histology*. Toronto: B.C. Decker, 380 pp.

Ayliffe LK, Chivas AR, Leakey MG. 1994. The retention of primary oxygen isotope composition of fossil elephant skeletal phosphate. *Geochimica et Cosmochimica Acta* 58:5291-5298.

Buss, I.O. 1990. *Elephant life: Fifteen years of high population density*. Ames: Iowa State University Press, 191 pp.

Coltrain, J.B., J.M. Harris, T.E. Cerling, J.R. Ehleringer, M.-D. Dearing, J. Ward, and J. Allen. 2004. Rancho La Brea stable isotope biogeochemistry and its implications for the palaeoecology of late Pleistocene, coastal southern California. *Palaeogeography, Palaeoclimatology, Palaeoecology* 205:199-219.

Dean, M.C. 1995. The nature and periodicity of incremental lines in primate dentine and their relationship to periradicular bands in OH 16 (*Homo habilis*). In *Aspects of dental biology: Paleontology, anthropology and evolution*, ed. J. Moggi-Cecchi, 239-265. Florence: International Institute for the Study of Man.

Dean, M.C. and A.E. Scandrett. 1996. The relation between long-period incremental markings in dentine and daily cross-striations in enamel in human teeth. *Archives of Oral Biology* 41:233-241.

Falconer, H. 1857. On the species of mastodon and elephant occurring in the fossil state in Great Britain. Part 1. *Mastodon. Quarterly Journal of the Geological Society of London* 13:307-360.

Feranec, R.S., E.A. Hadly, and A. Paytan. 2009. Stable isotopes reveal seasonal competition for resources between late Pleistocene bison (*Bison*) and horse (*Equus*) from Rancho La Brea, southern California. *Palaeogeography, Palaeoclimatology, Palaeoecology* 271:153-160.

Fisher, D.C. 1984. Taphonomic analysis of late Pleistocene mastodon occurrences: evidence of butchery by North American Paleo-Indians. *Paleobiology* 10:338-357.

Fisher, D.C. 1987. Mastodont procurement by Paleoindians of the Great Lakes region: Hunting or scavenging? In *The evolution of human hunting*, ed. M.H. Nitecki and D.V. Nitecki, 309-421. New York: Plenum Press.

Fisher, D.C. 1996. Extinction of proboscideans in North America. In *The Proboscidea: Evolution and palaeoecology of elephants and their relatives*, ed. J. Shoshani and P. Tassy, 296-315. Oxford: Oxford University Press.

Fisher, D.C. 2001. Season of death, growth rates, and life history of North American mammoths. In *Proceedings of the First International Conference on Mammoth Site Studies*, ed. D. West. Publications in Anthropology 22, 121-135.

Fisher, D.C. 2004. Season of musth and musth-related mortality in Pleistocene mammoths. *Journal of Vertebrate Paleontology* 24(Suppl. to 3):58A.

Fisher, D.C. 2007. Life history analysis of the Yukagir mammoth. In *The Yukagir*

mammoth, ed. G.G. Boeskorov, A.N. Tikhonov, and N. Suzuki, 142-156. St. Petersburg: Institute of Applied Ecology of the North [Yakutsk].

Fisher, D.C. 2008. Taphonomy and paleobiology of the Hyde Park mastodon. In *Mastodon paleobiology, taphonomy, and paleoenvironment in the late Pleistocene of New York state: studies on the Hyde Park, Chemung, and North Java sites*, ed. W. Allmon and P. Nestor. Palaeontographica Americana 61, 197-290.

Fisher, D.C., S. Beld, and A. Rountrey. 2008. Tusk record of the North Java mastodon. In *Mastodon paleobiology, taphonomy, and paleoenvironment in the late Pleistocene of New York state: studies on the Hyde Park, Chemung, and North Java sites*, ed. W. Allmon and P. Nestor. Palaeontographica Americana 61, 417-463.

Fisher, D.C., M.D. Cherney, C. Newton, A.N. Rountrey, Z.T. Calamari, R.K. Stuckey, C. Lucking, and L. Petrie. In review. Taxonomy and tusk growth analyses of Ziegler Reservoir proboscideans. *Quaternary Research*.

Fisher, D.C., and D.L. Fox. 2003. Season of death and terminal growth histories of Hiscock mastodons. In *The Hiscock Site: late Pleistocene and Holocene paleoecology and archaeology of western New York State*, ed. R. Laub, N. Miller, and D. Steadman. Bulletin of the Buffalo Society of Natural History, 37, 83-101.

Fisher, D.C., and D.L. Fox. 2007. Life history and unilateral loss of molar function in the Cohoes Mastodon: A case study in nutritional stress? *Journal of Vertebrate Paleontology* 27 (Suppl. to 3):74A-75A.

Fox, D.L. 2000. Growth increments in *Gomphotherium* tusks and implications for late Miocene climate change in North America. *Palaeogeography, Palaeoclimatology, Palaeoecology* 156:327-348.

Fuller, B., S. Fahrni, J. Harris, A. Farrell, J. Coltrain, L. Gerhart, J. Ward, R.E. Taylor, and J. Southon. In press. Ultrafiltration for asphalt removal from bone collagen for radiocarbon dating and isotopic analysis of Pleistocene fauna at the tar pits of Rancho La Brea, Los Angeles, California. *Quaternary Geochronology*.

Graham, R. 1986. Appendix 2. Part 2. Descriptions of the dentitions and stylohyoids of Mammuthus columbi from the Colby site. In *The Colby mammoth site: Taphonomy and archaeology of a Clovis kill in northern Wyoming*, ed. G.C. Frison and L.C. Todd, 171-90. Albuquerque: University of New Mexico Press.

Harris, J., A. Farrell, G. Takeuchi, S. Cox, and C. Howard. 2013. *Ex* Rancho La Brea" *Semper Aliquid Novum. Journal of Vertebrate Paleontology* 33:139A.

Heusser, L.E. 1998. Direct correlation of millennial-scale changes in western North America vegetation and climate with changes in the California Current system over the past ~60 kyr. *Paleoceanography* 13:252-262.

Keiss, R.E. 1969. Comparison of eruption-wear patterns and cementum annuli as age criteria in elk. *Journal of Wildlife Management* 33:175-180.

Koch, P.L., D.C. Fisher, and D. Dettman. 1989. Oxygen isotope variation in the tusks of extinct proboscideans: a measure of season of death and seasonality. *Geology* 17:515-519.

Koch, P.L., M.L. Fogel, and N. Tuross. 1994. Tracing the diets of fossil animals using stable isotopes. In *Stable isotopes in ecology and environmental science*, ed. K. Lajtha and R. H. Michener, 63-92. Oxford: Blackwell Scientific Publications.

Koch, P.L., N. Tuross, and M.L. Fogel. 1997. The effects of sample treatment and diagenesis on the isotopic integrity of carbonate in biogenic hydroxylapatite. *Journal of Archaeological Science* 24:417-29.

Komai, S. and T. Miyauti. 1938. Über die Parallelsteifen der Zahnwurzel ('Striae periradicales'). *Deutsche Zahn-, Mund- und Kieferheilkunde* 5:791-795.

Laws, R.M. 1952. A new method of age determination for mammals. *Nature* 169:972-973.

Laws, R.M. 1966. Age criteria for the African elephant, *Loxodonta a. africana*. *African Journal of Ecology* 4:1-37.

Lister, A.M. and L.D. Agenbroad. 1994. Gender determination of the Hot Springs mammoths. In *The Hot Springs mammoth site: A decade of field and laboratory research in paleontology, geology, and paleoecology*, ed. L.D. Agenbroad and J.I. Mead, 208-214. Hot Springs: The Mammoth Site of Hot Springs, South Dakota.

Minnich, R.A. 2007. Climate, paleoclimate, and paleovegetation. *Terrestrial vegetation of California* 3:43-70.

Osborn, H. F. 1936. *Proboscidea*. New York: The American Museum of Natural History.

Poole, J. 1996. The African elephant. In *Studying elephants*, ed. K. Kangwana, 1-8. African Wildlife Foundation.

Poole, J.H., and C.J. Moss. 1981. Musth in the African elephant, *Loxodonta africana*. *Nature*. 292:830–831.

Rasband, W.S. 1997. *ImageJ*. Bethesda, Maryland: US National Institutes of Health.

Rinaldi, C. and T.M. Cole. 2004. Environmental seasonality and incremental growth rates of beaver (*Castor canadensis*) incisors: implications for palaeobiology. *Palaeogeography, Palaeoclimatology, Palaeoecology* 206:289-301.

Rountrey, A.N. 2009. Life histories of juvenile woolly mammoths from Siberia: Stable isotope and elemental analyses of tooth dentin. Unpublished dissertation, University of Michigan, xiii+331 pp.

Rountrey, A.N., D.C. Fisher, A.N. Tikhonov, P.A. Kosintsev, P.A. Lazarev, G. Boeskorov, and B. Buigues. 2012. Early tooth development, gestation, and season of birth in mammoths. *Quaternary International* 255:196-205.

Saunders, J.J. 1970. The distribution and taxonomy of *Mammuthus* in Arizona. Unpublished M.S. thesis, University of Arizona, xi+115 pp.

Scheffer, V.B. 1950. Growth layers on the teeth of Pinnipedia as an indication of age. *Science* 112 (2907): 309-311.

Smith, K.M., and D.C. Fisher. 2011. Sexual dimorphism of structures showing indeterminate growth: tusks of American mastodons (*Mammut americanum*). *Paleobiology* 37:175-194.

Smith, K.M., and D.C. Fisher. 2013. Sexual dimorphism and inter-generic variation in proboscidean tusks: multivariate assessment of American mastodons (*Mammut americanum*) and extant African elephants. *Journal of Mammalian Evolution* 20:337-355.

Smith, T.M. and D.J. Reid. 2009. Temporal nature of periradicular bands ('striae periradicales') on mammalian tooth roots. In *Comparative Dental Morphology,* volume 13 eds. T. Koppe, G. Meyer, and K.W. Alt, 86-92. Basel:Karger.

Spaulding, W.G. 1990. Vegetational and climatic development of the Mojave Desert: the

last glacial maximum to the present. In *Packrat middens: the last 40,000 Years of Biotic Change* eds. J.L. Betancourt, T.R. Van Devender, and P.S. Martin, 166-199. Tucson: University of Arizona Press.

Table 2.1. Measurements of periradicular bands on Zed's left tusk. Bands are labeled backward in time, from the incomplete Year X, located at the proximal margin.

Distal Margin of Year	Distance to Proximal End (cm)	Extensional Length (cm) – of Year
X-10	54.7	
X-9	48.5	6.2 – X-10
X-8	43.4	5.1 – X-9
X-7	37.5	5.9 – X-8
X-6	32.6	4.9 – X-7
X-5	26.8	5.8 – X-6
X-4	21.6	5.2 – X-5
X-3	13.7	7.9 – X-4
X-2	9.2	4.5 – X-3
X-1	4.6	4.6 – X-2
X	0.6	4.0 – X-1
	0	0.6 – X (inc.)

Table 2.2. Molar measurements for Zed. Abbreviations: in mand., tooth in mandible, measurement not accessible; >, specimen incomplete or obscured by associated bone; @, loph number at which width is greatest.

Tooth	RM3	LM3	Rm3	Lm3
Occlusal length (cm)	25.8	27.0	23.7	23.4
Number of lophs	>14	16	>15	>15
Lophs/occlusal surface	9	10	10	10.5
Maximum width (cm)	12.0 @ 5	12.3 @ 5	12.0 @ 5	12.3 @ 5
Crown height (cm)	>25	>25	[in mand.]	[in mand.]
Lamellar frequency	3.5	3.7	4.0	4.0
Enamel thickness (mm)	3.0	3.0	3.5	3.7

Table 2.3. Measured isotope values for $\delta^{13}C$ (relative to VPDB) and $\delta^{18}O$ (relative to VSMOW) for hydroxylapatite in dentin. Distance is measured from the pulp cavity to the center of the sampling site. PC = pulp cavity.

Sample	$\delta^{13}C$	$\delta^{18}O$	Distance (mm)
PC	0.65	27.49	-0.35
PC-1	4.35	27.00	-1.05
PC-2	5.72	26.45	-1.75
PC-3	5.58	27.18	-2.45
PC-4	4.92	26.91	-3.15
PC-5	6.59	26.52	-3.85
PC-6	7.56	26.52	-4.55
PC-7	7.69	26.99	-5.25
PC-8	6.87	26.44	-5.95
PC-9	7.14	26.63	-6.65
PC-10	6.69	27.20	-7.35
PC-11	6.45	27.00	-8.05
PC-12	6.31	26.37	-8.75
PC-13	6.21	26.37	-9.45
PC-14	7.08	25.72	-10.15
PC-15	8.64	26.45	-10.85
PC-16	8.69	26.70	-11.55
PC-17	8.49	26.57	-12.25
PC-18	7.68	26.87	-12.95
PC-19	6.66	26.82	-13.65
PC-20	5.14	26.56	-14.35
PC-21	6.60	26.54	-15.05
PC-22	4.09	26.79	-15.75
PC-23	6.92	27.08	-16.45
PC-24	7.96	26.49	-17.15
PC-25	8.58	26.50	-17.85
PC-26	7.85	27.06	-18.55
PC-27	6.52	27.05	-19.25
PC-28	6.47	26.79	-19.95
PC-29	3.18	27.27	-20.65

Figure 2.1. Zed's left tusk, with proximal end in foreground (distal end in background), showing location of sample block used for microCT analysis, thin section production (for increment thickness analysis), and stable isotope sampling. White arrows mark boundaries of the last eight periradicular bands on the external surface. Breakage of the proximal margin has removed all but a small fragment of the extensional increment for the partial year (Year X, black font) that terminates the tusk record. The previous eight years of tusk extension are labelled (white font) within their respective periradicular bands. Scale bar is 10 cm.
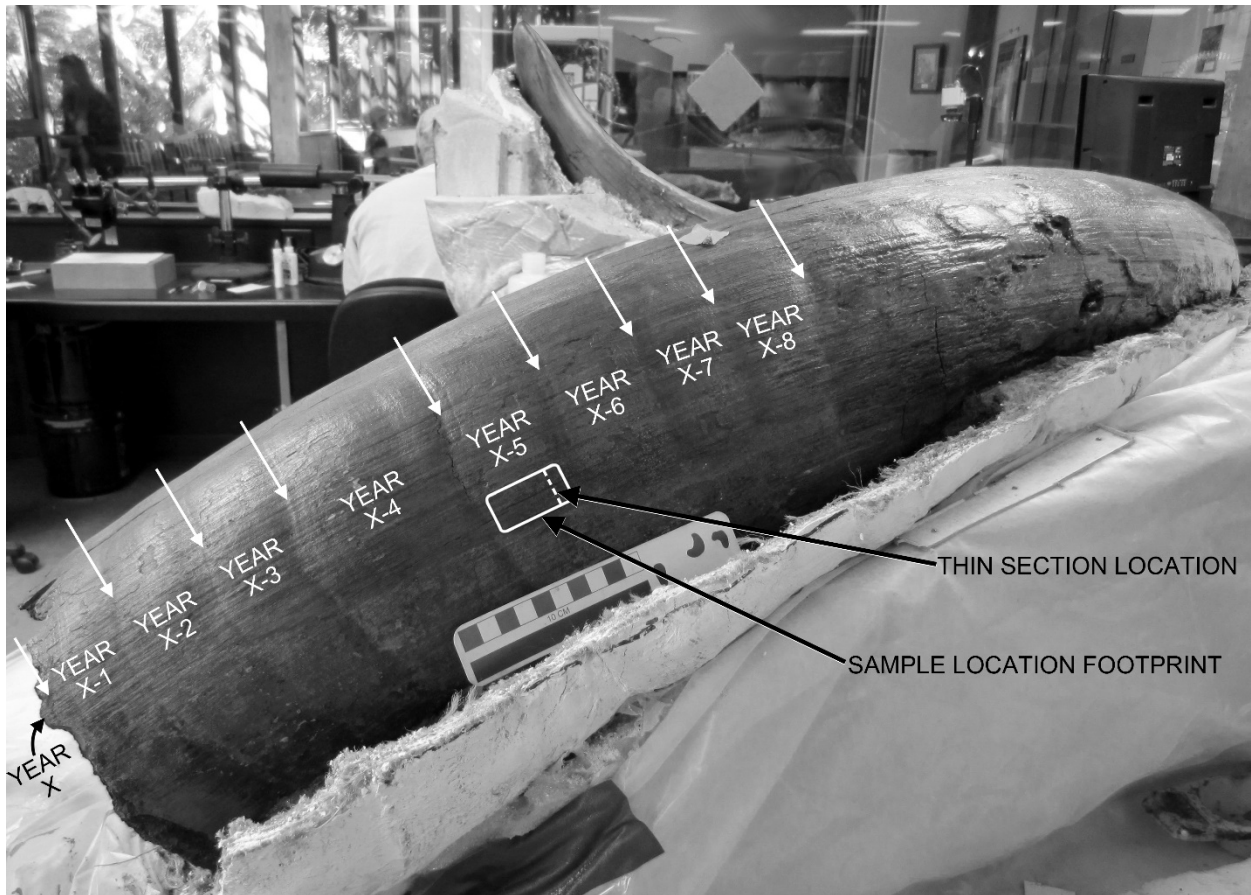
Figure 2.2. Occlusal view of Zed's mandible, showing left and right lower m3s.
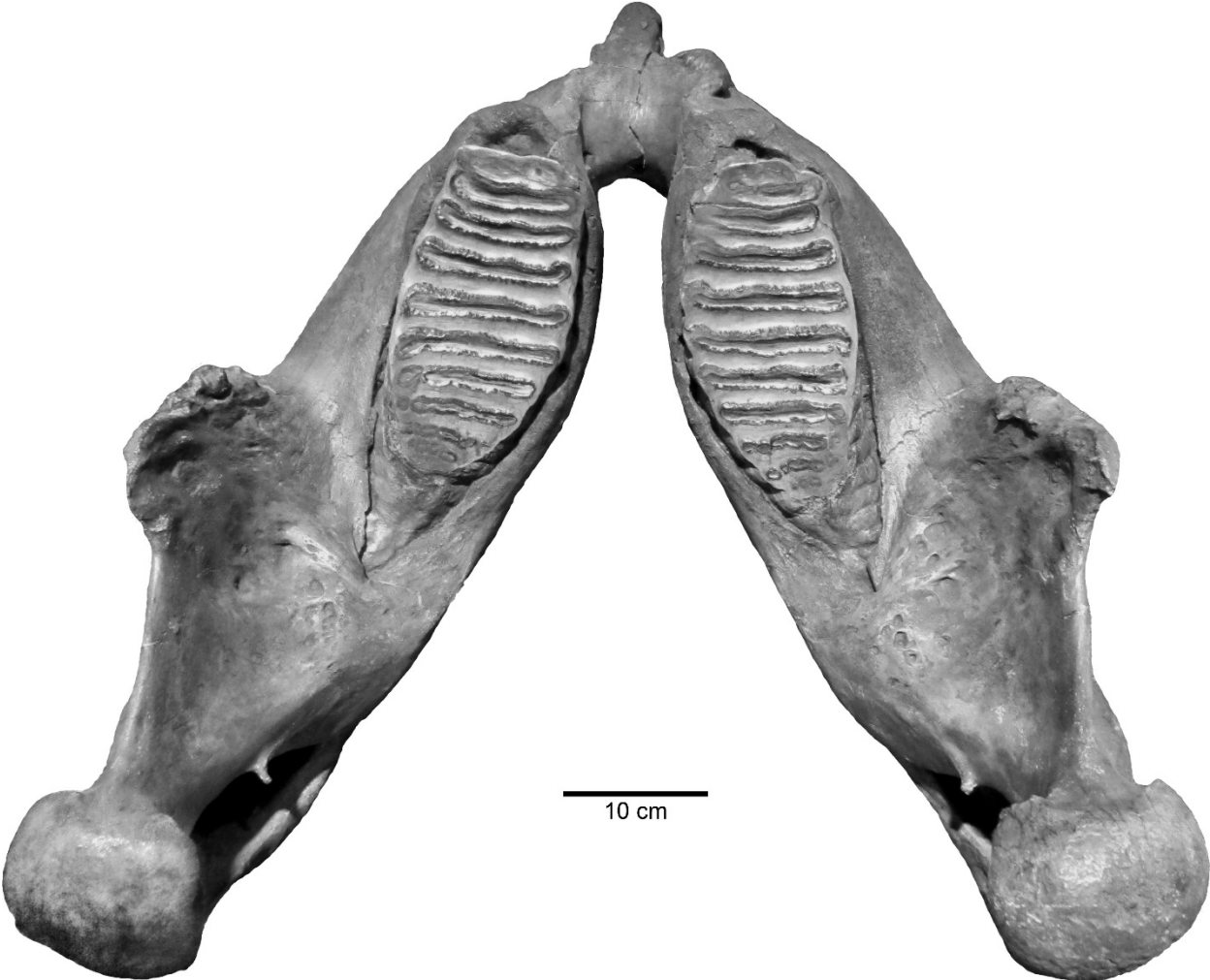
Figure 2.3. A, microCT image of a virtual transverse section of tusk cementum (brighter zone near upper, outer surface) and dentin (generally darker) extending from the dentin-cementum interface (large black arrow along right margin) to the surface of the pulp cavity (lower border of section). Smaller white arrows mark locations where there is an abrupt change (moving in the direction of apposition) from dentin with higher x-ray attenuation (brighter) to dentin with lower attenuation (darker). We hypothesize that these transitions mark approximate winter-spring boundaries. Annual increments of dentin apposition are labelled along the right margin, between white arrows, and correspond to years labelled in Figure 1. The bright circle in the upper part of the image is a ring artifact from the CT scan. B, photograph of a region (indicated in A by a black dashed rectangle) of the transverse thin section of tusk dentin showing weekly, and some daily, increments; numbers mark second-order increments included in the profile of variation in second-order increment thickness.

51
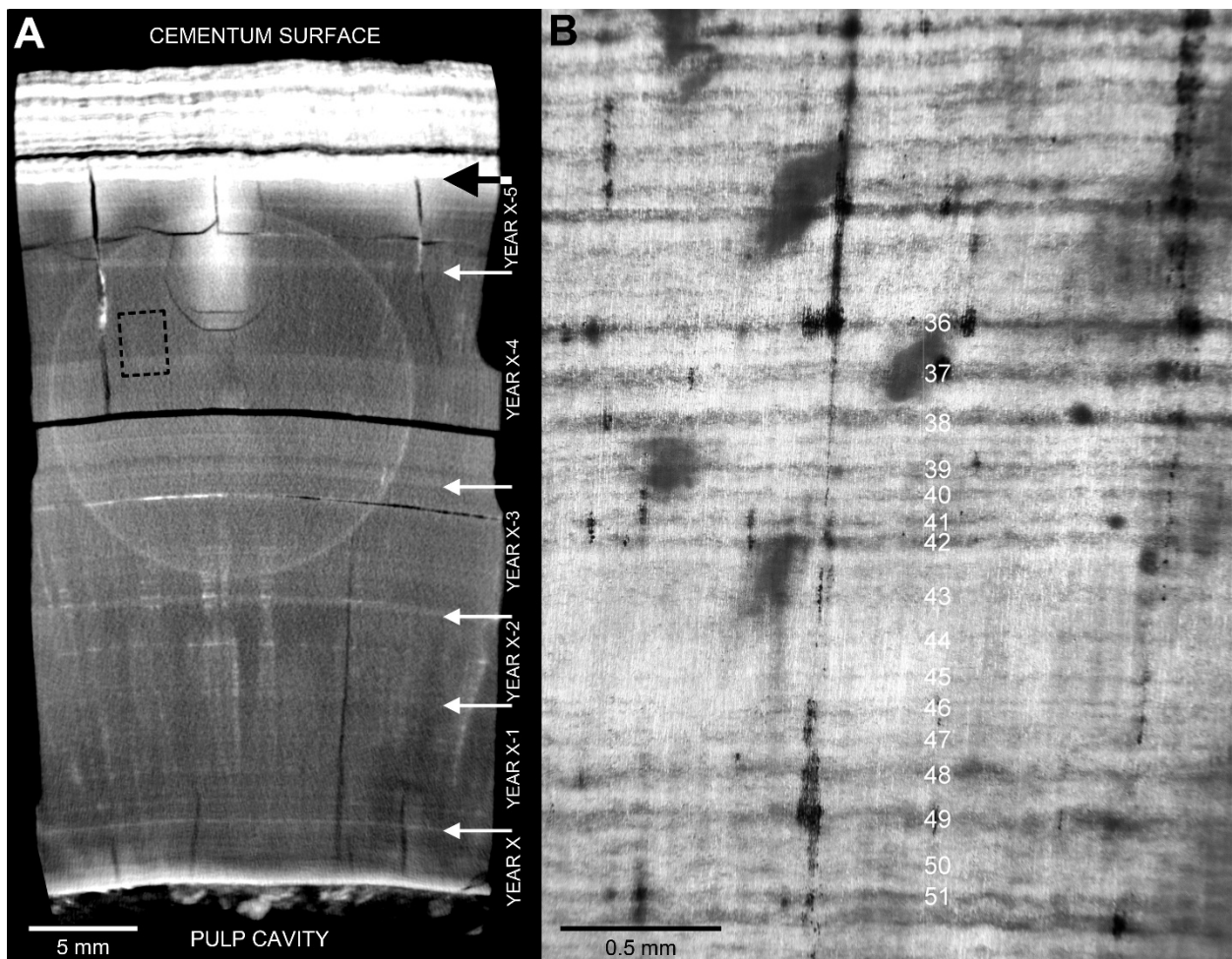
Figure 2.4. Sample slab used for stable isotope analysis. Internal fractures allowed several fragments to separate from the upper part of the slab (including most of the cementum layer; cementum-dentin interface indicated by white arrow) during polishing of this surface. A, black curved lines parallel to pulp cavity surface (lower border of sample slab) represent boundaries between planned serial samples to be collected along paths following second-order dentin increments. B, slab after milling, showing consistency of planned and implemented serial sampling.
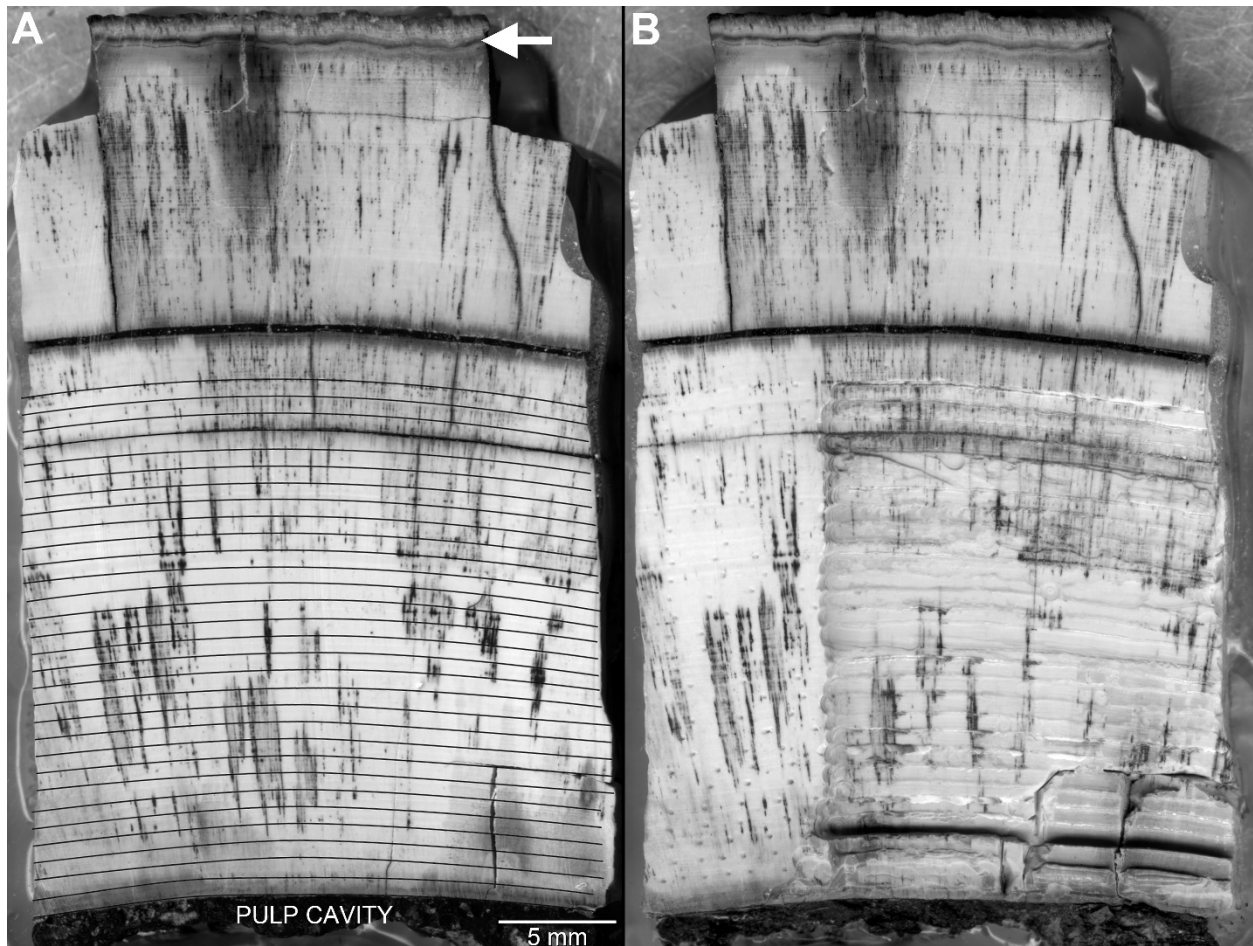
Figure 2.5. Graph showing extensional length of first-order periradicular bands between the gingival margin and the proximal margin of the tusk (data in Table 2.1.). Years are numbered as in Figure 1, with Year X excluded because it is incomplete.
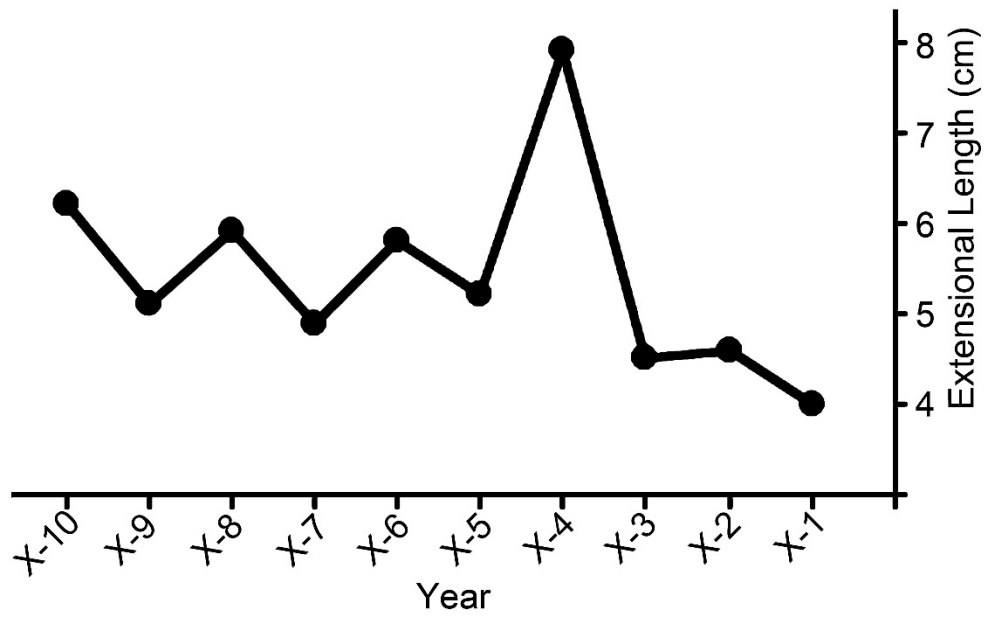
Figure 2.6. Results of tusk analysis. A, results of serial isotope analysis showing changes in $\delta^{13}C$ and $\delta^{18}O$ values through the last years of life. B, luminance values measured along a transect normal to appositional surface, acquired from a virtual section (microCT data) of the same years shown in A (this curve is truncated just before the high-luminance zone adjacent to the pulp surface). C, positions of density features observed in microCT images (symbolized by rectangles with left-to-right, white-to-black transitions). D, profile showing variation in thickness of weekly (second-order) appositional increments (increment numbers labelled for notably thick or thin increments). Continuous gray curve shows five-point moving average. Bracketed intervals labeled "M" or "M?" denote probable or possible musth episodes marked by low rates of dentin apposition during summer months. Vertical dotted lines represent hypothesized winter-spring boundaries demarcating years (labeled in C, matching labels in Figures 2.1. and 2.3.).
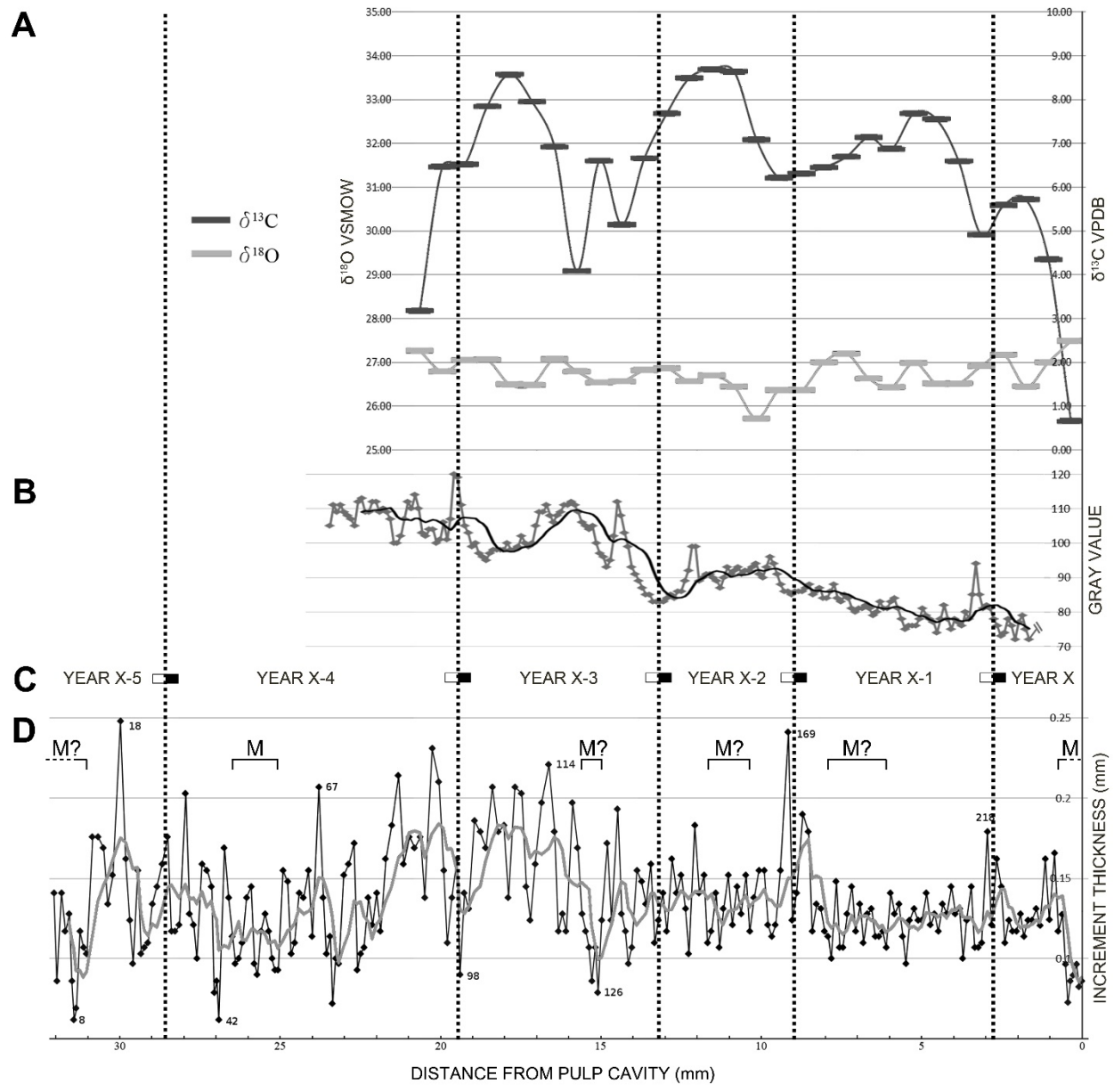
CHAPTER 3

First analysis of life history and season of death of a South American

gomphothere[2]

ABSTRACT

Excavations associated with wastewater treatment facilities in the Santiago Basin of

Chile uncovered remains of an adult male *Stegomastodon platensis* in Pleistocene

fluvial sediments. The specimen included a skull with both tusks still in their alveoli. A

small sample block of dentin and cementum was excised from the right tusk for analysis

of compositional and structural variation recorded in the sequence of dentin layers. The

sample was analyzed using serial isotope assays, microCT, and measurement of dentin

increments in thin-sections. These procedures allowed us to recover life history

information relating to the final four years of life. Analyses show seasonal variation in

composition, density, and growth rate, permitting identification of years. MicroCT

features appear to recur semiannually, which has not been observed previously in

proboscidean tusks; these features are interpreted to correspond to the winter-spring

boundary and some other aspect of environment or behavior recurring within each year.

Average annual apposition of dentin within the tusk is 10.4 mm for complete years

studied, suggesting that this individual was relatively healthy leading up to the final year

[2] El Adli, J.J., Fisher, D.C., Cherney, M.D., Labarca, R., Lacombat, F., 2017. First analysis of life history and season
of death of a South American gomphothere. Quaternary International.

of life. Recurrent periods of low rate of apposition measured in weekly dentin increments that formed during the summer are interpreted as representing periods of musth. Using the location of microCT features, annual appositional thickness, and the pattern of weekly growth within the final year of life, we interpret the season of death for this individual as being within the early autumn.

INTRODUCTION

Construction and mass grading in 2011 associated with a new wastewater treatment facility for the city of Santiago, Chile, exposed late Pleistocene to Holocene deposits containing fossil remains. This site (El Trebal 1) sits within the Santiago Basin and preserves alluvial, fluvial, and lacustrine deposits associated with the Maipo and Mapocho Rivers (Varela, 1991). The excavation site, located in the southwestern portion of the basin, lies within the watershed of the Mapocho River and contained sequences of sandy and conglomeratic layers that were interpreted as fluvial. The partial skull and tusks of a large gomphotheriid were discovered within the lower-most channel fill deposits of the excavation (ET1-10). Labarca et al. (2016) identified these remains as belonging to a male *Stegomastodon platensis* Ameghino, 1888. The assignment of this specimen to *Stegomastodon* rather than *Notiomastodon* may be controversial (see Mothé and Avilla, 2015), but discussions of taxonomy are beyond the scope of this paper. For consistency with the report of Labarca et al. (2016) we provisionally retain their species assignment of this specimen.

Due to degradation of collagen within the specimen (nicknamed "Marito"), an absolute age via radiocarbon dating could not be obtained (Labarca et al., 2016).

57

However, other gomphothere remains within the region have returned end-Pleistocene

ages, supporting the inferred geologic age of the unit in which Marito was found (Núñez

et al., 1994). The skull contains both upper M2s and M3s in different degrees of wear.

Both M2s are displaced medially with their anterior portions rotated toward the midline

(Fig. 1). The stage of molar wear and replacement observed in the specimen suggests

that this individual was an adult of reproductive age. The right tusk of the specimen

measures approximately 1.2 m in length (from the tip of the tusk to the alveolar margin)

with a greatest diameter of 19 cm at the alveolar margin (Labarca et al., 2016). Sexual

dimorphism was reported within skeletal elements of both trilophodont and

tetralophodont gomphotheres, as well as mammutids and elephantids (Madden, 1986;

Lister, 1996; Tassy, 1996; Smith and Fisher, 2011, 2013). Although not all of these

studies reported dimorphism specifically within tusks, Smith and Fisher (2013) found

that both *Mammut* and *Loxodonta* are relatively conservative in the aspects of tusk

morphology that display dimorphism (e.g., alveolar circumference). Due to this stability

in aspects of tusk dimorphism between disparate taxa, it seems most parsimonious,

from a phylogenetic perspective (Witmer, 1995), to expect similar sexual dimorphism in

Stegomastodon. Therefore, based on the diameter of the tusks relative to other

specimens of *Stegomastodon platensis* in South America (see Labarca et al., 2016),

Marito is inferred to be male.

The continuously growing tusks of gomphotheriids and other proboscideans

record an extended history of growth, which can be used to interpret life history. This

can be observed and interpreted via variation within first-order (annual), second-order

(weekly, containing seven third-order increments, or fortnightly, containing fourteen

third-order increments), and third-order (daily) growth increments observable within the dentin of tusks (Fisher, 2001). Within this paradigm, sets of lower-order increments have been shown to occur within increments of higher-order, but it is uncommon to observe all three orders continuously throughout a dentin sequence during any single analysis. Therefore, a series of analyses including microCT, thin section, and serial isotope sampling is often required to fully interpret growth history.

Due to the periodic nature of growth increments, increment thickness can be used to assess growth rates (e.g., thinner increments attributed to a given interval of time imply slower growth), which we in turn suggest may be related to an individual's nutritional status and health (i.e., thinner increments reflect poorer conditions for growth; Fisher, 1996). Comparing variations in appositional rates of dentin (i.e., changes in increment thickness) between growth layers with compositional and density changes, we can extract life history information and determine season of death for an individual. Specifically, thicker second- and third-order increments (marking more rapid apposition) would be expected in times of resource abundance and are typically associated with dentin showing oxygen isotope values characteristic of summer precipitation, whereas thinner increments that might indicate resource limitation are associated with oxygen isotope values expected for winter precipitation (e.g., Koch et al., 1989; Fisher and Fox, 2007). The causal basis for CT features is less clear, but we often see an abrupt transition to less dense dentin near the winter-spring boundary (Fisher et al., 2014; El Adli et al., 2015). Documenting such patterns over several years establishes a template on which smaller-scale features may appear. For example, in mature males, intervals of thin second-order increments in late spring or early summer have been interpreted as a

signature of musth, when mature male proboscideans tend to devote much of their attention to mating and to aggressive encounters with rival males (Poole, 1987). Although this time of year is not when thin second-order dentin increments would be expected based on available food, musth behavior is also associated with fasting, and in mammoths, its seasonality is offset from the season of calf birth by an interval matching the estimated gestation period. Such analyses have been conducted for both North American and Asian fossil proboscidean taxa, including *Mammut americanum*, *Mammuthus primigenius*, *Mammuthus columbi*, and *Gomphotherium* spp*. (Fisher, 1987, 1988, 1996, 2001; Fox, 2000; Rountrey et al., 2007; El Adli et al., 2015), but South American proboscideans are not yet similarly studied. Therefore, we present here the first analysis of life history and season of death for a South American gomphotheriid.

MATERIALS AND METHODS

Sample Block

A rectangular sample block measuring approximately 5 cm long and 3.5 cm wide was removed from the proximal end of the right tusk using a hand-held drill and a carbide bit. The sample extends from the outer cementum surface through a nearly continuous sequence of dentin to the pulp cavity surface. Due to delamination along growth layers within the tusk dentin, the sample was removed in four pieces. Three of these pieces could be refit unambiguously due to irregularities produced when the propagating fracture surface was deflected away from the appositional surface on which it began. However, the dentin fragment containing the pulp cavity surface could not be precisely placed because the fracture separating it from the rest of the dentin sequence

followed a single surface of apposition. Thus, the position of this piece had to be approximated. All pieces were reattached using quick-setting epoxy before conducting analyses.

The external surface of the tusk sample was relatively well preserved, with few surficial fractures. In transverse cross-section, the sample block is approximately 5 cm in appositional thickness with a 2 to 3 mm-thick layer of cementum. Unlike the relatively pristine outer surface of the sample, the dentin within the tusk was white and chalky in texture, in stark contrast to the more solid, and cream-colored dentin in fresh tusk material. This difference in color and texture is likely due to deterioration of the collagenous matrix during diagenesis. However, despite this apparent alteration, the dentin appeared to be structurally sound throughout most of its thickness, which allowed microCT, thin section, and isotopic analyses to proceed without undue difficulty.

MicroCT

The specimen was microCT-scanned at the University of Michigan with a SCANCO Medical μCT100 operating at 90kV, 78μA, and 500 ms, yielding uniform cubic voxels 60 μm per side. Amira 5.4.1 was used to visualize variations in X-ray attenuation within the tusk.

Thin Section

Two adjacent 7 mm-thick transverse sample blocks were cut from the specimen for use in analyses of microscopic growth increments. The slabs were cut perpendicular to the inclined surface of the pulp cavity using a diamond wafering blade on a Buehler

61

Isomet saw. The blade was lubricated with ethanol during cutting to avoid problems associated with water or oil as lubricants. The hygroscopic nature of the collagen in dentin drives increases in volume following hydration, leading to fractures, and oil permeates the dentin, compromising adhesion to the slide.

A thin section was made from one of the transverse sample blocks, utilizing the face of the block that was adjacent to the other sample block to maximize comparability between the two. The thin section was studied with a Leitz petrographic microscope at 40x magnification. Photomicrographs were taken under plane-polarized light from the available dentin sequence along a single transect of appositional growth. Kerosene was placed on the slide to enhance the visibility of growth increments. The IncMeas 1.3c plug-in (Rountrey, 2009) for ImageJ (Rasband, 1997) was used to measure second-order increment thicknesses from photomicrographs.

Isotope Analysis

The second sample block was used to collect a series of samples for measuring changes in stable isotope composition within the dentin during the last years of life. High-resolution images (acquired with a flatbed scanner) of the polished sample surface were aligned with a virtual section from the microCT scan. These were used to trace growth lines (mostly second-order features), creating mill paths to sample dentin that formed only within narrowly constrained intervals of time. These mill paths were then transferred to the slab surface where powdered dentin was collected using a carbide bit and a manual drilling stage under a stereomicroscope. In this way, we collected 24 samples of approximately equal thickness (0.7 mm) and depth (approximately 2 mm)

from approximately 2.5 cm-long mill paths.

Dentin powder samples were pretreated for isotopic analysis of structural carbonate following the methods described in Koch et al. (1997) and Rountrey (2009) (also see Crowley and Wheatley, 2014). Approximately 6.0 mg of each sample powder was vortexed in 0.5 ml of 30% H_2O_2 and then left for twenty-four hours in a closed fume hood. The samples were then rinsed in 1.0 ml of ultrapure water before being vortexed and then centrifuged for five minutes at 6,000 rpm. This rinse process was repeated five times with the supernatant being removed after each wash. Rinsed samples were vortexed in 0.5 ml of a 1 M calcium acetate buffered acetic acid solution, which was then left in a closed fume hood for a further twenty-four hours. Samples were then rinsed five more times with ultrapure water, as described above. Following the final rinse, the samples were freeze-dried overnight to remove all water. Once pretreatment was complete, a microbalance was used to load 0.75 mg of each sample into sample boats. Samples were then analyzed for carbon and oxygen isotope ratios using a Thermo Finnigan GasBench II coupled to the inlet of a Thermo Finnigan Delta V+ mass spectrometer. Isotope ratios were normalized to international standard NBS-19. All isotope values are reported in delta notation ($\delta = (\frac{R_{sample}}{R_{standard}} - 1) \times 1000$) with $\delta^{13}C$ values reported relative to Vienna Pee Dee Formation Belemnite (VPDB) and $\delta^{18}O$ values reported relative to Vienna Standard Mean Ocean Water (VSMOW).

RESULTS

MicroCT

X-ray computed microtomography (microCT) permitted us to visualize changes in

X-ray attenuation within tusk dentin (Fig. 2). In virtual section, the dentin-cementum junction appears as a rapid transition from higher attenuation values within the cementum to lower values within the dentin near the outside of the tusk. This outermost dentin, however (i.e., most of what we identify as year X-4 in Fig. 2A), appears to be poorly preserved and does not show the clearly zonal organization of subsequently formed dentin. In most of the rest of the dentin sequence, relatively regularly spaced variations in X-ray attenuation occur, forming clear zones that parallel the surface of apposition. With some variation, the dominant pattern is a succession of narrow (ca. 1 mm-thick) zones of low X-ray attenuation (low mineralization) followed by broader (ca. 5 mm-thick) zones of higher attenuation (high mineralization) after which the pattern repeats. Most of these major changes in attenuation are abrupt. Within the interval we identify as years X-3 to X (Fig. 2A), this pattern recurs eight times, with cycles having an average appositional thickness of 5.2 mm.

Adjacent to the pulp cavity is a zone of notably higher X-ray attenuation suggestive of enhanced mineralization, possibly caused by interaction with groundwater moving through porous sediment occupying the pulp cavity. This feature appears to be superimposed on the regular alternation of zones of contrasting density in most of the rest of the dentin sequence.

Thin Section

Our thin section was positioned to assess the same slice of dentin observed by microCT. Throughout most of the dentin sequence, it displays distinct banding of paired light and dark features that parallel the orientation of the pulp cavity surface. These

features are somewhat variable in thickness and occur over a range of 0.10 mm to 0.39 mm in appositional thickness. Although not consistently visible, finer and fainter bands of light and dark dentin were observed nested within some of the thicker light-dark couplets. These finer and fainter couplets, when measureable, were found to be on the order of tens of microns in thickness and were observed to occur in groups of seven per thicker light-dark couplet. The scale and hierarchical nature of these couplets match features described by Fisher (1987) as second- and third-order growth increments. Within this paradigm, the finer and fainter bands are the third-order increments (representing daily dentin apposition) and the thicker and higher-contrast bands are the second-order increments (representing approximately weekly dentin apposition). The number of third-order increments observed per second-order increment is the same as what was documented by Fox (2000) in tusks of *Gomphotherium*. This apparent weekly periodicity of second-order increments in gomphotheriids (as well as in *Mammuthus*) differs from the fortnightly second-order increments observed in *Mammut* (Fisher, 1987).

Thicknesses of second-order increments were measurable from approximately 1.5 cm below the dentin-cementum junction through to the pulp cavity. Delamination of dentin near the pulp cavity during extraction of the tusk sample (see Section 2) could have resulted in a loss of some material from the dentin sequence. We therefore regard the material observed in thin section as representing two continuous series of tusk material separated by a gap of missing dentin of unknown thickness. Although this gap seemed initially to be problematic, comparison of the pattern of change in increment thicknesses within and between the adjacent blocks (discussed below) may yet help

65

resolve whether material was in fact lost, and if so, how much.

Appositional thicknesses of second-order increments measured from the thin section were on average 0.23 mm with a range of 0.28 mm. In appositional order, these increments showed repeated variation from low to high and back to low growth rates over an average interval of 48 increments (Fig. 3). This roughly sinusoidal pattern of change in increment thickness recurs four times within the dentin sequence, with two complete cycles located in the middle portion of the dentin sequence and two incomplete cycles (one closer to the dentin-cementum junction and the other adjacent to the pulp cavity) of growth observed (Fig. 3C).

Isotope Analysis

Twenty-four serial samples were analyzed for oxygen and carbon isotopes within the structural carbonate in tusk dentin. These samples were collected from the same sequence of dentin as the last two cycles (near the pulp cavity) of low to high and back to low growth rate observed in second-order increments and the last four cycles of X-ray attenuation observed by microCT. The $\delta^{18}O$ values measured from the tusk show a cycle of variation over an interval of approximately 12 samples, with an amplitude of ca. 2‰ and an average value of 21.7‰ VSMOW (Table 1; Fig. 3). This average value is in line with $\delta^{18}O$ values recovered from enamel, dentin, and bone of other Pleistocene gomphotheriids from Chile (see Sánchez et al., 2004: table 1). Carbon values from the tusk also show an undulating pattern, but fluctuations have an amplitude of only ca. 1‰ around an average of -9.7‰ VPDB. The periodicity of changes in $\delta^{18}O$ values spans a similar thickness of dentin to that presenting a single cycle of change in second-order

66

increment thickness and two consecutive cycles of change in X-ray attenuation, but the

$\delta^{13}C$ record is less clearly cyclic. Nonetheless, the concordance between patterns of

variation in increment thicknesses and $\delta^{18}O$ values suggests that these features reflect

a fundamental cycle of change, probably equivalent to one year. This implies that the

cycle of change in X-ray attenuation is roughly semiannual, but this seems easier to

accept than a pattern of biennial change in rate of dentin apposition and $\delta^{18}O$ values.

Records of both $\delta^{18}O$ and $\delta^{13}C$ show unusually high values at the beginning of

our run of serial samples (farthest from the pulp cavity) – approximately 3.8‰ more

positive for $\delta^{18}O$ and 6.6‰ for $\delta^{13}C$ than values for the adjacent sample. The sample

that produced these extreme values was collected immediately adjacent to a

postmortem fracture that may have allowed groundwater penetration and subsequent

diagenetic alteration. Near the pulp cavity, $\delta^{13}C$ values rapidly increase by

approximately 3.5‰ over the span of three consecutive samples. The proximity of these

sample locations to the surface of the pulp cavity may have permitted alteration of

carbon values within this zone. Values of $\delta^{18}O$ decrease by 1.9‰ within the same

samples, the last two of which come from the hypermineralized zone noted in the

microCT record and may therefore be suspect.

DISCUSSION

Annual Growth

We have attempted to use distinct, recurring features of tusk structure and

composition to distinguish the largest scale of cyclic variation in this animal's growth

record, namely, first-order, or annual, increments. Synthesizing results from microCT,

thin section, and isotope analyses, we observed a set of patterns that repeat over similar spatial scales and that we interpret as reflecting annual growth (Figure 3). In thin section, appositional thicknesses of second-order increments were found to vary cyclically over intervals of about 48 increments. Similar patterns of change in appositional growth rate were reported for tusks of proboscideans from North America and Asia and were interpreted as changes in growth over a single year due to seasonal variation in conditions that modulate growth (Fisher, 1987; Fox et al., 2007; Fisher et al., 2014; El Adli et al., 2015). Series of thin second-order increments reflect growth during times when nutrient availability is low (e.g., winter), while thicker increments represent times of plenty (e.g., spring and summer). Abrupt changes from thin to thick second-order increments represent the change from winter to spring (i.e., the growing season for most vegetation). Given the similarity of the pattern of variation in second-order increment thickness within our sample to seasonal changes reported in other tusks, and given the average number of second-order growth increments observed per cycle of growth (~48 weeks), it is reasonable to interpret these patterns as annual features. We acknowledge that our estimate of the number of third-order (daily) increments per second-order increment and of the number of second-order increments per first-order increment (year) implies a deficit of about 30 days per year. However, failing to recognize even a few increments, especially in our tally of third-order increments per second-order increment, could easily explain this difference.

At the beginning of year X-1, the first full year for which we have stable isotope data and the next to last year of life, the $\delta^{18}O$ value is about 22‰, near the average for the year. With the next two samples, $\delta^{18}O$ drops to near 20‰ and then again rises to

oscillate near the average value for the rest of the year. Just after this, year X very nearly reproduces this pattern until about the position of its midyear density change, observed by microCT. Following this, $\delta^{18}O$ declines to anomalously low values, judging from the pattern of the previous year, but by this point, we are dealing with the hypermineralized zone near the pulp cavity surface. As for what the overall pattern means, the drop in $\delta^{18}O$ could reflect the animal's first spring access to drinking water sources influenced by snowmelt at higher altitudes. Following this, $\delta^{18}O$ returns to higher, but notably variable values. The Santiago Basin is a relatively low-elevation region, but on all sides save the southwest, it is framed by higher montane regions that may be expected to complicate weather patterns for the Basin. Although the annual $\delta^{18}O$ pattern is by no means a simple sinusoid, the similarity of at least the first half of each of these two years is close enough that we consider it as corroborating our hypothesis of what constitutes a single year in this system.

Unfortunately, we cannot say as much for the pattern of variation in $\delta^{13}C$ values. The pattern within year X-1 is not sinusoidal, nor is it obviously repeated from year X-1 to year X. Except for an upward drift of $\delta^{13}C$ values toward the surface of the pulp cavity, which we take to be suggestive of diagenetic alteration (Fisher et al., 2014), the range of values is consistent with expectation for a herbivore browsing on C_3 vegetation. However, the pattern of variation in $\delta^{13}C$ values neither corroborates nor refutes our hypothesis of what constitutes a year. This pattern (or lack thereof) may be reflective of a relatively stable dietary source (with excursions representing exploitation of a more ephemeral food source) and could suggest minimal change in the floral assemblage throughout the year. Regardless, $\delta^{13}C$ provides no aid in our assessment

69

of annual intervals for this specimen.

Fortunately, our thin section gave us access to a longer record of time than we were able to sample for stable isotopes. We observed parts of four annual cycles of variation in rate of apposition recorded by second-order increments, with three abrupt transitions from low to high rate interpretable as marking the onset of spring. Each of these changes in growth rate was co-located with an abrupt transition from high to low X-ray attenuation (see section 3.1). Patterns of zonation in X-ray attenuation have been used to identify season of apposition within tusk dentin of *Mammut* and *Mammuthus* (Fisher et al., 2014; El Adli et al., 2015). Those authors identified high levels of dentin mineralization during the winter season, dropping to a lower level of mineralization in the spring. In most previously described cases, this abrupt change is followed by a gradual transition back to higher mineralization during the winter, completing the yearly cycle of appositional growth. However in the microCT section studied here, not every transition from high to low attenuation was associated with the same type of shift in second-order increment thickness. In fact, the sample contains twice as many microCT density cycles as it does cyclical patterns in isotope values and second-order increment thickness (Figs. 2, 3). These "additional" density features are indistinguishable from those that co-occur at winter-spring boundaries as we currently recognize them. At least within the three years for which we can evaluate the pattern using our current sample, these "extra" microCT features are found just after a brief decline in second-order increment thicknesses bracketed by relatively thick increments. In the case of two years (X and X-2; see Fig. 3) the "extra" microCT feature occurs several second-order increments after the recovery from this decline in thickness, but in one year (X-1) the

70

feature occurs slightly later and is observed at the start of a series of thin second-order increments. The repeated presence and somewhat consistent location of non-winter-spring microCT features suggests that these features are real and likely represent some aspect of life history or environment, but we cannot yet identify their cause with certainty.

Semiannually recurring density features have not been observed in tusks of other proboscidean taxa (Fisher et al., 2014; El Adli et al., 2015). However, a new pattern found in a new context does not contradict or refute earlier work on annual microCT density cycles. In fact, this discovery highlights the necessity of conducting multiple independent analyses (e.g., microCT, thin section, serial isotope, etc) before determining the periodicity of different tusk features within each specimen. To date, the number of tusks that have undergone microCT analyses is small. Therefore it is not yet clear whether variation in the periodicity of different tusk features (including the "extra" density features in Marito's tusk) is 1) unique to specific individuals, 2) associated with some local population, or 3) characteristic of a taxonomic group. This problem merits further study, but will require assessment across different individuals, regions, and taxa, which is far beyond the scope of this paper.

As in many other similar studies of proboscidean tusk growth, we recognize annual growth based on the telltale signatures of the boundary between winter and spring (Fisher, 1987; Koch et al., 1989; Fox and Fisher, 1994; El Adli et al., 2015). All three sets of data recovered from Marito's tusk show an arguably annual pattern of growth with relatively synchronous changes in pattern approximating what we expect to be the boundary between winter and spring (Figs. 2, 3). Here, we follow the methods of

El Adli et al. (2015) and use the location of microCT density features (i.e., the change from high attenuation to low) collocated with changes in growth patterns of second-order increments (i.e., the transition between a series of relatively thin increments rapidly shifting to thicker increments) to designate the boundary between years. Given these criteria for identifying annual boundaries, we observe two complete and two partial years of growth within Marito's tusk sample (Fig. 3). The two complete years of life are similar in thickness (10.7 mm for year X-1 and 10.0 mm for year X-2). These measurements of annual appositional thickness are similar to the growth rates observed in mature male mammoths and mastodons from the late Pleistocene of North America (see Fisher, 2001, 2008; El Adli et al., 2015). With respect to partial years of growth, the first-order (annual) increment located furthest from the pulp cavity (Year X-3) appears to be incomplete due to degradation of the tusk sample, obscuring growth increments. Therefore, all we can say is that this year was thicker than 6.7 mm. The final year of life (Year X) was adjacent to the pulp cavity and recorded appositional growth totaling only 6.1 mm. This year is thin because Marito died before a full year was completed.

Season of Death

Given our interpretation of annual increments of tusk growth, we can use data from Marito's tusk to interpret his season of death. Within the final year of life (year X), we observe 25 second-order increments between the winter-spring boundary marking its beginning and the pulp cavity surface. However, this count may be incomplete as the early portion of year X contains a break in the sequence of dentin due to damage during extraction of the sample from the tusk, resulting in a discontinuity and possible gap (see

Material and methods; Fig. 3). Further complicating our interpretation of the final year of life, values recovered from isotopic analyses (especially for $\delta^{13}C$) appear to be diagenetically altered in this region, so the annual pattern of change in values is likely overprinted with misleading isotopic ratios. This leaves us dependent on the pattern of change in thickness of second-order increments (in comparison to previous years of growth) and microCT features as lines of evidence for our interpretation. With respect to the former, the final year of life shows an initial rise in growth rates following the winter-spring boundary, but then a decline toward the time of death, interrupted by a short sequence of thin second-order increments separating the sequence of thick increments from the final sequence of progressively thinner increments. Comparing the pattern of second-order increment thicknesses in previous complete years (years X-1 and X-2) to year X, the final year of life appears to follow a pattern similar to that of previous years across the break in the dentin sequence, which suggests that little material was lost along this interface during extraction. Given the pattern from previous years, the final year appears to terminate around what we expect to be the end of a series of declining second-order increment thicknesses preceding a series of thin increments. If we divide each growth year into four seasons of equal duration, the end of this declining sequence would represent late summer to early autumn. The observed pattern of growth seems consistent with a time near the summer-autumn boundary as food quality and availability would likely be declining as part of the transition toward winter.

The final year of life also contains a non-winter-spring microCT density feature. This feature and the non-winter-spring density feature observed in year X-2 are both preceded by a similar number of second-order increments following the previous winter-

spring boundary, suggesting that they form during a similar time of year. Furthermore, the non-winter-spring features in year X and X-2 are located within a sequence of second-order increments of decreasing thickness, which are immediately preceded by an abrupt decrease and increase in thickness following a series of distinctly thick increments (Fig. 3). The non-winter-spring density feature in year X-1 appears later in the annual cycle than in years X or X-2, but not so much later as to suggest that these features do not all form during a similar season. Using our previously described premise for identifying seasons from second-order increment thicknesses, these non-winter-spring density features appear to form in the middle to late summer. With regard to the final year of life, this summer density feature is followed by apposition of eight second-order increments before the pulp cavity surface. Unlike the count of increments from the last winter-spring boundary, this section of dentin is continuous and unbroken, giving us a complete record of growth from the final density transition until death. Thus, given the thickness of the final year of growth relative to previous years, the pattern of second-order increment growth, and the presence of a non-winter-spring microCT feature representing middle to late summer growth followed by a series of further second-order increments, we infer that death came in the latest summer to early autumn, a time period unusual for a natural death.

Cause of Death and Life History Interpretation

While season of death can often be inferred from a tusk sample containing the pulp cavity surface, cause of death is more complicated. The thickness of complete years of growth (Year X-1 and X-2) recorded within the dentin of Marito's tusk suggests

that this individual was relatively healthy leading up to the final year of life. Similarly, the final year of life (Year X), when compared with the thickness recorded during a similar amount of time within Years X-1 and X-2, shows that Marito was on track to grow another annual layer of comparable thickness. Furthermore, the profile of second-order increment thicknesses shows no unusual pattern of growth or sustained periods of low growth near the time of death (such as was described in a male *M. columbi* by El Adli et al., 2015), suggesting that there was no extended period of morbidity preceding death. The abrupt, non-winter death of a seemingly healthy individual seems to rule out attrition from nutritional stress or disease as potential causes of death.

One aspect of male proboscidean life history that has been proposed as a cause of premature death in North American mammoths and mastodons is musth (Fisher, 2004, 2007, 2008; Fisher and Fox, 2007; El Adli et al., 2015). In modern elephants musth is a period of aggression between males over potential mates that lasts up to a maximum of three months (Poole and Moss, 1981; Poole, 1996). Musth is associated with extended periods of fasting, which we expect to result in decreases in tusk growth rates. This behavior recurs annually and at predicable times in large, healthy males of reproductive age, but can be more sporadic in occurrence for smaller and younger individuals. Timing of musth in elephants is not highly synchronized within a population, but musth individuals are found to be more frequent during and just after the rainy season (Poole, 1987; Kahl and Armstrong, 2002). This increase in frequency of musth males around the rainy season suggests some optimum for timing of reproduction and is likely associated with optimal birth season (i.e., the start of the rainy season, which would be followed by enhanced food availability). Given that gestation in elephants is

approximately 22 months (Poole, 1996), the optimal time for conception (and thus musth) is several months after the beginning of optimal foraging conditions. In modern African elephants, optimal foraging is associated with the rainy seasons (the so-called "long rains" and "short rains"). However, in a climate system where temperature variation assumes a greater role, the optimal birth season is near the onset of spring, making summer the optimal time for musth.

Although we do not currently have direct evidence to support a similar gestation time or the occurrence of musth in gomphotheriids, we suggest that this behavior may be conserved. Within North American proboscidean taxa, both mammoth and mastodon males show evidence of having undergone periods of musth (Fisher, 2004, 2007, 2008, 2009; Fisher and Fox, 2007; El Adli et al., 2015). In all cases, musth was associated with summer, and in several of these cases, musth battles were inferred to have been the cause of death. Despite the wide phylogenetic separation of mammutids and elephantids, sexual dimorphism appears to be widespread throughout Proboscidea, which suggests conservation of behavior and physiology throughout much of the group (Smith and Fisher, 2013). Thus it seems reasonable to infer, through phylogenetic bracketing (Witmer, 1995), that mature male *Stegomastodon* likely also went into musth during a time of year that would have optimized season of birth.

Within Marito's tusk sample, we note three short periods of sustained decrease in second-order increment thickness found within stretches of conspicuously high growth rate (see brackets labeled "M": Fig. 3). Placing these periods within the context of years, we observe these short durations of low growth rate to occur between 10 and 12 increments after the inferred winter-spring boundary (Fig. 3). In all three cases, these

76

periods of low growth are found to be near, but not precisely coinciding with non-winter-spring microCT features. Given our interpretation of seasons in patterns of second-order increment thicknesses and in non-winter-spring microCT features, these thin second-order increments appear to form in the early summer, an ideal mating period for an early spring birth given a 22 month gestation. Considering the recurring nature of these features, the appropriate seasonal association, and the resemblance to similar patterns of second-order increment growth in other male proboscideans (see El Adli et al., 2015), we interpret these periods of thin second-order increments within the context of early summer as representing musth.

One of the inferred musth periods occurs within the final year of life (Year X). However, musth appears to predate time of death by 10 second-order increments. El Adli et al. (2015) showed a similarly long period of dentin apposition following musth in a large male *Mammuthus columbi* from California. Those authors suggested that this sequence of second-order increments following musth represented an extended period of morbidity following injury during a musth battle, which was evidenced by a sudden decrease in second-order increment thicknesses following the characteristically thin growth increments inferred as representing musth. In the case of Marito, growth rates briefly increase beyond musth and then steadily decline afterwards, which is similar to growth patterns observed in previous years. In other words, we do not observe a markedly different pattern from an average growth year. Thus we do not treat musth injury as a probable cause of death.

Other interpretations of cause of death are hard to invoke without further evidence. If predation were the cause of death, we might expect to see feeding-related

77

damage on bone, which even then would not rule out scavenging. However, no such features are observed on the remains recovered for Marito (although they are, admittedly, few). In the Great Lakes region of North America, Fisher (1987, 1995) has associated an autumn season of death with several male mastodons that were clearly butchered and utilized by humans. Such an interpretation is unwarranted here due to a lack of taphonomic evidence. Furthermore, the relatively imprecise Pleistocene age of the specimen does not allow us to assess whether such a cause of death is even reasonable. Accidental death (e.g., drowning) is a further plausible cause for mortality, but no evidence is available for or against such a hypothesis. Therefore, given no further clues regarding the demise of Marito we are left with an unfortunate unknown. What can be said is that, based on the evidence recorded within the dentin of Marito's tusk, he was a healthy male *Stegomastodon* of prime reproductive age who died relatively abruptly during the autumn. The information provided by these analyses of growth and life history provides some of the first insights into the behavior and ecology of a South American proboscidean taxon. Future studies of a similar nature will doubtless provide further information into these animals' lifestyle and may elucidate some of the lingering questions uncovered within this initial investigation.

CONCLUSION

We performed a series of analyses on the tusk of an adult male *Stegomastodon* from central Chile. This study represents the first life history analysis performed on a South American proboscidean and provides new insights into the lives of gomphotheres from the southern hemisphere. Thin section analysis reveals seasonal variation in

78

weekly increment thicknesses over two complete and two incomplete years. Serial

isotope sampling shows an annual pattern of compositional variation in $\delta^{18}O$, but $\delta^{13}C$

values show no clear annual pattern. MicroCT reveals semiannually-recurring cycles of

density change, which have not been documented in any other proboscidean.

Combined, these analyses suggest that this individual was relatively healthy in his final

years of life, with rates of annual tusk growth similar to those documented in male

proboscidean tusks from North America. We also find evidence to suggest that this

individual consistently underwent a short period of musth in the early summer during the

final three years of life. The final year of life shows a truncated pattern of growth relative

to earlier years. Based on comparison with complete years of growth, it appears that

this individual died in the late summer to early autumn.

ACKNOWLEDGEMENTS

REFERENCES

Ameghino, F., 1888. Rápidas diagnosis de algunos mamíferos fósiles nuevos de la República Argentina. Obras Completas, Buenos Aires V, 469–480.

Crowley, B.E., Wheatley, P.V., 2014. To bleach or not to bleach? Comparing treatment methods for isolating biogenic carbonate. Chemical Geology 381, 234–242.

El Adli, J.J., Cherney, M.D., Fisher, D.C., Harris, J.M., Farrell, A.B., Cox, S.M., 2015. Last years of life and season of death of a Columbian mammoth from Rancho La Brea. In: Harris, J.M. (Ed.), La Brea and beyond: The paleontology of asphalt-preserved biotas. Natural History Museum of Los Angeles County, Science Series vol 42, pp. 65–80.

Fisher, D.C., 1987. Mastodont procurement by Paleoindians of the Great Lakes Region: Hunting or scavenging? In: Nitecki, M.H., Nitecki, D.V. (Eds.), The evolution of human hunting. Plenum, New York, pp 309–421.

Fisher, D.C., 1988. Season of death of the Hiscock mastodonts. Bulletin of the Buffalo Society of Natural Sciences 33, 115–125.

Fisher, D.C., 1995. Experiments on subaqueous meat caching. Current Research in the Pleistocene 12, 77–80.

Fisher, D.C., 1996. Extinction of proboscideans in North America. In: Shoshani, J., Tassy, P. (Eds.), The Proboscidea: Evolution and palaeoecology of elephants and their relatives. Oxford University Press, Oxford, pp 296–315.

Fisher, D.C., 2001. Season of death, growth rates, and life history of North American mammoths. In: West, D.L. (Ed.), Mammoth site studies: Proceedings of the first international conference on mammoth site studies. Publications in Anthropology vol. 22, University of Kansas, Lawrence, pp. 121–135.

Fisher, D.C., 2004. Season of musth and musth-related mortality in Pleistocene mammoths. Journal of Vertebrate Paleontology 24 (Supplement to 3), 58A.

Fisher, D.C., 2007. Life history analysis of the Yukagir mammoth. In: Boeskorov, G.G., Tikhonov, A.N., Suzuki, N. (Eds.), The Yukagir mammoth. Institute of Applied Ecology of the North [Yakutsk], St. Petersburg, pp. 142–156.

Fisher, D.C., 2008. Taphonomy and paleobiology of the Hyde Park mastodon. In: Allmon, W.D., Nester, P.L. (Eds.), Mastodon paleobiology, taphonomy, and paleoenvironment in the late Pleistocene of New York State: Studies on the Hyde Park, Chemung, and Java sites. Palaeontographica Americana vol. 61, pp. 197–289.

Fisher, D.C., 2009. Paleobiology and extinction of proboscideans in the Great Lakes region of North America. In: Haynes, G. (Ed.), American megafaunal extinctions at the end of the Pleistocene, Springer, New York, pp. 55–75.

Fisher, D.C., Cherney, M.D., Newton, C., Rountrey A.N., Calamari, Z.T., Stucky, R.K., Lucking, C., Petrie, L., 2014. Taxonomic overview and tusk growth analyses of Ziegler Reservoir proboscideans. Quaternary Research 82, 518–532.

Fisher, D.C., Fox, D.L., 2007. Season of death of the Dent mammoths: Distinguishing single from multiple mortality events. In: Brunswig, R.H., Pitblado, B.L. (Eds.). Frontiers in Colorado Paleoindian archaeology: From the Dent site to the Rocky Mountains. University Press of Colorado, Boulder, Colorado, pp. 123–153.

Fox, D.L., 2000. Growth increments in *Gomphotherium* tusks and implications for late

Miocene climate change in North America. Palaeogeography, Palaeoclimatology, Palaeoecology 156, 327–348.

Fox, D.L., Fisher, D.C., 1994. Tusk growth rate in *Loxodonta africana* as recorded by incremental laminae in tusk dentin. Journal of Vertebrate Paleontology 14, 26A

Fox, D.L., Fisher, D.C., Vartanyan, S., Tikhonov, A.N., Mol, D., Buigues, B., 2007. Paleoclimatic implications of oxygen isotopic variation in late Pleistocene and Holocene tusks of *Mammuthus primigenius* from northern Eurasia. Quaternary International 169, 154–165.

Kahl, P.M., Armstrong, B.D., 2002. Visual displays of wild African elephants during musth. Mammalia 66, 159–172.

Koch, P.L., Fisher, D.C., Dettman, D., 1989. Oxygen isotope variation in the tusks of extinct proboscideans: A measure of season of death and seasonality. Geology 17, 515–519.

Koch, P.L., Tuross, N., Fogel, M.L., 1997. The effects of sample treatment and diagenesis on the isotopic integrity of carbonate in biogenic hydroxylapatite. Journal of Archaeological Science 24, 417-429.

Labarca, R., Alberdi, M.T., Prado, J.L., Mansilla, P., Mourgues, F.A., 2016. Nuevas evidencias acerca de la presencia de *Stegomastodon platensis* Ameghino 1888, Proboscidea: Gomphotheriidae, en el Pleistoceno tardío de Chile central. Estudios Geológicos 72 (1), doi: http://dx.doi.org/10.3989/egeol.42199.385 (in Spanish)

Lister, A. M. 1996. Sexual dimorphism in the mammoth pelvis: an aid to gender determination. In: Shoshani, J., Tassy, P. (Eds.), The Proboscidea: Evolution and palaeoecology of elephants and their relatives. Oxford University Press, Oxford, pp. 254–259.

Madden, C.T., 1986. *Stegomastodon* associated with *Mammuthus* in Arizona during the Quaternary. Quaternary Research 26, 266–271.

Mothé, D., Avilla, L., 2015. Mythbusting evolutionary issues on South American Gomphotheriidae (Mammalia: Proboscidea). Quaternary Science Reviews 110, 23–35.

Núñez, L., Varela, J., Casamiquela, R., Schiappacasse, V., Niemeyer, H., Villagrán, C., 1994. Cuenca de Taguatagua en Chile: el ambiente del Pleistoceno superior y ocupaciones humanas. Revista Chilena de Historia Natural 67, 503–519. (in Spanish)

Poole, J., 1987. Rutting behavior in African elephants: the phenomenon of musth. Behavior 102, 283–316

Poole, J., 1996. The African elephant. In: Kaugwana, K. (Ed.). Studying elephants. African Wildlife Foundation, Washington, D.C., pp. 1–8.

Poole, J.H., Moss, C.J., 1981. Musth in the African elephant, *Loxodonta africana*. Nature 292, 830–831.

Rasband, W.S., 1997. ImageJ. United States National Institutes of Health, Bethesda, Maryland. http://imagej.nih.gov/ij/.

Rountrey, A.N., Fisher, D.C., Vartanyan, S., Fox, D.L., 2007. Carbon and nitrogen isotope analyses of a juvenile woolly mammoth tusk: evidence of weaning. Quaternary International 169, 166–173.

Rountrey, A.N., 2009. Life histories of juvenile woolly mammoths from Siberia: Stable

isotope and elemental analyses of tooth dentin. Ph.D. dissertation, University of Michigan, xiii+331 pp.

Sánchez, B., Prado, J.L., Alberdi, M.T., 2004. Feeding ecology, dispersal, and extinction of South American Pleistocene gomphotheres (Gomphotheriidae, Proboscidea). Paleobiology 30, 146–161.

Smith, K.M., Fisher, D.C., 2011. Sexual dimorphism of structures showing indeterminate growth: tusks of American mastodons (*Mammut americanum*). Paleobiology 37 (2), 175–194.

Smith, K.M., Fisher, D.C., 2013. Sexual dimorphism and inter-generic variation in Proboscidean tusks: multivariate assessment of American mastodons (*Mammut americanum*) and extant African elephants. Journal of Mammalian Evolution 20 (4), 337–355.

Tassy, P., 1996. Who is who among the Proboscidea. In: Shoshani, J., Tassy, P. (Eds.), The Proboscidea: Evolution and palaeoecology of elephants and their relatives. Oxford University Press, Oxford, pp. 39–48.

Varela, J., 1991. Geología del Cuaternario de la Depresión Central de Chile en la Zona de la Cuenca de Santiago, región Metropolitana, Chile. Congreso Geológico Chileno No. 6. Resúmenes expandidos, 593–596. (in Spanish)

Witmer, L.M., 1995. The extant phylogenetic bracket and the importance of reconstructing soft tissues in fossils. In: Thomason, J.J. (Ed.), Functional Morphology in Vertebrate Paleontology. Cambridge University Press, New York, pp. 19–33.

Table 3.1. Isotope values for δ¹³C (relative to VPDB) and δ¹⁸O (relative to VSMOW) for carbonate in dentin within the tusk sample. Distance is measured in millimeters from the pulp cavity (PC) to the middle of the sampling site.

Sample	$\delta^{13}C$	$\delta^{18}O$	Distance (mm)
PC	-6.2	20.4	0.44
PC-1	-8.3	21.2	1.31
PC-2	-9.1	21.4	2.21
PC-3	-9.7	22.2	3.13
PC-4	-9.7	22.0	3.97
PC-5	-9.5	21.2	4.76
PC-6	-9.7	20.5	5.57
PC-7	-9.5	21.7	6.41
PC-8	-9.8	21.7	7.33
PC-9	-10.6	22.6	8.27
PC-10	-10.3	22.2	9.57
PC-11	-10.3	21.5	9.88
PC-12	-10.1	21.8	10.67
PC-13	-10.1	22.5	11.42
PC-14	-11.0	21.3	12.15
PC-15	-10.7	22.5	12.88
PC-16	-10.3	21.9	13.61
PC-17	-10.5	21.1	14.36
PC-18	-10.4	20.4	15.10
PC-19	-10.3	20.4	15.85
PC-20	-10.2	22.0	16.58
PC-21	-11.0	22.0	17.33
PC-22	-11.1	21.5	18.08
PC-23	-4.5	25.3	18.81

Figure 3.1. Ventromedial view of broken right tusk and palate of *Stegomastodon platensis* recovered from El Trebal 1. Black electrical tape marks the location of the extracted tusk sample. Abbreviations: A = anterior; D = dorsal; M2 = second upper molar; M3 = third upper molar; pmx = premaxilla.
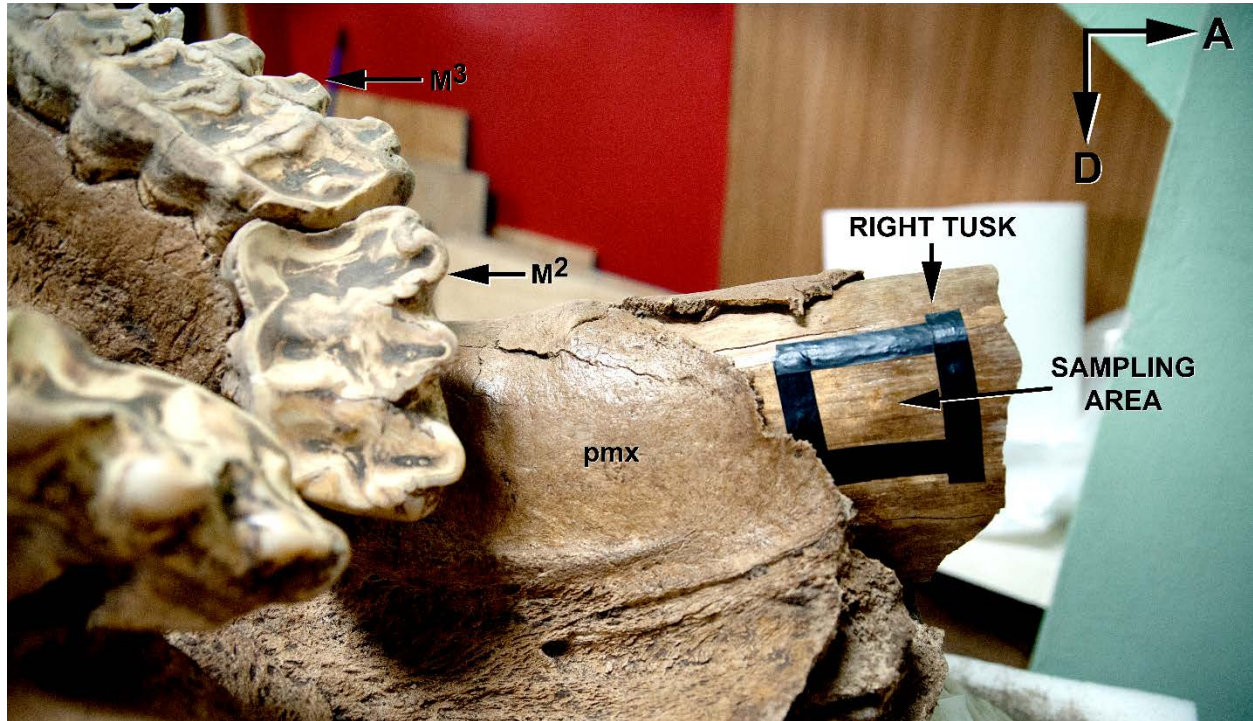
Figure 3.2. MicroCT image and photomicrograph of a transverse section of tusk. A, MicroCT image of a transverse section of tusk material showing density features (marked by white arrows). White dotted box shows the location of the thin section view shown in B. DCJ = dentin-cementum junction. B, photomicrograph of a transverse thin section of tusk material showing weekly (marked by white arrows) and daily increments of dentin apposition.
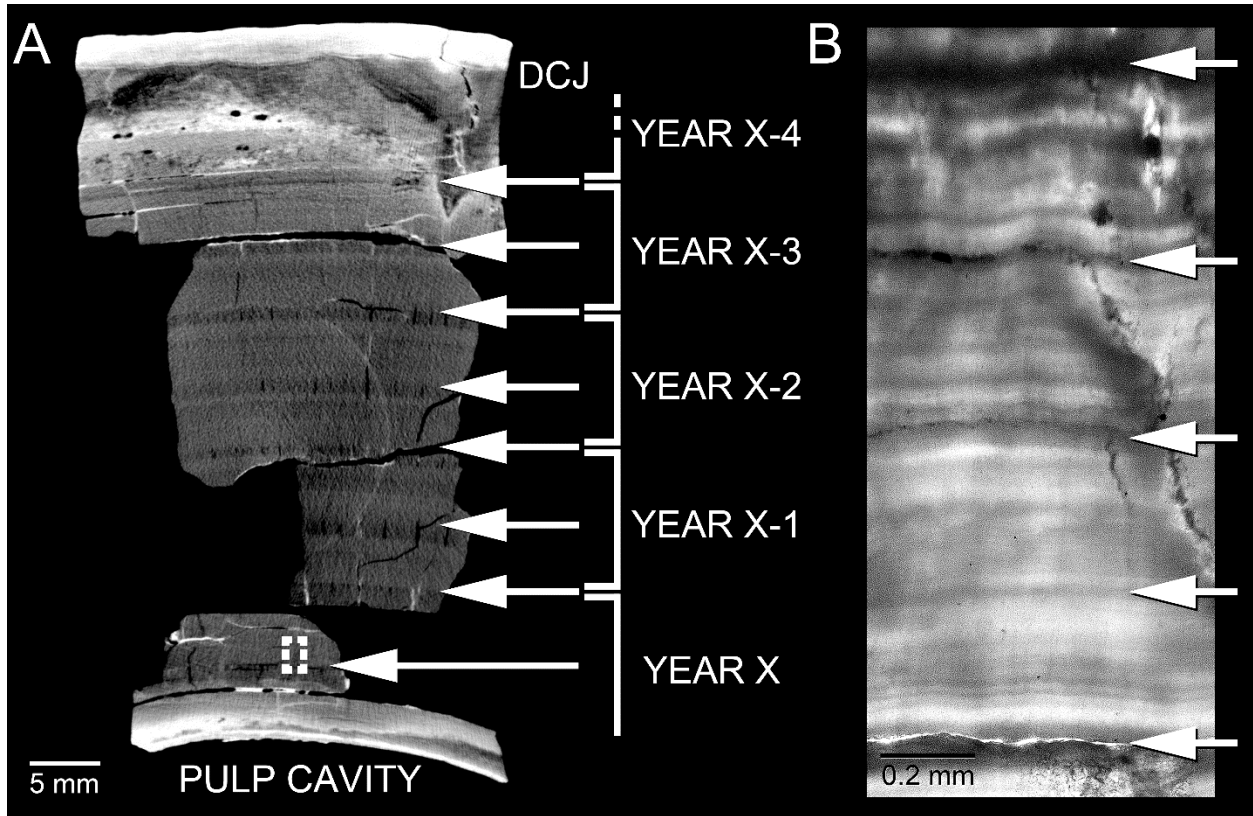
Figure 3.3. Results of tusk analysis. A, Results of serial isotope analysis showing changes in δ¹³C and δ¹⁸O values through the last years of life. B, positions of density features observed in microCT images (shown as white-to-black rectangles). C, profile showing variations in thickness of weekly (second-order) increments. Vertical dotted lines represent hypothesized winter-spring boundaries demarcating years (labeled in B); bracketed intervals labeled "M" correspond to inferred musth episodes, as evidenced by low rates of dentin apposition during summer months. The dagger symbol shows the final increment representing the time of death.
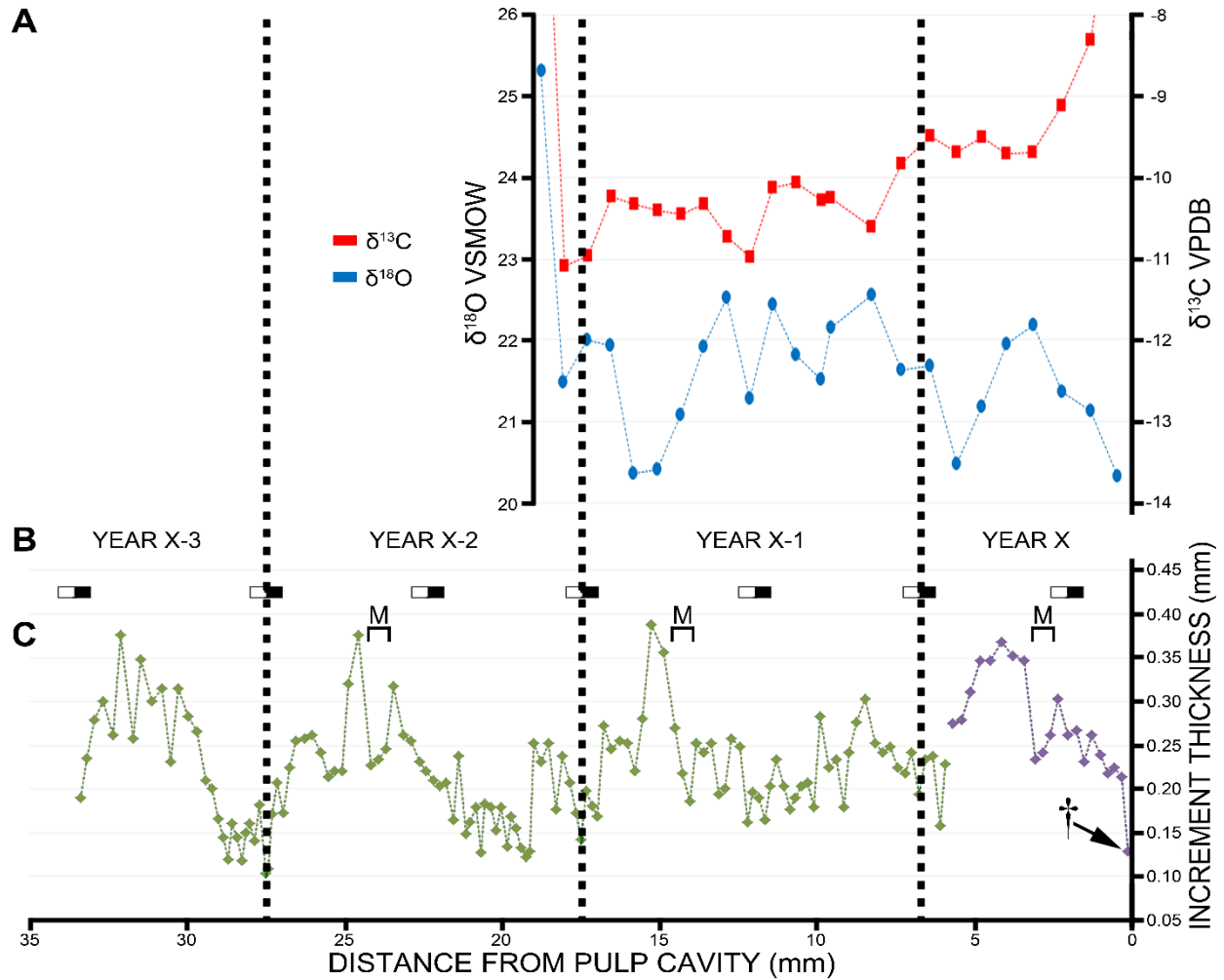
CHAPTER 4

Final years of life and seasons of death of woolly mammoths from Wrangel Island and mainland Chukotka, Russian Federation[3]

ABSTRACT

The tusks of proboscideans contain a continuous record of growth throughout much of an individual's life. Proximal portions of isolated tusks from five individuals of *Mammuthus primigenius* from Chukotka and Wrangel Island, Russian Federation, were analyzed to extract life history information from the last years of life. All five individuals are identified as adults based on the shallowness of their pulp cavities and the reverse-taper of the tusks proximal to the gingival margin. Given this, these individuals are interpreted as female due to the relatively small circumference of their tusks. However, based on these features, there appears to be a range in ontogenetic age among these individuals. Radiocarbon dating of the specimens yields absolute age estimates ranging from approximately 5,000 to 7,500 $C^{14}yrBP$ (5,600 to 8,550 calBP) for the Wrangel Island specimens and 15,000 and 26,000 $C^{14}yrBP$ (18,350 to 30,950 calBP) for the Chukotka specimens. Isotopic, thin section, and x-ray microtomographic analyses were performed on each specimen to determine the boundaries between years and to understand both inter- and intra-annual variation in tusk growth. Variation

---

[3] El Adli, J.J., Fisher, D.C., Vartanyan, S.L., Tikhonov, A.N., 2016. Final years of life and seasons of death of woolly mammoths from Wrangel Island and mainland Chukotka, Russian Federation. Quaternary International.

within and between years is then used to interpret season of death and relevant life history information for each individual. Each tusk segment recorded approximately five to nine years of growth. Based on the patterns observed in dentin density and comparison with previous years, all five individuals are interpreted as having died in late winter. With the exception of one specimen representing a younger individual, all of the tusks display a sinusoidal change in annual appositional tusk growth over an interval of approximately four to five years. These variations in annual growth are interpreted as calving cycles. Changes in average growth rate between Wrangel Island and Chukotka specimens can be explained based on differences in ontogenetic age and a shift to an insular environment. Further analyses of tusk samples from Wrangel Island and Chukotka will allow for an increased understanding of shifts in the patterns of life histories within mammoth populations through time and will ultimately allow for greater interpretative power in deducing the cause of their extinction.

INTRODUCTION

The end of the Pleistocene was marked by extinctions of many large terrestrial mammals, and on the continents, the woolly mammoth (*Mammuthus primigenius*) was no exception. However, Wrangel Island, located in the Arctic Ocean approximately 140 km off the coast of Chukotka in northeastern Russian Federation, provided a refugium for a relict population of woolly mammoths that survived until ca. 3,700 $C^{14}yrBP$ (Boeskerov, 2006; Bryson et al., 2010; Vartanyan et al., 1993; Vartanyan et al., 2008). The island is relatively large at approximately 7,600 km^2 in area and is topographically heterogeneous. A narrow coastal plain extends along the southern margin, and a

broader lowland makes up the northern portion of the island. The eastern and western ends of the island are dominated by plateaus, and an east-west trending mountain belt (greatest elevation, ~1100 m) occupies the central region. The island has been free of large glaciers for the past 64,000 years (Alekseev, 1998; Ehlers and Gibbard, 2007; Gualtieri et al., 2003; Stauch and Gualtieri, 2008) and was connected to mainland Chukotka during times of low sea level during much of the late Pleistocene until approximately 12,000 ybp (Hopkins, 1973). Thus the Wrangel Island population of mammoths was likely reproductively isolated from the mainland population of *M. primigenius* before the onset of the Holocene.

It was initially hypothesized that Wrangel Island supported a relict floral community throughout much of the Holocene, but palynological data suggest that a modern flora and climate was in place by the onset of the Holocene (Lozhkin et al., 2001; Lohzkin et al., 2011). Artifact remains of human hunters have also been found on the island dating to just after the latest known mammoth remains (Dikov, 1988). No clear evidence has been found that demonstrates hunting of woolly mammoths by ancient humans on Wrangel, but this may simply reflect poor sampling due to the relative inaccessibility of the island.

There is, as of yet, little support for any hypothesis on the cause of mammoth extinction on Wrangel Island (Abramson et al., 2015; Monjeau et al., 2015), but the key to understanding this phenomenon may be to learn more about patterns of growth and reproduction in these animals. The two most commonly hypothesized causes of mammoth extinction, human predation and climate change, each have a different set of predictable effects on individuals and populations. Therefore shifts in biological

processes through time and across many individuals can provide a signature for

different drivers of extinction. For example, if rapid climate change was the cause of

extinction, we would expect populations to show effects of nutritional stress due to

changes in the quality and/or abundance of food. Conversely if predation was the main

driver of extinction, we would expect to observe little negative impact on the health of

individuals, but would instead see changes in life history such as decrease in age of

maturation, increase in growth rates, and decrease in calving intervals (Fisher, 2009).

The record of conditions found in mammoth tusks can provide information on the life

history of individuals, allowing collection of data that can be used to test competing

extinction hypotheses.

Tusks as a record

The tusks of mammoths are enlarged incisors composed largely of dentin, which

grows by apposition at the surface of the pulp cavity. Tusk dentin, like all mammalian

dental tissues, is mostly composed of hydroxylapatite and, to a lesser extent, collagen.

Previous studies have recovered bulk compositional information from carbon, nitrogen,

and oxygen, which have been broadly informative about the environment and ecology of

mammoths (Bocherens et al., 1994, 1996; Drucker et al., 1999; Iacumin et al., 2000).

However, the ever-growing nature of tusk dentin allows for finer-scale analyses over a

continuous record of growth covering the final years of an individual's life up until the

day of death (recorded at the pulp cavity). This record is accessed through analyses of

compositional and structural variation within and among periodically-formed dentin

increments. Such growth features are frequently preserved in mammalian teeth and

have been studied extensively (Gysi, 1931; Laws, 1952; Dean, 1987; Fisher, 1987; Fox and Fisher, 1994; Fisher, 2001). In mammoths, these increments have been interpreted to form on annual (first-order), approximately weekly (second-order), and daily (third-order) intervals (Fisher, 2001). Sets of lower-order increments are nested within increments of higher-order, although all three types of increment are rarely observable simultaneously under the same viewing conditions. Variations within and between growth increments have been used to extract life history information and determine season of death (Fisher, 1987). Therefore, with a large enough sample of individuals across a broad temporal range, we should be able to use life history information extracted from tusks to test competing hypotheses of extinction (Fisher, 2009).

MATERIAL AND METHODS

Portions of isolated tusks from five individuals (CHM-10, ZCHM-13, 39M, 41M, and 42M) of *Mammuthus primigenius* from northeastern Siberia were analyzed in this study. Two of these specimens (CHM-10 and ZCHM-13) were recovered from the northern coast of Chukotka by SV, DCF, ANT, and others, and these will serve as a control group. The remaining three specimens (39-M, 41-M, and 42-M) were collected on Wrangel Island by SV. These specimens were recovered from coarse-grained (sands and gravels) fluvial deposits along the southern portion of the island. All of the Wrangel Island specimens were proximal sections cut from more complete specimens (in the field) using a handsaw. Only parts of tusks were collected during this phase of our work because of the logistic difficulties of collecting and exporting larger samples. Similarly, the two Chukotka specimens were removed from the field as larger, though

91

still incomplete, tusks, which were later transversely cut to remove the proximal ends. These five specimens were shipped to the University of Michigan where the majority of the analyses occurred. Each specimen underwent similar treatment, as described below.

All three of the Wrangel Island specimens were digitized using a Creaform HandyScan 3D laser scanner to record external morphological features of the tusks, which could be lost during sampling of the specimens. Each of the five specimens was then radiographically imaged at the MicroCT Core Facility at the University of Michigan School of Dentistry, using a SCANCO Medical μCT100 operating at 90kV, 78μA, and 500 ms, yielding uniform cubic voxels 60 μm per side. Patterns of variation in x-ray attenuation within the tusks were visualized using Amira 5.4.1. Zones of high and low x-ray attenuation were noted by eye, but were also quantified by luminance measurements.

Luminance was measured along a transect parallel to the direction of dentin apposition in a single microCT slice. At each position along this transect, the grayscale values of ten neighboring pixels representing dentin that formed at the same time were averaged in Adobe Photoshop CS5. This averaging of values reduced the influence of local features (e.g., computational artifacts, vacuities, dentinal tubules) on the luminance trend. The "Measure" tool in ImageJ (Rasband, 1997) was used to recover grayscale values for each position (pixel) along the transect.

Approximately one cubic centimeter of dentin was removed from the distal portion of each specimen using a coping saw. These dentin blocks were sent to Beta Analytic for collagen extraction and AMS dating. Age estimates for each specimen are

presented in Table 1 as ^{14}C yr BP (before present) and as calibrated dates in calendar years BP (calibrated using IntCal13; Reimer et al., 2013).

Drying of these tusks following collection resulted in minor fracturing of dentin, often following incremental features. Prior to sampling, epoxy resin was poured into these fractures to ensure recovery of an intact dentin sequence during later removal of sample blocks. Specimens were then placed in a vacuum for several minutes to remove air trapped within the fractures and allow more complete penetration by epoxy. After void space was filled, the pulp cavity surface was coated with epoxy to reduce loss of material from near the time of death during cutting of the specimens.

For analysis of microscopic growth features, a 5 to 10 mm-thick longitudinal slab was cut from each tusk using a Delta 14" metal-cutting (low-speed) band saw. Each slab was cut so that it contained the outside curve of the tusk as well as the apex of the pulp cavity. From these longitudinal sections, a smaller sample block was cut in the transverse plane normal to the surface of apposition (perpendicular to the pulp cavity surface) using a Buehler Isomet saw and a diamond wafering blade. Ethanol was used as a cutting lubricant rather than water because the collagen in dentin is hygroscopic; exposure to water causes dentin to expand, spalling away from adjacent dentin that has not yet absorbed as much water.

Transverse thin sections were made from the cut transverse slabs, using ethanol for cutting and polishing as in Fisher and Fox (2003). These thin sections were examined at 40x magnification under a Leitz petrographic microscope. Photomicrographs were taken along a transect from the cementum to the pulp cavity surface under plane-polarized light. Kerosene was added to each slide to enhance the

contrast of various growth features. Photomicrographs were analyzed using the

IncMeas 1.3c plug-in (Rountrey, 2009) for ImageJ to measure second-order increment

thicknesses.

RESULTS

ZCHM-13

ZCHM-13 is the largest of the five tusk samples studied, with a greatest

circumference of 231 mm (Table 1). The external surface of the tusk, especially on the

outside curve, is abraded due to a combination of weathering and interaction with

sediment in a moderately energetic, rapidly eroding, coastal environment. Most of this

abrasion affected the outermost cementum and did not penetrate as far as dentin. As a

consequence of abrasion, neither periradicular features (following the usage of Fisher,

2008 and El Adli et al., 2015), this term is used to describe topographic expression of

incremental features along the dentin-cementum interface, sometimes visible also along

the external surface of cementum) nor evidence of the gingival (or alveolar) margin

were observed on the surface of the tusk. Likewise, the proximal margin of the tusk has

been damaged along its entire circumference so that at its thinnest, the proximal margin

is approximately 1 cm thick. The pulp cavity, however, appears to be intact near its

apex, which allows for an accurate determination of season of death. Within the tusk,

the dentin has partially or completely delaminated along several of the conical

appositional surfaces due to heterogeneous desiccation-induced volume loss after

removal from the field. The dentin itself is a pale cream color and contains few regions

94

of chalky texture, suggesting that there has been little degradation of the original collagen matrix.

X-ray computed microtomography was used to observe density differences within the tusk. Density transitions within tusk dentin have been used in previous studies to identify seasons and have aided in identification of winter-spring boundaries (Fisher et al., 2014; El Adli et al., 2015). In CT section, several anatomical features are readily identifiable. The junction between dentin and cementum is displayed as an abrupt transition from higher values of attenuation (cementum) to lower values (dentin) adjacent to and approximately paralleling the outer surface of the tusk. The pulp cavity surface is identified by the sharp transition in density from dentin to air on the internal surface of the tusk, which is inclined relative to the outer surface and the dentin-cementum junction. Within the dentin sequence, finer-scale changes in density (both gradual and step-wise) appear at orientations that roughly parallel the pulp cavity surface. Step-wise examples of such change appear at fairly regular intervals and appear to represent boundaries separating dentin that formed just before and just after some short-term change in the physical properties of dentin. These patterns imply regular, time-dependent variation in attenuation values along transects normal to the surface of apposition.

Previous studies have suggested that dentin density varies seasonally in premaxillary and mandibular tusks in proboscideans (Fisher, 1987; Fisher et al., 2014; El Adli et al., 2015). Those studies suggest that during late winter months, dentin is more highly mineralized, whereas during spring, there is an abrupt transition from higher to lower levels of mineralization before gradually transitioning back to greater

mineralization in the next winter (Fig. 1). Within the part of the tusk studied from ZCHM-13, five abrupt transitions from high to low attenuation are observed, which we provisionally use to mark boundaries between years as this feature is the most readily locatable "event" within each seasonal cycle (Fisher, 1987). A zone of high attenuation is also observed immediately adjacent to the pulp cavity, but this feature differs in its exceptionally high x-ray attenuation relative to the rest of the dentin in the tusk and therefore probably represents diagenetic precipitation of secondary carbonate from groundwater during burial and has no bearing on interpretation of life history.

The realization that density features (in particular, the step-wise transition from high to low attenuation values) are associated with the boundary between winter and spring allows annual dentin increments to be distinguished and measured through a succession of years. The geometry of these annual increments, as observed in microCT, is generally conical. However, in *Mammuthus*, these cones taper proximally in appositional thickness, and thus any measurement of appositional thicknesses must be taken at a consistent position within the cone to be comparable from one year to the next and among individuals. In our study, all measurements of first-order increment thickness were taken at a position halfway along the proximodistal length of the inclined surface of each cone. In years where the apex of the cone was not visible, measurements were taken based on the location of the midpoint of the inclined surface of the cone from the following year, which was then translated in position to the surface of the adjacent increment to be measured. However, to limit the uncertainty associated with this protocol, we still required that the appositional thickness measurement be made directly, from one winter-spring boundary to the next and thus that the middle

96

portion of the "dentin cone" for a given year be preserved. As we attempted measurements in earlier-formed parts of tusks than were fully preserved in our specimens, there were almost always years that could be identified and counted (and might even yield second-order increment data for a "complete" year) but that did not yield a first-order thickness measurement.

Using the above methods, the four complete years and the single partial year observed in the microCT image of ZCHM-13 record the final years of life of this individual up to the time of death. Among complete years (Year X-1, X-2, X-3, and X-4; Fig. 2A) there is some fluctuation in annual appositional thickness with a range of 4.7 to 6.2 mm (average of 5.5 mm; standard deviation of 0.6). The final year of the animal's life (Year X) recorded the lowest annual growth (appositional thickness of 4.3 mm) observed within this individual. However, this is almost certainly due in part to Year X representing less than a full year of growth. Although microCT is broadly informative in locating winter-spring boundaries, finer scale analyses of dentin microstructure in thin section provides greater detail about inter- and intra-annual appositional growth within the tusk.

Thin sections were initially examined under reflected light through a stereomicroscope at low magnification (25x). At regular intervals within the dentin sequence, we observed alternating zones of high polish/high topography and low polish/low topography whose limits along the direction of apposition were conformable with visible dentin growth layers that generally paralleled the pulp cavity surface. Overall, the dentin sequence is characterized by abrupt transitions from high polish/high topography zones to low polish/low topography zones in the direction of growth,

97

followed by a more gradual transition from low to high polish. We took the differing appearance and elevation of these features as evidence for differences in degree of mineralization of dentin, with more polished zones being harder than intervening low-polish dentin. We suspect that these variations in hardness reflect regular, seasonal changes in tusk structure or composition. Within the ZCHM-13 sample, we observed and marked five zones of harder dentin in the thin section. As described above for microCT features, tusk dentin varies seasonally in its level of mineralization. Upon comparison between the locations of the most highly mineralized zones in microCT and the harder zones of high polish/high elevation, we found that the spatial boundaries of these features were coincident. Therefore, we interpret the five abrupt transitions from high polish/high topography to low polish/low topography as located approximately at boundaries between winter and spring.

After initial reconnaissance, the thin section was observed under plane-polarized light at 40x magnification, revealing distinct light-dark couplets identified as second-order increments within the dentin. Although not visible within most second-order increments, daily (third-order) increments were occasionally observed within second-order increments as fainter and narrower light-dark couplets. When visible, second-order increments were observed to contain approximately seven third-order increments, suggesting that second-order increments represent approximately weekly intervals of growth within the tusk, as has been demonstrated previously (Fisher et al., 2003). It remains possible that some of these growth increments vary in their periodicity, but as a first approximation, measurement of successive second-order increment thicknesses normal to the appositional surface allows us to construct a history of appositional growth

98

in the years leading up to the time of death (i.e., the last dentin deposited at the pulp cavity surface).

Second-order increment thickness was measured from near the dentin-cementum junction through to the pulp cavity surface (Year X-5 to Year X). On average, measured second-order increment thicknesses were 0.11 mm with a standard deviation of 0.04 mm. These increments displayed fairly regular fluctuations from low to high rate of apposition, repeating over a period of approximately 46 second-order increments (Fig. 3A). Sinusoidal changes in appositional rate have previously been recorded in proboscidean tusks from Siberia and North America, and have been interpreted as seasonal changes in growth (Fisher, 1987; Koch et al., 1989; Fox et al., 2007). Rapid transitions from low to high rates of apposition are interpreted as occurring near the transition from winter to spring and the beginning of the growing season for vegetation. Five of these transitions are observed within the thin section of CHM-10 (Fig. 3A), each of which also approximates the location of a transition from a zone of high polish/high topography to low polish/low topography in the thin section and a transition from high x-ray attenuation to low attenuation in microCT (as discussed above). The co-occurrence of these features is consistent with our interpretation that these regions represent the transition between winter and spring, which (following established usage; Fisher, 1987) we use to define the boundary between successive years (i.e., first-order increments). Based on the position of these first-order increment boundaries and the regular sinusoidal pattern of variation in second-order apposition between them, the partial tusk of ZCHM-13 recorded four complete and two partial years of growth (Figs. 2A, 3A). The first-formed of these partial years is from the most distal most part of the specimen,

located near the dentin-cementum junction. However, the second partial year occurs immediately adjacent to the pulp cavity and thus represents the partial year just prior to this individual's death. We expect an incomplete seasonal pattern of variation in second-order increment thickness to be a truncated portion of a complete annual pattern of growth with changes in second-order increment thicknesses reflecting identifiable (based on observations of patterns of growth in complete years within the same individual) periods of time within a given seasonal cycle. Given this, we are able to identify the individual's season of death based on the number of second-order increments and pattern of second-order increment thicknesses since the last winter-spring boundary. ZCHM-13 recorded 31 second-order increments from the previous winter-spring boundary to the pulp cavity surface, suggesting (based on previous years) that this individual died during the winter.

CHM-10

The external surface of CHM-10 has been abraded, removing some of the layers of cementum. The proximal end of the tusk was also damaged prior to collection, leaving an incomplete proximal margin. At the most nearly complete part of this margin, the tusk tapers to 2 mm in thickness before abruptly ending at an abraded surface. Three large, longitudinal fractures extend from near the apex of the pulp cavity to the external surface of the tusk. Furthermore, the dentin sequence has delaminated in several places, mostly along appositional growth surfaces. However, enough of the specimen remained intact to extract a continuous, undamaged block of dentin to analyze in thin section and microCT.

MicroCT analysis of the specimen reveals regular shifts in x-ray attenuation within the dentin sequence. As in ZCHM-13, these repeating changes from high to low attenuation occur along a transect perpendicular to the surface of the pulp cavity and probably represent seasonal shifts in levels of dentin mineralization. Five transitions are observed within the dentin studied for CHM-10, representing two partial and four complete years of growth.

The four complete years of life recorded in the microCT section (bounded by the density features described above) are relatively uniform in thickness, with the exception of the last complete year of life (Year X-1, Fig. 2B). In Year X-2 through Year X-4, yearly appositional thicknesses averaged 6.4 mm with a standard deviation of 0.3. However, appositional thickness for Year X-1 was only 4.1 mm, significantly lower than in previous years. The final year of the animal's life (Year X) also records less appositional growth (appositional thickness of 3.7 mm), but this is at least partly due to the increment representing less than a full year, because the individual died before another density feature representing spring growth could form.

Thin section analysis revealed a continuous sequence of second-order increments from near the dentin-cementum junction to around the time of the animal's death. On average, these increments measured 0.13 mm in thickness with a standard deviation of 0.05 mm, but the difference between minimum and maximum thicknesses was relatively large (0.05 mm and 0.27 mm, respectively). As in ZCHM-13, second-order increments showed regular, seasonal fluctuations in rate of apposition over a period of approximately 44 second-order increments (Fig. 3B). MicroCT density features (discussed above) again approximate the location of the inflection point between

101

sequences of thin increments (winter growth) transitioning into those with thicker increments (spring/summer growth). Using the location of high to low attenuation transitions in microCT to define boundaries between first-order increments, we observed four complete (Year X-1, X-2, X-3, and X-4) and two partial (Year X and Year X-5) years of growth. The year adjacent to the pulp cavity (Year X) is the final year of life and records 31 second-order increments from the previous winter-spring boundary until the time of death (recorded at the pulp cavity). Based on this second-order increment count and the seasonal pattern of growth relative to previous years, CHM-10 appears to have died during winter.

41-M

41-M is the second largest Wrangel Island tusk studied (at 207 mm greatest circumference) and the second smallest tusk overall. The tusk has been slightly abraded on the outer surface, but still shows first-order periradicular banding. Five such periradicular bands are visible and record relatively uniform extensional growth rates over the last five years of life (average of 1.9 cm and standard deviation of 0.1). The exception to this pattern is the final year of life, which is notably short. However, this is likely due to the final year of life not representing a complete year, as well as abrasion of the proximal-most margin of the tusk. The pulp cavity of 41-M is undoubtedly the deepest of the five tusks studied, with a relatively acute apex in longitudinal cross-section. Within the tusk, the dentin is cream-colored with few regions of chalky texture. This suggests that the dentin within the study region has had little degradation of the original collagen matrix.

MicroCT analysis of dentin within the tusk reveals regular shifts in x-ray attenuation along an appositional thickness transect, which we interpret as seasonal shifts in mineralization. Six transitions from high to low x-ray attenuation are observed within the longitudinal section. This includes five complete and two partial years of growth leading up to the time of death. Of the complete years, only three were measurable for appositional thickness due to the relatively deep pulp cavity, which meant that only the last few years preserve the middle of the dentin "cones" for measurement (Fig. 2C). These annual growth increments appear to be relatively uniform in thickness, with a relatively low range of 5.6 to 6.2 mm (average 5.8 mm; standard deviation of 0.3).The final year of life is, again, appositionally thinner than previous years, probably due to this increment representing less than a complete year of growth.

Measurements of second-order growth increment thicknesses within the dentin using thin section analysis reveal seasonal fluctuations in growth over a period of approximately 43 second-order increments (Fig. 3C). Increment thicknesses vary over a range of 0.04 to 0.22 mm with an average thickness of 0.10 mm and a standard deviation of 0.04. Abrupt transitions from high to low x-ray attenuation observed in microCT approximate the locations of seasonal change from low to high growth rates within the dentin and are thus used to approximate the boundary between winter and spring. With these boundaries defining years, we observe seven first-order increments within the thin section sample (two partial and five complete years). The final year of life for 41-M recorded 34 second-order growth increments, with death occurring following a

series of relatively thin increments. Given these data and comparisons with earlier, complete years of growth, 41-M appears to have died during winter.

42-M

42-M is the largest of the Wrangel Island specimens and third largest overall, with a greatest circumference of 216 mm. The outer surface of the tusk has been abraded so that no periradicular bands are visible. Likewise, the entire proximal margin of the tusk is worn and rounded, with about 1 cm of material missing from the proximal-most portion. The pulp cavity is largely intact but has been partially split longitudinally by a post-mortem fracture. Some of the conical dentin layers within the tusk have also partially delaminated from each other, likely as a result of desiccation after exhumation. The dentin contains several small, chalky-textured regions (especially in areas surrounding longitudinal fractures) suggesting some local degradation of the original collagenous matrix. However, the majority of the dentin within the part of the specimen used for analysis appeared to be unaltered.

Analysis of x-ray attenuation throughout the dentin sequence using microCT shows regular density changes interpreted to represent seasonal shifts in mineralization within the tusk. Six attenuation transitions are observed within the dentin sequence studied for 42-M. These transitions represent a sequence of two partial and five complete years of growth from the last seven years of life up to the time of death. With respect to the five measurable and complete years of life recorded within the section, annual growth increment thicknesses appear to fluctuate in a sinusoidal pattern (Fig. 2D). This shift occurs over a range of 3.6 to 5.5 mm (average 4.5 mm; standard

deviation of 0.8) and appears to occur on a period of approximately five years. Perhaps surprisingly, the next to last year of life (Year X-1) is the thickest first-order increment measured within the tusk (at 5.5 mm in thickness). Furthermore, the final year of life, though incomplete, was already above the average thickness based on previous complete years (at 4.8 mm in thickness). Since variations in tusk apposition reflect conditions during growth, the fact that the final year of life is already thicker than the average for previous complete years suggests that Year X, despite being the year of death, was not a particularly difficult for the animal.

Thin section analysis reveals a continuous sequence of second-order increments from near the dentin-cementum junction to the pulp cavity. Second-order increments measured within the thin section averaged 0.09 mm in thickness with a standard deviation of 0.03 and a range of 0.20 to 0.03 mm. These increments reveal seasonal fluctuations in growth over a period of approximately 42 second-order increments (Fig. 3D). When compared with microCT data, regions of the thin section containing sequences of thin second-order increments that abruptly transition to thicker second-order increments are associated with a similarly abrupt transition from high x-ray attenuation to low attenuation, which we interpret to be the boundary between winter and spring (which we use to mark the boundary between years). Using these features to mark first-order increment boundaries, we observed five complete (Year X-1, X-2, X-3, X-4, and X-5) and two partial (Year X and Year X-6) years of growth. From the last winter-spring boundary until the time of death (Year X), we record 39 second-order increments. Compared to previous complete years of growth, Year X appears to be near the number of second-order increments expected for previous years. This fact,

coupled with the patterns of growth and x-ray attenuation seen in previous years, suggests that 42-M died in late winter.

39-M

39-M is the smallest of the five tusk samples studied with a greatest circumference of 165 mm. The external surface shows moderate abrasion, especially on the proximal margin and along the inside curve of the tusk. The pulp cavity surface is well-preserved and has the shallowest and least acute apex of any tusk studied. Unlike the other tusks, 39-M has little internal fracturing of tusk dentin. Likely as a result of this, the dentin within the tusk is exceptionally well preserved and has few regions of chalky texture.

Analysis of x-ray attenuation within the dentin by micoCT reveals regular shifts in density along a transect perpendicular to the surface of the pulp cavity. These transitions from high to low x-ray attenuation repeat nine times within 39-M, representing seven complete and two incomplete years of growth (Figs. 1, 2E). With respect to complete years of growth, five were measurable for appositional thickness in microCT (Year X-1, X-2, X-3, X-4, and X-5). These years averaged 3.8 mm in thickness with a standard deviation of 0.3 and a range of 3.4 to 4.3 mm. The final year of life (Year X) is approximately as thick as Year X-4 (3.4 mm in appositional thickness), the thinnest complete year of life measured. Due to the fact that Year X is within the range of thickness of previous complete years, the final year of life likely represents nearly a complete year of growth.

Thin section analysis reveals a continuous sequence of second-order increments within the dentin. However, unlike in other tusks analyzed in this study, second-order increments were not visible for measurement within two millimeters of the pulp cavity surface. It is unclear why increments in this region are obscured, but it may be due to degradation of the dentin nearest the pulp cavity. With respect to measured second-order increments in 39-M, increments showed regular, seasonal fluctuations in thickness over periods of approximately 43 second-order increments (Fig. 3E). On average, these increments measured 0.08 mm in thickness with a standard deviation of 0.05 and a range of 0.03 to 0.27 mm. When compared with the location of abrupt transitions from high to low x-ray attenuation (as discussed above), density features approximate the location of change from sequences of thin second-order increments to sequences of thicker increments. These microCT features are therefore used to define the boundaries between winter and spring (and thus the boundaries between years). Using this criterion, the thin section records five complete (Year X-1, X-2, X-3, X-4, and X-5) and two incomplete (Year X and X-6) years. The final year (Year X) records 21 second-order increments following the previous winter-spring boundary, but as previously stated, increments could not be measured all the way to the pulp cavity. Based on the thickness of the last year of life relative to previous years (3.6 mm Year X thickness vs. 3.8 mm average annual thickness) and the lack of visible transition in x-ray attenuation near the pulp cavity, this individual appears to have died during winter.

DISCUSSION

Sex and Stage of Ontogenetic Development

All five of the specimens analyzed in this study were collected as isolated partial tusks with no further dental or postcranial elements to provide a Laws' Age Class for each individual (Laws, 1966; Lister, 1999). In complete or nearly complete tusks, presence of annual growth increments could provide an absolute ontogenetic age, but none of the tusks sampled represent anything near a complete history of growth. However, aspects of tusk morphology, as observed in both *Loxodonta* and *Mammut*, have been shown to provide relevant information on ontogenetic age, as well as the sex of the individual (Smith and Fisher, 2011; 2013). Though such a study has not been performed for *Mammuthus primigenius*, Smith and Fisher (2013) found tusk morphology associated with sexual dimorphism and ontogenetic age to be highly conserved between evolutionarily distant taxa (*L. africana* and *M. americanum*), suggesting that these findings likely hold true within Elephantidae, providing a point of reference for this study.

Three features of tusk morphology relevant for determining stage of ontogeny and sex are of particular importance for individuals in this study. Firstly, measurements of tusk diameter and circumference can be used to differentiate male and female individuals, with males of a given ontogenetic age having larger tusks than similarly-aged females (Fisher, 2008; Smith and Fisher, 2013). Secondly, the axial depth of the pulp cavity (and thus the relative acuteness of the apex of the pulp cavity) is both an indicator of sex and changes during ontogeny. In general, males have a much deeper pulp cavity than females of a similar ontogenetic age, and can even have pulp cavity apices that extend distal to the alveolar margin. Furthermore, the axial depth of the pulp cavity appears to shorten over ontogeny (especially in females), with older female

individuals having exceptionally shallow pulp cavities with less acute apices (Fisher, 2008). Finally, ontogenetically older individuals tend to display a visible tapering of the proximal portion of the tusk near the proximal margin.

Based on the criteria above, several interpretations can be made about the specimens in this study. Measurements of tusk circumference (Table 1) suggest that these specimens either represent young individuals or are all adult females. However, all of the specimens possess a shallow pulp cavity (Fig. 1). Given normal patterns of sexual dimorphism in proboscidean tusks (Fisher, 2008; Smith and Fisher, 2013), these two features allow us to interpret all individuals in this study as female. With regard to ontogeny, we cannot assign a specific age to any of the specimens, but we can interpret their ages relative to one another. 39-M possesses the shortest pulp cavity, the least acute pulp cavity apex, and has the most distinct reverse tapering of the proximal end of the tusk. These features suggest that this individual was an older female and is almost certainly the oldest individual in this study. Conversely, 41-M has the deepest pulp cavity, most acute pulp cavity apex, and lacks visible tapering of the proximal end of the tusk. Therefore, this individual is interpreted as a younger adult female and is likely the ontogenetically youngest individual studied. The other three tusks (CHM-10, ZCHM-13, and 42-M) are all similarly intermediate with respect to these three features and are thus interpreted as being from adult females of ontogenetic stage between that of 39-M and 41-M.

Second-order incremental growth record

All five of the tusks studied show strong patterns of seasonal (intra-annual) variation in second-order increment appositional thickness. With regard to number of second-order increments per first-order increment, only a single year within a single individual (ZCHM-13) was found to have 52 second-order increments per first-order increment, as has been found in mammoth tusks from temperate latitudes (Fisher, 2001). All other years within the individuals studied have complete years containing approximately 42 second-order features, with the number of third-order increments per second-order increment varying from seven to eleven during the year. This change from consistently circaseptan second-order increments to increments showing a different hierarchical pattern has been documented repeatedly in *M. primigenius* tusks from above the Arctic Circle (Fisher and Fox, 2003; Fox et al., 2007). Fisher (2001) suggested that the presence of this shift in the pattern of second-order increment formation in high-latitude mammoths may be due to a complex interaction between circadian rhythms (which are responsible for third-order increment formation) and an unknown aspect of dentin mineralization within the tusk. This hypothesis has yet to be fully explored and is outside of the scope of this paper. Regardless, this phenomenon appears to be consistent within individuals living above the Arctic Circle, which allows for two assumptions: 1) comparisons of seasonal patterns of variation in second-order increment thicknesses between different individuals should be valid, even when first-order increments are found to contain a lower-than-expected number of second-order increments; and 2) differences in number of second-order increments per first-order increment could be a coarse indicator of latitudinal movement of an individual from year to year (such as in ZCM-13), as proposed previously for the Yukagir mammoth (Fisher,

110

2007), where years with as many as 52 second-order increments were interpreted as representing time spent below the Arctic Circle.

With regard to patterns of change in growth rates measured from second-order increment thicknesses, there appears to be great variability in degree of seasonality across these five individuals. In general, periods of rapid growth (reflecting favorable foraging conditions) immediately following the boundary between winter and spring are relatively short in CHM-10, 39-M, and in several years in ZCHM-13 and 41-M, resulting in an exceptionally peaked appearance of second-order increment profiles (Fig. 3). Other years appear to show extended periods of favorable conditions resulting in longer sequences of high growth rate (see ZCHM-13 Year X-2 and CHM-10 Year X-3). Conversely, 42-M shows little change in observed growth rate within years (especially Years X-2 and X-3; Fig. 3) and generally moderate growth rates overall, suggesting relatively constant conditions during the final years of life. The relatively high and seasonally focused variability of second-order increment profiles from CHM-10, ZCHM-13, 39-M, and 41-M suggest an extremely seasonal environment that was also variable among years (Fig. 3). This is especially true in the Wrangel Island specimens, which is expected given the high latitude and insular location. However, annual patterns of second-order increment growth in individuals from the Pleistocene of Chukotka and the Holocene of Wrangel Island do not seem to suggest exceptional hardship for either of these two populations. Nor on their own do they appear to provide clues to the cause of extinction of either group.

First-order incremental growth record

111

First-order increments are the temporally longest recurring growth features observed in tusk dentin and are likely formed due to the cycling of the seasons during the solar year. Measurements of first-order increment thicknesses allow inter-annual comparisons of growth within individuals. Variations in growth within individuals could reflect either difference in forage availability between years (likely due to degree of seasonal severity within each year), different aspects of life history, or changes in growth rate over ontogeny.

All five individuals in this study show inter-annual variation in annual appositional growth. However, in at least four of these individuals (CHM-10, ZCHM-13, 39-M, and 42-M) the pattern of change in appositional growth for sequences of complete years appears to be consistently sinusoidal. Although not enough data is available from any specimen to see the pattern repeat within a single individual, all of the sinusoidal changes in annual appositional growth appear to occur over a period of four to five years (Fig. 2). The range of variation in appositional thickness for complete years in three of these samples (CHM-10, ZCHM-13, and 42-M) is significantly greater than the range in 41-M (average of ca. 2 mm in the former and 0.6 mm in the latter), and it is not clear whether 41-M shows the sinusoidal pattern. This suggests that either this pattern was not recognizable with the limited number of complete years recovered from 41-M or that whatever aspect of life history this pattern reflects might not have been a factor during these years of 41-M. It should be noted that while 39-M does not have as large a range of growth rates as do the three other specimens that show a sinusoidal growth pattern, when compared relative to greatest transverse diameter, the value observed in 39-M falls closer to the other three than it does to 41-M (range in annual increment

thickness divided by external diameter: CHM-10, 0.037; 42-M, 0.028; ZCHM-13, 0.020; 39-M, 0.018; 41-M, 0.009). Therefore, we consider the pattern observed in 39-M to be similar to that of CHM-10, ZCHM-13, and 42-M, and it therefore may reflect the same aspect of life history. Interestingly, 41-M is ontogenetically the youngest individual in this study. This suggests that the aspect of life history recorded in the other tusks either occurs only at a later ontogenetic age than this individual or that it is discontinuous in occurrence.

Fisher (1996) observed regular changes in annual increment length between periradicular bands of tusks from adult female *Mammut americanum* in the Great Lakes region of North America that were different from patterns observed in the tusks of adult males and juveniles of either sex. These measurements of extensional growth revealed a pattern of sinusoidal change in adult female mastodons that was similar to what we observe in adult female mammoth tusks from Siberia. Fisher et al. (2008) documented a similar pattern in appositional thickness measurements from three mastodon tusks from the state of New York and found annual variations in growth rate to recur over average periods of three to four years. These authors associated this pattern with reproductive life history and, more specifically, interpreted it as representing calving intervals. Although mammutids and elephantids (including *Mammuthus*) share a relatively distant common ancestor, many aspects of their life histories have been found to be conserved between the two groups (Fisher, 2009). It is therefore reasonable to assume that patterns observed in *Mammuthus* reflect aspects of life history similar to those observed in *Mammut*. Thus, we tentatively interpret the sinusoidal patterns of change in appositional growth within CHM-10, ZCHM-13, 39-M, and 42-M as representing calving

intervals (with 41-M either representing an individual below reproductive age or between calves near the time of death). The four- to five-year calving intervals suggested for *M. primigenius* by this sample are directly in line with the duration of calving intervals in modern populations of *Loxodonta* (Whitehouse and Hall-Martin, 2000; Moss, 2001).

Growth rates through time

Fisher (1996) hypothesized that changes in life history through time could be used as a test for the two most often-cited drivers of mammoth extinction. He argued that climate-driven and hunting-driven extinctions each have a different set of predictable (and often antithetical) effects on individuals and populations. Therefore shifts in biological processes through time and across many individuals could provide clues for different drivers of extinction. For example, if rapid climate change resulting in lesser quality and/or abundance of vegetative food sources was the cause of extinction, we would expect populations to show effects of nutritional stress, such as increases in age of maturation, decreases in growth rates, and increases in calving interval. Conversely, if predation were the main driver of extinction, we would expect to observe little negative impact on health of individuals, but would instead see changes in life history such as decreases in age of maturation, increases in growth rates, and decreases in calving interval, as have been observed in modern elephants and other vertebrates under hunting pressure (Carrick and Ingham, 1962; Douglas-Hamilton, 1973). Using information collected from tusks, Fisher (2009: fig. 4.3) showed that age of maturation in mastodons from the Great Lakes region appears to decrease toward the time of extinction, which is in line with predictions of the hypothesis that hunting was the

114

main driver of extinction. Although these data may indeed reflect the cause of extinction within this portion of North America, the megafaunal extinction at the end of the Pleistocene was nearly global and does not necessarily require a common cause. Therefore, it is crucial to test these extinction hypotheses on many different populations of individuals across many different regions to fully understand the demise of proboscideans and other megafauna at the end of the Pleistocene..

The sample of Wrangel Island and Chukotka mammoths studied here may begin to provide insight into changes in life history in woolly mammoths that, respectively, survived and did not survive the end-Pleistocene. However, of the aspects of life history that could be recorded within these tusk samples, few can be interpreted due to the incompleteness of each specimen. Given the above results for this sample and the discussion thereof, we are left with two aspects of life history that have been extracted from these tusks: average annual appositional growth and calving interval. Although in future studies calving interval may prove to be the more important feature of life history for determining cause of extinction, we chose to focus on average annual growth rates here, due to one major deficiency in our record of calving intervals from the data at hand: none of the specimens in this study contained enough years to demonstrate a complete and repeated sinusoidal pattern of change in annual growth. Due to this fact, we cannot be certain that any of these specimens record a complete calving interval, and we therefore must estimate the duration of the inferred calving interval based on a series of incomplete patterns. Since all four of the inferred calving intervals showed a similar duration (+/- 1 year), any error associated with this estimate would make it difficult to observe any change through time. Of course, this apparent stasis in calving

interval could be real, in which case it is notable that their magnitude is not nearly as great as what has been observed for drought-stressed *L. africana.* Still, any strong statement on calving intervals in *M. primigenius* would require longer intervals of life history from each individual and a larger sample of individuals.

Annual appositional thicknesses were taken from each specimen using microCT and averaged for complete years. When these data are compared between populations, there is a noticeable difference in the mean of the average appositional thicknesses, with the Pleistocene-age Chukotka mammoths having generally thicker increments than those of the Holocene-age Wrangel Island specimens. This is perhaps unsurprising, given that the population on Wrangel Island, initially reported as dwarfed, was smaller in body size than the mainland population (Vartanyan et al., 1993). Thus we might expect them to have thinner annual increments on average. Considering data within the Chukotka sample, annual appositional growth appears to be relatively stable through time and only shows a 0.3 mm increase between ZCHM-13 and CHM-10. Obviously, these data only represent two individuals, which complicates interpretation, but this lack of clear change in growth rate may suggest either similar living conditions during the times when these individuals were alive or that the driver of extinction was not yet affecting this population by 18,500 calBP. With respect to trends in average annual appositional growth within the Wrangel Island population, there appears to be a strong trend of decline in annual appositional thickness toward the time of extinction. Although it may seem appropriate to suggest that this pattern reflects support for the climate change hypothesis, there are several important factors to consider with respect to this sample.

The declining trend in appositional growth across the three Wrangel Island individuals could represent one of (or some combination of) three main factors: pressure from some driver of extinction, insular dwarfing, and/or ontogeny. The first has already been discussed with respect to its meaning for a population and would only be considered compelling evidence if the other two were factored out. As mentioned above, the Wrangel Island population of mammoths underwent a reduction in body size once isolated from the Siberian mainland. Vartanyan et al. (1993) suggested, based on tooth measurements, a minimum 30% decrease in body size during the first 5,000 years of mammoth occupation of the isolated island. If we compare the chronologically oldest specimen in our sample (41-M, at ca. 8,400 calBP) to the youngest specimen (39-M, at ca. 5,700 calBP) there appears to be a similar reduction of 35% in annual appositional thickness. Although it is difficult to compare decreases in tusk growth rate directly to decreases in body size, it is reasonable to assume that there would be some correlation. It would be, however, somewhat surprising if insular dwarfism was solely responsible for this trend. This is not because such a rate of decline is inherently unreasonable (35% in ~3,000 years), but more because that hypothesis would imply that reduction in size only began to occur ~3,500 years after the island was isolated (as 41-M was found to have a similar average annual appositional thickness to the two Chukotka specimens), which contradicts the findings of Vartanyan et al., (1993). Insular dwarfing might explain some of the downward trend in growth rates within the Wrangel Island population, but the 3,500 year lapse before the pattern begins is still difficult to explain. The final factor to consider is stage of ontogenetic development. This topic was discussed in prior sections of this study with regard to the developmental age of each

individual, but its implications for this trend of declining growth rates through time bears further consideration.

Fisher et al. (2014), using estimated annual increment volumes in microCT, showed a relatively consistent tusk growth trajectory throughout the lives of mastodons from Colorado. Those authors, as well as others (Fisher, 1996; Fisher, 2009; Fisher et al., 2008), show data that suggest a general decline in the annual growth of female tusks leading up to the time of death. This suggests that growth rates peak in younger individuals but then decline towards senescence. Interestingly, the chronological and relative ontogenetic ages of the three Wrangel Island specimens are antithetic (i.e, the chronologically oldest specimen was found to be the ontogenetically youngest and vice versa), which could lead to an apparent trend of declining annual growth through time that is, in reality, a reflection of ontogeny.

Although it is enticing to suggest that these data represent changes in life history as a consequence of some extrinsic pressure that would eventually lead to mammoth demise, it is clear that any trend observed here, especially within the Wrangel Island sample, may be obscured by other intrinsic factors. Utilizing annual growth rates, the sample sizes used within this study for both the Wrangel Island and Chukotka populations are too small to parse out the signals of change in growth due to ontogeny or change due to insular dwarfing from any pattern of life history change through time. Other aspects of life history such as calving interval or age of maturation may better serve as tests for these types of patterns, but more work is required to determine accurately their signals within tusks. Regardless, a larger sample is clearly needed in

order to determine the cause of extinction of both the insular and continental populations of mammoths in northeastern Siberia.

ACKNOWLEDGEMENTS

REFERENCES

Abramson, G., Laguna, M.F., Kuperman, M.N., Monjeau, J.A., Lanata, J.L., 2015. On the roles of hunting and habitat size on the extinction of megafauna. Quaternary International. http://dx.doi.org/10.1016/j.quaint.2015.08.043.

Alekseev, M.N, 1997. Paleogeography and geochronology in the Russian eastern Arctic during the second half of the quaternary. Quaternary International 41/42, 11-15.

Bocherens, H., Fizet, M., Mariotti, A., Gangloff, R.A., Burns, J.A., 1994. Contribution of isotopic biogeochemistry (^{13}C, ^{15}N, ^{18}O) to the paleoecology of mammoths (*Mammuthus primigenius*). Historical Biology 7, 187-202.

Bocherens, H., Pacaud, G., Lazarev, P.A., Mariotti, A., 1996. Stable isotope abundances (^{13}C, ^{15}N) in collagen and soft tissues from Pleistocene mammals from Yakutia: implications for the palaeobiology of the Mammoth Steppe. Palaeogeography, Palaeoclimatology, Palaeoecology 126, 31–44.

Boeskerov, G.G., 2006. Arctic Siberia: refuge of the Mammoth fauna in the Holocene. Quaternary International 142/143, 119-123.

Bryson, R.A., Agenbroad, L.D., McEnaney DeWall, K., 2010. Paleoclimate modeling and paleoenvironmental interpretations for three instances of island dwelling mammoths. Quaternary International 217, 6-9.

Carrick, R., Ingham, S.E., 1962. Studies on the southern elephant seal, *Mirounga leonina* (L.). V. Population dynamics and utilization. Wildlife Research 7 (2): 198-206.

Dean, M.C., 1987. Growth layers and incremental markings in hard tissues, a review of the literature and some preliminary observations about enamel structure in *Paranthropus boisei*. Journal of Human Evolution 16, 157-172.

Dikov, N.N., 1988. The earliest sea mammal hunters of Wrangell Island. Arctic Anthropology 25 (1), 80-93.

Douglas-Hamilton, I., 1973. On the ecology and behaviour of the Lake Manyara elephants. African Journal of Ecology 11 (3), 401-403.

Drucker, D., Bocherens, H., Mariotti, A., Lévêque, F., Vandermeersch, B., Guadelli, J.L., 1999. Conservation des signatures isotopiques du collagène d'os et de dents du Pléistocène supérieur (Saint-Césaire, France): implications pour les reconstitutions des régimes alimentaires des Néandertaliens. Bulletins et Mémoires de la Société d'Anthropologie de Paris 11 (3-4), 289-305.

Ehlers, J., Gibbard, P.L., 2007. The extent and chronology of Cenozoic global glaciation. Quaternary International 164/165, 6-20.

El Adli, J.J., Cherney, M.D., Fisher, D.C., Harris, J.M., Farrell, A.B., Cox, S.M., 2015. Last years of life and season of death of a Columbian mammoth from Rancho La Brea. In: Harris, J.M. (Ed.), La Brea and beyond: The paleontology of asphalt-preserved biotas. Natural History Museum of Los Angeles County, Science Series vol 42, pp. 65-80.

Fisher, D.C., 1987. Mastodont procurement by Paleoindians of the Great Lakes Region: Hunting or scavenging? In: Nitecki, M.H., Nitecki, D.V. (Eds.), The evolution of human hunting. Plenum, New York, pp 309–421.

Fisher, D.C., 1996. Extinction of proboscideans in North America. In: Shoshani, J., Tassy, P. (Eds.), The Proboscidea: Evolution and palaeoecology of elephants and their relatives. Oxford University Press, Oxford, pp 296–315.

Fisher, D.C., 2001. Season of death, growth rates, and life history of North American mammoths. In: West, D.L. (Ed.), Mammoth site studies: Proceedings of the first international conference on mammoth site studies. Publications in Anthropology vol. 22, University of Kansas, Lawrence, pp. 121–135.

Fisher, D.C., 2007. Life history analysis of the Yukagir mammoth. In: Boeskorov, G.G., Tikhonov, A.N., Suzuki, N. (Eds.), The Yukagir mammoth. Institute of Applied Ecology of the North [Yakutsk], St. Petersburg, pp. 142–156.

Fisher, D.C., 2008. Taphonomy and paleobiology of the Hyde Park mastodon. In: Allmon, W.D., Nester, P.L. (Eds.), Mastodon paleobiology, taphonomy, and paleoenvironment in the late Pleistocene of New York State: Studies on the Hyde Park, Chemung, and Java sites. Palaeontographica Americana vol. 61, pp. 197–289.

Fisher, D.C., 2009. Paleobiology and extinction of proboscideans in the Great Lakes region of North America. In: Haynes, G. (Ed.), American megafaunal extinctions at the end of the Pleistocene, Springer, New York, pp. 55–75.

Fisher, D.C., Beld, S.G., Rountrey, A.N., 2008. Tusk record of the North Java mastodon. In: Allmon, W.D., Nester, P.L. (Eds.). Mastodon paleobiology, taphonomy, and paleoenvironment in the late Pleistocene of New York State: Studies on the Hyde Park, Chemung, and Java sites. Palaeontographica Americana vol 61, pp. 417-463.

Fisher, D.C., Cherney, M.D., Newton, C., Rountrey A.N., Calamari, Z.T., Stucky, R.K., Lucking, C., Petrie, L., 2014. Taxonomic overview and tusk growth analyses of Ziegler Reservoir proboscideans. Quaternary Research 82 (3), 518-532.

Fisher, D.C., Fox, D.L., Agenbroad, L.D., 2003. Tusk growth rate and season of death of Mammuthus columbi from Hot Springs, South Dakota, USA. In: Reumer, J.W.F., De Vos, J., Mol, D. (Eds.), Advances in mammoth research (Proceedings of the Second International Mammoth Conference, Rotterdam, May 16–20 1999) vol. 9, Deinsea, pp. 117–133.

Fisher, D.C., Fox, D.L., 2003. Season of death and terminal growth histories of Hiscock mastodons. In: Laub, R., Miller, N., Steadman, D. (Eds.), The Hiscock Site: Late Pleistocene and Holocene paleoecology and archaeology of western New York State, Bulletin of the Buffalo Society of Natural History vol. 37, Buffalo, New York, pp. 83-101.

Fox, D.L., Fisher, D.C., 1994. Tusk growth rate in *Loxodonta africana* as recorded by incremental laminae in tusk dentin. Journal of Vertebrate Paleontology 14, 26A

Fox, D.L., Fisher, D.C., Vartanyan, S., Tikhonov, A.N., Mol, D., Buigues, B., 2007. Paleoclimatic implications of oxygen isotopic variation in late Pleistocene and Holocene tusks of *Mammuthus primigenius* from northern Eurasia. Quaternary International 169, 154–165.

Gualtieri, L., Vartanyan, S., Brigham-Grette, J., Anderson, P.A., 2003. Pleistocene raised marine deposits on Wrangel Island, northeast Siberia and implications for the presence of an Eastern Siberian ice sheet. Quaternary Research 59, 399-410.

121

Gysi, A., 1931. Metabolism in adult enamel. Dent. Digest 37, 661-668.

Hopkins, D.M., 1973. Sea level history in Beringia during the past 250,000 years. Quaternary Research 3 (4), 520-540.

Iacumin, P., Nikolaev, V., Ramigni, M., 2000. C and N stable isotope measurements on Eurasian fossil mammals, 40 000 to 10 000 years BP: herbivore physiologies and palaeoenvironmental reconstruction. Palaeogeography, Palaeoclimatology, Palaeoecology 163, 33-47.

Koch, P.L., Fisher, D.C., Dettman, D., 1989. Oxygen isotope variation in the tusks of extinct proboscideans: A measure of season of death and seasonality. Geology 17, 515–519.

Laws, R.M., 1952. A new method of age determination for mammals. Nature 169, 972.

Laws, R.M., 1966. Age criteria for the African elephant, *Loxodonta a. africana*. East African Wildlife Journal 4, 1-37.

Lister, A.M., 1999. Epiphyseal fusion and postcranial age determination in the woolly mammoth *Mammuthus primigenius*. Deinsea 6, 79-87.

Lozhkin, A.V., Anderson, P.M., Vartanyan, S.L., Brown, T.A., Belaya, B.V., Kotov, A.N., 2001. Late Quaternary paleoenvironments and modern pollen data from Wrangel Island (Northern Chukotka). Quaternary Science Reviews 20 (1), 217-233.

Lozhkin, A.V., Anderson, P.M., Vazhenina, L.N., 2011. Younger Dryas and Early Holocene Peats from northern Far East Russia. Quaternary International 237, 54–64.

Monjeau, J.A., Araujo, B., Lanata, J.L., Laguna, M.F., Abramson, G., Kuperman, M.N., 2015. The controversy space about Quaternary megafaunal extinctions. Quaternary International. http://dx.doi.org/10.1016/j.quaint.2015.10.022.

Moss, C.J., 2001. The demography of an African elephant (*Loxodonta africana*) population in Amboseli, Kenya. Journal of Zoology 255 (2), 145-156.

Rasband, W.S., 1997. ImageJ. United States National Institutes of Health, Bethesda, Maryland. http://imagej.nih.gov/ij/.

Reimer, P.J., Bard, E., Bayliss, A., Beck, J.W., Blackwell, P.G., Ramsey, C.B., Buck, C.E., Cheng, H., Edwards, R.L., Friedrich, M., Grootes, P. M., 2013. IntCal13 and Marine13 radiocarbon age calibration curves 0–50,000 years cal BP. Radiocarbon 55 (4), 1869-1887.

Rountrey, A.N., 2009. Life histories of juvenile woolly mammoths from Siberia: Stable isotope and elemental analyses of tooth dentin. Ph.D. dissertation, University of Michigan, xiii+331 pp.

Smith, K.M., Fisher, D.C., 2011. Sexual dimorphism of structures showing indeterminate growth: tusks of American mastodons (*Mammut americanum*). Paleobiology 37 (2), 175-194.

Smith, K.M., Fisher, D.C., 2013. Sexual dimorphism and inter-generic variation in proboscidean tusks: multivariate assessment of American mastodons (*Mammut americanum*) and extant African elephants. Journal of Mammalian Evolution 20 (4), 337-355.

Stauch, G., Gualtieri, L., 2008. Late Quaternary glaciations in northeastern Russia. Journal of Quaternary Science 23, 545-558.

Vartanyan, S. L., Garutt, V.E., Sher, A.V., 1993. Holocene dwarf mammoths from Wrangel Island in the Siberian Arctic. Nature 362, 337-340.

Vartanyan, S.L., Arslanov, K.A., Karhu, J.A., Possnert, G., Sulerzhitsky, L.D., 2008. Collection of radiocarbon dates on the mammoths (*Mammuthus primigenius*) and other genera of Wrangel Island, northeast Siberia, Russia. Quaternary Research 70 (1), 51-59.

Whitehouse, A.M., Hall-Martin, A.J., 2000. Elephants in Addo Elephant National Park, South Africa: reconstruction of the population's history. Oryx 34 (1), 46-55.

Table 4.1. ^{14}C dates and calibrated ages of Wrangel Island and Chukotka specimens. Circ.= greatest circumference (in mm); Diam.=greatest diameter (in mm).

Sample	Laboratory Number	^{14}C age BP	Calibrated age BP	Circ. (Diam.)
ZCHM-13	CAMS-10324	26,370±150	30,335 – 30,976	231 (75)
CHM-10	CAMS-10323	15,235±50	18,353 – 18,653	224 (73)
41-M	AA-98464	7,597±79	8,286 – 8,555	207 (63)
42-M	AA-98465	6,255±70	6,971 – 7,321	216 (66)
39-M	AA-98463	4,972±41	5,604 – 5,756	165 (50)

Figure 4.1. Micro-computed tomographic slice of tusk 39-M in longitudinal cross section showing annual variations in density. White arrows mark hypothesized winter-spring boundaries with hypothesized years labeled in between. White dash arrows mark the edges of a CT scan artifact. DCJ = dentin-cementum junction (marked by black and white dashed line). Scale bar is 1 cm.
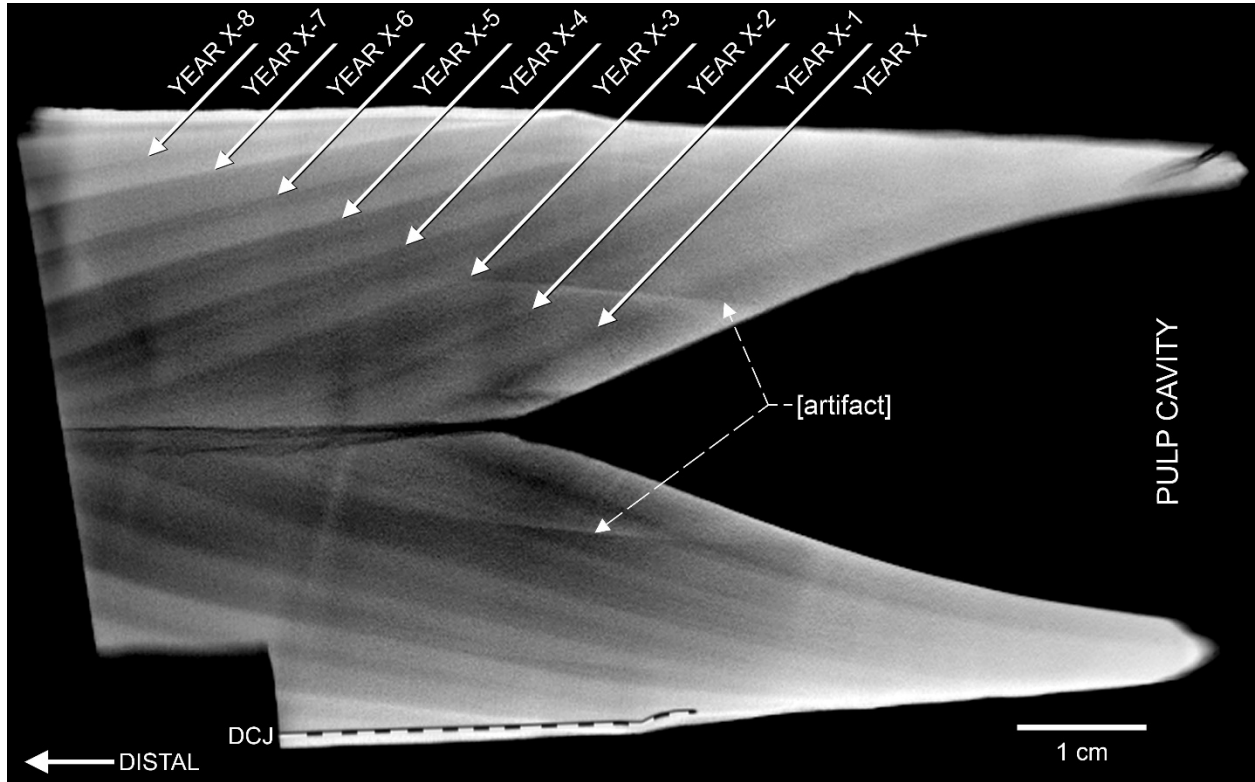
Figure 4.2. Measurements of first-order (annual) increment thickness from microCT images for A) ZCHM-13, B) CHM-10, C) 41-M, D) 42-M, and E) 39-M. Year X is the final, incomplete year of life recorded at the pulp cavity, and each year numbered following the convention "X-1" is from earlier in that individual's life.
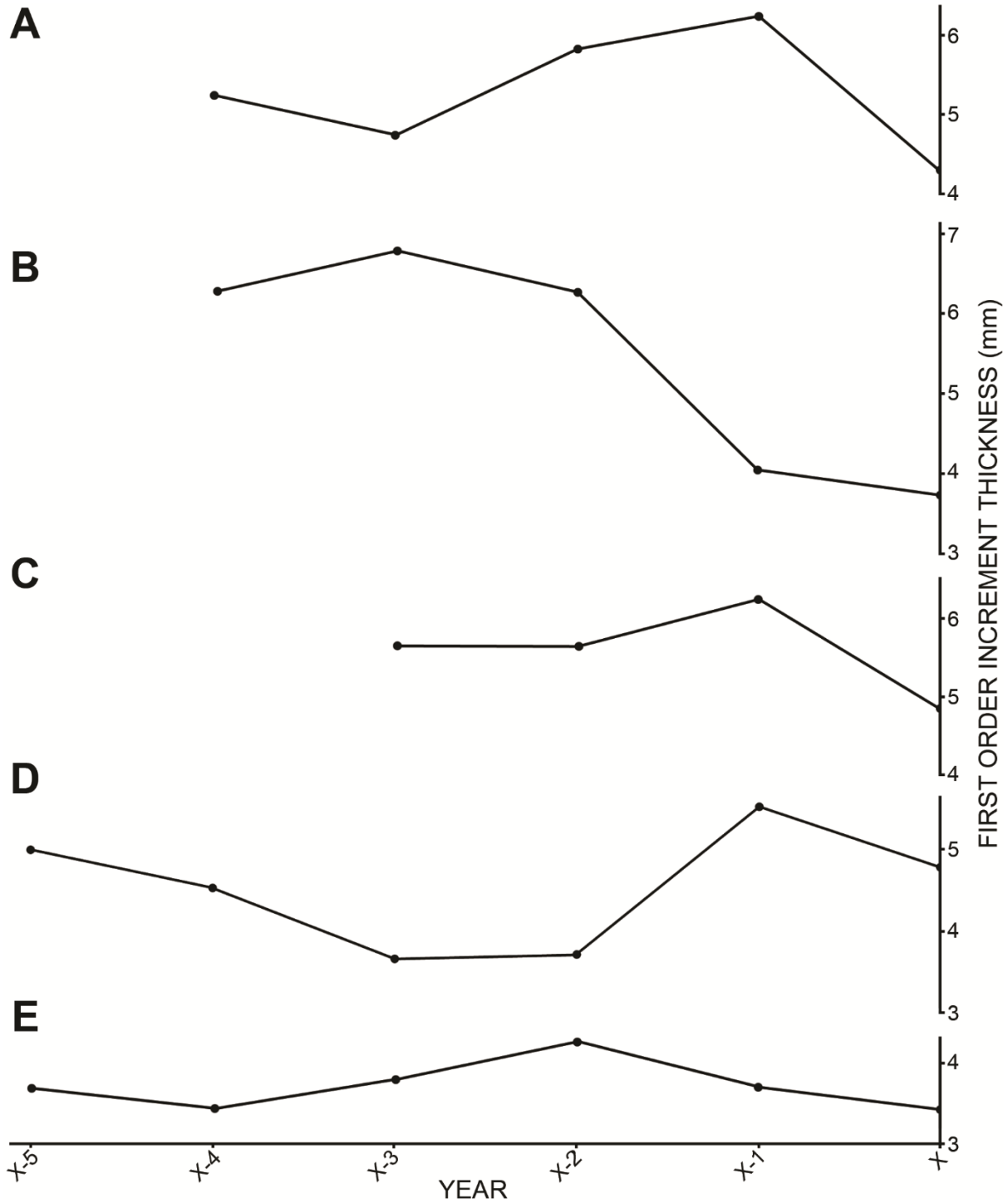
Figure 4.3. Results of thin section and microCT analyses showing patterns of second-order (weekly) increment growth for A) ZCHM-13, B) CHM-10, C) 41-M, D) 42-M, and E) 39-M. Years are labeled as in Figures 1 and 2 and are bounded by zones of transition from high to low x-ray attenuation in microCT (symbolized by white-to-black rectangles). Vertical dashed lines represent hypothesized winter-spring boundaries. 2^0 = number of second-order increments within each year of tusk growth.

128
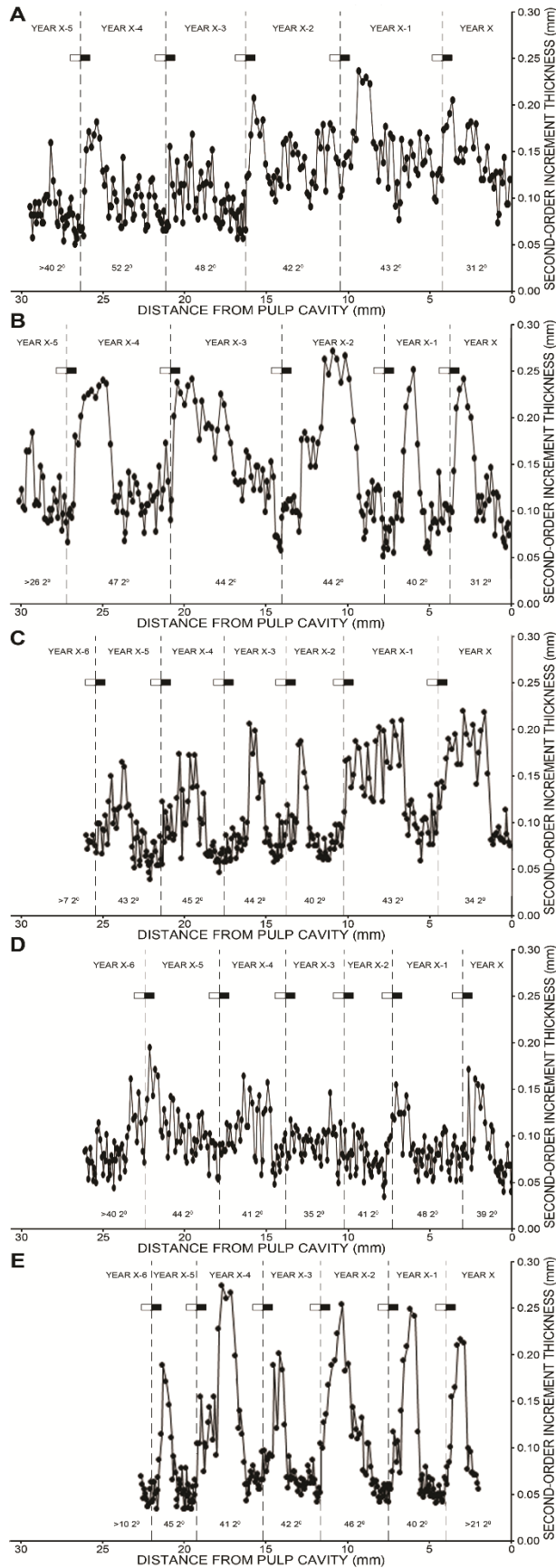
Figure 4.4. Average first-order (annual) increment thickness (in mm) for Chukotka and Wrangel Island specimens relative to AMS age estimate. calBP = calibrated years before present.
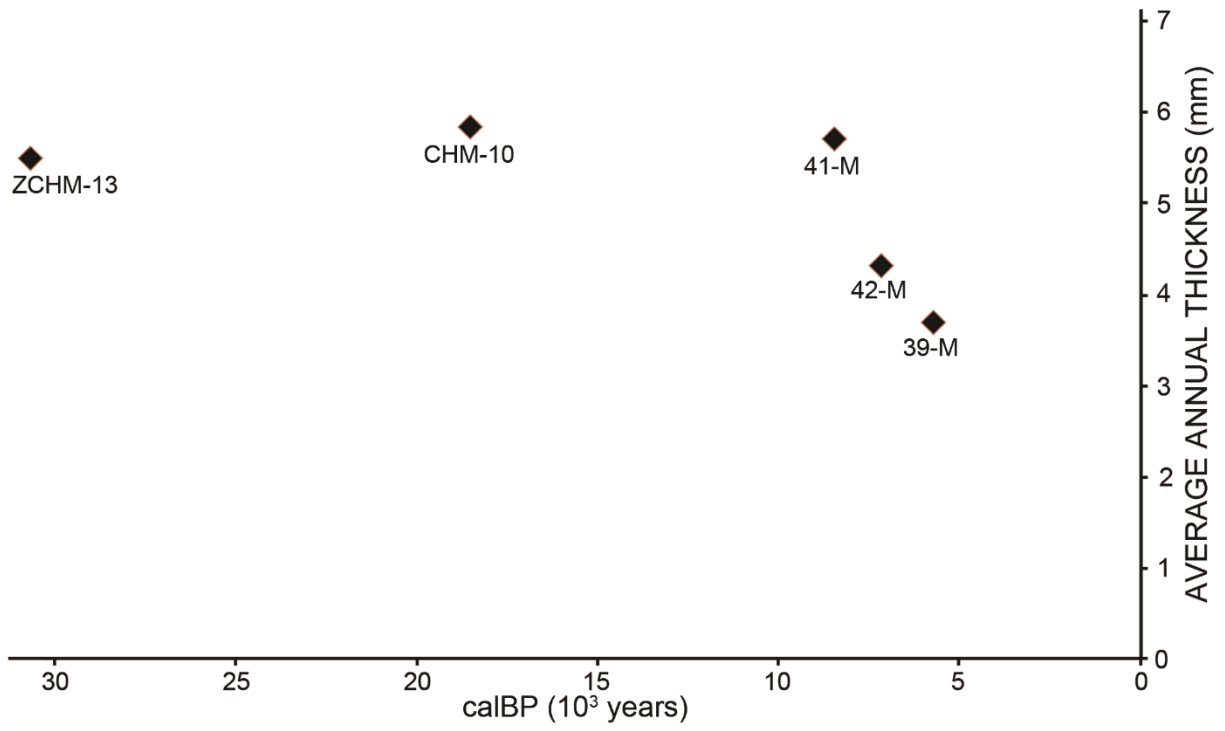
CHAPTER 5

Reproductive life histories of female woolly mammoths from microCT scans of whole tusks

INTRODUCTION

The debate over the cause of the near-global extinction of large mammals at the end of the Pleistocene has taken place over the last two centuries with no clear consensus (Grayson, 1984). Current dominant hypotheses for the cause of this extinction can be broken down into two major categories: climate-related and human hunting-related drivers (or some combination of both) (Koch and Barnosky, 2006). Studies in support of either extinction hypothesis frequently rely on strictly temporal data (e.g., timing of human migration into a region relative to timing of extinction) to argue their cases. However, the action of these two potential agents of extinction is broadly coeval with the presumed period of mammoth decline (and with each other), which makes it difficult to decouple their effects (if any). There is also an issue, especially in the case of climate change, of determining cause and effect. For example, northerly shifts of the taiga in northern Siberia at the end of the Pleistocene could either be interpreted as relating to disappearance of the mammoth steppe biome due to changing climate or as change in floral communities due to reduction in herbivore populations as a consequence of human hunting (Zimov et al., 1995; Augustine and McNaughton, 1998; Zimov, 2005; Johnson, 2009; Barnosky et al., 2016). Finally, the sparse record of

humans in the Pleistocene makes it difficult to identify accurately the timing of human arrival in a given region. Given these issues, alternative approaches to assessing cause(s) of extinction may be more viable.

Fisher (1996) argued that changes in the timing and duration of different aspects of life history could provide a test for cause of extinction in proboscideans. He suggested that some aspects of life history should change predictably and differently under a climate change- versus hunting-driven cause. Therefore, assessing life history in populations before and during the extinction and observing how life history changes could fingerprint the overall cause of extinction. Two such aspects of life history, calving interval and age of maturation, are expected to be antithetically effected under a hunting- versus climate change-driven extinction (Fisher et al., 2008; Fisher, 2009). The detailed record of growth found in proboscidean tusks can provide valuable information about life history from extinct taxa (Fisher, 1996; 2009; Fisher et al., 2008; 2014; Rountrey et al., 2007; El Adli et al., 2015; 2016; 2017; Cherney, 2016; Grigoriev et al., 2017). These tusk growth records could provide extensive data on calving history over the lives of female mammoths, a potentially vital key to our understanding of end-Pleistocene extinction (Fisher, 1996; Fisher et al., 2008; El Adli et al., 2016).

Tusks are the enlarged, continuously-erupting incisor teeth of proboscideans. They are capped at the distal tip by enamel and are covered externally by cementum. However, the overwhelming bulk and volume of each tusk is composed of dentin (hydroxylapatite and a collagen component), which makes up the internal portion of the tusk. Dentin forms through apposition of conical layers at the pulp cavity surface. The tusks of all elephantimorphs that have been studied to date contain a nested hierarchy

131

of periodically-forming dentin increments. In mammoths, these features have been found to form on a daily, weekly, and yearly basis (Fisher, 2001). Assessment of these compositional and structural growth increments has been accomplished through serial isotopic analyses, plane-polarized light microscopy, and high-resolution X-ray computed tomography (microCT) (Koch et al., 1989; Fisher, 1996; Rountrey et al., 2007; Fisher et al., 2014; El Adli et al., 2016).

In the past half-decade, microCT analyses of portions of proboscidean tusks have documented regular changes in density within dentin corresponding to years of growth (Fisher et al., 2014; El Adli et al., 2015; 2016; Cherney, 2016). This finding allows for analysis of interannual variation in tusk growth rates without the need for destructive sampling, which may otherwise prohibit the investigation of a specimen. However, these previous analyses were conducted on small portions of tusk (less than ~10 cm in length and diameter) due to size constraints of available microCT scanners. Until recently, industrial microCT scanners large enough for analyses of complete adult tusks were inaccessible, while most medical CT scanners lack the necessary power and resolution to image tusk density features. The recent acquisition of a large-bed industrial microCT scanner at the University of Michigan has allowed for imaging of the internal structure of whole tusks of woolly mammoths, which allows access to these extensive datasets of growth history from an individual mammoth's life. We here use these data to interpret multiple decades of life history information for Siberian woolly mammoths and assess any changes in ontogenetic timing and/or duration of different aspects of life history at the end of the Pleistocene.

MATERIALS AND METHODS

Sample Selection

Complete or nearly-complete tusks from 10 individuals (43-M, 48-M, 2007/003, Malolyakhovsky, TA-3, ZCHM-28, ZCHM-29, ZCHM-30, ZCHM-38, and ZCHM-46) of *Mammuthus primigenius* from northern Siberia were analyzed in this study. Specimens bearing the field designation "ZCHM" were collected from the northern portion of Chukotka. Specimens marked "TA" and "2007" were collected on the Taymyr Peninsula. The Malolyakhovsky individual was found on Maly Lyakhovsky Island (one of the New Siberian Islands; see Grigoriev et al., 2017). Specimens labelled "M" were collected from Wrangel Island. Table 5.1 provides a list of specimens along with their sex, provenance, and radiochronological age. Sex was determined for each specimen based on aspects of tusk morphology (see Chapter 4 discussion) and, in the case of TA-3 and ZCHM-46, from aDNA (Cherney, pers. comm.). All tusks were recovered from permafrost, which allowed for exceptional preservation of most of the study specimens. All tusks internally preserve the cream-white coloration and consistency of fresh ivory, as observed where dentin is exposed. Small portions of dentin in some tusks showed a whiter color and chalky texture, suggesting some degree alteration during burial. Although great care was taken to dry each specimen as slowly and evenly as possible following recovery from the field, desiccation fractures are common within the dentin and cementum layers of many of the tusks in this sample.

Radiometric Dating

A small (~1 cm^3) sample block of dentin was cut from each tusk using a coping saw or hacksaw. Each dentin block was weighed, wrapped in aluminum foil, and placed in an individual plastic sample bag. Samples were sent to either Beta Analytic (Beta), NSF-Arizona AMS Facility (AA), or Centre for Isotope Research at the University of Groningen (GrA) for collagen extraction and Accelerator Mass Spectrometry (AMS) dating. Radiometric dates were reported by each facility as radiocarbon years before present (^{14}C age BP), but were converted to calibrated dates in calendar years before present (calBP) using IntCal13 (Reimer et al., 2013). Both calibrated and uncalibrated dates for each specimen are reported in Table 5.1.

CT Scanning Procedures

Each tusk was cut into multiple ~1 m sections in order to fit inside the available CT scanner. Tusks were cut using either a coping saw, hacksaw, or bandsaw with a bimetal or carbide grit blade. Almost all tusk sections were scanned using the Nikon X TH 225 ST industrial microCT scanner housed at the University of Michigan Department of Earth and Environmental Sciences. The only exceptions to this were TA-3 and the distal third of ZCHM-46, which both had previously been cut into small segments and scanned on a SCANCO Medical μCT100 at the MicroCT Core Facility at the University of Michigan School of Dentistry by M Lynch as a portion of the dissertation research of MD Cherney (see Cherney, 2016). The Malolyakhovsky specimen was scanned in Yakutsk, Russian Federation, in a Siemens Somatom Definition AS medical CT scanner by DC Fisher and colleagues.

Tusks scanned in the Nikon X TH 225 ST were held vertically within the scanner

using a five gallon plastic bucket weighted with sand for support and polyethylene foam to secure the tusk's orientation within the bucket. Each tusk section required multiple, partially-overlapping scans in order to image the complete specimen. When possible, the "batch scan" setting was used in Nikon Inspect-X to automate multiple scans along a specimen; otherwise they were scanned individually.

Female tusks were scanned at a resolution of 60 μm to 80 μm uniform cubic voxels, while male tusks yielded 120 μm uniform cubic voxels. Differences in scanning resolution between specimens are a result of the practical limitations of the scanner at a given tusk diameter (i.e., due to the nature of the cone beam, higher-resolution scans have smaller fields of view and therefore cannot fully image specimens over a certain diameter). Despite the quartered resolution of the specimens imaged using the coarsest versus finest settings, the internal density features which this study relies on were visible in all specimens scanned. Further stemming from differences in diameter along the length of each tusk and between different tusks, scan settings were optimized for each individual and were modified for different sections within the same tusk where necessary (see Table 5.2 for a detailed list of scanning parameters for each specimen). All specimens were scanned using the "minimize ring artifacts" setting in Nikon Inspect-X.

CT Visualization and Scan Alignment

Once scans were completed, projections were then reconstructed using Nikon CT Pro 3D. Center of rotation was determined automatically using two different slices (dual slice selection). Beam hardening was minimized using beam hardening reduction

setting 2 or 3. The scans were then reconstructed and exported as either 32- or 16-bit floating point .vol files or as a tiff stack.

Volume files from each scan were visualized using Amira 6.0.1 on an HP Z840 Workstation with an Intel Xenon CPU E5-2623 v3 3.00 GHz processor and 128 GB of RAM, located in the University of Michigan Museum of Paleontology 3D Laboratory. Due to limitations in available RAM, each scan was first resampled using Lanczos filtering to produce 100 µm uniform cubic voxels. Individual scans within each tusk section were then aligned with each other using a combination of automated registration and manual alignment of internal and external features of the tusk, as well as alignment of thermoplastic adhesive markers placed on the specimen at the time of scanning. Alignment between complete tusk sections was done manually using the aid of photogrammetrically produced 3D surface models of the whole tusk. Once the whole tusk was aligned, each scan was filtered using a Gaussian filter set to 3D interpretation and kernel Type set to Standard. Standard deviation in the X, Y, and Z planes was set to 2 and kernel size [px] was set to between 3 and 5 in the X and Y planes and 2 in the Z plane. This minimal filtering removes noise from each scan, which makes annual X-ray attenuation features within the tusk easier to visualize. Individual scans are then merged using "standard" interpolation to produce a single volume file of the whole tusk.

Curved slices were produced using the "curved slice" module in Amira 6.0.1 by creating a B-spline curve that passes through each slice at the center of the tusk and then projecting two perpendicular curved planes through the tusk (Fig. 5.1). The "ortho slice" module was used to find the center of the tusk at a given slice. Control points for the B-spline curve were added every 20 slices and the B-spline curve is generated

136

using interpolation mode and "degree" set to 3. Sampling along the curved slice was set to "finest" and the colormap was adjusted manually to improve the appearance of density features. Each curved slice was extracted in orthographic view as a high-resolution (>10k x 10k pixels) tiff using the "snapshot" module and the "render tiles" option set to greater than 5 x 5 with antialiasing set to 1.

Annual Increment Measurements

All measurements of annual features (see Figure 5.2) were done using ImageJ (Rasband, 1997). Annual increment areas were measured using the Polygon Selection tool and were saved as Report Object Instance (ROI) sets. Extensional increments were measured between tips of annual increment cones along the center of the tusk. Appositional thicknesses were measured normal to the inclined surface of each cone beginning at the halfway point between the cone tip and proximal margin on the trailing edge of each cone. Angular measurements of cone apices were made on both the leading and trailing edge of each annual increment cone and were then averaged for each year. Tusk radius measurements were made from the apex of each annual cone to the external surface. Measurements were made on both of the perpendicular curved slices, where appropriate, and were then averaged to account for variability in the cross-sectional shape of each annual increment.

Generalized Additive Models

We used generalized additive models (GAMs) and generalized additive mixed models (GAMMs) to identify regular patterns of tusk growth. Generalized additive

137

models are modifications of the generalized linear model (which itself is a simplified

form of linear regression) combined with aspects of non-parametric additive models

(Hastie and Tibshirani, 1986). GAMs presuppose that the relationships between

variables follow a smooth pattern, which can be either linear or nonlinear. These models

employ a penalty for complexity (e.g., "non-smoothness", "wiggliness", or departure

from linearity), but are allowed to depart from simplicity if a more complex pattern is

supported by a given dataset. GAMMs further modify GAMs by incorporating

components of mixed-effects models. Such models can account for fixed effects within

the dataset, such as those related to provenance or sex of the specimen (or a

combination of both). Within this study, we employed GAMs to model the patterns of

growth within individuals, while GAMMs were used to generalize trends in growth

across the study sample.

GAMs and GAMMs within this study are explored using the "mgcv" package in R.

Both analyses are conducted using spline-based smooth terms with cubic regression

splines set as the smooth class. Penalization of cubic regression splines is based on the

integrated square second derivative cubic spline penalty (see Wood, 2006). The

settings for the tuning parameters used differed for GAMs and GAMMs.

For GAMs, the tuning parameter "k" (i.e., basis dimension of the smoothing

matrix for each smooth term) was set to n-1 where "n" is the number of data points for

the specimen analyzed. This was done to allow the GAM the most freedom to identify

potentially complex patterns within the relatively small set of data for each specimen. To

check our GAMs and ensure that our values for "k" were not too large, we confirmed

that the effective degrees of freedom (edf) were less than k-1 for each model, as

suggested by Wood (2006).

The tuning parameters of our GAMMs were optimized by minimizing the generalized cross-validation score (GCV), while iteratively increasing "k" from an initial value of approximately n/2 until the lowest GCV is attained. Fixed effects for all GAMMs within this study were specimens (i.e., effects of data nested within a specimen) and regions (i.e., effects of specimens nested within a region). Males were not included in GAMMs due to the low number of specimens and data points.

<center>RESULTS</center>

MicroCT Features

X-ray computed microtomography (microCT) reveals numerous density features within the dentin occurring throughout each tusk. These features match the conical shape of the pulp cavity surface, indicating that they are features related to tusk growth. In terms of X-ray attenuation, the features can be described (moving in the direction of time of formation) as a sequence of lower-attenuation dentin gradually transitioning to higher attenuation before abruptly returning to lower attenuation and then repeating the pattern. Overall, these features are predominantly composed of lower-attenuation dentin, with higher attenuation dentin often making up less than a quarter of the appositional thickness of the sequence. Studies of similar density features in other proboscidean tusks that utilized a combination of microCT, thin section, and stable isotope analyses (Fisher et al., 2014; El Adli et al., 2015; 2016) determined that each full cycle in dentin density represents a year of tusk growth. Furthermore, El Adli et al. (2016; see Chapter 4) observed that the abrupt transition from high- to low-attenuation

in each density cycle consistently coincided with a rapid change from thin to thick second-order (weekly-forming) increments in Siberian specimens of *Mammuthus primigenius*. Those authors reasoned that the abrupt density transition in each cycle likely reflects the seasonal change from winter to spring. This abrupt shift in X-ray attenuation provides an ideal visual marker for identifying annual growth features within a tusk and is therefore used in this study to mark the boundary between years. Furthermore, we frequently observe partial delamination of annual increments from one another along the abrupt density transition at the winter-spring boundary and parallel to the orientation of the pulp cavity surface. This type of delamination between dentin layers is common in proboscidean tusks and occurs in response to stresses associated with uneven desiccation of the hygroscopic dentin following removal from permafrost and storage in a drier environment. Since delamination appears often to occur along the winter-spring boundary, this provides a further visual aid in identifying the boundary between years.

Within ZCHM-28, we observed 35 abrupt density transitions from the distal tip to the pulp cavity. Of these visible density features, 32 are complete enough to allow for measurement (Table 5.3). The three remaining annual features are located at the broken distal tip, where abrasion of the tusk during life has removed material from the portion of the tusk containing the record of earlier life and has left behind only the proximal ends of the distal-most three years. Abrasion of the tusk during life is common in proboscideans (especially on the outside curve, near the distal end of the tusk). This wear can remove the outer cementum and enamel layers from the tusk and eventually obliterate the external-most portions of dentin increments (Fisher, 1996).

Density features observed in ZCHM-29 are relatively distinct and are clearly visible throughout the tusk's length. Of the 29 density features observed in the tusk, 26 years of growth are complete enough to make most of our measurements (Table 5.4). As was the case with ZCHM-28, 3 years of growth at the distal end of the tusk are too incomplete for measurement. However, unlike the abraded tusk tip of ZCHM-28, the tip of the tusk of ZCHM-29 was not available for study. With regard to the proximal portion of the tusk (which was available for study), the proximal margin has been broken and abraded leaving a thick proximal end (in contrast to the blade-like edge of a complete tusk). This degree of abrasion in the proximal region makes it difficult to estimate annual areas accurately for the final five years of life due to a lack of proximal portions for those increments. Measurements of tusk radii, angles of cone apices, extensional lengths, and appositional thicknesses are still feasible, however, for the last five years of life, because these measurements utilize aspects of the distal half of each cone.

ZCHM-30 shows variable preservation of X-ray density features, with increments being most visible in the middle section of the tusk, less visible in the proximal section, and faint in the distal section. The muted features in the distal portion make measurement difficult in this region of the tusk. However, multiple delaminations between dentin layers along winter-spring boundaries facilitate recognition of annual boundaries and make consistent measurement possible. Within ZCHM-30, we observe 37 density features, 34 of which permit measurements (Table 5.5). The difference between measurable and unmeasurable increments, as in ZCHM-29, is due to the tip of the tusk being removed from the specimen and being unavailable for study, which has resulted in only partial increments being visible near the distal-most part of the tusk.

ZCHM-46 preserves only faint density features throughout the tusk, making several types of measurements (e.g., area and appositional thickness) unreasonable to collect for this individual. Density features are consistently visible near the center of the tusk, but tend to quickly fade toward the outer surface. Identification of years, especially in the proximal portion of the tusk, was aided by the location of delaminations within the dentin. Based on these features, we were able to record 41 density increments within ZCHM-46, all of which allowed measurements of extensional length (Table 5.6).

The Malolyakhovsky specimen exhibits exceptional preservation of X-ray attenuation features throughout the entirety of the tusk (Fig. 5.1). Unlike the other specimens in this study, this individual was stored in an ice cave for several years and did not experience extended periods of drying within a museum collection before being CT-scanned. This may speak to the importance of scanning "wet" specimens recently removed from the field in order to obtain best results in CT. The proximal-most 20 annual increments have delaminated from adjacent increments near the external surface of the tusk, but these delaminations have not progressed to the center of the tusk. Due to the lack of delamination near the center of the tusk, we can observe that each delamination coincides with an abrupt transition from high to low X-ray attenuation, confirming that these features of desiccation do consistently occur at the boundary between dentin that formed in the winter and dentin that formed in the spring. In the Malolyakhovsky tusk, we observed 42 annual growth features for measurement (Table 5.7).

Tusk 2007/003 preserves relatively faint microCT features, but unlike the features in ZCHM-46, they are visible throughout the tusk. Attenuation features are

142

clearest in the middle portion of the tusk's length and become increasingly more difficult to identify near the proximal and distal ends. Despite this issue, we were able to confidently take measurements throughout the entirety of the tusk after careful inspection of the curved microCT slices. We observed 17 annual density features and could make measurements on 16 of them (Table 5.8). The single unmeasurable year occurs at the distal tip of the tusk where abrasion during life has removed the distal portion of the cone.

We observed 11 moderately well preserved density features throughout the tusk of TA-3. Measurements of appositional thickness, extensional length, tusk radius, and apex angle were measured for all of these 11 annual increments (Table 5.9). However, the proximal end of the tusk (containing the pulp cavity) was not available for study and, as a consequence, the proximal-most portions of the final two years were not within our dataset, making area measurements for those years unavailable.

Specimen 43-M has 20 readily visible density features in the tusk. Attenuation features were variably discernible throughout the tusk (although always visible), with the high-attenuation portions of some years being significantly brighter than those of other years. Due to a transversely broken tusk tip, we were only able to measure annual areas, extensional lengths, tusk radii, and apex angles for the proximal-most 17 increments (Table 5.10). Enough of the proximal portions of two earlier years of life were present to warrant appositional thickness measurements from those distal-most years.

Tusk 48-M shows variable preservation of X-ray density features. The proximal and distal portions of the tusk show the clearest density features, while features in the

middle portion are less visible. Likewise, the portions of density features near the external surface of the tusk are often more difficult to observe than in the central portion of the tusk. We were able to document 24 increments from which we could measure extensional lengths and tusk radii. We were only able to make measurements of area, appositional thickness, and apex angle when enough of the proximal portion of an increment was visible to make measurement, which resulted in sporadic documentation of these features in 48-M (Table 5.11).

ZCHM-38 contains the faintest attenuation features of the tusks in this study. Although attenuation features can be seen throughout the tusk's length, they are most readily visible in the middle portion of the tusk and are increasingly less visible in the proximal and distal regions. Furthermore, these density features are most easily identified in the center of the tusk, but rapidly become imperceptible towards the cementum. This lack of clear features throughout the tusk makes accurate measurements of area, appositional thickness, and cone apex angle impossible. However, extensional length can be measured, as that relies on the more visible portions of the density features at the center of the tusk. With that in mind, we observed and measured 17 density transitions within ZCHM-38 (Table 5.12).

Tusk Radius

In the past, authors such as Elder (1970), Pilgram & Western (1986), Sukumar et al. (1988), Fisher (1996, 2009), and Smith & Fisher (2011, 2013) have documented the circumferences of proboscidean tusks and discussed their growth patterns and differences between sexes. Those authors used circumference rather than radius or

diameter to avoid issues of variability in cross-sectional geometry that occur throughout

ontogeny and among individuals. Although we recognize this issue, we have opted to

document the greatest tusk radius for each year from either curved slice to allow for

measurements in tusks that are missing portions of the outside surface (such as TA-3,

ZCHM-38, and ZCHM-46).

Measurements of the greatest tusk radius at the tip of each annual dentin cone

were taken for all tusks within the study sample. All specimens show an overall trend of

increasing tusk radius from distal to proximal, but there is variation in the greatest

thickness for each tusk (Fig. 5.3). Fisher (2008) compared degree of tooth eruption and

wear to tusk circumference at the alveolar margin in *Mammut* and documented a

general increase in circumference with higher Laws Age Group (Laws, 1966), as well as

significantly larger circumferences in males relative to females for individuals of similar

ontogenetic ages. As such, years with narrower radii generally formed earlier in life than

those with greater radii. However, it should be noted that near the tusk tip abrasion

during life can reshape the tusk, leading to a smaller radius than expected given the age

of formation for that year. Furthermore, Smith and Fisher (2011, 2013) documented a

moderate proximal tapering of tusk circumference with advanced age. Applying these

principles, tusks within this study with a relatively small maximum radius (e.g., TA-3 and

2007/003) likely represent individuals that died at a much younger age than those with

greater radii (e.g., ZCHM-28, ZCHM-29, ZCHM-30, ZCHM-46, 43-M, and the

Malolyakhovsky specimen). This assessment is further corroborated by the fact that

specimens with greater tusk radii also have generally greater tusk lengths, as well as

shallower pulp cavities (see results on cone apex angle below; also see Fisher, 1996,

2009; Smith and Fisher, 2011, 2013).

Factoring in relative ontogenetic age of the individuals within the study, the overall pattern of growth (with respect to tusk radius) appears to be a consistent year-to-year increase in tusk radial thickness during early years of life, with rates of increase in radius eventually slowing at some point during adulthood. Tusks that contain multiple decades of growth (such as ZCHM-28, ZCHM-30, ZCHM-46, and the Malolyakhovsky specimen) also show a decrease in tusk radius within the final decade of life. This constriction of the proximal portion of the tusk was also documented by Smith and Fisher (2013) who suggested that this was a feature of old age. Applying a generalized additive mixed model to the dataset recovers an overall trend that matches our interpretation of ontogenetic trend based on this observation (Fig. 5.4; Table 5.13).

Cone Apex Angle

Annual increments in tusks, as has been noted repeatedly above, are conical in shape. Although their geometry is admittedly more complex than that of a simple cone, such a generalization is often appropriate as a first-order approximation. As such, we can simplify the shape of a former pulp cavity surface in longitudinal section to that of a triangle. In this simplification, the base of the triangle is the diameter of the tusk and the height is the depth of the pulp cavity. Using basic trigonometric functions (e.g., sine or cosine), we can then easily calculate the depth of the pulp cavity from the angle of the apex of each annual cone and the diameter of the tusk at that year. Furthermore, when diameter is the same between different years but the angles of the cone apices change, then there must be a corresponding change in pulp cavity depth. Therefore, angular

146

measurements of annual cone apices give a relative approximation of the depth of the

pulp cavity at the time when the increment formed (given a known tusk diameter). As

such, more acute (lower-angle) cone apices can be associated with a deeper pulp

cavity at time of formation, while less acute (higher-angle) cone apices are associated

with a shallower pulp cavity. Smith and Fisher (2011, 2013) documented both sexual

dimorphism and an ontogenetic trend in pulp cavity depth in *Mammut* and *Loxodonta*.

Those authors, along with Fisher (1996), reported the general trend that pulp cavity

depth decreases with increasing ontogenetic age. In other words, older individuals tend

to have shallower pulp cavities than younger individuals. This pattern is further modified

when factoring in the individual's sex, in that males tend to have deeper pulp cavities

than females of a similar age. These past studies involving pulp cavity depth have relied

on single measurements of pulp cavity depth per specimen (i.e., pulp cavity depth at

death) across multiple specimens to make these observations. Our data provide the first

documentation of this feature throughout the life of an individual, which gives us more

detailed insights into the changes in pulp cavity depth throughout ontogeny. To a first

order, our data corroborate both the ontogenetic trend documented by Fisher (1996)

and Smith and Fisher (2011, 2013) in *Mammuthus primigenius*, as well as the pattern of

sexual dimorphism (Fig. 5.5).

     All tusks in our study for which measurements of cone apex angles could be

made show either a general increase in the angle of each cone apex toward the pulp

cavity (becoming less acute through time) within each individual or, in the case of TA-3,

no significant change in angle (Fig. 5.5). When removed from any context of relative

ontogenetic age, these specimens appear to have significant spread in the possible

range of angle measurements within individuals and often little overlap among individuals. However, when these angle measurements are compared relative to the radius of the tusk at a given year (a rough approximation of relative age), a coarse relationship emerges in which lower-angle cone apices are associated with narrower tusks and vice versa (Fig. 5.6). This suggests that the spread in the range of cone apex angles among individuals observed in Figure 5.5 is likely due to differences in the ontogenetic ages of the individuals rather than intraspecific variation. Furthermore, fitting a generalized additive mixed model to these data shows a statistically significant, near-linear (effective degrees of freedom = 1.875; $p<0.05$) positive trend between cone apex and distance from the pulp cavity (Fig. 5.7; Table 5.14).

Although the overall trend of decreasing pulp cavity depth with age is clearly present in the study sample, the pattern appears to be variable within each individual. All individuals show extended runs of years with a seemingly steady increase in the angle of cone apices, but many have a pattern of growth marked by an undulating change in angle over a period of several years with a net increase in cone angle overall (Fig. 5.5). This undulation in angle can vary over a range of up to eleven degrees (in the case of the Malolyakhovsky specimen), but more often varies by less than five degrees. The frequency of this undulating pattern is variable both within specimens and among specimens and can range from as little as three years to up to nine years. The cause of this pattern is unclear, but likely has to do with changes in the rates of apposition relative to extension due to conditions during life.

In general, years associated with shorter tusk radii (<30 mm) and more acute cone apex angles (<20 degrees) tend to have little to no increase in angle over an

148

extended series of years (see TA-3 and 2007/003, as well as the distal-most years in ZCHM-29, ZCHM-30, and the Malolyakhovsky specimen; Fig. 5.6). Years associated with greater tusk radii and higher cone apex angles are more likely to be associated with either a trend of steady increase or an undulating pattern of cone apex angle. 48-M, by contrast, has relatively narrow cone angles given its radius due to the fact that this individual is a male. In ZCHM-29, ZCHM-30, and the Malolyakhovsky specimen, a trend of steady increase in apex angle (of variable duration) precedes the onset of the undulating pattern, and, in the case of ZCHM-30 and the Malolyakhovsky specimen, follows a period of little change in angle during the earliest years of life recorded. It is not clear if this represents a general ontogenetic pattern, but it may warrant investigation in future studies.

Annual Increment Area

Annual area measurements, measured in longitudinal section, were possible to make in seven of the ten tusks analyzed, all of which were females. Five of these individuals (43-M, ZCHM-28, ZCHM-29, ZCHM-30, and the Malolyakhovsky specimen) show an overall trend of steady decline in annual area toward the pulp cavity (Figs. 5.8–5.12). The two remaining specimens (2007/003 and TA-3) both record a rapid year-to-year increase in annual area, but in the case of 2007/003, this trend abruptly shifts to an apparent decline in growth rate following the largest increment measured in the specimen (Figs. 5.13 and 5.14). An overall positive versus negative trend in area throughout life seems like a major discrepancy among individuals, which could lead one to argue for high variability in mammoth tusk growth rates. However, when ontogenetic

age of the specimens is taken into account, a clear pattern emerges.

Based on measurements of tusk radius and depth of the pulp cavity (see above; Figs. 5.3–5.7), both 2007/003 and TA-3 represent young individuals, whereas the other specimens are clearly older animals. Furthermore, Cherney (2016) analyzed TA-3 and concluded, using measurements of estimated annual increment volumes, that the tusk contained portions of years 3 through 17 (from birth). Based on Cherney's (2016) analysis, our measurements of area in TA-3 span ages 5 to 13 in the animal's life. Although we could not make a similar estimate of age from birth for 2007/003, the ranges in tusk radius and length suggest that this individual died at a slightly greater age than TA-3, with some overlap in age between the two individuals probably recorded in the tusk. If these two specimens represent individuals containing juvenile years and the other four specimens contain adult years, then a consistent pattern emerges where area increases rapidly in younger individuals but then steadily declines throughout adulthood.

Beyond the general primary trend of decreasing annual areas during adulthood, a more complex secondary pattern is visible within the sequences of annual growth measurements in all of the adult individuals, as well as in the portion of the 2007/003 tusk containing an overall decline in growth rate. This secondary pattern occurs over a period of three to five years in duration (measured from peak to peak) and is composed of two parts: 1) a successive decrease in area over a period of two to four years, which is then followed by 2) a successive increase in area over one to three years. In nearly every cycle of this undulating pattern, the portion containing the sequential increase in growth rates rarely returns to or exceeds the area at the start of the preceding decline

150

(i.e., an overall decrease in area from peak to peak, as seen in Figs. 5.8–5.13).

Furthermore, when considering the number of years associated with a decreasing

versus increasing trend in growth rate, most cycles are composed of more than 50% of

years within the decline (Fig. 5.15). A generalized additive model applied to each

individual recovers this pattern in all individuals with the exception of TA-3 and ZCHM-

29 (Figs. 5.8–5.14; Tables 5.15 – 5.22). It is unclear why generalized additive modelling

is not be able to recover the pattern in ZCHM-29 (even though the pattern seems

apparent in Fig. 5.9), but it should be noted that this individual seems to be different

from the other specimens in that more than half of the undulations within ZCHM-29

contain a majority of years in the portion of the cycle defined by increasing growth rates

rather than decreasing.

Annual Extensional Length

Extensional lengths were measured in all specimens within the study and often

allowed for the most consecutive yearly measurements made for each individual (e.g.,

as in 48-M, TA-3, ZCHM-29, and 2007/003). Additionally, measurements of extension

could be made on three individuals (48-M, ZCHM-38, and ZCHM-46) for which annual

areas could not, due to difficulty in visualization of attenuation features in microCT

slices. In general, all specimens, except for 48-M and ZCHM-38, show similar primary

and secondary patterns of growth to those in annual area measurements (see above;

Figs. 5.8–5.14 and 5.15–5.17; Tables 5.15 – 5.24). In the case of the undulating

secondary pattern, the largest increment within each cycle occurs within the same year

for both extensional and area measurements in all specimens studied.

In 2007/003 and TA-3, both individuals show an initial rapid rise in rate of extension in the distal portions of the tusk, but following the year of greatest extension recorded for each, extensional lengths decline and begin to undulate over a 3-to-5 year period, as in the secondary pattern discussed in the preceding section. This undulating pattern was not observed in measurements of area for TA-3, because the years during which the undulatory pattern should have been expressed did not have well enough preserved boundaries to permit measurement of area. Applying a generalized additive model to both these specimens recovers the transition from a year-to-year rapid increase in extensional length to a 3- to 5-year undulating pattern in extension (Figs. 5.13 and 5.14, Tables 5.19 – 5.20).

ZCHM-46, a specimen from which we were unable to take accurate area measurements, had a record of 41 consecutive years that were suitable for making extensional length measurements. The distal-most 9 years of the specimen show a year-to-year increase in extensional length that is similar to that seen in the distal years of both 2007/003 and TA-3 (Fig. 5.16). Cherney (2016) analyzed the distal 7 of these 9 years and concluded, using the trajectory of changes in tusk diameter, that those years were formed from ages 5 to 13 from birth. This, along with the similar radii of these years to those of the other two tusks (Fig. 5.3), fits with the hypothesis that this pattern is associated with early life. Also as in 2007/003 and TA-3, ZCHM-46 displays a repeated 3- to 5-year-long pattern of decreasing and then increasing extensional lengths, which begins immediately following the year with the greatest extensional length recorded in the tusk. The multi-year undulating pattern of growth repeats six times within this specimen before the individual's death, and each of these undulations

is recovered when a generalized additive model is applied (Fig. 5.16, Table 5.23).

Due to damage on the proximal-most edge, we were unable to measure annual areas for the final five years of life in ZCHM-29, but this did not affect our ability to measure extensional lengths for those years. As with area measurements, ZCHM-29 shows a repeated pattern of decrease and increase in extensional lengths over a period of 3 to 5 years (Fig. 5.8). Generalized additive modelling of extensional length measurements was able to recover the multi-year undulating pattern (Table 5.16). The proximal-most year in ZCHM-29 has significantly less extension than do the earlier-forming years. As this proximal-most year is adjacent to the pulp cavity, this represents the final year of life for this individual and contains the last layers of dentin laid down before the animal's death. Significant deviation from the observed extensional lengths of previous years suggests that this individual died not long after the previous winter-spring boundary. Accurate assessment of season of death for this individual is beyond the scope of this study (requiring finer scale analyses of second-order increments; see Chapters 2-4), but based on the extensional lengths of previous years, this individual appears to have died within the summer or fall, unusual for an adult female proboscidean.

As with ZCHM-46, we were unable to make accurate annual area measurements of ZCHM-38 due to inadequate contrast in density within the tusk, especially in the middle and outer portions. Measurements of extensional lengths, however, were possible for 17 consecutive years in this individual (Fig. 5.18). ZCHM-38, a male, shows an overall trend of decreasing annual extensional lengths toward the pulp cavity, similar to the primary pattern observed in both area and extensional length measurements of

the female specimens. However, unlike the females, this specimen does not show the consistent multi-year-long pattern of decreasing and then increasing growth rates. Instead, this specimen is marked by mostly year-to-year fluctuations in extensional lengths; a pattern not observed in any of the females. The only series of years within ZCHM-38 that shows a 3-year undulating pattern also differs from the one observed in females in that 1) more years are associated with the trend of increasing growth rates than the trend of decreasing growth rates and 2) the final year in the positive trend has a much greater extensional length than at the start of the negative trend. Also, applying a generalized additive model to the extensional length data from ZCHM-38 returns only the primary negative trend in growth rates through time and is unable to recognize any secondary pattern as was observed in all female specimens (Fig. 5.18, Table 5.24). The lack of a recognizable secondary pattern could potentially be due to the low number of data points for this specimen, but when a generalized additive model is applied to each adult female specimen using a reduced number of extensional years to match that of ZCHM-38, we are still able to recover the undulating pattern in all of those individuals. This suggests that the secondary pattern observed in female specimens is not present in ZCHM-38.

Measurements of extensional length in 48-M, another male, show a gradual decline through life, a trend that appears to be present in all specimens within the dataset. However, like ZCHM-38, this individual does not appear to show a pattern similar to that of the secondary pattern of growth. Instead, the pattern of growth appears to be marked by year-to-year fluctuations and extended excursions of thicker or thinner years. Applying a generalized additive model to the data confirms this observation (Fig.

154

5.17, Table 5.22), which further suggests that the secondary pattern is not present in either of the males studied.

In order to assess the overall, primary pattern of growth across all individuals within the study sample, we applied a generalized additive mixed model to the entire dataset (Fig. 5.19, Table 5.25). This model shows a consistent year-to-year rise in extensional length during the distal-most years, before eventually reaching a peak extensional length and beginning a steady decline in growth rate toward the time of death. Given the multi-decadal record documented within some of these specimens, the wide range of ontogenetic ages within this study, and our observations of growth trends at different ontogenetic stages (see this and the preceding section), it seems reasonable to interpret this pattern as the general trend in growth expected over the course of the full life of an individual.

Annual Appositional Thickness

Measurements of annual appositional thicknesses could be taken on eight of the study specimens (ZCHM-28, ZCHM-29, ZCHM-30, 2007/003, TA-3, 43-M, 48-M, and the Malolyakhovsky specimen). To a first approximation, tusks with smaller radii (i.e., 2007/003 and TA-3) have a generally positive trend in appositional thickness towards the pulp cavity and larger tusks (i.e., ZCHM-28, ZCHM-29, ZCHM-30, and the Malolyakhovsky specimen) have an overall negative trend through time (Figs. 5.8–5.14 and 5.17), as was observed in both extensional length and area measurements. In 43-M, 48-M, ZCHM-29 and ZCHM-30, this trend is very weak and has a slope of nearly zero when a simple linear regression is applied. This near lack of trend in appositional

155

thickness measurements is consistent with findings in Great Lakes Region mastodons by Fisher (2008) and Fisher et al. (2008).

Each tusk displays a wide range of year-to-year and multiyear fluctuations in appositional thickness over periods of 2 to 7 years. These fluctuations do not appear to be regular, unlike what was documented in both area and extensional length measurements. Furthermore, the years containing local maxima or minima within a given fluctuation are sometimes not the same as those for area and extensional length. Local maxima documented in appositional thickness generally approximate those documented in area and extension, but there is often some offset of the maximum by up to several years. Furthermore, some of the local maxima measured for apposition are not present in the extension or area measurements at all. The overall pattern of growth may also be different. This is emphasized in 2007/003, which records a relatively continuous year-to-year increase in appositional thickness throughout the distal-most 12 years of the tusk, rather than for the distal-most 5 years as was observed in both extension and area.

Applying generalized additive models to each tusk corroborates our interpretation that no clear secondary pattern of growth is present in our measurements of appositional thickness (Figs. 5.8–5.14 and 5.17; Table 5.15 – 5.22). Out of the eight tusks to which this model was applied, only ZCHM-28 and the Malolyakhovsky specimen recover an undulating multiyear pattern in apposition. The model for the Malolyakhovsky specimen recovers two major undulations throughout the individual's life with durations of 19 and 12 years, clearly different from the secondary pattern observed in area and extensional measurements. In fact, this pattern appears to be an

abrupt shift from on-average thicker years of apposition to relatively thinner years

starting after year X-22, rather than a repeated pattern of appositional growth. For

ZCHM-28, the model does recover a repeated undulating pattern that has a periodicity

of 4 to 7 years. These undulations, however, do not match up with those observed in

area and extensional measurements, and are fewer in number (five for apposition

versus seven for extension and area). We also observed year-to-year fluctuations in

appositional thickness within some of the modeled undulations for ZCHM-28, whereas

the pattern of undulations in measurements of area and extension is relatively smooth

and consistent from year-to-year. Generalized additive models based on appositional

measurements for the other individuals are relatively linear, and in some cases, have

minimal support and explain little of the variation within the data (e.g., ZCHM-29,

ZCHM-30, 43-M, 48-M, and TA-3; Tables 5.16, 5.17, 5.19, 5.21, and 5.22).

DISCUSSION

Correlated Aspects of Tusk Growth

The overall volume of a given dentin increment within a tusk is determined by an

interplay between appositional and extensional growth rates (Fisher, 2001). Although it

may seem that apposition and extension would be linked, Fisher (2008) and Fisher et

al. (2008) reported variation in the rates of increase of one relative to the other. Those

authors observed that appositional thicknesses remain nearly constant throughout much

of life, while extensional lengths show an overall negative trend through time. Our data

largely support this, although in the case of appositional thicknesses, we find a high

degree of variability within and among individuals (e.g., the Malolyakhovsky specimen,

Figs. 5.8–5.14 and 5.17).

Our dataset allows for assessment of the input of both extension and apposition as they relate to increment area (and likely volume). Correlation of extensional length and appositional thickness on area reveals an overall positive trend for both types of measurement (Figs. 5.20 and 5.21). Correlation between these measurements and area is significantly stronger when only considering measurements within each specimen, especially with regard to extensional length where R values range from 0.84 to 0.95 (p<0.05). As was noted above, the pattern of year-to-year change in extensional length appears to closely mirror that of area, while apposition appears to show a roughly similar pattern in some specimens and a dissimilar pattern in others (Figs. 5.8–5.14, 5.16–5.18, and 5.21). This suggests a degree of decoupling between rates of apposition and extension within the tusk. The cause of this difference in growth rates is unclear, but it is possible that rates of apposition and extension are modulated by different components of diet (e.g., mineral vs. protein; Fisher, 2001). With respect to each measure's contributions to the size of annual dentin cones, apposition seems to only minutely affect the area of each annual increment relative to extension, which appears to be the main contributor to increment area for each year, unsurprising given their order of magnitude difference in value. Figure 5.22 illustrates this point, showing that even at relatively large appositional thicknesses increment area remains small without significant increase in extensional length. Therefore in the absence of area measurements, extensional length likely provides the best proxy for area.

Calving Histories of Female Woolly Mammoths

Fisher (1996) was the first to document an undulating three-to-six-year pattern of change in extensional length of annual increments marked by first-order periradicular features in a proboscidean tusk, which he interpreted as the signal for calving intervals. This pattern was observed in the four female American mastodons studied, while a different pattern was observed in juveniles and males. Since that study, other papers have noted patterns of similar duration in female mastodons and mammoths (Fisher et al., 2008; Fisher, 2009; El Adli et al., 2016 [see Chapter 4]). As discussed above, we documented this pattern in measurements of both extensional length and area in female woolly mammoth tusks, which we have described as a "secondary pattern". In this section, we use our more extensive dataset to corroborate this interpretation of Fisher (1996).

The secondary pattern described above has a consistent sex and ontogenetic distribution within our study sample, matching the findings of Fisher (1996) and Fisher et al. (2008). The pattern is observed in all female individuals in increments clearly representing growth during adult years (based on tusk radius and cone apex angle measurements). However, the pattern was absent in ZCHM-38 and 48-M, both males, and was not observed in increments formed during early, likely juvenile years (the distal portions of 2007/003, TA-3, and ZCHM-46). The presence of this pattern only within the adult years of females suggests that it is likely reflective of reproductive life history.

The duration of each cycle in the secondary pattern gives further credence to a calving interval interpretation. The life histories of *Loxodonta* and, to a slightly lesser degree, *Elephas*, have been studied in various game reserves and wildlife refuges across both Africa and Asia (Douglas-Hamilton, 1973; Laws et al., 1975; Moss, 2001;

159

Sukumar, 2003; Baskaran et al., 2009). These authors document calving intervals ranging from 3 to 12 years with 4 and 5 years being by far the most common interval. Moss (2001) reported that most females studied in the Amboseli *Loxodonta* population reproduce continuously throughout adulthood and into old age, with only 9 of 38 individuals over the age of 50 showing signs of reproductive senescence. Females within our study show a range in the periodicity of the undulating secondary pattern between 3 and 6 years (counting between peaks in each cycle), with 4- and 5-year cycles being the most common and 6-year cycles being rare (i.e., only observed twice within the study sample). These periodicities fall well within the range of observed calving intervals for both *Loxodonta* and *Elephas*, and in no instance fall below or above a reasonable value for an elephantid calving interval. No other aspect of female life history occurs over a similar interval and is pervasive throughout adult life.

The multiyear change in growth rates that defines the undulating secondary pattern is also easily explained in the context of a calving interval interpretation. Both fetal tissues (especially the ossification of bones) and dentin require calcium and phosphate. During gestation, this requirement causes the concentration of calcium and phosphate in serum to decrease (Rasmussen, 1977; Luciano et al., 1978; Kovacs and Kronenberg, 1997; Kovacs, 2001; Ozbek et al., 2009), which reduces the available material to form dentin increments in tusks. As such, a female mammoth without a calf or gestating fetus should be able to form a thicker annual dentin increment than a female with calf. However during the roughly 22-month gestation of a fetus (Moss, 1983; Meyer et al., 2004; Rountrey et al., 2012), an increasingly larger portion of the mother's budget of calcium and phosphate that would otherwise go to the formation of new tusk

160

material is instead allocated to the fetus, thus resulting in decreasing increment size during gestation.

Once the calf is born, milk formation should have some negative effect on the rate of tusk growth, but it is unclear whether this would be greater or less than the nutrient deficit during gestation. In lactating human females, both phosphate and ionized calcium in serum are elevated relative to pregnancy (falling within or exceeding the normal range) (Kovacs, 2001). Such an increase in mineral levels could allow for growth of larger dentin increments during lactation. Ozbek et al. (2009) further noted a change in the texture and morphology of enamel and dentin of rodent incisors formed during pregnancy relative to non-pregnant females with a gradual return to "normal" tooth growth during lactation; however, tooth growth rates in these individuals were not documented.

Regardless of expected changes in tusk growth rates during nursing, after the mother begins the process of weaning, the percentage of her nutrient intake allocated to the calf should gradually decrease, which should result in an increase in tusk growth rates. Subsequent conception of another calf would repeat the cycle. However, in *Loxodonta* and *Elephas* there is often some overlap between nursing of an older calf and gestation of a new fetus, with weaning of the older calf occurring shortly before the birth of the new sibling (Moss, 1988). The nutritional burden of a gestating fetus while still nursing an incompletely weaned calf would likely prohibit tusk growth rates from reaching the level of years prior to conception of the initial calf. Furthermore, this would also result in a return to a declining trend in growth rates until the weaning of the older calf and subsequent birth of the new calf.

161

Given the distribution, periodicity, and shape of the secondary pattern observed within female woolly mammoth tusks, an explanation of each cycle as representing a calving interval is the most reasonable interpretation. This interpretation further supports the similar findings of Fisher (1996) and Fisher et al. (2008) for *Mammut americanum*. Interestingly, the duration of calving intervals across such distantly related taxa as mammutids and elephantids suggests that long gestation and extended periods of parental care evolved relatively early in proboscidean history, likely as a consequence of large body size.

Age of Maturation

Three general multi-year patterns of growth can be observed in measurements of tusks in this study sample. The first is the year-to-year increase in growth rates observed only in the distal portions of tusks with relatively small radii (Figs. 5.13, 5.14, and 5.16; also see Cherney, 2016). The second is the undulating secondary pattern occurring only in adult females, which we have interpreted above as representing the signal for calving intervals. Finally, the third is the primary pattern of a roughly linear, negative trend in growth rates with increasing age observed in portions of both adult male and female tusks (e.g., Figs. 5.8–5.11). Based on tusk radius and cone apex angle measurements, the first pattern is associated with juvenile growth, while the second and third patterns reflect aspects of growth associated with adulthood. If correct, then it stands to reason that in female mammoths the cessation of the first pattern and the onset of the second and third patterns would indicate the beginning of adulthood, and the year in which this change occurs would be the age of maturation. Maturation in

males is a two-step process (i.e., eviction from the matriarchal family unit and first onset of musth), requiring a different approach for identification (see Fisher, 2008).

In all three tusks containing the positive year-to-year trend in growth rates (2007/003, TA-3, and ZCHM-46), there is an abrupt onset of the secondary pattern that coincides with termination of the positive trend. This change occurs at the year with the highest growth rate recorded in the entire tusk for both area and extension measurements in each individual. In 2007/003 and ZCHM-46, this largest growth year also marks the onset of the primary negative trend in growth rates, which continues until death. In TA-3, the presence (or absence) of this negative trend is ambiguous, as only four years beyond the largest growth year occur before death. Given the end of the juvenile pattern and onset of the adult patterns at this largest growth increment in all three specimens, it is reasonable to interpret this transition year as the age of maturation for these individuals. Figure 5.23 shows these interpretations of patterns related to calving and age of maturation applied to ZCHM-46.

Patterns in Life History through Time

The timing of the onset of different aspects of life history or (for recurring aspects of life) the duration over which they occur have been shown to vary based on extrinsic factors experienced during life (Hanks and Mcintosh, 1973; Stearns, 1977; Fowler, 1981; Rutberg, 1987; Moss, 2001; Ryan et al., 2007). Furthermore, different extrinsic factors may have distinct and predictable effects on life history. Fisher (1996) used such theory and data to hypothesize that changes in life history throughout the Pleistocene could be used to test the cause of extinction in proboscideans. Such tests of extinction

using life history are ideal for the end-Pleistocene as the two oft-hypothesized causes of extinction, climate change and human hunting, are expected to have antithetical effects on some aspects of life history.

Climate change, itself, has no inherent positive or negative effects on organisms, in general. However, climate change could drive extinction in herbivore populations by changing the composition of local flora. Such changes could result in a decline in the abundance or quality of preferred vegetation available to herbivores (as well as in the availability of water), leading to their demise. Changes in vegetation and water availability have been shown to have a dramatic effect on life history in extant proboscideans. During periods of extended drought (where resources are limited), populations of *Loxodonta* delay maturation and increase time between calves (Douglas-Hamilton, 1973; Laws et al., 1975; Moss, 1988; 2001). In *Loxodonta*, the median age of first conception is approximately 12 years old while mean calving interval is 4.5 years, with some minor variation among different populations (Eltringham, 1982). However, during periods of nutritional limitation, calving intervals have been documented to be as long as 12 years and age of first conception as late as age 22 (Laws et al., 1975; Eltringham, 1982; Moss, 2001). Analogous (but less extensive) studies of *Elephas* have yielded similar average calving intervals and slightly older average age at first conception to those documented in *Loxodonta*, but no study has yet attempted to document life history responses under nutritional limitation (Daniel et al., 1987; Sukumar, 2003; Baskaran et al., 2009). Regardless, the pattern observed in *Loxodonta* seems clear in that both age of maturation and calving intervals increase in response to nutrient limitation, as might be expected with a decrease in the quality and/or

abundance of food sources under the scenario of a climate change-driven extinction.

Changes in reproductive life histories as a consequence of hunting have been documented in several vertebrate taxa. Such studies have shown that reduction in population size due to hunting (even in groups as disparate as teleosts, pinnipeds, and cetaceans) results in a decrease in average age of maturation (Carrick and Ingham, 1962; Lockyer, 1972; 1984; Rijnsdorp, 1993; Trippel, 1995; Rochet, 1998; Festa-Bianchet, 2003, Gabriele et al., 2007). Likewise, increased fecundity has been documented in overhunted populations of teleost fish (Bagenal, 1966; Healey, 1978; Horwood and Howlett, 1986; Kelly and Stevenson, 1985), while birthing interval decreases in various iteroparous tetrapod species (Anderson and Burnham, 1976; Swihart et al., 1998; Gosselin et al., 2015). Similar studies have not been conducted for modern proboscideans, but the link of hunting pressures to earlier reproductive schedules and increased birth rates across many distantly related vertebrate groups suggests that a similar response should be expected in *Mammuthus*.

In terms of using reproductive life history as a test for cause of extinction, our dataset suffers from a lack of finite radiocarbon dates for individuals studied (n = 3). Of the individuals with finite dates, only a single specimen (TA-3) approximates the timing of extinction for woolly mammoths in Siberia (Koch and Barnosky, 2006). Despite this issue, some general observations can be made about patterns of change in life history within the dataset, though further analyses of tusks spanning the end-Pleistocene will be required to fully test extinction hypotheses.

Average calving interval within an individual ranged from 4 to 4.5 years, a relatively minor variation in length (Fig. 5.24). The three female individuals that returned

165

infinite radiocarbon ages (ZCHM-28, ZCHM-30, and ZCHM-46) together have an average calving interval of 4.3 years in duration (range of 4.2 to 4.5 years). ZCHM-29 and the Malolyakhovsky specimen, both with calibrated radiocarbon ages of ~33,000 years BP, together average 4.1 years in average calving interval, while TA-3, at ~10,000 years in age, has a single measurable calving interval of 4 years in length. This apparent weak negative trend in calving interval toward the time of extinction is mirrored in estimates of age at maturation, with the onset of the first calving interval beginning at age 13 for ZCHM-46 and at age 11 for TA-3.

It is not clear whether the decreases in average calving interval and age at maturation (supporting the hunting-induced extinction hypothesis) found within this study reflect real shifts in life history or are an artifact of low sampling. However, Fisher (2009) found a similar decrease in the age of maturation of American mastodon from the Great Lakes Region of North America at the end of the Pleistocene. Furthermore, Cherney (2016) found a decrease in weaning age in Siberian woolly mammoths toward the time of extinction, which also supports hunting as the primary agent of mammoth extinction in northeast Asia. These similar findings using several aspects of life history across multiple regions and taxa represent a pattern of consilience between data sources that supports a hunting-caused extinction for proboscideans to the exclusion of the climate-change hypothesis. Regardless of trend, the relatively young age of maturation and short calving interval for TA-3 at the end of the Pleistocene is not suggestive of an individual living in a state of nutritional stress, as would be expected under a climate change-related extinction.

The results presented above contain some of the longest records of growth yet

documented for individual proboscideans. The analyses used to obtain these data required little to no damage to specimens and collecting of data occurred relatively rapidly compared to more invasive techniques (e.g., thin sectioning). We thus have assembled a protocol for analysis of multi-decadal records of tusk growth using techniques that can produce results relatively quickly and easily, and may allow access to growth records for specimens that could not be analyzed destructively. These extensive records of growth for many individual mammoths allow us to make compelling interpretations of different aspects of life history. Perhaps even more importantly, this type of data is beginning to shed light on the cause of proboscidean extinction at the end of the Pleistocene.

Moving forward with this work, analyses of more tusks will surely be needed to provide sufficient documentation of changes in life history through time and an adequate test of the cause of mammoth extinction. The exact number of specimens that will be required depends on whether the overall pattern that emerges is simple or complex. Beyond the obvious need to fill in the large temporal gaps of our dataset, we are also obliged to analyze multiple specimens from similar periods of time to see if results are replicated. This could either reveal a wide spread or only a narrow range in calving intervals and ages of maturation within a given time interval. More specimens would likely be required to document patterns of change in life history if there is high variability in average calving interval and age of maturation. Finally, the cause of extinction need not be the same for every region or population. It will eventually be necessary to analyze populations across multiple continents to discover whether life history changes in the same way for disparate populations (indicating a single overall cause of extinction

for proboscideans) or differs in response regionally (indicating different agents of extinction for each population). Completing such a body of work will require the efforts of multiple researchers over many years, but will likely provide some of the most compelling tests for the cause of the end-Pleistocene extinction. The research presented in this chapter is a step along the way to this overall goal.

REFERENCES

Anderson, D.R., Burnham, K.P., 1976. Population ecology of the mallard: VI. The effect of exploitation on survival. US Fish and Wildlife Service.

Augustine, D.J., McNaughton, S.J., 1998. Ungulate effects on the functional species composition of plant communities: herbivore selectivity and plant tolerance. The Journal of Wildlife Management, 1165-1183.

Bagenal, T., 1966. The ecological and geographical aspects of the fecundity of the plaice. Journal of the Marine Biological Association of the United Kingdom 46, 161-186.

Barnosky, A.D., Lindsey, E.L., Villavicencio, N.A., Bostelmann, E., Hadly, E.A., Wanket, J., Marshall, C.R., 2016. Variable impact of late-Quaternary megafaunal extinction in causing ecological state shifts in North and South America. Proceedings of the National Academy of Sciences 113, 856-861.

Baskaran, N., Das, S., Sukumar, R., 2009. Population, reproduction and management of captive Asian elephants (*Elephas maximus*) in Jaldapara Wildlife Sanctuary, West Bengal, India. Indian Forester 135, 1545.

Carrick, R., Ingham, S.E., 1962. Studies on the southern elephant seal, *Mirounga leonina* (L.). V. Population dynamics and utilization. CSIRO Wildlife Research 7, 198-206.

Cherney, M.D., 2016. Records of Growth and Weaning in Fossil Proboscidean Tusks as Tests of Pleistocene Extinction Mechanisms.

Daniel, J., Desai, A., Sivaganesan, N., 1987. Ecology of Asian elephant in Mudumalai Wildlife Sanctuary. Annual report 1987.

Douglas-Hamilton, I., 1973. On the ecology and behaviour of the Lake Manyara elephants. African Journal of Ecology 11, 401-403.

El Adli, J.J., Cherney, M.D., Fisher, D.C., Harris, J.M., Farrell, A.B., Cox, S.M., 2015. Last years of life and season of death of a Columbian mammoth from Rancho La Brea. In: Harris, J.M. (Ed.), La Brea and beyond: The paleontology of asphalt-preserved biotas. Natural History Museum of Los Angeles County, Science Series vol 42, pp. 65-80.

El Adli, J.J., Fisher, D.C., Cherney, M.D., Labarca, R., Lacombat, F., 2017. First analysis of life history and season of death of a South American gomphothere. Quaternary International.

El Adli, J.J., Fisher, D.C., Vartanyan, S.L., Tikhonov, A.N., 2016. Final years of life and seasons of death of woolly mammoths from Wrangel Island and mainland Chukotka, Russian Federation. Quaternary International.

Elder, W., 1970. Morphometry of elephant tusks. African Zoology 5.

Eltringham, S.K., 1982. Elephants. Blandford Press, Link House, West Street.

Festa-Bianchet, M., 2003. Exploitative wildlife management as a selective pressure for the life-history evolution of large mammals. Animal behavior and wildlife conservation, 191-207.

Fisher, D.C., 1996. Extinction of proboscideans in North America. In: Shoshani, J., Tassy, P. (Eds.), The Proboscidea: Evolution and palaeoecology of elephants and their relatives. Oxford University Press, Oxford, pp 296–315.

Fisher, D.C., 2001. Season of death, growth rates, and life history of North American

mammoths. In: West, D.L. (Ed.), Mammoth site studies: Proceedings of the first international conference on mammoth site studies. Publications in Anthropology vol. 22, University of Kansas, Lawrence, pp. 121–135.

Fisher, D.C., 2008. Taphonomy and paleobiology of the Hyde Park mastodon. In: Allmon, W.D., Nester, P.L. (Eds.), Mastodon paleobiology, taphonomy, and paleoenvironment in the late Pleistocene of New York State: Studies on the Hyde Park, Chemung, and Java sites. Palaeontographica Americana vol. 61, pp. 197–289.

Fisher, D.C., 2009. Paleobiology and extinction of proboscideans in the Great Lakes region of North America. In: Haynes, G. (Ed.), American megafaunal extinctions at the end of the Pleistocene, Springer, New York, pp. 55–75.

Fisher, D.C., Beld, S.G., Rountrey, A.N., 2008. Tusk record of the North Java mastodon. In: Allmon, W.D., Nester, P.L. (Eds.). Mastodon paleobiology, taphonomy, and paleoenvironment in the late Pleistocene of New York State: Studies on the Hyde Park, Chemung, and Java sites. Palaeontographica Americana vol 61, pp. 417-463.

Fisher, D.C., Cherney, M.D., Newton, C., Rountrey, A.N., Calamari, Z.T., Stucky, R.K., Lucking, C., Petrie, L., 2014. Taxonomic overview and tusk growth analyses of Ziegler Reservoir proboscideans. Quaternary Research 82, 518-532.

Fowler, C.W., 1981. Density dependence as related to life history strategy. Ecology 62, 602-610.

Gabriele, C.M., Straley, J.M., Neilson, J.L., 2007. Age at first calving of female humpback whales in southeastern Alaska. Marine Mammal Science 23, 226-239.

Gosselin, J., Zedrosser, A., Swenson, J.E., Pelletier, F., 2015. The relative importance of direct and indirect effects of hunting mortality on the population dynamics of brown bears. Proceedings of the Royal Society B: Biological Sciences 282.

Grayson, D.K., 1984. Nineteenth century explanations of Pleistocene extinctions: A review and analysis.

Grigoriev, S.E., Fisher, D.C., Obadă, T., Shirley, E.A., Rountrey, A.N., Savvinov, G.N., Garmaeva, D.K., Novgorodov, G.P., Cheprasov, M.Y., Vasilev, S.E., 2017. A woolly mammoth (*Mammuthus primigenius*) carcass from Maly Lyakhovsky Island (New Siberian Islands, Russian Federation). Quaternary International.

Hanks, J., McIntosh, J.E.A., 1973. Population dynamics of the African elephant (*Loxodonta africana*). Journal of Zoology 169, 29-38.

Hastie, T., Tibshirani, R. 1986. Generalized Additive Models. Statistical Science 1(3), 297-318.

Healey, M., 1978. Fecundity changes in exploited populations of lake whitefish (*Coregonus clupeaformis*) and lake trout (*Salvelinus namaycush*). Journal of the Fisheries Board of Canada 35, 945-950.

Horwood, J., Bannister, R., Howlett, G., 1986. Comparative fecundity of North Sea plaice (*Pleuronectes platessa* L.). Proceedings of the Royal Society of London B: Biological Sciences 228, 401-431.

Johnson, C.N., 2009. Ecological consequences of Late Quaternary extinctions of megafauna. Proceedings of the Royal Society B: Biological Sciences.

Kelly, K.H., Stevenson, D.K., 1985. Fecundity of Atlantic herring (*Clupea harengus*) from three spawning areas in the western Gulf of Maine, 1969 and 1982. J.

Northw. Atl. Fish. Sci 6, 149-155.

Koch, P.L., Barnosky, A.D., 2006. Late Quaternary Extinctions: State of the Debate. Annual Review of Ecology, Evolution, and Systematics 37, 215-250.

Koch, P.L., Fisher, D.C., Dettman, D., 1989. Oxygen isotope variation in the tusks of extinct proboscideans: a measure of season of death and seasonality. Geology 17, 515-519.

Kovacs, C.S., 2001. Calcium and Bone Metabolism in Pregnancy and Lactation. The Journal of Clinical Endocrinology & Metabolism 86, 2344-2348.

Laws, R.M., 1966. Age criteria for the African elephant, Loxodonta a. africana. East African Wildlife Journal 4, 1-37.

Laws, R.M., Parker, I.S., Johnstone, R.C., 1975. Elephants and their habitats. Clarendon Press.

Lockyer, C., 1972. The age at sexual maturity of the southern fin whale (*Balaenoptera physalus*) using annual layer counts in the ear plug. ICES Journal of Marine Science 34, 276-294.

Lockyer, C., 1984. Review of baleen whale (Mysticeti) reproduction and implications for management. Reports of the International Whaling Commission, Special, 27-50.

Loe, L.E., Bonenfant, C., Mysterud, A., Gaillard, J.M., Langvatn, R., Klein, F., Calenge, C., Ergon, T., Pettorelli, N., Stenseth, N.C., 2005. Climate predictability and breeding phenology in red deer: timing and synchrony of rutting and calving in Norway and France. Journal of Animal Ecology 74, 579-588.

Luciano, D.S., Vander, A.J., Sherman, J.H., 1978. Human function and structure. McGraw-Hill Companies.

Meyer, J.M., Walker, S.L., Freeman, E.W., Steinetz, B.G., Brown, J.L., 2004. Species and fetal gender effects on the endocrinology of pregnancy in elephants. General and comparative endocrinology 138, 263-270.

Moss, C.J., 1983. Oestrous behaviour and female choice in the African elephant. Behaviour 86, 167-195.

Moss, C.J., 1988. Elephant memories: thirteen years in the life of an elephant family. William and Morrow Company, New York.

Moss, C.J., 2001. The demography of an African elephant (*Loxodonta africana*) population in Amboseli, Kenya. Journal of Zoology 255, 145-156.

Ozbek, M., Dural, S., Kanli, A., Tuncel, M., Orhan, K., 2009. Morphological evaluation of rat incisor enamel and dentin induced by pregnancy and lactation using a scanning electron microscope. Journal of Veterinary Medical Science 71, 1273-1277.

Pilgram, T., Western, D., 1986. Inferring the sex and age of African elephants from tusk measurements. Biological conservation 36, 39-52.

Rasband, W.S., 1997. ImageJ. United States National Institutes of Health, Bethesda, Maryland. http://imagej.nih.gov/ij/.

Rasmussen, P., 1977. Calcium deficiency, pregnancy and lactation in rats. Journal of Periodontal Research 12, 491-499.

Reimer, P.J., Bard, E., Bayliss, A., Beck, J.W., Blackwell, P.G., Ramsey, C.B., Buck, C.E., Cheng, H., Edwards, R.L., Friedrich, M., 2013. IntCal13 and Marine13 radiocarbon age calibration curves 0–50,000 years cal BP. Radiocarbon 55, 1869-1887.

Rijnsdorp, A., 1993. Fisheries as a large-scale experiment on life-history evolution: disentangling phenotypic and genetic effects in changes in maturation and reproduction of North Sea plaice, *Pleuronectes platessa* L. Oecologia 96, 391-401.

Rochet, M.-J., 1998. Short-term effects of fishing on life history traits of fishes. ICES Journal of marine Science 55, 371-391.

Rountrey, A.N., Fisher, D.C., Vartanyan, S., Fox, D.L., 2007. Carbon and nitrogen isotope analyses of a juvenile woolly mammoth tusk: evidence of weaning. Quaternary International 169, 166-173.

Rountrey, A.N., Fisher, D.C., Tikhonov, A.N., Kosintsev, P.A., Lazarev, P.A., Boeskorov, G., Buigues, B., 2012. Early tooth development, gestation, and season of birth in mammoths. Quaternary International 255, 196-205.

Rutberg, A.T., 1987. Adaptive hypotheses of birth synchrony in ruminants: an interspecific test. The American Naturalist 130, 692-710.

Ryan, S.J., Knechtel, C.U., Getz, W.M., 2007. Ecological cues, gestation length, and birth timing in African buffalo (*Syncerus caffer*). Behavioral Ecology 18, 635-644.

Smith, K.M., Fisher, D.C., 2011. Sexual dimorphism of structures showing indeterminate growth: tusks of American mastodons (*Mammut americanum*). Paleobiology 37, 175-194.

Smith, K.M., Fisher, D.C., 2013. Sexual dimorphism and inter-generic variation in proboscidean tusks: Multivariate assessment of American mastodons (*Mammut americanum*) and extant African elephants. Journal of Mammalian Evolution 20, 337-355.

Stearns, S.C., 1977. The evolution of life history traits: a critique of the theory and a review of the data. Annual Review of Ecology and Systematics 8, 145-171.

Sukumar, R., 2003. The living elephants: evolutionary ecology, behaviour, and conservation. Oxford University Press.

Sukumar, R., Joshi, N., Krishnamurthy, V., 1988. Growth in the Asian elephant. Proceedings: Animal Sciences 97, 561-571.

Swihart, R.K., Weeks, J.H.P., Easter-Pilcher, A.L., DeNicola, A.J., 1998. Nutritional condition and fertility of white-tailed deer (*Odocoileus virginianus*) from areas with contrasting histories of hunting. Canadian Journal of Zoology 76, 1932-1941.

Trippel, E.A., 1995. Age at maturity as a stress indicator in fisheries. Bioscience 45, 759-771.

Wittemyer, G., Barner Rasmussen, H., Douglas-Hamilton, I., 2007. Breeding phenology in relation to NDVI variability in free-ranging African elephant. Ecography 30, 42-50.

Wood, S.N. 2006. Generalized Additive Models: an introduction with R. Chapman and Hall/CRC Press.

Zimov, S.A., 2005. Pleistocene Park: Return of the Mammoth's Ecosystem. Science 308, 796-798.

Zimov, S.A., Chuprynin, V.I., Oreshko, A.P., III, F.S.C., Reynolds, J.F., Chapin, M.C., 1995. Steppe-Tundra Transition: A Herbivore-Driven Biome Shift at the End of the Pleistocene. The American Naturalist 146, 765-794.

Table 5.1. Specimens used for study of internal density features. F = female; M = male; CHK = Chukotka; NSI = New Siberian Islands; TMR = Taymyr Peninsula, WRA = Wrangel Island.

Specimen	Sex	Provenance	Laboratory Number	^{14}C age BP	Calibrated age BP
ZCHM-28	F	CHK	Beta 468134	>43,500	-
ZCHM-29	F	CHK	Beta 468135	29,010±140	33,625–32,826
ZCHM-30	F	CHK	Beta 413316	>43,500	-
ZCHM-46	F	CHK	Beta 413320	>43,500	-
Malolyakhovsky	F	NSI	GrA-60044	28,610±110	32,930–32,480
2007/003	F	TMR	Beta 468136	>43,500	-
TA-3	F	TMR	AA98473	10,480±100	12,662–12,064
43-M	F	WRA	AA98466	4,542±60	5,448–5,017
48-M	M	WRA	Beta 413313	7,260±30	8,165–8,005
ZCHM-38	M	CHK	none	unknown	unknown

Table 5.2. Scan parameters used for individual tusks and tusk sections.

Specimen	Section	kV	μA	ms	Voxel Size (μm)	Filter Material	Filter Thickness (mm)
ZCHM-28	Proximal	170	195	2829	90	Copper	2.00
	Distal	170	195	2829	90	Copper	2.00
ZCHM-29	Proximal	195	205	1415	80	Copper	1.50
	Distal	195	205	1415	70	Copper	1.50
ZCHM-30	Proximal	192	190	2829	64	Copper	2.00
	Middle	200	200	2000	64	Copper	2.00
	Distal	205	215	2000	64	Copper	2.50
ZCHM-46	Proximal	205	215	1000	80	Copper	1.25
	Middle	205	215	1000	90	Copper	1.25
	Distal	90	78	500	60	Aluminum	0.50
Malolyakhovsky	Whole	120	75	1000	600	Unknown	Unknown
2007/003	Proximal	190	195	2000	80	Copper	2.00
	Distal	195	200	1415	82	Copper	1.50
TA-3	Proximal	90	78	500	60	Aluminum	0.50
	Distal	90	78	500	60	Aluminum	0.50
43-M	Proximal	205	245	1000	50	Copper	1.50
	Distal	205	245	1000	50	Copper	1.50
48-M	1	185	215	708	100	Aluminum	11.00
	2	205	240	2829	100	Copper	3.50
	3	200	230	500	100	Aluminum	8.40
	4	205	250	2829	100	Copper	3.50
ZCHM-38	Proximal	195	205	4000	120	Copper	3.50
	Distal	195	205	4000	120	Copper	3.50

Table 5.3. Measurements of density features observed in ZCHM-28. PC = pulp cavity. Years are listed as distance from the pulp cavity with Year X being the year containing the pulp cavity surface and Year X-1 being one year distal to Year X. All measurements (except extensional length) are averages of measurements taken from curved slices along the X and Y planes.

Year (from PC)	Radius (mm)	Area (mm²)	Extensional Length (mm)	Appositional Thickness (mm)	Angle (°)
X	29.4	763.2	14.7	2.3	36.7
X-1	28.8	1119.0	23.1	4.1	34.0
X-2	29.8	1438.7	26.1	4.0	30.4
X-3	31.3	1116.3	18.4	5.8	30.0
X-4	32.2	1085.7	21.0	4.2	33.0
X-5	34.7	1765.3	28.6	5.9	34.9
X-6	35.7	1423.9	20.8	4.0	33.9
X-7	36.5	1314.1	21.9	4.3	32.9
X-8	37.5	1585.0	24.5	3.9	30.3
X-9	37.8	2281.7	36.2	7.3	28.3
X-10	37.7	2157.9	31.0	6.3	28.2
X-11	36.7	1948.9	28.0	5.9	27.8
X-12	36.1	2102.6	30.7	5.3	28.3
X-13	35.0	2638.3	42.0	4.6	28.0
X-14	34.1	2006.8	33.3	3.7	25.7
X-15	34.2	2120.9	34.8	4.1	24.3
X-16	34.8	2408.4	36.2	5.7	25.4
X-17	36.1	2836.9	44.2	5.5	27.3
X-18	35.8	2251.8	33.3	5.0	27.7
X-19	36.2	1585.3	27.9	3.7	25.7
X-20	34.5	2321.2	34.7	6.7	24.6
X-21	35.1	2387.5	37.2	6.9	24.8
X-22	34.9	2629.9	39.0	5.8	24.0
X-23	34.3	3084.6	47.0	6.7	24.1
X-24	33.4	2413.3	39.8	6.1	24.2
X-25	31.0	2300.4	40.3	5.0	23.1
X-26	29.4	2717.4	44.2	5.8	20.7
X-27	28.4	3320.3	51.9	6.9	20.7
X-28	26.7	2584.9	47.3	6.7	20.8
X-29	26.2	2306.1	44.4	5.2	18.8
X-30	24.2	2380.7	46.4	6.0	18.4
X-31	21.2	2822.0	51.4	7.2	19.9

Table 5.4. Measurements of density features observed in ZCHM-29. PC = pulp cavity. Years are listed as distance from the pulp cavity with Year X being the year containing the pulp cavity surface and Year X-1 being one year distal to Year X. All measurements (except extensional length) are averages of measurements taken from curved slices along the X and Y planes. "-" = increment too incomplete to obtain measurement."

Year (from PC)	Radius (mm)	Area (mm²)	Extensional Length (mm)	Appositional Thickness (mm)	Angle (°)
X	37	-	14	3.2	27
X-1	38	-	33	5.2	28
X-2	38	-	38	5.5	25
X-3	37	-	37	5.9	22
X-4	36	-	46	6.9	20
X-5	37	2148	411	5.9	90
X-6	37	1632	27	5.2	22
X-7	37	2315	42	5.8	23
X-8	36	2480	43	6.1	21
X-9	36	2910	57	6.3	19
X-10	35	2393	41	5.9	19
X-11	35	2149	36	6.7	21
X-12	33	2895	51	5.8	21
X-13	33	2765	49	7.0	18
X-14	32	2272	43	6.0	18
X-15	32	2644	43	6.4	18
X-16	31	3119	51	7.1	18
X-17	31	3245	54	7.0	19
X-18	32	2949	50	7.5	19
X-19	32	2491	46	5.3	18
X-20	31	3536	59	7.8	18
X-21	29	2741	50	6.6	18
X-22	26	2699	47	5.6	18
X-23	26	2212	36	4.6	19
X-24	27	3427	55	7.7	19
X-25	25	2672	43	5.9	18

Table 5.5. Measurements of density features observed in ZCHM-30. PC = pulp cavity. Years are listed as distance from the pulp cavity with Year X being the year containing the pulp cavity surface and Year X-1 being one year distal to Year X. All measurements (except extensional length) are averages of measurements taken from curved slices along the X and Y planes.

Year (from PC)	Radius (mm)	Area (mm²)	Extensional Length (mm)	Appositional Thickness (mm)	Angle (°)
X	36.5	2100.1	29.0	4.8	32.8
X-1	38.2	2341.8	40.0	5.6	35.4
X-2	38.3	1546.7	21.3	3.3	34.7
X-3	39.5	2130.7	28.5	5.7	31.8
X-4	39.9	2297.9	32.7	6.0	28.6
X-5	41.7	2678.7	42.8	7.1	27.6
X-6	42.2	2671.2	43.4	6.7	26.9
X-7	43.3	1748.1	18.9	4.2	27.6
X-8	43.6	2904.0	45.5	6.6	29.2
X-9	42.4	2958.7	47.7	7.0	26.0
X-10	44.4	3528.9	58.5	7.7	24.1
X-11	45.5	3333.7	53.7	6.6	25.7
X-12	45.5	2550.8	32.9	4.1	25.4
X-13	44.4	2606.9	33.0	4.3	22.6
X-14	45.6	3470.0	51.1	7.8	22.6
X-15	45.7	2080.0	22.8	3.2	25.9
X-16	45.9	2449.3	36.8	5.0	25.9
X-17	45.3	2591.2	38.5	5.2	22.3
X-18	45.2	3613.6	48.1	7.2	20.6
X-19	44.1	2638.4	36.6	4.8	22.2
X-20	44.4	2751.2	41.1	4.7	23.9
X-21	43.5	3021.9	40.5	5.4	25.9
X-22	42.2	3366.8	51.2	6.2	24.3
X-23	41.3	2444.6	33.2	3.8	22.5
X-24	41.1	2820.3	42.2	5.2	22.9
X-25	40.3	3497.7	60.9	7.2	23.2
X-26	40.3	2687.5	31.8	4.8	21.4
X-27	40.2	3174.9	44.6	5.3	19.6
X-28	40.3	3710.9	55.6	7.7	20.2
X-29	40.7	3291.8	59.4	5.4	21.9
X-30	39.8	2669.9	41.4	4.2	21.3
X-31	40.0	2761.5	39.4	5.3	20.1
X-32	37.0	3398.3	44.7	5.9	21.1
X-33	36.4	3806.2	58.1	6.9	19.8

Table 5.6. Measurements of density features observed in ZCHM-46. PC = pulp cavity. Years are listed as distance from the pulp cavity with Year X being the year containing the pulp cavity surface and Year X-1 being one year distal to Year X. All measurements (except extensional length) are averages of measurements taken from curved slices along the X and Y planes. "-" = increment too incomplete to obtain measurement.

Year (from PC)	Radius (mm)	Area (mm²)	Extensional Length (mm)	Appositional Thickness (mm)	Angle (°)
X	37.9	-	17.2	-	-
X-1	38.6	-	22.9	-	-
X-2	39.4	-	25.9	-	-
X-3	38.9	-	29.3	-	-
X-4	39.5	-	28.1	-	-
X-5	40.0	-	35.6	-	-
X-6	39.4	-	14.1	-	-
X-7	39.3	-	29.7	-	-
X-8	39.6	-	28.4	-	-
X-9	39.3	-	34.0	-	-
X-10	39.0	-	45.5	-	-
X-11	40.2	-	35.7	-	-
X-12	39.9	-	25.7	-	-
X-13	39.5	-	22.5	-	-
X-14	42.7	-	32.2	-	-
X-15	37.6	-	49.0	-	-
X-16	37.5	-	26.8	-	-
X-17	37.3	-	34.6	-	-
X-18	36.8	-	44.0	-	-
X-19	36.6	-	29.6	-	-
X-20	35.8	-	33.9	-	-
X-21	34.7	-	44.5	-	-
X-22	32.2	-	51.7	-	-
X-23	38.6	-	30.1	-	-
X-24	38.3	-	45.8	-	-
X-25	37.0	-	46.4	-	-
X-26	36.6	-	54.0	-	-
X-27	36.1	-	63.6	-	-
X-28	34.5	-	47.0	-	-
X-29	30.3	-	37.0	-	-
X-30	27.8	-	52.0	-	-
X-31	24.7	-	64.8	-	-
X-32	23.9	-	74.3	-	-
X-33	24.5	-	57.3	-	-
X-34	22.5	-	49.3	-	-
X-35	21.0	-	53.1	-	-
X-36	20.7	-	48.1	-	-
X-37	19.3	-	49.4	-	-

X-38	18.3	-	51.5	-	-
X-39	17.2	-	40.0	-	-
X-40	14.8	-	35.1	-	-

Table 5.7. Measurements of density features observed in the Malolyakhovsky specimen. PC = pulp cavity. Years are listed as distance from the pulp cavity with Year X being the year containing the pulp cavity surface and Year X-1 being one year distal to Year X. All measurements (except extensional length) are averages of measurements taken from curved slices along the X and Y planes. "-" = increment too incomplete to obtain measurement.

Year (from PC)	Radius (mm)	Area (mm²)	Extensional Length (mm)	Appositional Thickness (mm)	Angle (°)
X	48.2	933.4	18.9	4.1	45.3
X-1	48.9	1105.9	20.9	4.4	44.1
X-2	49.6	1252.5	22.9	4.6	42.1
X-3	49.4	1578.6	27.2	5.1	36.5
X-4	49.8	1322.9	16.6	3.9	34.7
X-5	50.6	1422.6	21.4	3.9	37.6
X-6	50.5	1566.1	23.7	4.6	38.4
X-7	52.1	1833.4	26.8	6.1	39.1
X-8	54.2	1611.2	22.2	4.2	39.7
X-9	54.1	1579.2	19.8	4.8	40.1
X-10	54.1	1675.7	26.0	5.3	38.9
X-11	53.7	1893.3	28.5	5.8	35.1
X-12	52.8	2103.1	31.5	6.3	32.0
X-13	52.4	1699.4	23.0	4.6	30.8
X-14	51.2	1945.6	25.5	5.4	33.1
X-15	51.1	2121.5	28.5	4.8	34.6
X-16	49.5	2675.2	35.6	5.6	35.7
X-17	49.1	1715.1	19.0	2.9	40.0
X-18	49.2	1918.6	26.1	5.1	42.1
X-19	48.7	2273.7	31.0	4.7	41.2
X-20	48.4	1820.0	25.2	3.5	38.8
X-21	48.7	1673.6	25.2	5.7	34.5
X-22	47.9	1924.1	29.9	7.7	33.2
X-23	47.4	2092.3	30.0	7.4	33.8
X-24	47.5	2573.4	37.8	7.3	32.1
X-25	46.2	2272.1	34.3	5.5	29.9
X-26	46.7	2305.0	31.8	7.1	28.4
X-27	44.9	2648.5	33.5	7.3	28.4
X-28	45.9	2731.1	37.2	7.8	27.8
X-29	44.9	3058.9	41.3	7.4	26.3
X-30	44.1	2786.6	29.8	7.7	25.8
X-31	42.9	2663.8	37.0	7.5	24.9
X-32	41.3	3467.9	51.7	8.6	23.5
X-33	40.1	3090.8	43.5	7.9	23.7
X-34	38.8	3067.9	39.7	7.9	22.6
X-35	37.0	3229.7	39.0	7.6	22.0
X-36	35.3	3471.5	47.3	7.0	24.2

X-37	33.0	3299.0	40.6	7.0	23.8
X-38	30.8	2919.7	41.0	7.7	22.3
X-39	25.3	2806.6	40.6	6.2	21.7
X-40	19.0	2998.6	43.4	5.8	21.9
X-41	13.9	3301.3	48.2	4.8	23.7

Table 5.8. Measurements of density features observed in 2007/003. PC = pulp cavity. Years are listed as distance from the pulp cavity with Year X being the year containing the pulp cavity surface and Year X-1 being one year distal to Year X. All measurements (except extensional length) are averages of measurements taken from curved slices along the X and Y planes. "-" = increment too incomplete to obtain measurement.

Year (from PC)	Radius (mm)	Area (mm²)	Extensional Length (mm)	Appositional Thickness (mm)	Angle (°)
X	30.6	-	39.4	4.5	20.0
X-1	29.7	-	36.5	4.9	18.8
X-2	29.4	1980.0	44.8	6.3	19.1
X-3	29.0	1929.3	45.1	6.6	19.5
X-4	28.5	2403.5	51.2	7.7	19.0
X-5	25.8	1905.0	44.2	7.0	19.3
X-6	25.4	2247.0	53.5	6.1	18.7
X-7	24.1	2516.6	57.1	6.9	17.2
X-8	22.8	1915.0	46.5	6.3	17.2
X-9	21.2	2017.9	53.2	5.4	16.9
X-10	21.2	2230.4	60.0	6.4	15.5
X-11	21.6	2775.6	69.3	6.5	15.3
X-12	19.1	2429.3	63.1	5.5	15.0
X-13	17.7	1413.4	46.9	5.3	16.1
X-14	16.5	1443.8	45.3	4.9	19.1
X-15	14.0	1350.2	40.1	5.0	20.1

Table 5.9. Measurements of density features observed in TA-3. PC = pulp cavity. Years are listed as distance from the proximal end of the tusk (pulp cavity not preserved in specimen) with Year Y being the most proximal year and Year Y-1 being one year distal to Year Y. All measurements (except extensional length) are averages of measurements taken from curved slices along the X and Y planes. "-" = increment too incomplete to obtain measurement.

Year (from PC)	Radius (mm)	Area (mm²)	Extensional Length (mm)	Appositional Thickness (mm)	Angle (°)
Y	29.7	-	58.7	8.4	17.7
Y-1	29.9	-	56.7	6.2	16.3
Y-2	27.5	2523.8	47.3	6.1	16.7
Y-3	26.5	2156.9	43.2	7.1	16.5
Y-4	25.2	3004.0	60.6	5.4	17.7
Y-5	25.9	2570.1	55.3	7.8	18.7
Y-6	24.0	2124.1	50.3	7.0	17.6
Y-7	22.6	2236.5	52.3	5.6	17.1
Y-8	21.0	2048.8	50.0	5.7	18.6
Y-9	20.2	1975.6	48.8	5.1	19.5
Y-10	17.8	1205.2	36.8	6.8	19.6

Table 5.10. Measurements of density features observed in 43-M. PC = pulp cavity. Years are listed as distance from the pulp cavity with Year X being the year containing the pulp cavity surface and Year X-1 being one year distal to Year X. All measurements (except extensional length) are averages of measurements taken from curved slices along the X and Y planes.

Year (from PC)	Radius (mm)	Area (mm²)	Extensional Length (mm)	Appositional Thickness (mm)	Angle (°)
X	28.1	831.0	21.3	2.6	30.1
X-1	28.6	994.3	15.9	3.8	29.4
X-2	29.3	1478.8	29.9	2.9	28.4
X-3	28.9	1413.6	27.0	3.0	30.0
X-4	29.4	1282.3	19.9	3.8	31.9
X-5	29.7	1600.8	25.4	3.6	32.8
X-6	30.5	1673.4	27.2	3.2	32.9
X-7	30.0	1265.6	19.5	3.0	31.1
X-8	30.5	1469.5	24.3	2.3	29.9
X-9	31.1	1588.7	28.5	3.6	29.5
X-10	31.1	1152.1	23.3	3.2	28.6
X-11	31.9	1045.3	23.3	2.5	27.9
X-12	31.7	1196.9	26.2	2.9	25.8
X-13	32.0	1173.9	26.8	2.1	22.1
X-14	31.3	1542.3	29.9	3.3	21.2
X-15	30.6	1862.7	33.9	3.4	19.2
X-16	30.3	1378.8	25.5	3.3	16.6
X-17				2.9	
X-18				2.6	

Table 5.11. Measurements of density features observed in 48-M. PC = pulp cavity. Years are listed as distance from the pulp cavity with Year X being the year containing the pulp cavity surface and Year X-1 being one year distal to Year X. All measurements (except extensional length) are averages of measurements taken from curved slices along the X and Y planes.

Year (from PC)	Radius (mm)	Area (mm²)	Extensional Length (mm)	Appositional Thickness (mm)	Angle (°)
X	64.9		24.9	4.0	18.9
X-1	67.2		24.9	4.2	17.6
X-2	66.8		57.4	6.3	17.5
X-3	67.2		53.2	6.9	18.3
X-4	67.2		32.3	4.8	18.1
X-5	66.2	3649.3	32.0	5.2	20.1
X-6	66.4	3832.8	33.1	5.1	22.3
X-7	66.4	2963.5	27.9	4.7	20.6
X-8	66.4	4448.4	49.9	4.8	16.7
X-9	64.7	5644.6	78.4	8.0	16.2
X-10	64.9	5163.2	54.4	5.0	17.2
X-11	63.6		62.4		
X-12	62.3		53.6		
X-13	60.0		57.9		
X-14	57.5		46.4		14.5
X-15	56.8	4507.1	65.4	7.2	14.5
X-16	53.6	3324.8	28.6	5.4	16.1
X-17	51.5	3364.9	34.8	5.4	18.1
X-18	49.5		57.0	5.6	
X-19	46.5		32.7	4.7	
X-20	43.2		66.5	6.3	
X-21	41.2	4246.7	59.8	5.2	17.6
X-22	40.4	3001.2	35.7	4.4	17.3
X-23	35.9	3266.3	41.5	5.3	16.8

Table 5.12. Measurements of density features observed in ZCHM-38. PC = pulp cavity. Years are listed as distance from the pulp cavity with Year X being the year containing the pulp cavity surface and Year X-1 being one year distal to Year X. All measurements (except extensional length) are averages of measurements taken from curved slices along the X and Y planes. "-" = increment too incomplete to obtain measurement.

Year (from PC)	Radius (mm)	Area (mm²)	Extensional Length (mm)	Appositional Thickness (mm)	Angle (°)
X	71.6	-	52.6	-	-
X-1	69.9	-	55.6	-	-
X-2	69.5	-	32.8	-	-
X-3	68.2	-	65.1	-	-
X-4	67.3	-	69.9	-	-
X-5	67.5	-	50.0	-	-
X-6	66.3	-	91.1	-	-
X-7	67.0	-	76.3	-	-
X-8	65.0	-	93.2	-	-
X-9	65.7	-	77.2	-	-
X-10	65.2	-	57.9	-	-
X-11	62.5	-	79.2	-	-
X-12	62.3	-	70.1	-	-
X-13	62.7	-	80.9	-	-
X-14	63.4	-	73.7	-	-
X-15	63.1	-	87.5	-	-
X-16	62.2	-	74.0	-	-

Table 5.13. Results of a generalized additive mixed model on the relationship of radius as a function of year from the pulp cavity. The model factors in the effects of variation within specimens and regions. edf = effective degrees of freedom, GCV = generalized cross-validation score, Ref.df = reference degrees of freedom, Std. Error = standard error.

Parametric coefficients:

	Estimate	Std. Error	t value	Pr(>|t|)
(Intercept)	28.1917	0.214	131.713	<0.05
New Siberian Islands	9.7701	0.2574	37.957	<0.05
Taymyr	-8.0843	0.7116	-11.36	<0.05
Malolyakhovsky	9.7701	0.2574	37.957	<0.05
TA-3	1.058	1.2368	0.855	0.393
ZCHM-28	3.5002	0.5127	6.827	<0.05
ZCHM-29	2.1781	0.5631	3.868	0.757
ZCHM-30	13.2566	0.4998	26.522	<0.05
ZCHM-46	7.5711	0.4775	15.857	<0.05

Approximate significance of smooth terms:

	edf	Ref.df	F	p-value
s(year from pulp cavity)	1.995	2	290.2	<0.05

R^2(adj) = 0.883
GCV = 10.411

Table 5.14. Results of a generalized additive mixed model on the relationship of cone apex angle as a function of year from the pulp cavity. The model factors in the effects of variation within specimens and regions. edf = effective degrees of freedom, GCV = generalized cross-validation score, Ref.df = reference degrees of freedom, Std. Error = standard error.

Parametric coefficients:

	Estimate	Std. Error	t value	Pr(>|t|)
(Intercept)	18.7649	0.1821	103.068	<0.05
New Siberian Islands	8.0234	0.2072	38.731	<0.05
Taymyr	-4.1421	0.5334	-7.766	<0.05
Malolyakhovsky	8.0234	0.2072	38.731	<0.05
TA-3	-0.648	0.95	-0.682	0.496
ZCHM-28	8.0858	0.3883	20.822	<0.05
ZCHM-29	0.1314	0.4232	0.31	0.757
ZCHM-30	6.6664	0.3807	17.511	<0.05

Approximate significance of smooth terms:

	edf	Ref.df	F	p-value
s(year from pulp cavity)	1.875	1.984	236.9	<0.05

R2(adj) = 0.882

GCV = 6.168

Table 5.15. Results of generalized additive models on the relationships of area, extension, and apposition as a function of year from the pulp cavity in ZCHM-28. edf = effective degrees of freedom, GCV = generalized cross-validation score, Ref.df = reference degrees of freedom, Std. Error = standard error.

Area

Parametric coefficients:

	Estimate	Std. Error	t value	Pr(>|t|)
(Intercept)	2100.59	30.74	68.33	<0.05

Approximate significance of smooth terms:

	edf	Ref.df	F	p-value
s(year from pulp cavity)	21.88	25.44	14.91	<0.05

R^2(adj) = 0.923
GCV = 1.06e05

Extension

Parametric coefficients:

	Estimate	Std. Error	t value	Pr(>|t|)
(Intercept)	34.39	0.55	62.89	<0.05

Approximate significance of smooth terms:

	edf	Ref.df	F	p-value
s(year from pulp cavity)	18.8	22.45	13.51	<0.05

R^2(adj) = 0.91
GCV = 25.096

Apposition

Parametric coefficients:

	Estimate	Std. Error	t value	Pr(>|t|)
(Intercept)	5.33	0.15	36.26	<0.05

Approximate significance of smooth terms:

	edf	Ref.df	F	p-value
s(year from pulp cavity)	12.13	14.96	2.93	<0.05

R^2(adj) = 0.56

GCV = 1.17

Table 5.16. Results of generalized additive models on the relationships of area, extension, and apposition as a function of year from the pulp cavity in ZCHM-29. edf = effective degrees of freedom, GCV = generalized cross-validation score, Ref.df = reference degrees of freedom, Std. Error = standard error.

Area

Parametric coefficients:

	Estimate	Std. Error	t value	Pr(>|t|)
(Intercept)	2652.13	85.32	31.08	<0.05

Approximate significance of smooth terms:

	edf	Ref.df	F	p-value
s(year from pulp cavity)	1.634	2.03	4.457	<0.05

R^2(adj) = 0.29
GCV = 1.75e05

Extension

Parametric coefficients:

	Estimate	Std. Error	t value	Pr(>|t|)
(Intercept)	44.77	1.15	39.03	<0.05

Approximate significance of smooth terms:

	edf	Ref.df	F	p-value
s(year from pulp cavity)	12.46	14.01	2.074	0.11

R^2(adj) = 0.462
GCV = 71.096

Apposition

Parametric coefficients:

	Estimate	Std. Error	t value	Pr(>|t|)
(Intercept)	6.22	0.16	39.36	<0.05

Approximate significance of smooth terms:

	edf	Ref.df	F	p-value
s(year from pulp cavity)	1.54	1.90	1.86	0.24

R^2(adj) = 0.08

GCV = 0.70

Table 5.17. Results of generalized additive models on the relationships of area, extension, and apposition as a function of year from the pulp cavity in ZCHM-30. edf = effective degrees of freedom, GCV = generalized cross-validation score, Ref.df = reference degrees of freedom, Std. Error = standard error.

Area

Parametric coefficients:

	Estimate	Std. Error	t value	Pr(>|t|)
(Intercept)	2813.1	54.8	51.33	<0.05

Approximate significance of smooth terms:

	edf	Ref.df	F	p-value
s(year from pulp cavity)	20.09	22.52	3.572	<0.05

R^2(adj) = 0.678
GCV = 2.69e05

Extension

Parametric coefficients:

	Estimate	Std. Error	t value	Pr(>|t|)
(Intercept)	41.36	1.22	33.98	<0.05

Approximate significance of smooth terms:

	edf	Ref.df	F	p-value
s(year from pulp cavity)	20.52	22.8	2.40	0.05

R^2(adj) = 0.58
GCV = 137.2

Apposition

Parametric coefficients:

	Estimate	Std. Error	t value	Pr(>|t|)
(Intercept)	5.61	0.22	25.1	<0.05

Approximate significance of smooth terms:

	edf	Ref.df	F	p-value
s(year from pulp cavity)	1.91	2.39	0.06	0.95

R^2(adj) = -0.03

GCV = 1.86

Table 5.18. Results of generalized additive models on the relationships of area, extension, and apposition as a function of year from the pulp cavity in the Malolyakhovsky specimen. edf = effective degrees of freedom, GCV = generalized cross-validation score, Ref.df = reference degrees of freedom, Std. Error = standard error.

Area

Parametric coefficients:

	Estimate	Std. Error	t value	Pr(>|t|)
(Intercept)	2248.32	25.65	87.66	<0.05

Approximate significance of smooth terms:

	edf	Ref.df	F	p-value
s(year from pulp cavity)	25.27	30.75	22.65	<0.05

R^2(adj) = 0.944
GCV = 73786

Extension

Parametric coefficients:

	Estimate	Std. Error	t value	Pr(>|t|)
(Intercept)	31.51	0.52	60.58	<0.05

Approximate significance of smooth terms:

	edf	Ref.df	F	p-value
s(year from pulp cavity)	24.14	28.97	8.87	<0.05

R^2(adj) = 0.857
GCV = 28.295

Apposition

Parametric coefficients:

	Estimate	Std. Error	t value	Pr(>|t|)
(Intercept)	5.92	0.12	49.97	<0.05

Approximate significance of smooth terms:

	edf	Ref.df	F	p-value
s(year from pulp cavity)	7.77	9.70	11.7	<0.05

R^2(adj) = 0.73
GCV = 0.74

Table 5.19. Results of generalized additive models on the relationships of area, extension, and apposition as a function of year from the pulp cavity in the 2007/003. edf = effective degrees of freedom, GCV = generalized cross-validation score, Ref.df = reference degrees of freedom, Std. Error = standard error.

Area

Parametric coefficients:

	Estimate	Std. Error	t value	Pr(>|t|)
(Intercept)	2039.79	36.33	56.15	<0.05

Approximate significance of smooth terms:

	edf	Ref.df	F	p-value
s(year from pulp cavity)	10.49	10.94	11.37	<0.05

R^2(adj) = 0.9
GCV = 1.03e5

Extension

Parametric coefficients:

	Estimate	Std. Error	t value	Pr(>|t|)
(Intercept)	49.76	0.88	56.73	<0.05

Approximate significance of smooth terms:

	edf	Ref.df	F	p-value
s(year from pulp cavity)	8.14	8.79	10.49	<0.05

R^2(adj) = 0.85
GCV = 58.70

Apposition

Parametric coefficients:

	Estimate	Std. Error	t value	Pr(>|t|)
(Intercept)	5.96	0.12	48.93	<0.05

Approximate significance of smooth terms:

	edf	Ref.df	F	p-value
s(year from pulp cavity)	4.27	5.23	7.42	<0.05

R^2(adj) = 0.72

GCV = 0.35

Table 5.20. Results of generalized additive models on the relationships of area, extension, and apposition as a function of year from the pulp cavity in the TA-3. edf = effective degrees of freedom, GCV = generalized cross-validation score, Ref.df = reference degrees of freedom, Std. Error = standard error.

Area

Parametric coefficients:

	Estimate	Std. Error	t value	Pr(>|t|)
(Intercept)	2205.0	102.7	21.48	<0.05

Approximate significance of smooth terms:

	Edf	Ref.df	F	p-value
s(year from pulp cavity)	1.791	2.222	6.061	<0.05

R^2(adj) = 0.613
GCV = 1.37e5

Extension

Parametric coefficients:

	Estimate	Std. Error	t value	Pr(>|t|)
(Intercept)	50.93	0.94	53.95	<0.05

Approximate significance of smooth terms:

	Edf	Ref.df	F	p-value
s(year from pulp cavity)	7.45	8.36	5.12	.13

R^2(adj) = 0.80
GCV = 42.26

Apposition

Parametric coefficients:

	Estimate	Std. Error	t value	Pr(>|t|)
(Intercept)	6.74	0.30	21.72	<0.05

Approximate significance of smooth terms:

	edf	Ref.df	F	p-value
s(year from pulp cavity)	1.00	1.00	1.97	0.19

R^2(adj) = 0.09

GCV = 1.19

Table 5.21. Results of generalized additive models on the relationships of area, extension, and apposition as a function of year from the pulp cavity in the 43-M. edf = effective degrees of freedom, GCV = generalized cross-validation score, Ref.df = reference degrees of freedom, Std. Error = standard error.

Area

Parametric coefficients:

	Estimate	Std. Error	t value	Pr(>|t|)
(Intercept)	1350.0	8.29	162.9	<0.05

Approximate significance of smooth terms:

	Edf	Ref.df	F	p-value
s(year from pulp cavity)	12.85	13	73.35	<0.05

R^2(adj) = 0.98
GCV = 6299.9

Extension

Parametric coefficients:

	Estimate	Std. Error	t value	Pr(>|t|)
(Intercept)	25.17	0.30	84	<0.05

Approximate significance of smooth terms:

	Edf	Ref.df	F	p-value
s(year from pulp cavity)	12.68	12.98	15.07	<0.05

R^2(adj) = 0.92
GCV = 7.81

Apposition

Parametric coefficients:

	Estimate	Std. Error	t value	Pr(>|t|)
(Intercept)	3.06	0.11	27.2	<0.05

Approximate significance of smooth terms:

	Edf	Ref.df	F	p-value
s(year from pulp cavity)	1.00	1.00	0.839	0.37

R^2(adj) = 0.01

GCV = 0.27

Table 5.22. Results of generalized additive models on the relationships of area, extension, and apposition as a function of year from the pulp cavity in the 48-M. edf = effective degrees of freedom, GCV = generalized cross-validation score, Ref.df = reference degrees of freedom, Std. Error = standard error.

Area

Parametric coefficients:

	Estimate	Std. Error	t value	Pr(>|t|)
(Intercept)	3951.1	168.7	23.42	<0.05

Approximate significance of smooth terms:

	Edf	Ref.df	F	p-value
s(year from pulp cavity)	4.475	5.164	3.036	<0.05

R^2(adj) = 0.54
GCV = 6.28e5

Extension

Parametric coefficients:

	Estimate	Std. Error	t value	Pr(>|t|)
(Intercept)	46.278	2.96	15.61	<0.05

Approximate significance of smooth terms:

	Edf	Ref.df	F	p-value
s(year from pulp cavity)	1.76	2.19	1.47	0.24

R^2(adj) = 0.01
GCV = 238.44

Apposition

Parametric coefficients:

	Estimate	Std. Error	t value	Pr(>|t|)
(Intercept)	5.42	0.23	23.6	<0.05

Approximate significance of smooth terms:

	edf	Ref.df	F	p-value
s(year from pulp cavity)	1.58	1.97	0.63	0.56

R^2(adj) = 0.02

GCV = 1.21

Table 5.23. Results of a generalized additive model on the relationship of extensional length as a function of year from the pulp cavity in ZCHM-46. edf = effective degrees of freedom, GCV = generalized cross-validation score, Ref.df = reference degrees of freedom, Std. Error = standard error.

Parametric coefficients:

	Estimate	Std. Error	t value
(Intercept)	39.99	1.01	39.64

Approximate significance of smooth terms:

	edf	Ref.df	F
s(year from pulp cavity)	19.73	24.07	5.89

R^2(adj) = 0.769
GCV = 84.44

Table 5.24. Results of a generalized additive model on the relationship of extensional length as a function of year from the pulp cavity in ZCHM-38. edf = effective degrees of freedom, GCV = generalized cross-validation score, Ref.df = reference degrees of freedom, Std. Error = standard error.

Parametric coefficients:

	Estimate	Std. Error	t value	
(Intercept)	69.82	3.12	22.41	

Approximate significance of smooth terms:

	edf	Ref.df	F	
s(year from pulp cavity)	1.70	2.12	4.45	

R^2(adj) = 0.35
GCV = 196.25

Table 5.25. Results of a generalized additive mixed model on the relationship of extensional length as a function of year from the pulp cavity. The model factors in the effects of variation within regions. edf = effective degrees of freedom, GCV = generalized cross-validation score, Ref.df = reference degrees of freedom, Std. Error = standard error.

Parametric coefficients:

	Estimate	Std. Error	t value	Pr(>|t|)
(Intercept)	39.96	0.68	59.06	<0.05
New Siberian Islands	-2.69	1.46	-1.84	0.07
Taymyr	-0.03	1.94	-0.02	0.99

Approximate significance of smooth terms:

	edf	Ref.df	F	p-value
s(year from pulp cavity)	6.68	7.80	25.82	<0.05

R^2(adj) = 0.60
GCV = 61.00

Figure 5.1. A, longitudinal curved virtual slice from the left tusk of the Malolyakhovsky mammoth. The pulp cavity is visible in the upper right. B, magnified section from the longitudinal curved slice showing X-ray attenuation features interpreted as bounding annual growth increments. White lines locate some of the abrupt transitions from higher attenuation to lower attenuation (interpreted as the seasonal boundary between winter and spring), which we use to distinguish years.
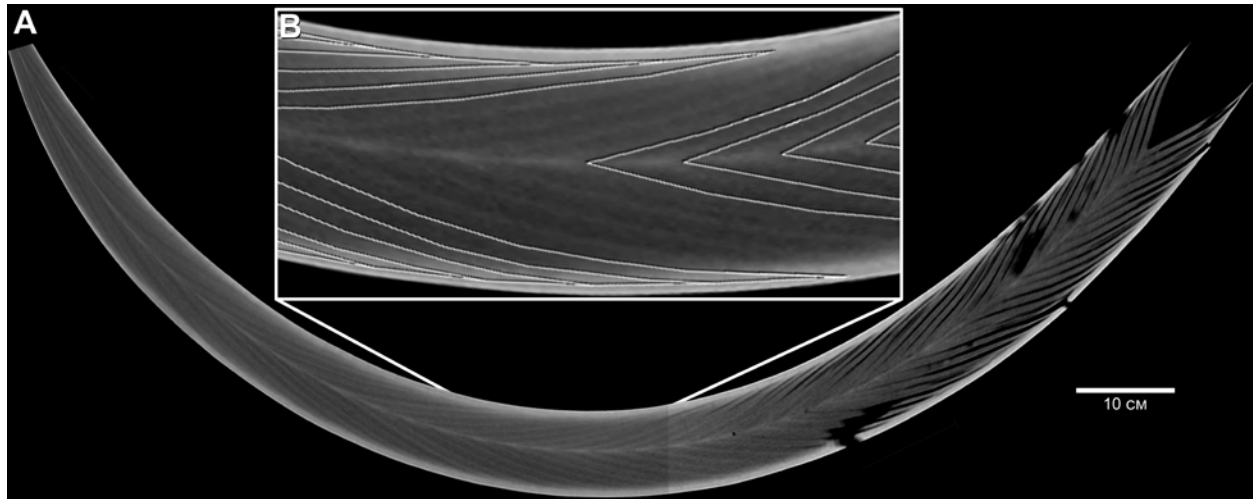
Figure 5.2. Measurement protocol for microCT curved slices. One of the longitudinal slices of the middle section of the left tusk of the Malolyakhovsky mammoth (in orthographic view), showing the five variables used here to characterize annual rates of tusk growth: 1) radius, 2) area, 3) extensional length, 4) cone apex angle, and 5) appositional thickness. Measurements 1 and 2 are shown for the same year, as are 3 and 5. 4a and 4b show the location of angular measurements at both boundaries of a single year. White dashed line marks the boundary between dentin and cementum. White solid lines following former pulp cavity surfaces bounding a single annual increment within the tusk, which is used for measurement of area. White dotted lines mark a portion of the boundaries between annual increments near the cone apex to aid in visualization of the location for extensional length measurement. Dash-dot lines show the arms of each angle used for measurements of cone apex angle. Measurements are made on two perpendicular longitudinal slices for all specimens, and are then averaged together.
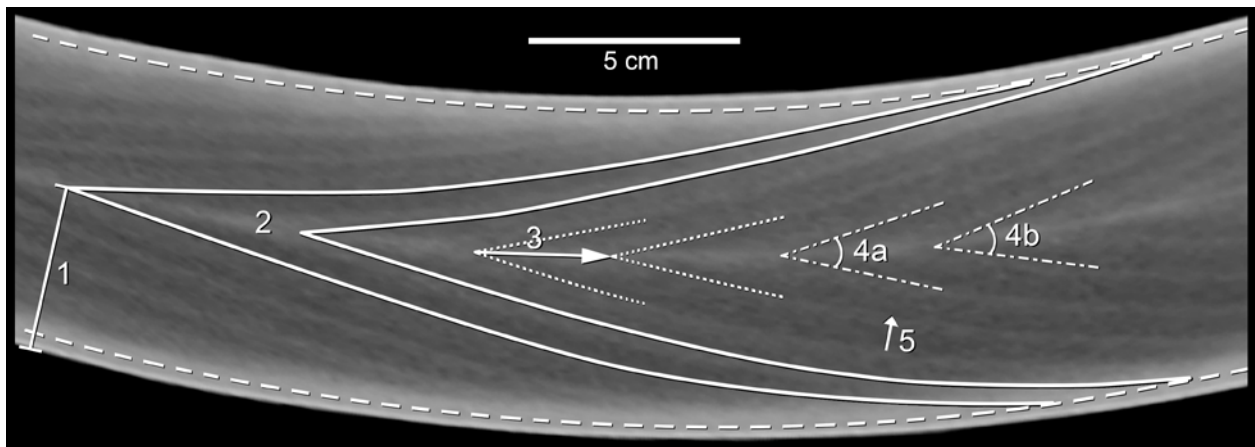
Figure 5.3. Graph of greatest tusk radius measurements relative to years from the pulp cavity. Specimens are identified based on their color. Circles denote specimens from Chukotka, squares are specimens from the Taymyr Peninsula, triangles represent specimens from the New Siberian Islands, and crosses mark specimens from Wrangel Island.
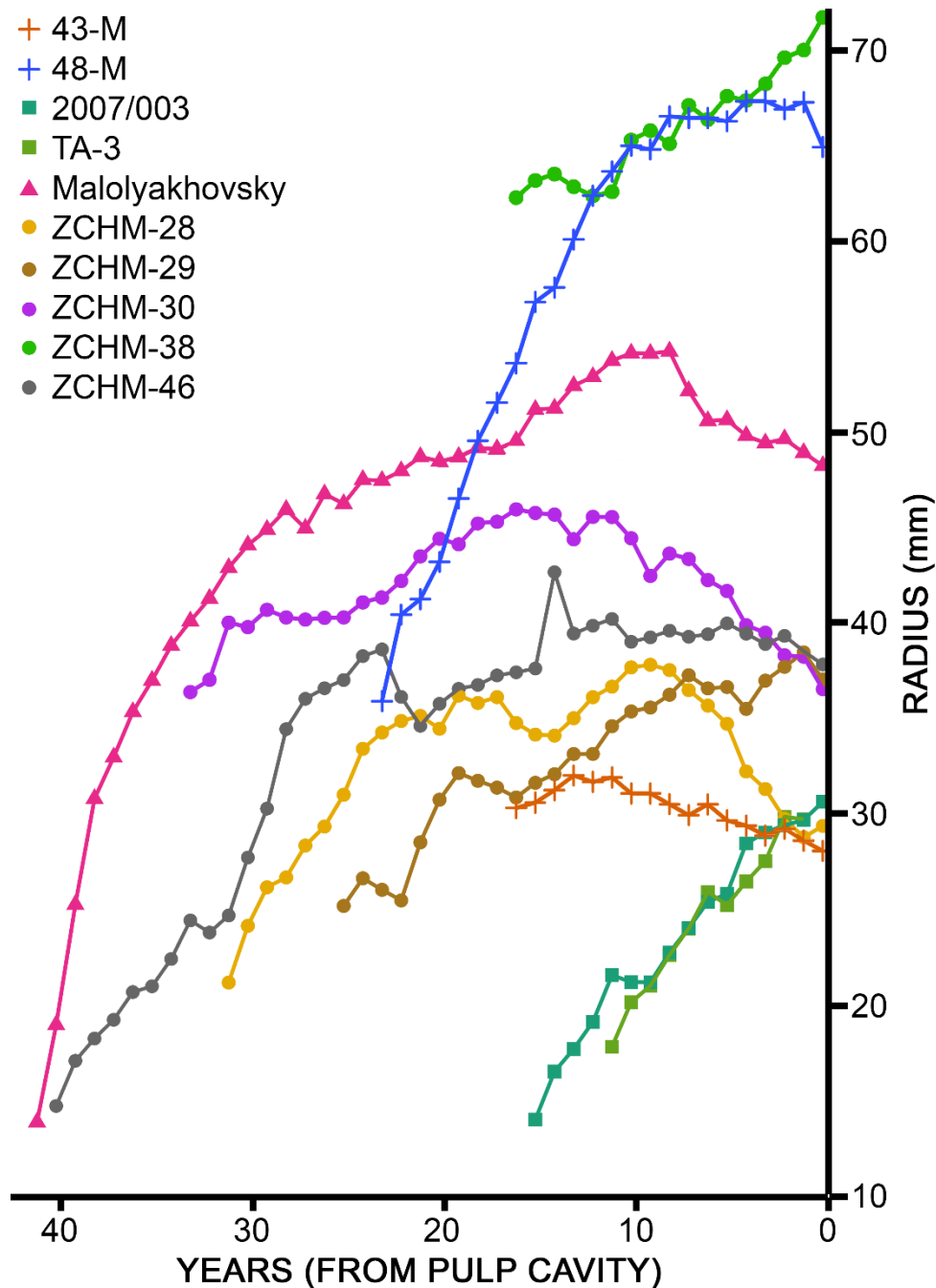
Figure 5.4. Generalized additive mixed model of tusk radius on years from the pulp cavity for all female specimens. The blue line shows the model, while the grey shading is the associated standard error. See Table 5.13 for statistical results of model.
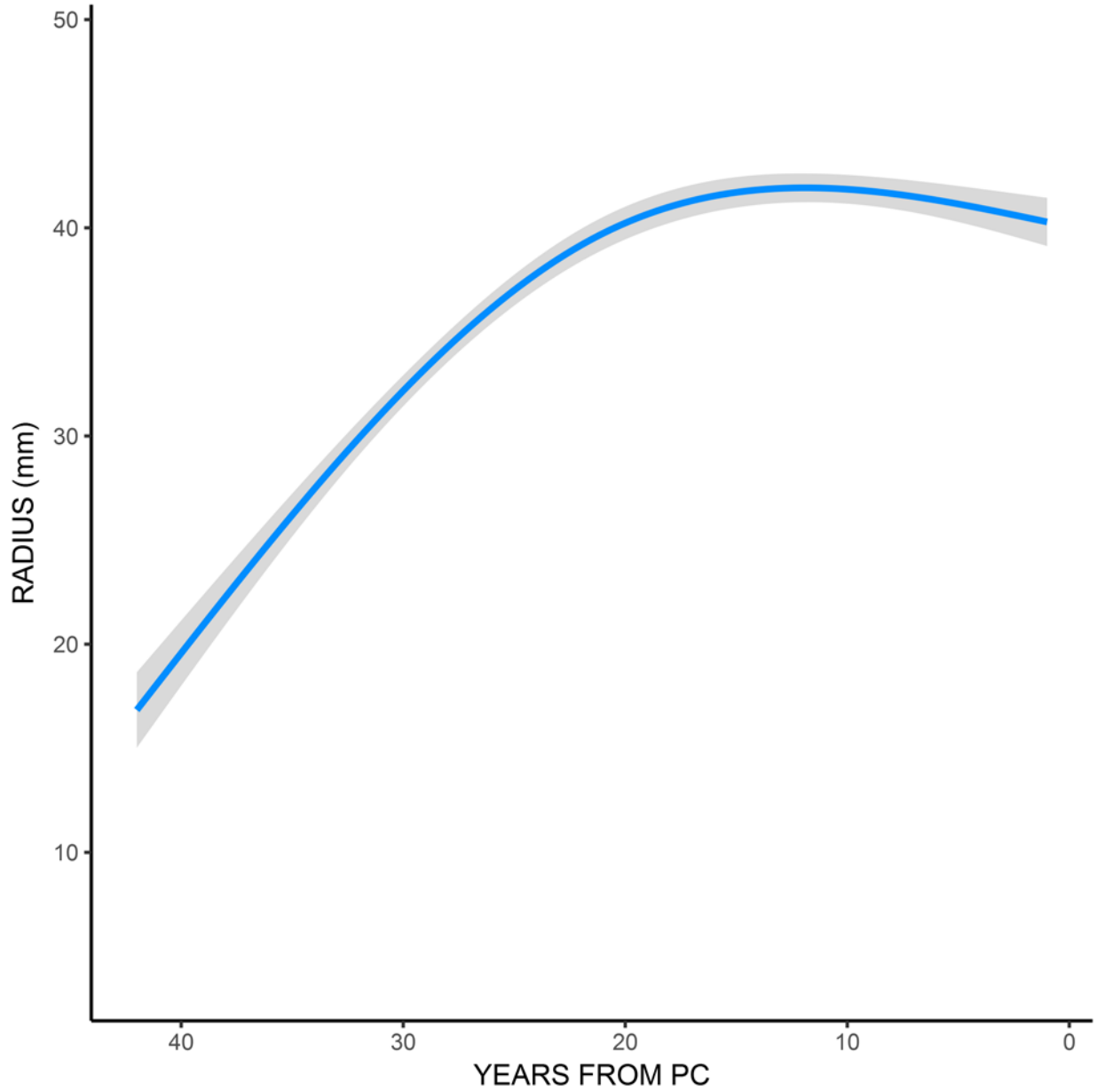
Figure 5.5. Graph of cone apex angle measurements relative to years from the pulp cavity. Specimens are identified based on their color. Circles denote specimens from Chukotka, squares are specimens from the Taymyr Peninsula, triangles represent specimens from the New Siberian Islands, and crosses mark specimens from Wrangel Island.
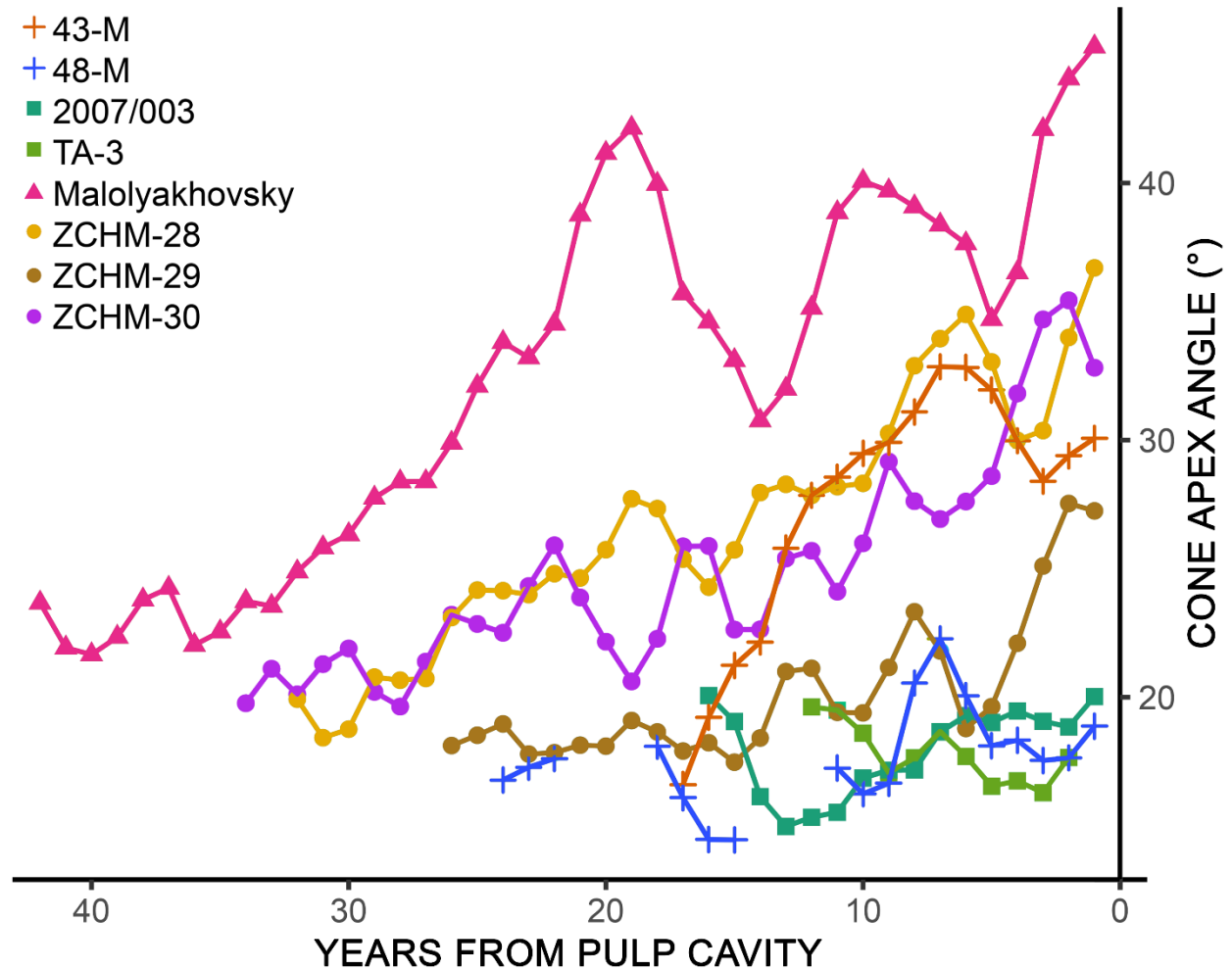
Figure 5.6. Graph of cone apex angle measurements relative to radius. Specimens are identified based on their color. Circles denote specimens from Chukotka, squares are specimens from the Taymyr Peninsula, triangles represent specimens from the New Siberian Islands, and crosses mark specimens from Wrangel Island.
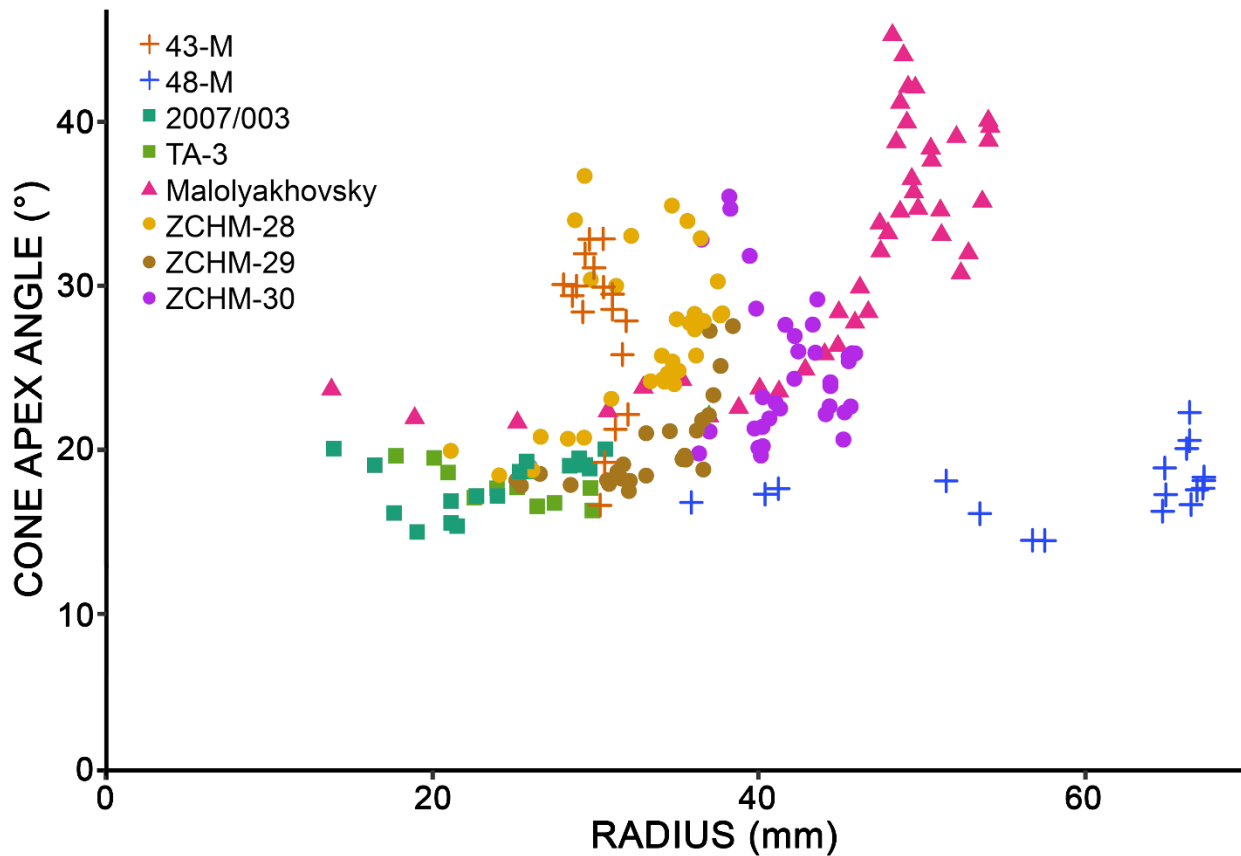
Figure 5.7. Generalized additive mixed model of cone apex angle on years from the pulp cavity for all female specimens. The blue line shows the model, while the grey shading is the associated standard error. See Table 5.14 for statistical results of model.
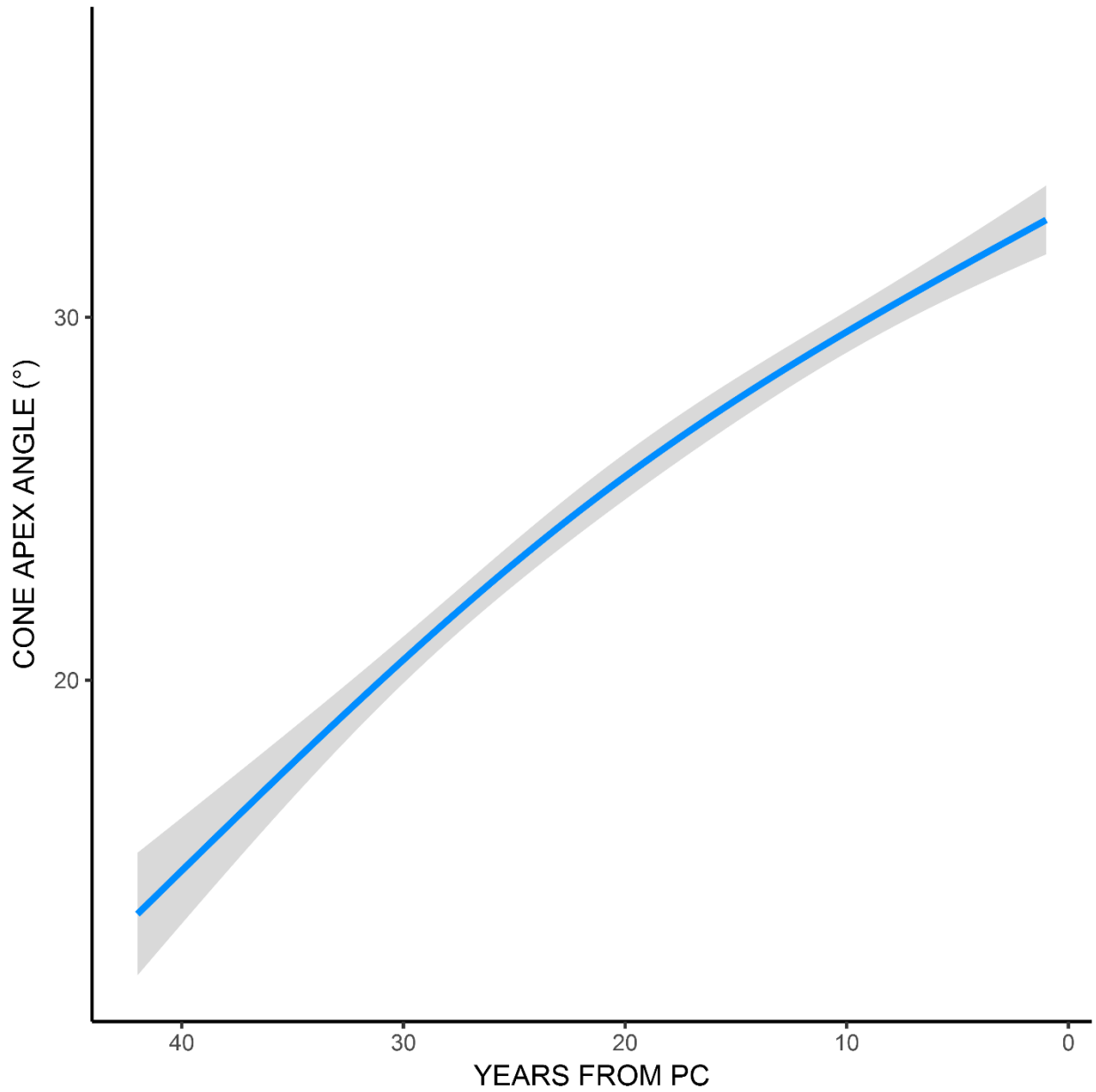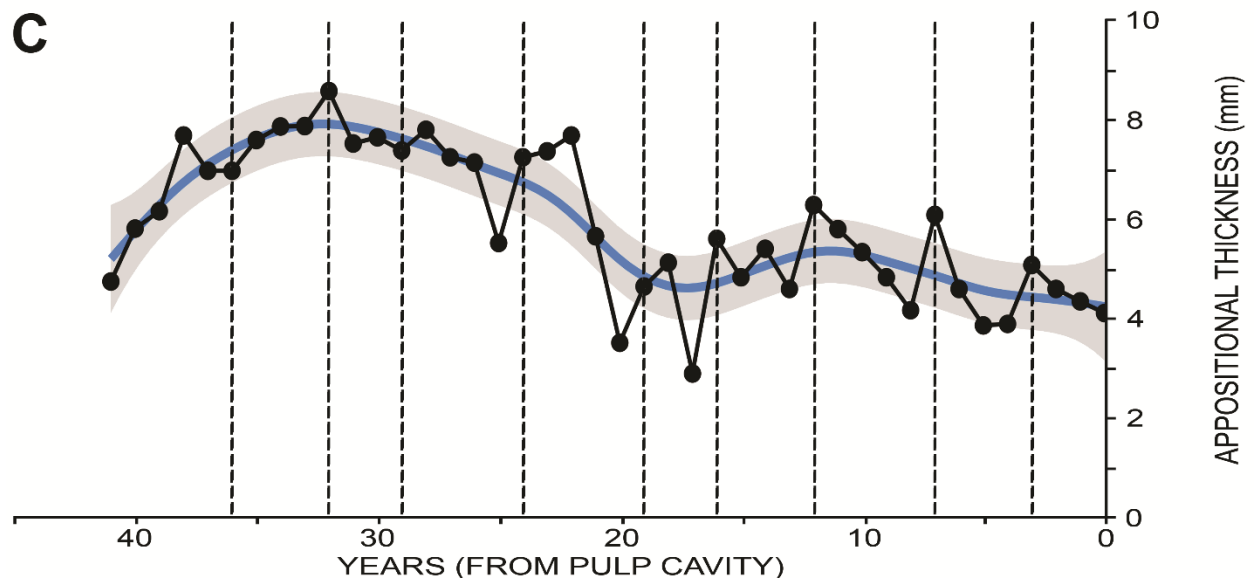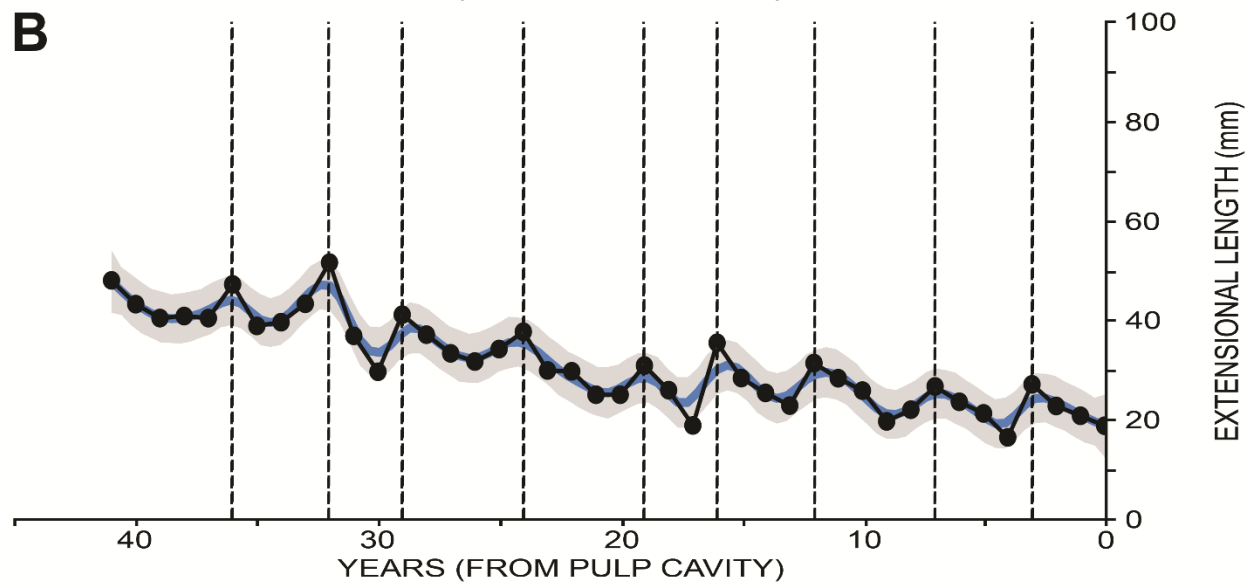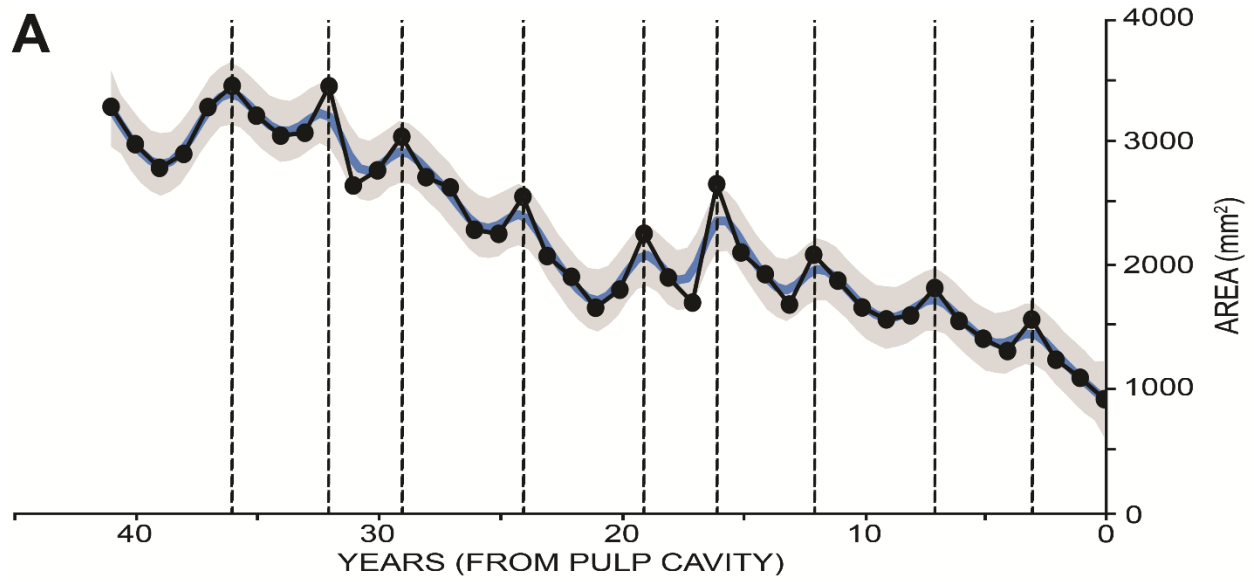
Figure 5.8. Graphs of annual measurements taken from ZCHM-28 showing A) area, B) extensional length, and C) appositional thickness. The year of death (year X) is recorded at 0 years from the pulp cavity. Black dots connected by black lines are the measured values for each year. The blue lines and grey shading are the generalized additive models and associated standard errors, respectively. Vertical dashed lines mark local peaks within the pattern of annual area measurements and are projected down onto the same year in the graphs for the other measurements. These peaks mark the boundaries between undulations within the secondary pattern observed in both annual areas and extensional lengths. See Table 5.15 for statistical results of model.
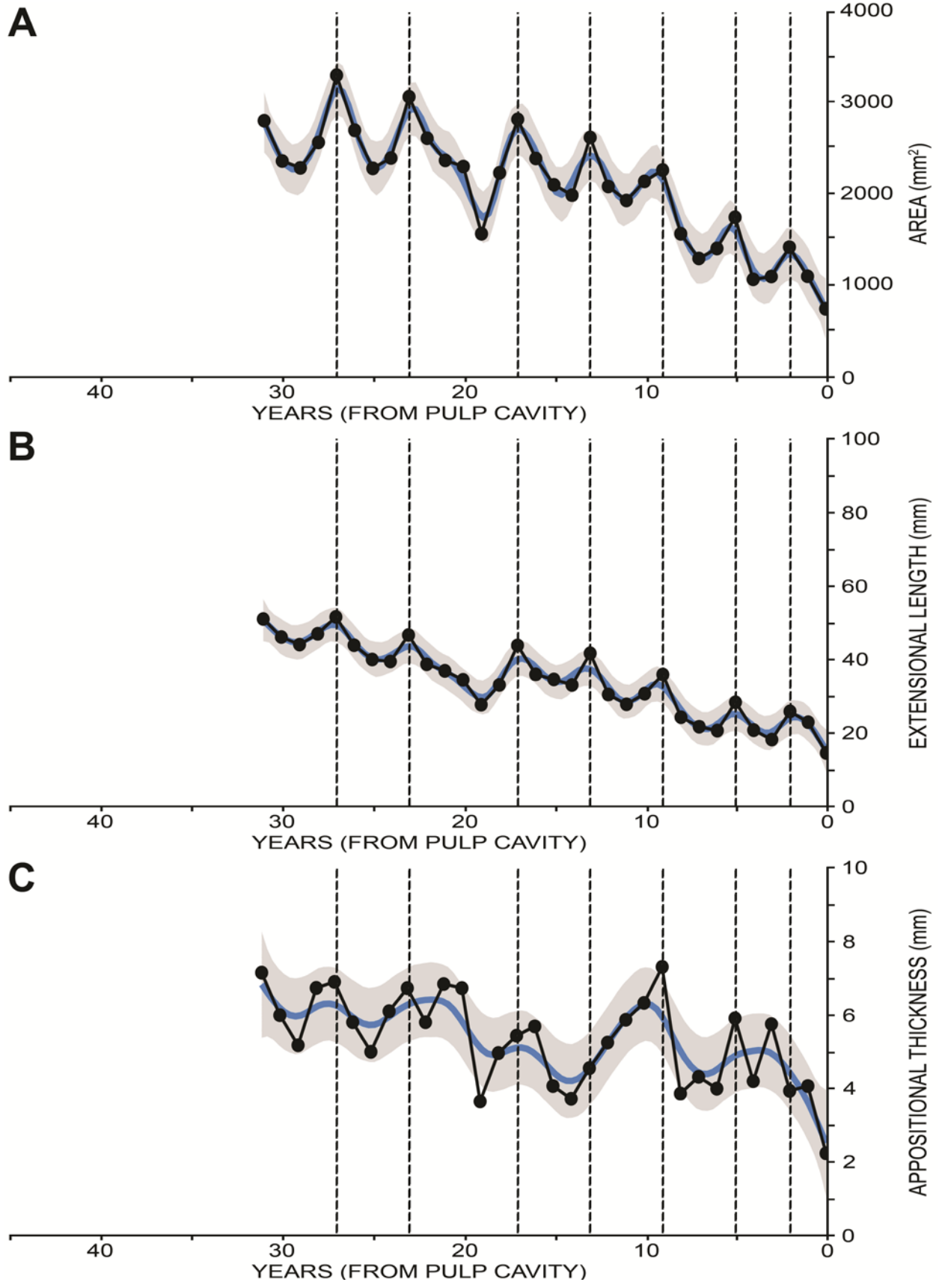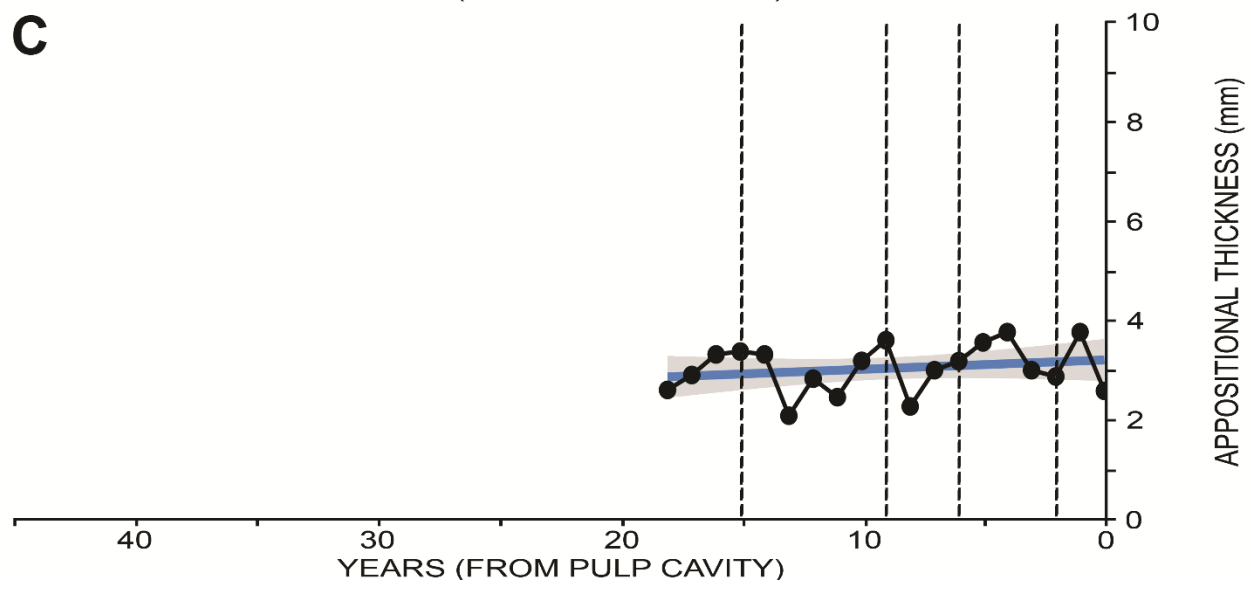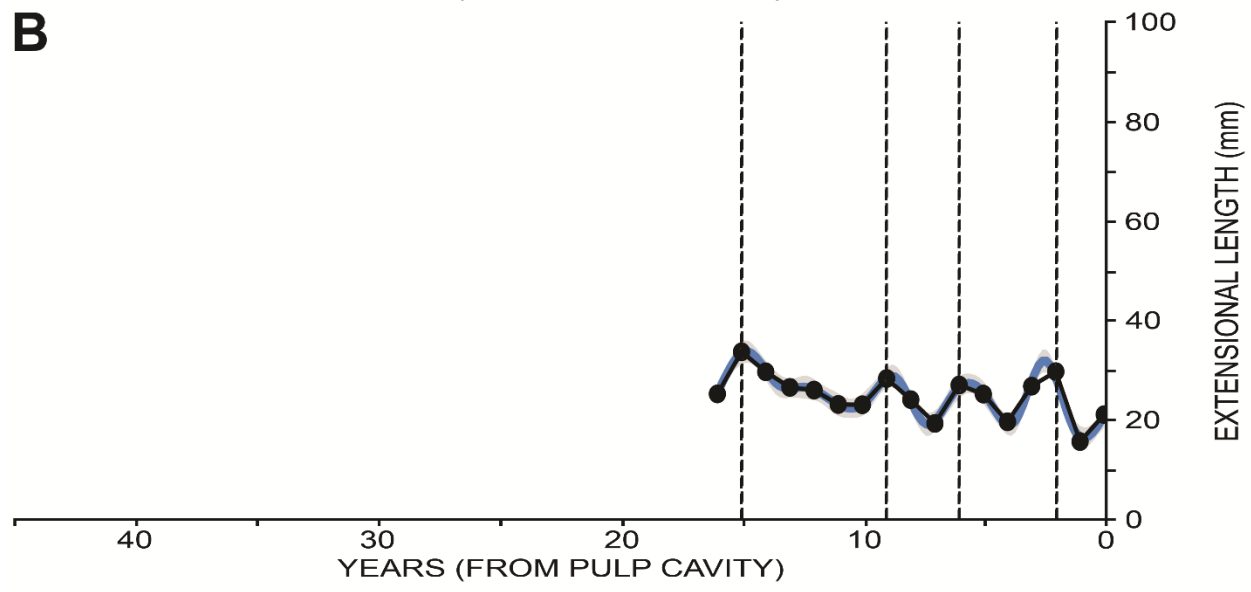
Figure 5.9. Graphs of annual measurements taken from ZCHM-29 showing A) areas, B) extensional lengths, and C) appositional thicknesses. The year of death (year X) is recorded at 0 years from the pulp cavity. Black dots connected by black lines are the measured values for each year. The blue lines and grey shadings are the generalized additive models and associated standard errors, respectively. Vertical dashed lines mark local peaks within the pattern of annual area measurements and are projected down onto the same year in the graphs for the other measurements. These peaks mark the boundaries between undulations within the secondary pattern observed in both annual areas and extensional lengths. See Table 5.16 for statistical results of model.
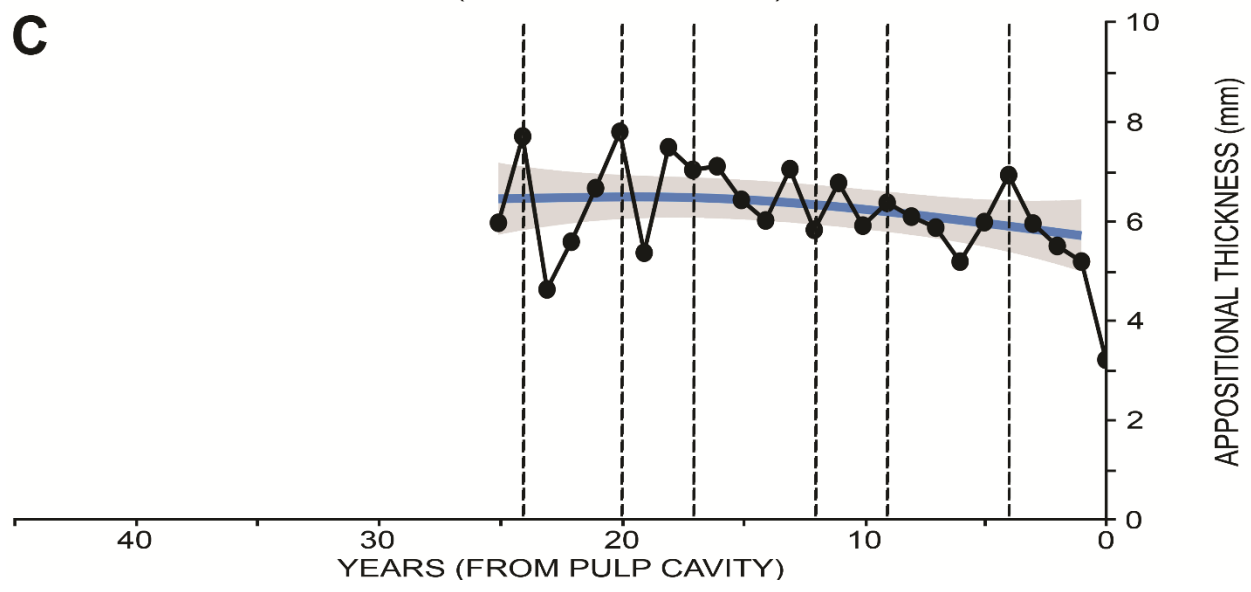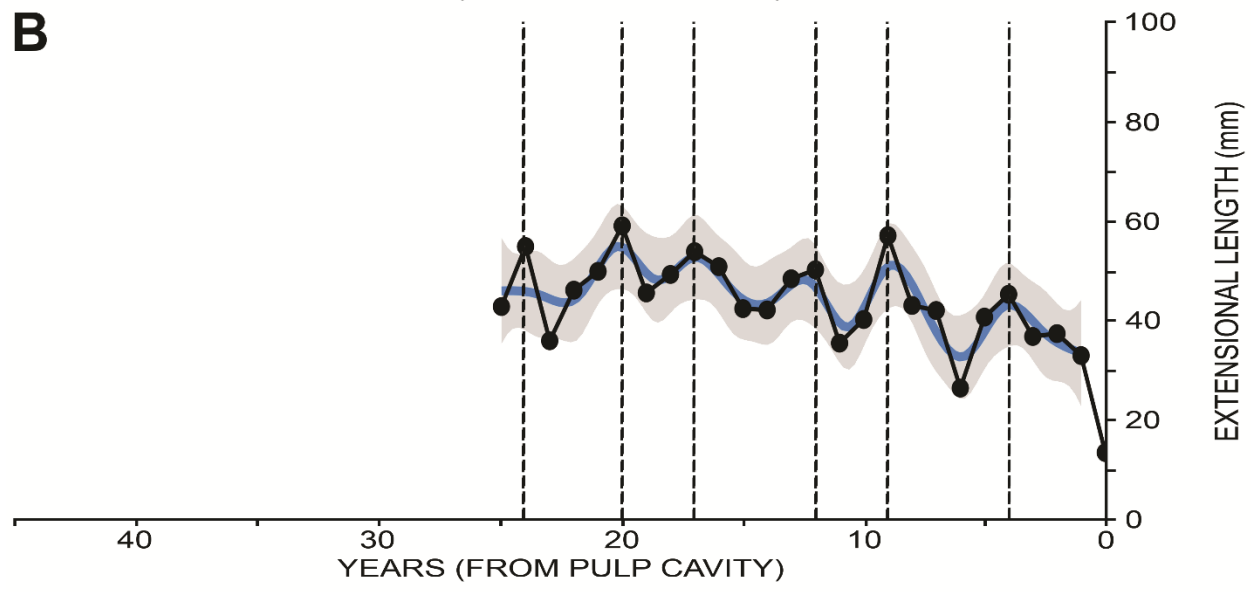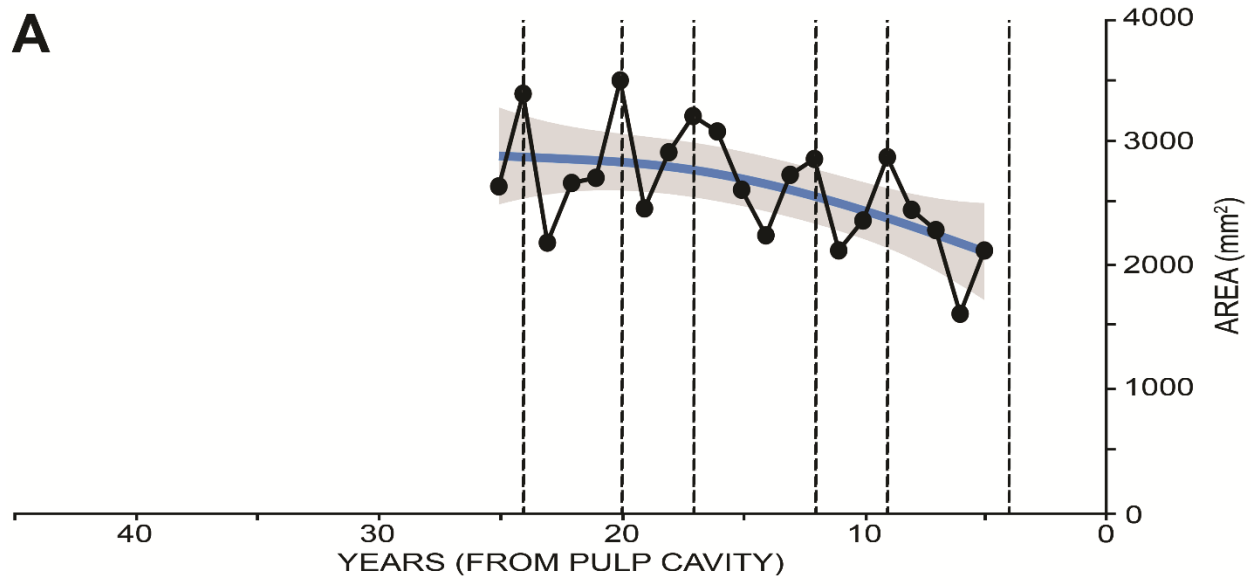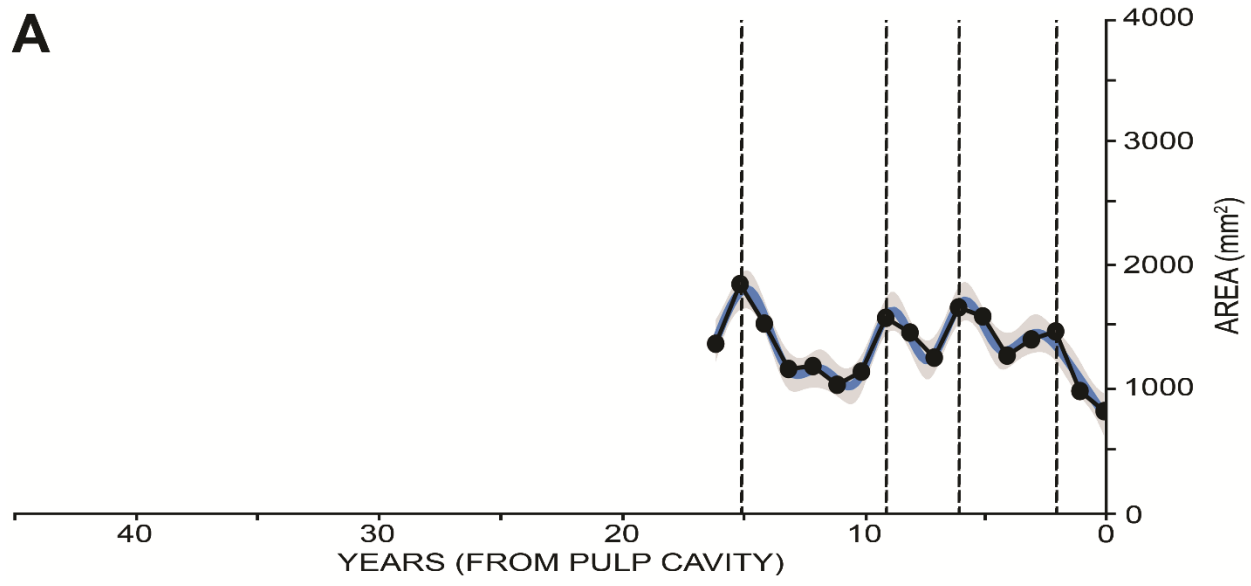
Figure 5.10. Graphs of annual measurements taken from ZCHM-30 showing A) areas, B) extensional lengths, and C) appositional thicknesses. The year of death (year X) is recorded at 0 years from the pulp cavity. Black dots connected by black lines are the measured values for each year. The blue lines and grey shadings are the generalized additive models and associated standard errors, respectively. Vertical dashed lines mark local peaks within the pattern of annual area measurements and are projected down onto the same year in the graphs for the other measurements. These peaks mark the boundaries between undulations within the secondary pattern observed in both annual areas and extensional lengths. See Table 5.17 for statistical results of model.
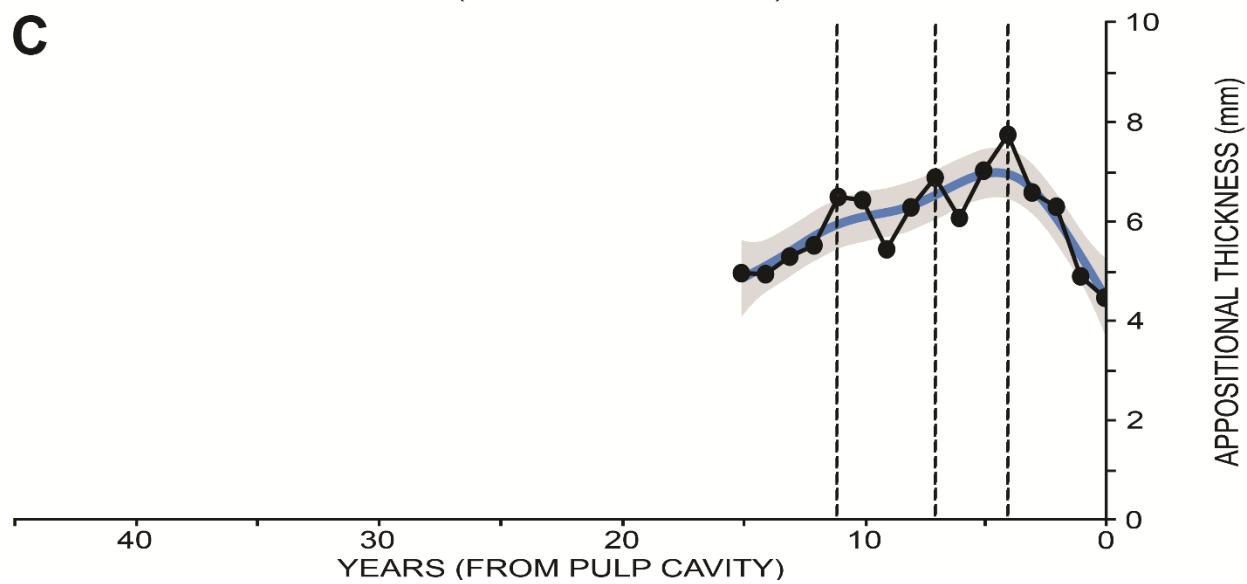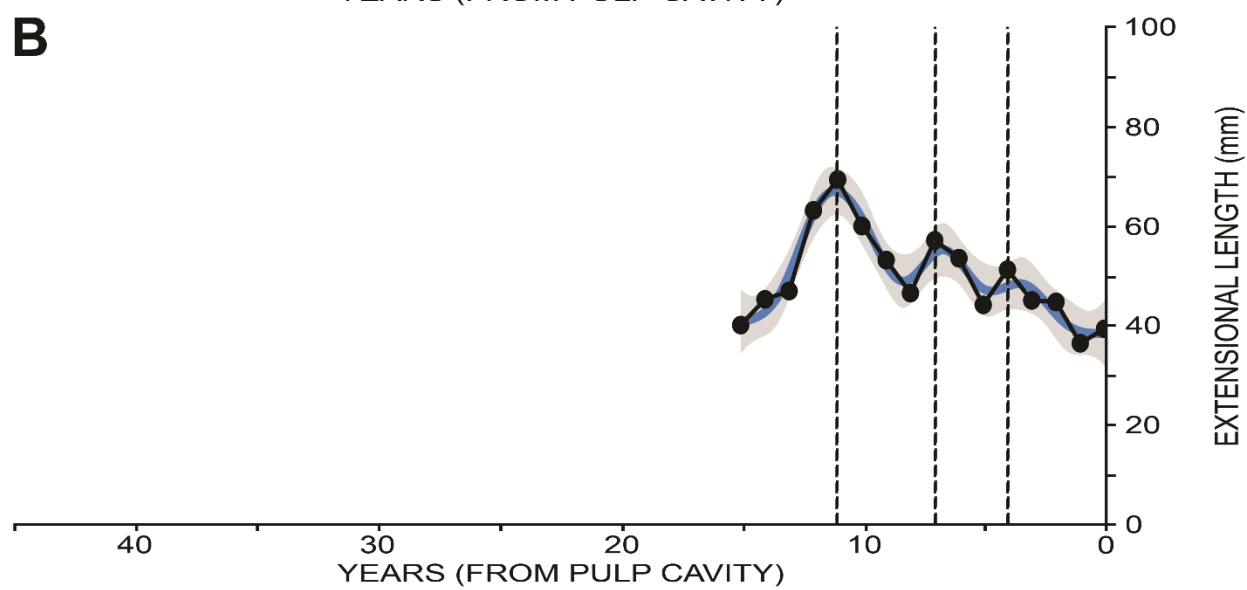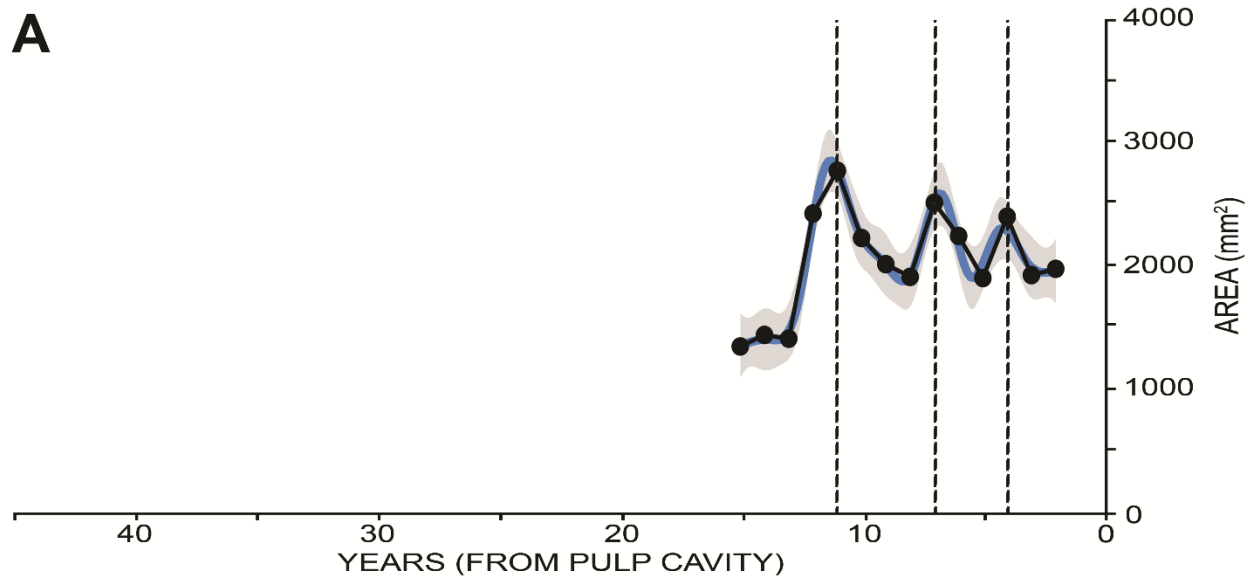
221
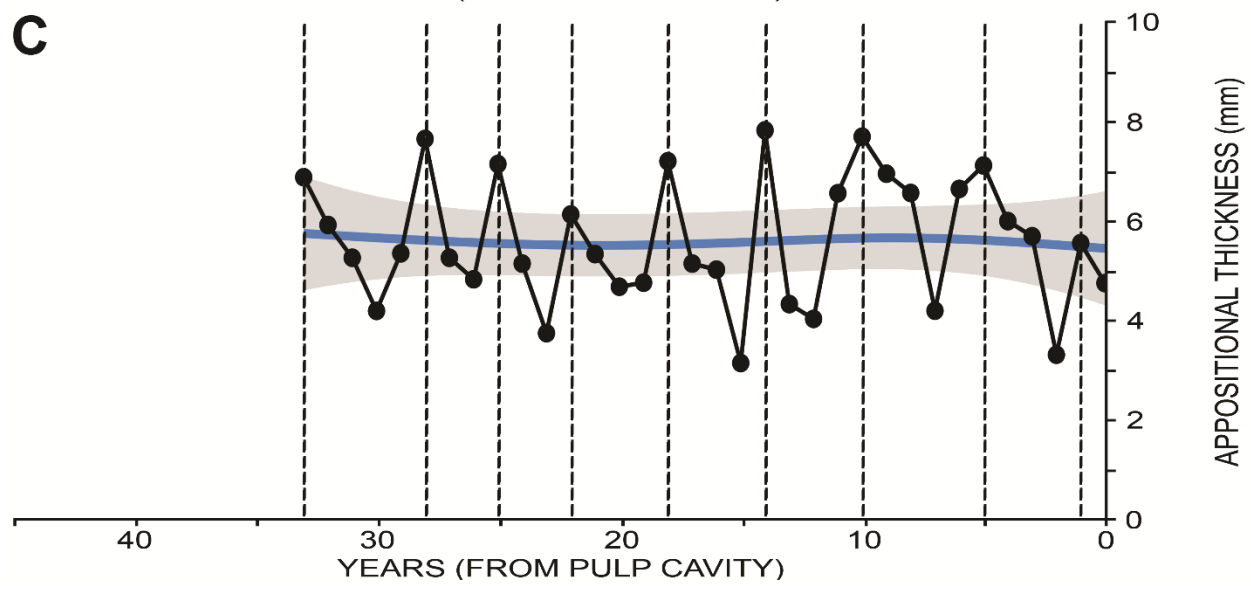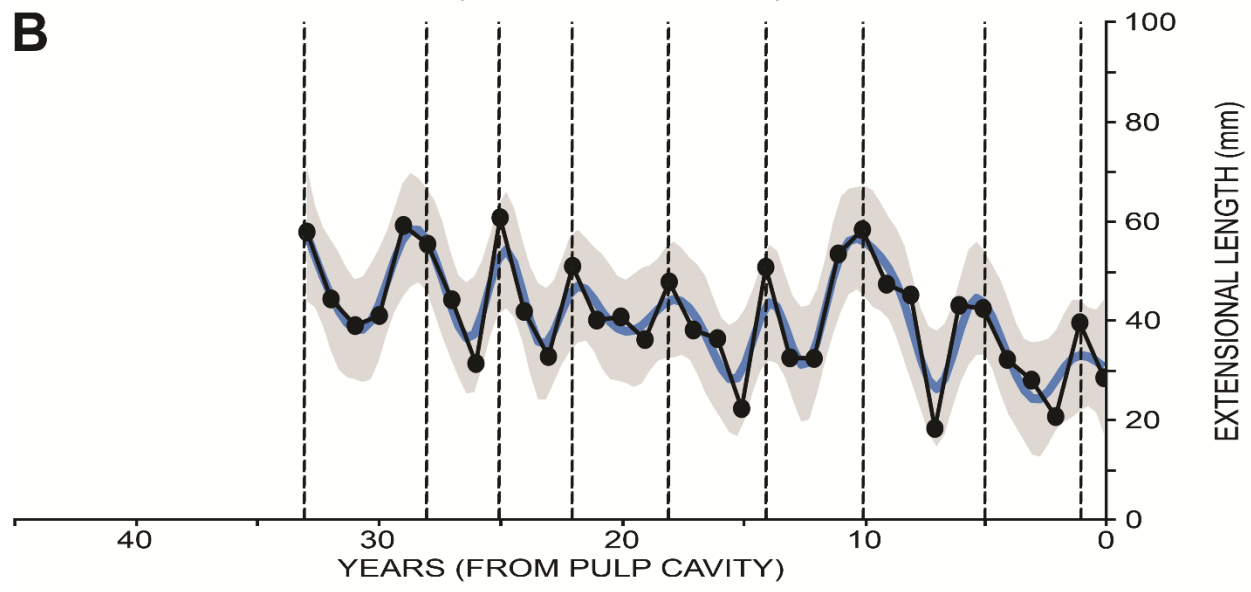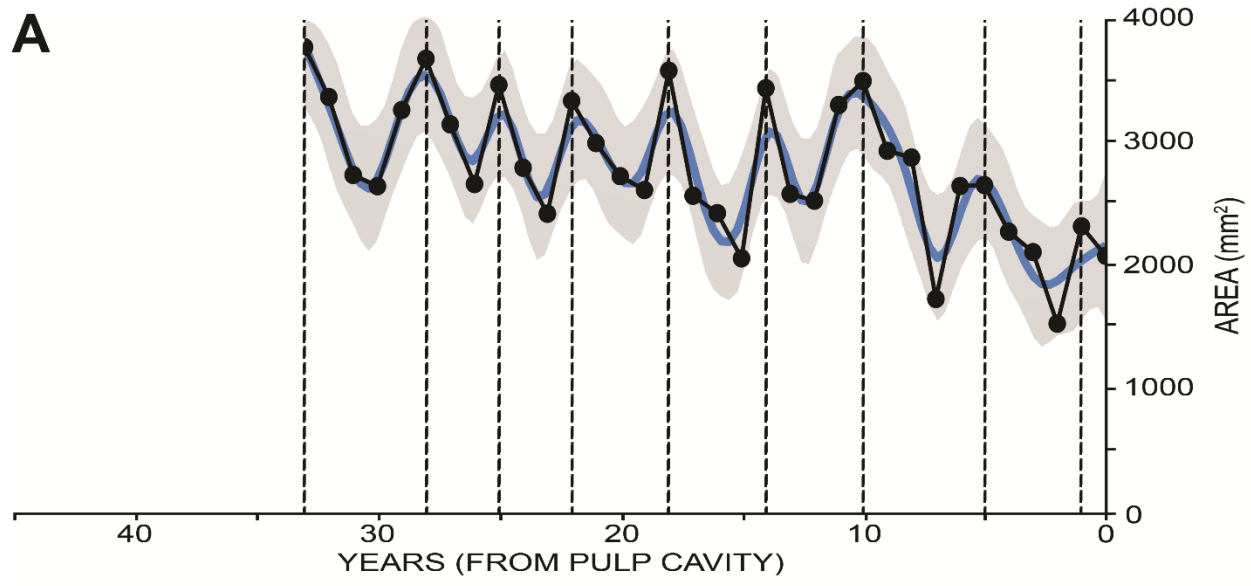
Figure 5.11. Graphs of annual measurements taken from the Malolyakhovsky specimen showing A) areas, B) extensional lengths, and C) appositional thicknesses. The year of death (year X) is recorded at 0 years from the pulp cavity. Black dots connected by black lines are the measured values for each year. The blue lines and grey shadings are the generalized additive models and associated standard errors, respectively. Vertical dashed lines mark local peaks within the pattern of annual area measurements and are projected down onto the same year in the graphs for the other measurements. These peaks mark the boundaries between undulations within the secondary pattern observed in both annual areas and extensional lengths. See Table 5.18 for statistical results of model.
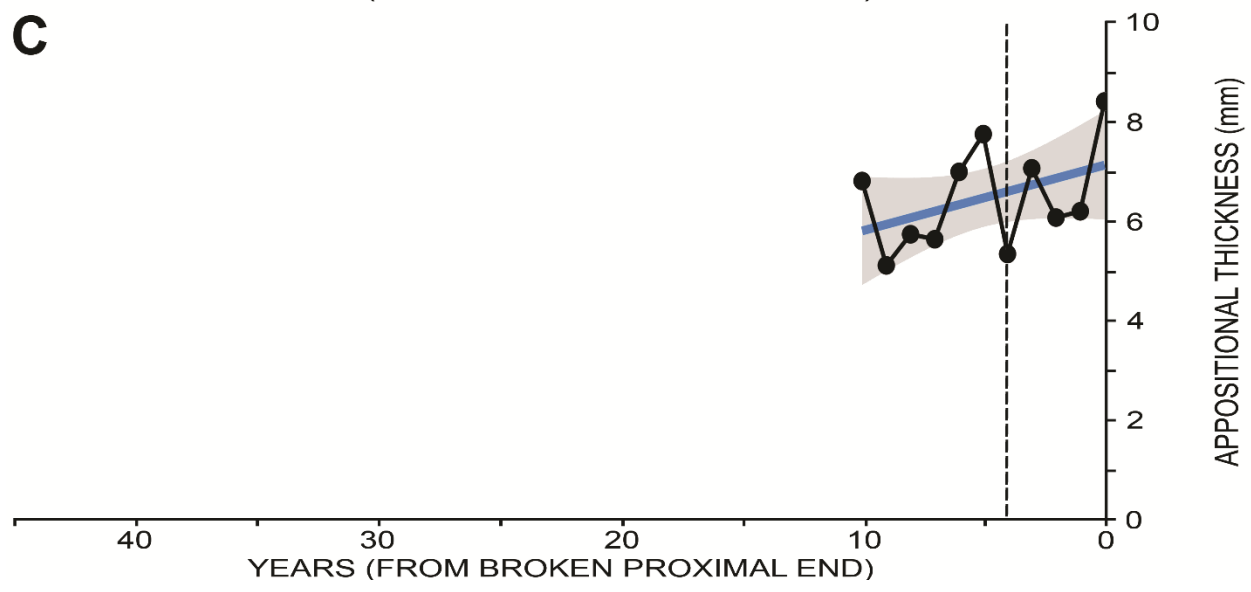
223

Figure 5.12. Graphs of annual measurements taken from 43-M showing A) areas, B) extensional lengths, and C) appositional thicknesses. The year of death (year X) is recorded at 0 years from the pulp cavity. Black dots connected by black lines are the measured values for each year. The blue lines and grey shadings are the generalized additive models and associated standard errors, respectively. Vertical dashed lines mark local peaks within the pattern of annual area measurements and are projected down onto the same year in the graphs for the other measurements. These peaks mark the boundaries between undulations within the secondary pattern observed in both annual areas and extensional lengths. See Table 5.21 for statistical results of model.
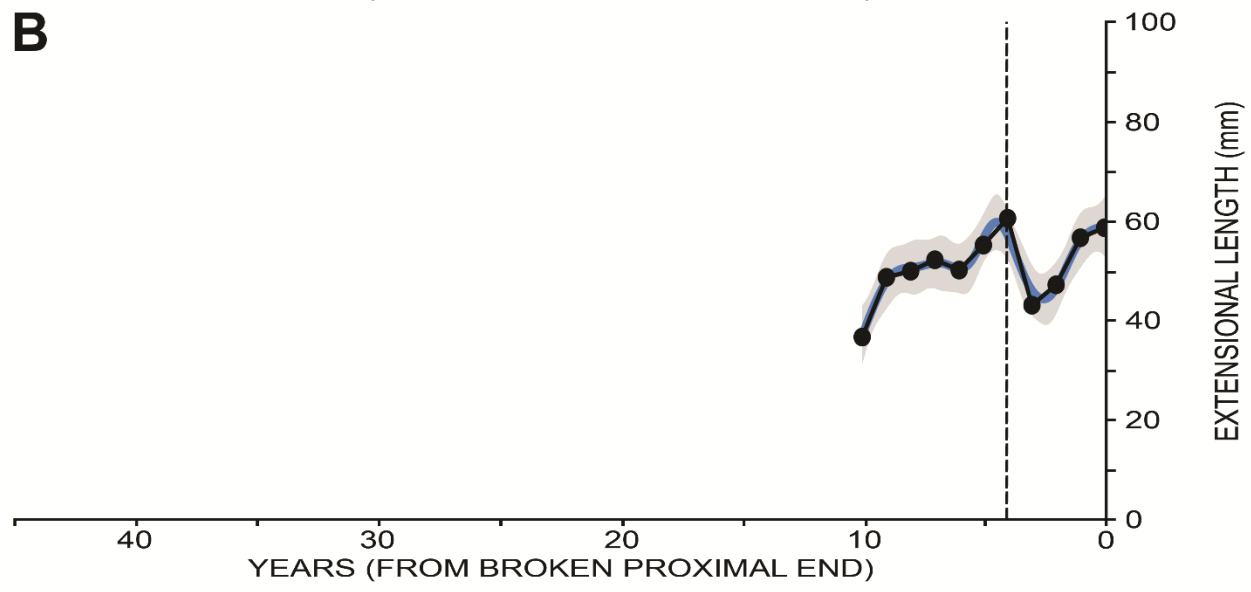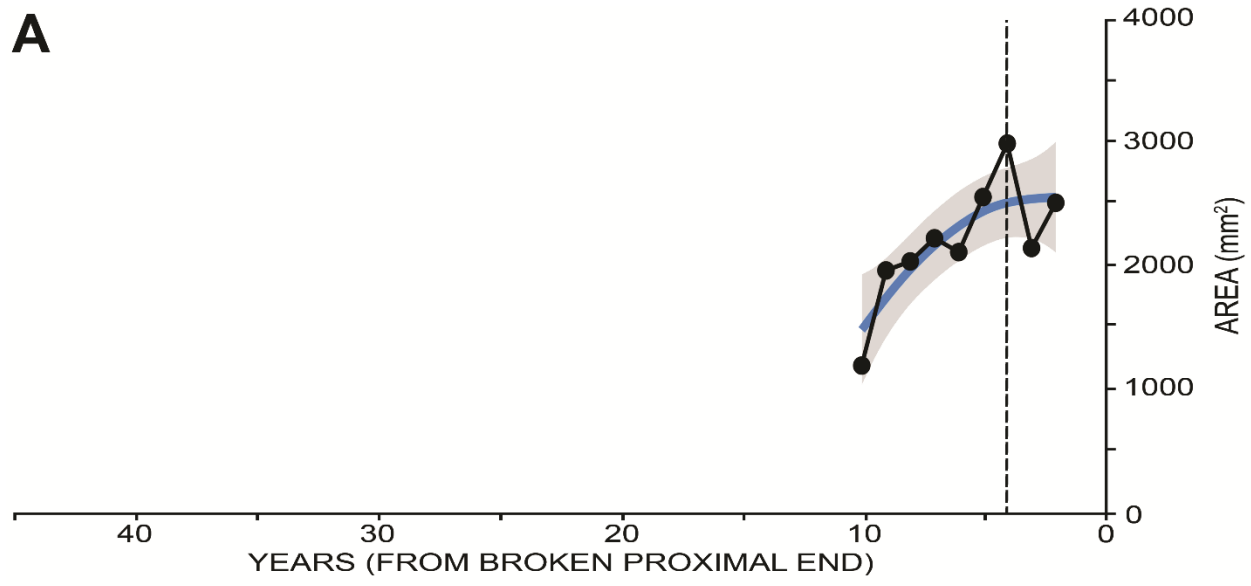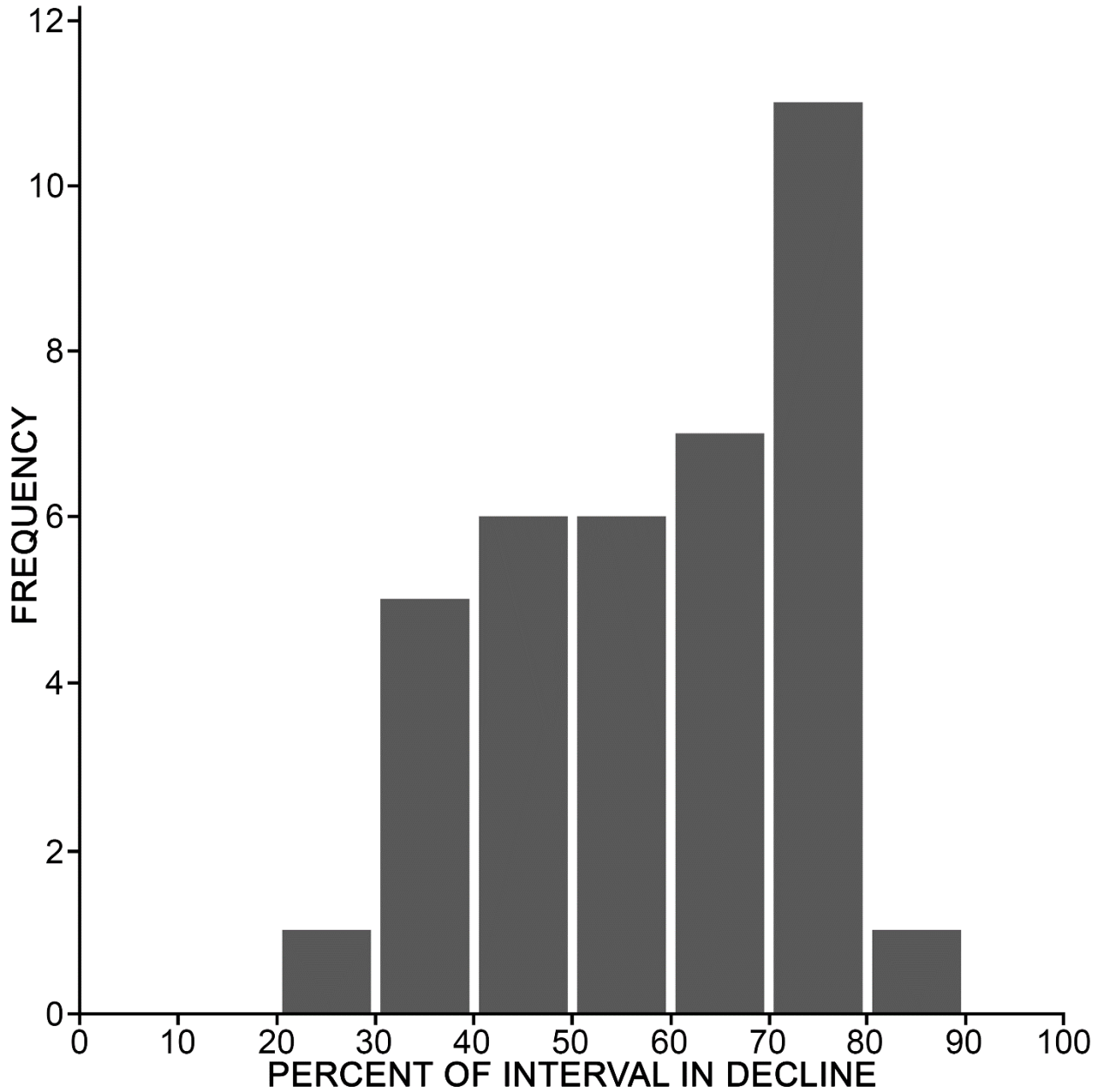
Figure 5.13. Graphs of annual measurements taken from 2007/003 showing A) areas, B) extensional lengths, and C) appositional thicknesses. The year of death (year X) is recorded at 0 years from the pulp cavity. Black dots connected by black lines are the measured values for each year. The blue lines and grey shadings are the generalized additive models and associated standard errors, respectively. Vertical dashed lines mark local peaks within the pattern of annual area measurements and are projected down onto the same year in the graphs for the other measurements. These peaks mark the boundaries between undulations within the secondary pattern observed in both annual areas and extensional lengths. See Table 5.19 for statistical results of model.

Figure 5.14. Graphs of annual measurements taken from TA-3 showing A) areas, B) extensional lengths, and C) appositional thicknesses. The year of death (year X) is recorded at 0 years from the pulp cavity. Black dots connected by black lines are the measured values for each year. The blue lines and grey shadings are the generalized additive models and associated standard errors, respectively. Vertical dashed lines mark local peaks within the pattern of annual area measurements and are projected down onto the same year in the graphs for the other measurements. These peaks mark the boundaries between undulations within the secondary pattern observed in both annual areas and extensional lengths. See Table 5.20 for statistical results of model.

A

B

C

YEARS (FROM BROKEN PROXIMAL END)

229

Figure 5.15. Histogram showing the frequency of observed cases within all complete undulations of the secondary pattern where "n" years of sustained decline in annual area are documented, expressed as a percentage of the total interval of "m" years until the beginning of the next undulation (i.e., $\frac{n}{m} \times 100$). Bar widths in the chart reflect the span of data contained within each bin (10% bins).
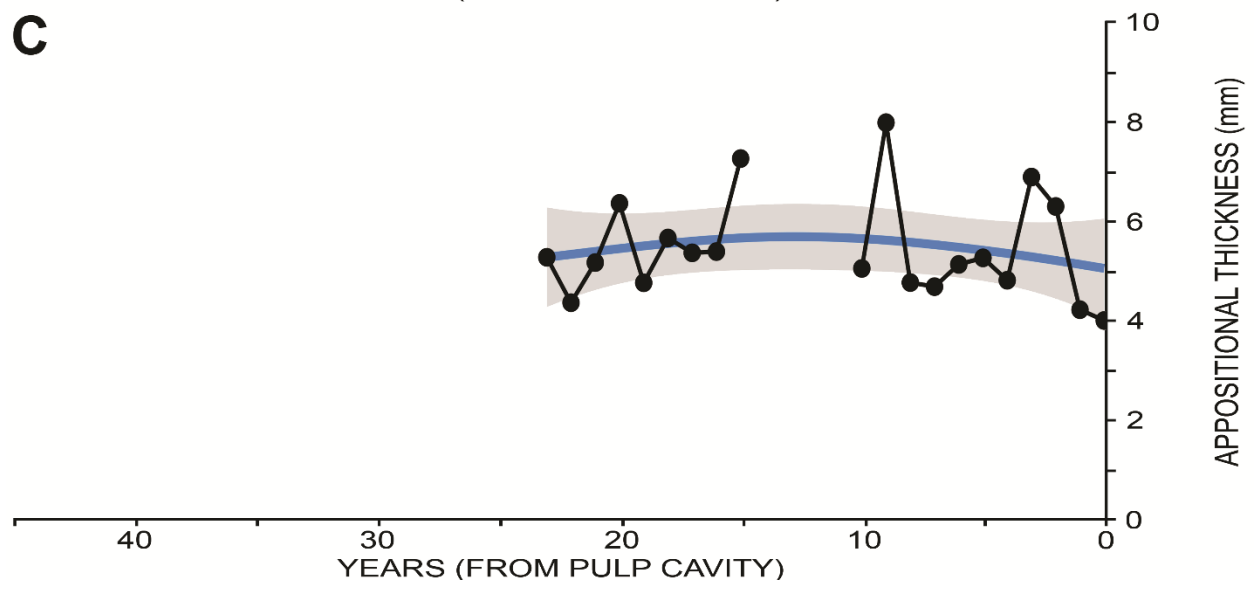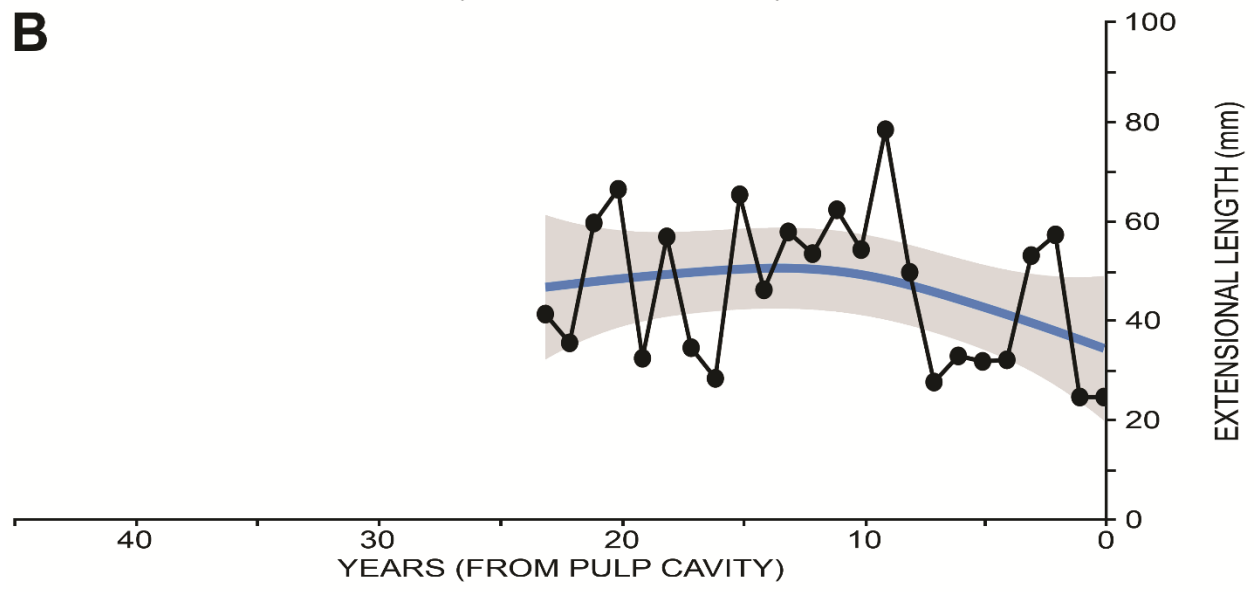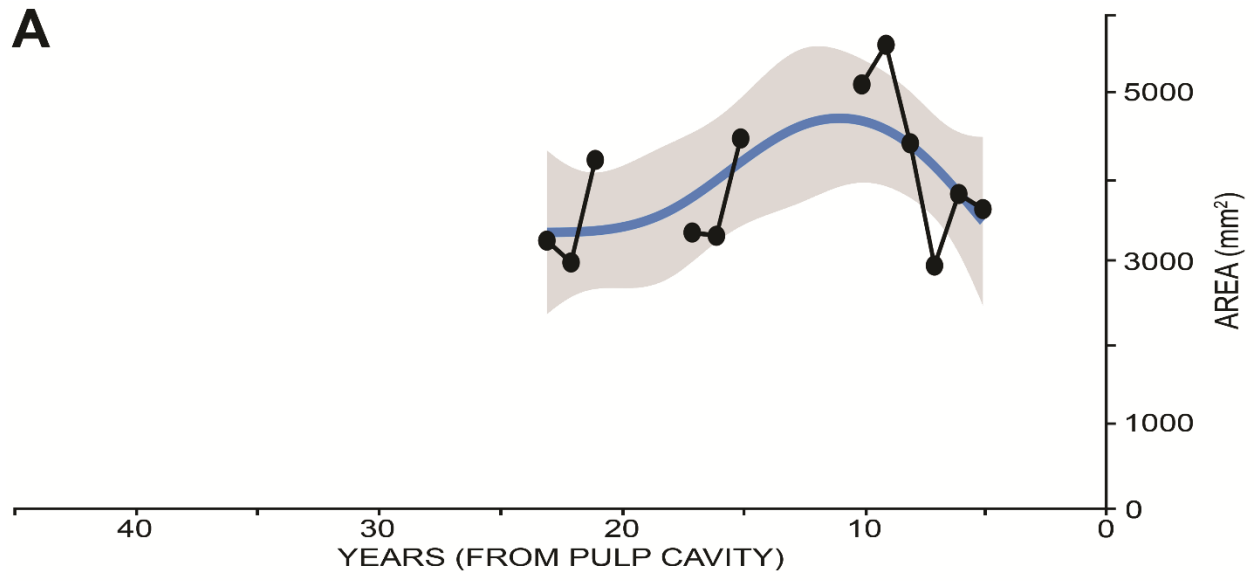
Figure 5.16. Graphs of annual measurements taken from ZCHM-46 showing A) areas, B) extensional lengths, and C) appositional thicknesses. Lack of visibility of some aspects of microCT features within the tusk made measurement of both annual areas and appositional thicknesses impossible for this specimen. The year of death (year X) is recorded at 0 years from the pulp cavity. Black dots connected by black lines are the measured values for each year. The blue lines and grey shadings are the generalized additive models and associated standard errors, respectively. Vertical dashed lines mark local peaks within the pattern of annual area measurements and are projected down onto the same year in the graphs for the other measurements. These peaks mark the boundaries between undulations within the secondary pattern observed in both annual areas and extensional lengths. See Table 5.23 for statistical results of model.
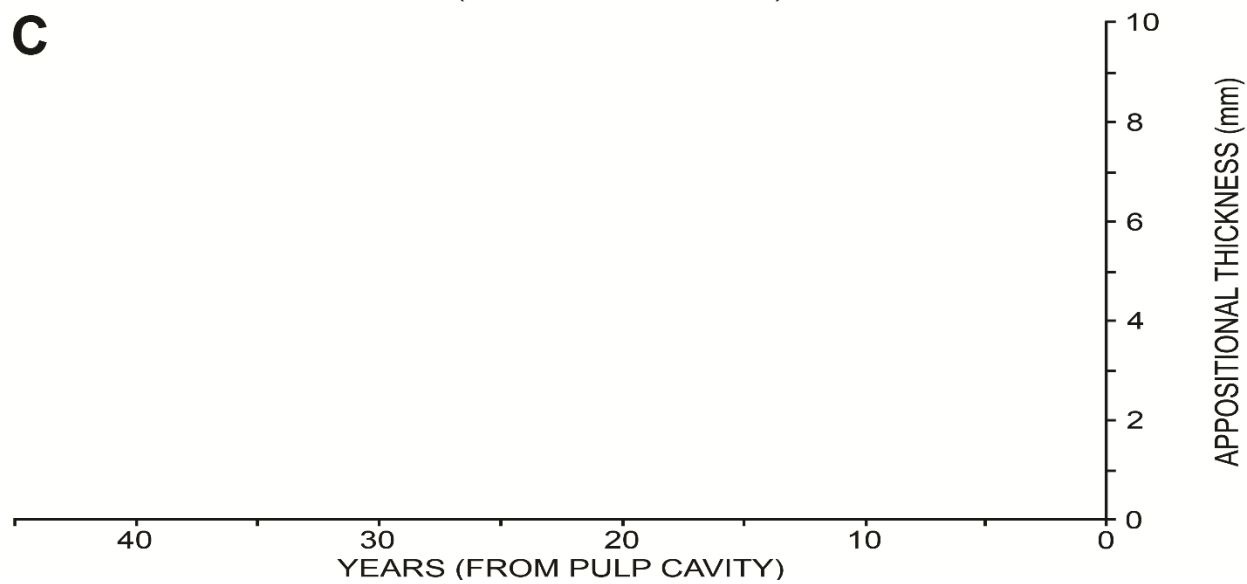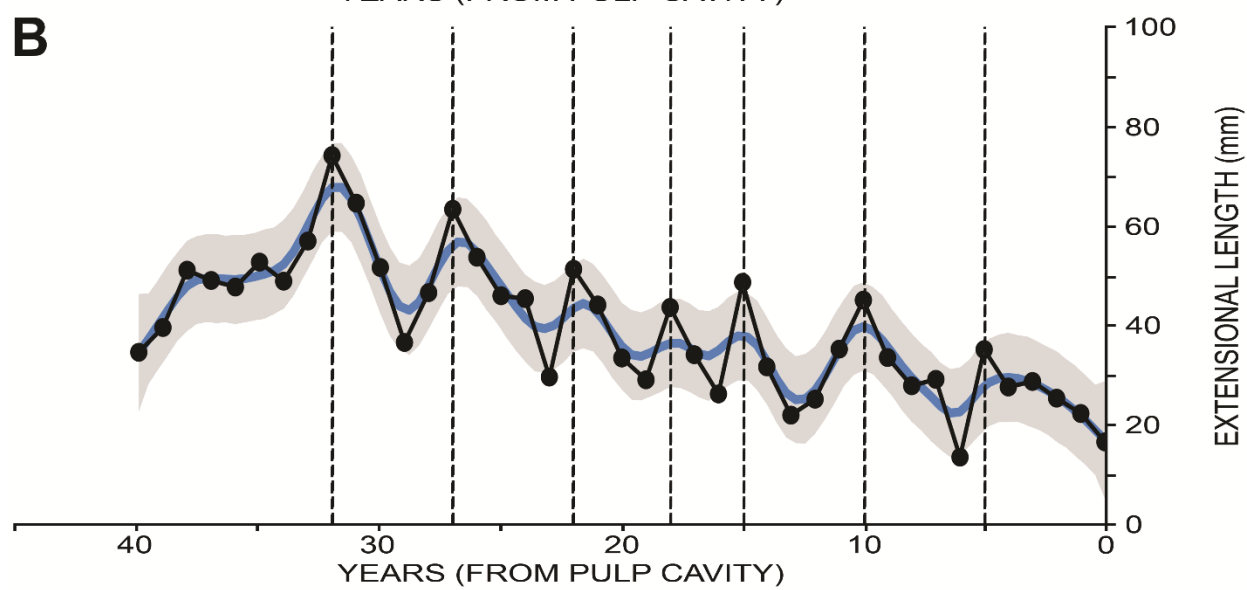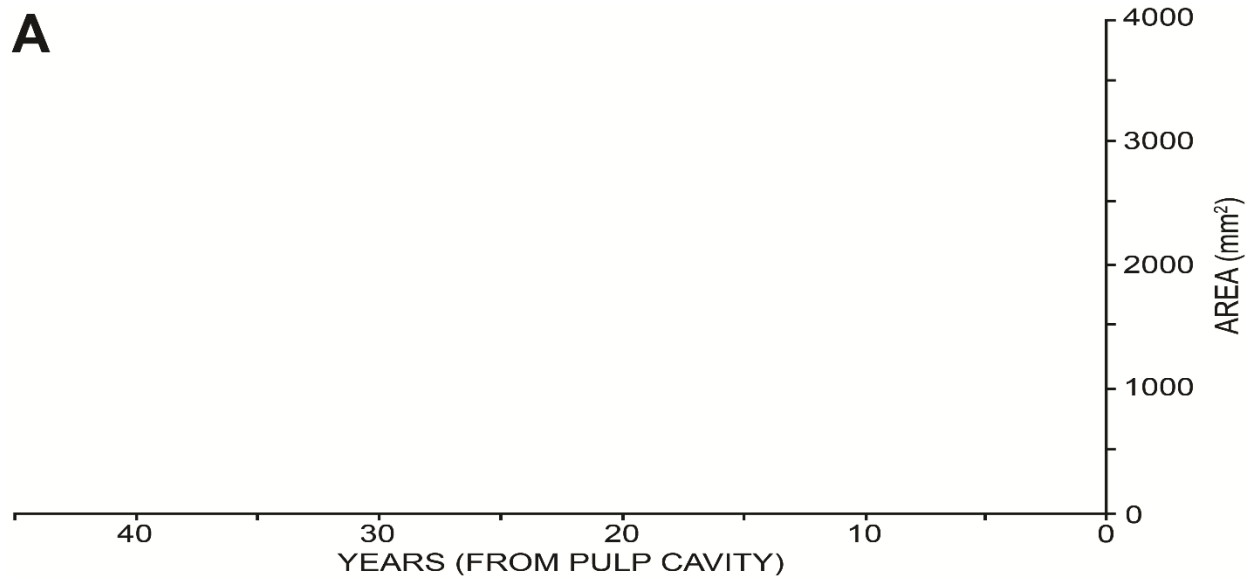
Figure 5.17. Graphs of annual measurements taken from 48-M showing A) areas, B) extensional lengths, and C) appositional thicknesses. The year of death (year X) is recorded at 0 years from the pulp cavity. Black dots connected by black lines are the measured values for each year. Lack of a black line connecting a black dot represents a break in the data where some number of years was not visible for that type of measurement. The blue lines and grey shadings are the generalized additive models and associated standard errors, respectively. See Table 5.22 for statistical results of model.
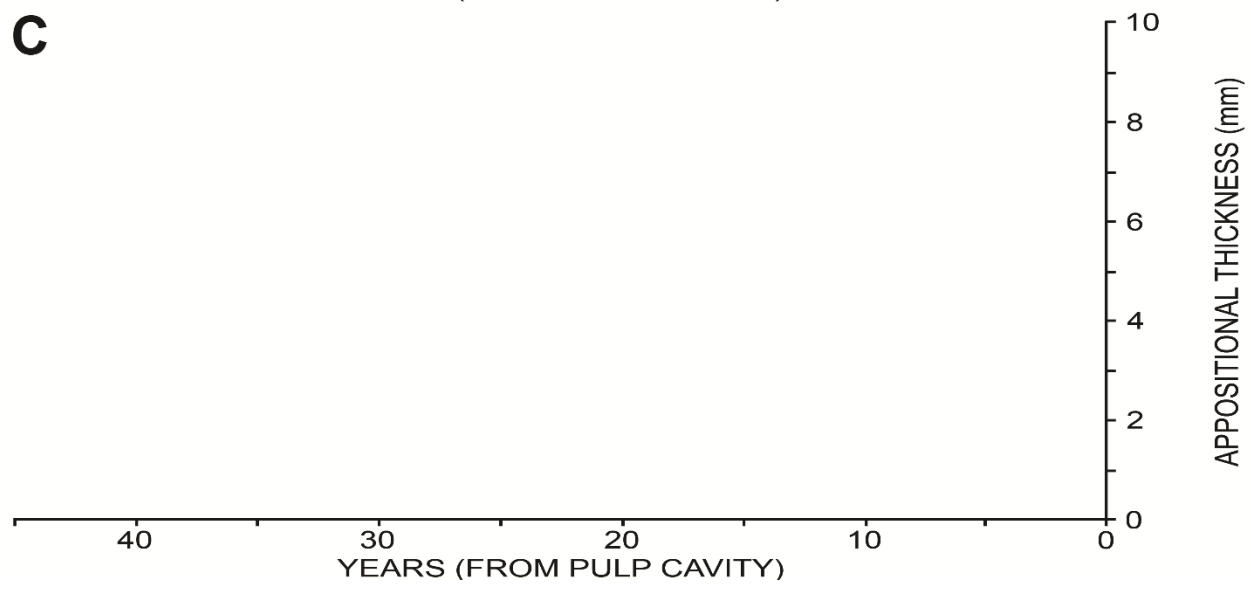
A

B

C

234

Figure 5.18. Graphs of annual measurements taken from ZCHM-38 showing A) areas, B) extensional lengths, and C) appositional thicknesses. Lack of visibility of some aspects of microCT features within the tusk made measurement of both annual areas and appositional thicknesses impossible for this specimen. The year of death (year X) is recorded at 0 years from the pulp cavity. Black dots connected by black lines are the measured values for each year. The blue lines and grey shadings are the generalized additive models and associated standard errors, respectively. See Table 5.24 for statistical results of model.

A

AREA (mm²)

YEARS (FROM PULP CAVITY)

B

EXTENSIONAL LENGTH (mm)

YEARS (FROM PULP CAVITY)

C

APPOSITIONAL THICKNESS (mm)
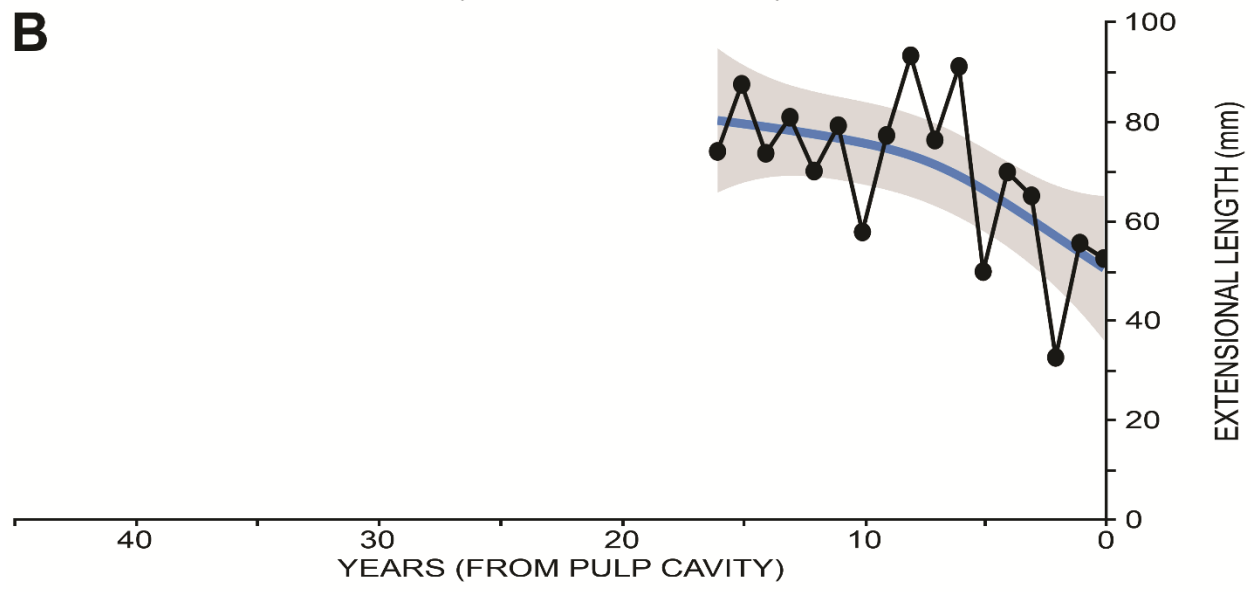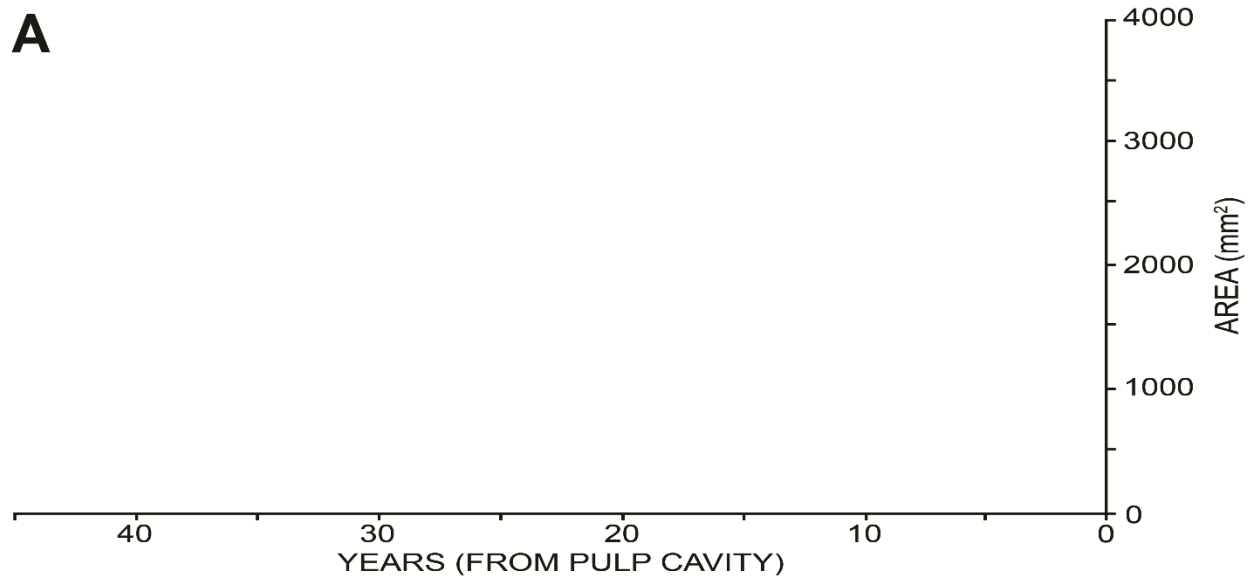
YEARS (FROM PULP CAVITY)

236

Figure 5.19. Generalized additive mixed model of annual extensional length on years from the pulp cavity for all female specimens. The blue line shows the model, while the grey shading is the associated standard error. See Table 5.25 for statistical results of model.
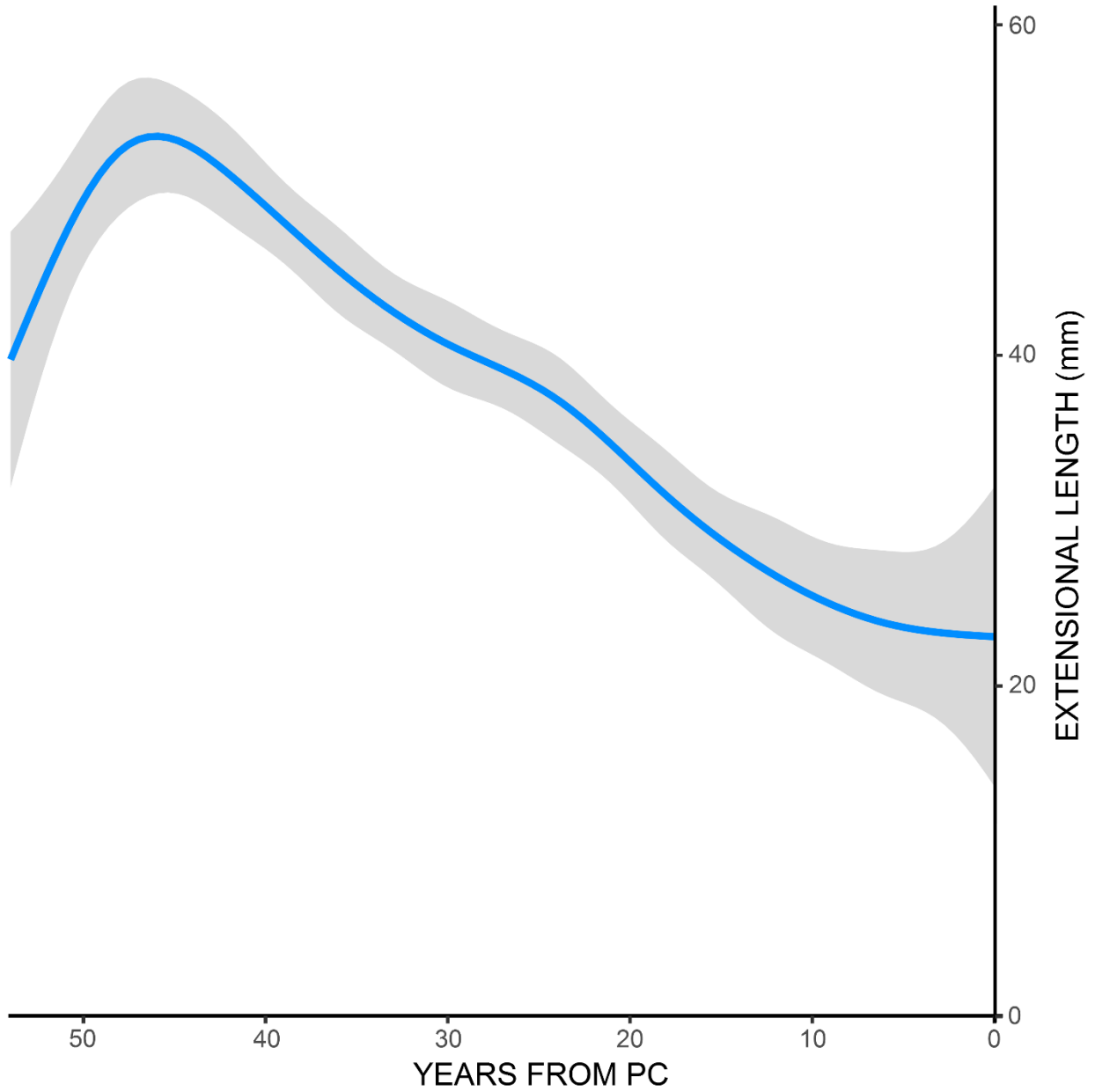
Figure 5.20. Graph of appositional thickness measurements relative to annual area. Specimens are identified based on their color. Circles denote specimens from Chukotka, squares are specimens from the Taymyr Peninsula, triangles represent specimens from the New Siberian Islands, and crosses mark specimens from Wrangel Island.
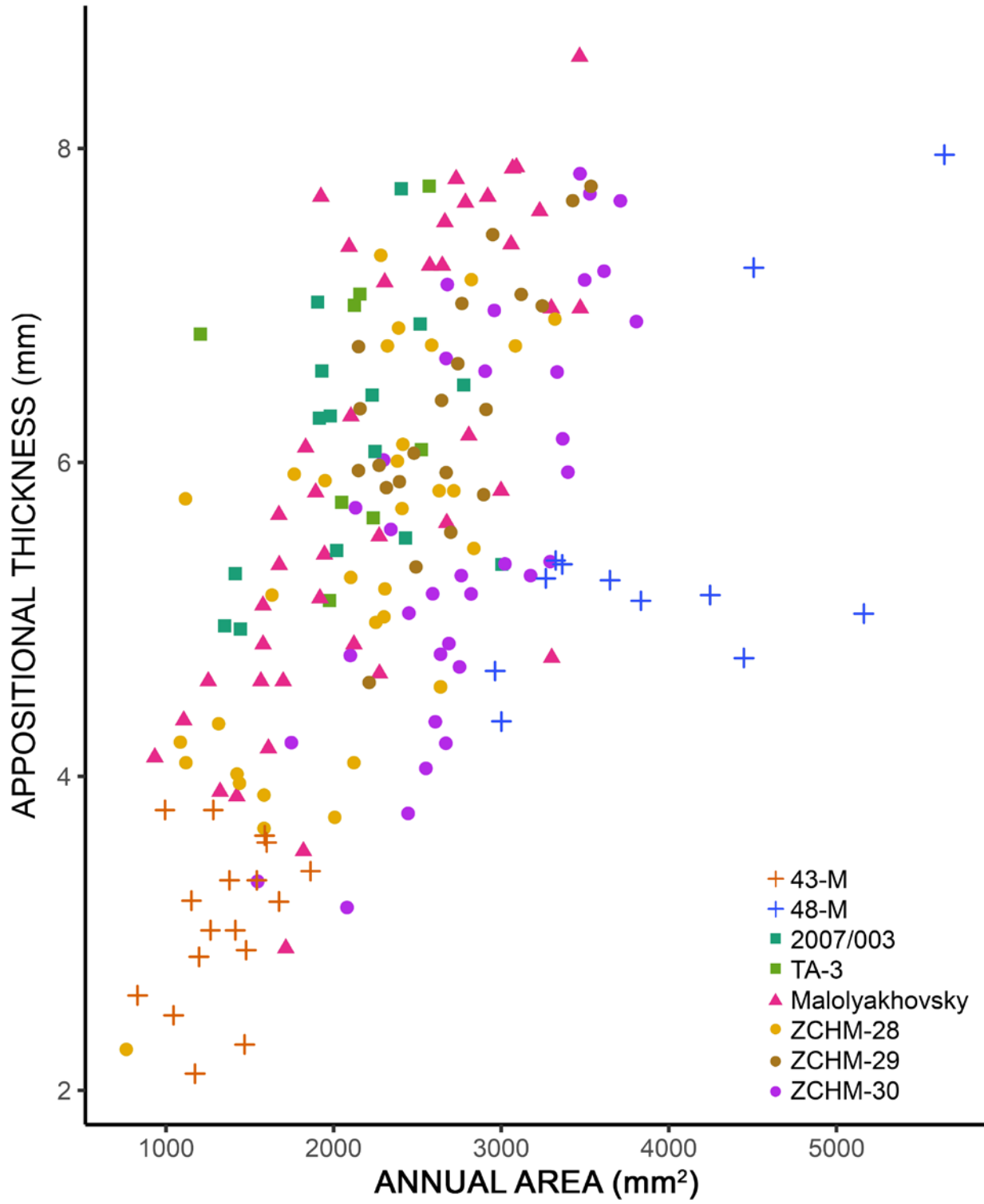
Figure 5.21. Graph of extensional length measurements relative to annual area. Specimens are identified based on their color. Circles denote specimens from Chukotka, squares are specimens from the Taymyr Peninsula, triangles represent specimens from the New Siberian Islands, and crosses mark specimens from Wrangel Island.
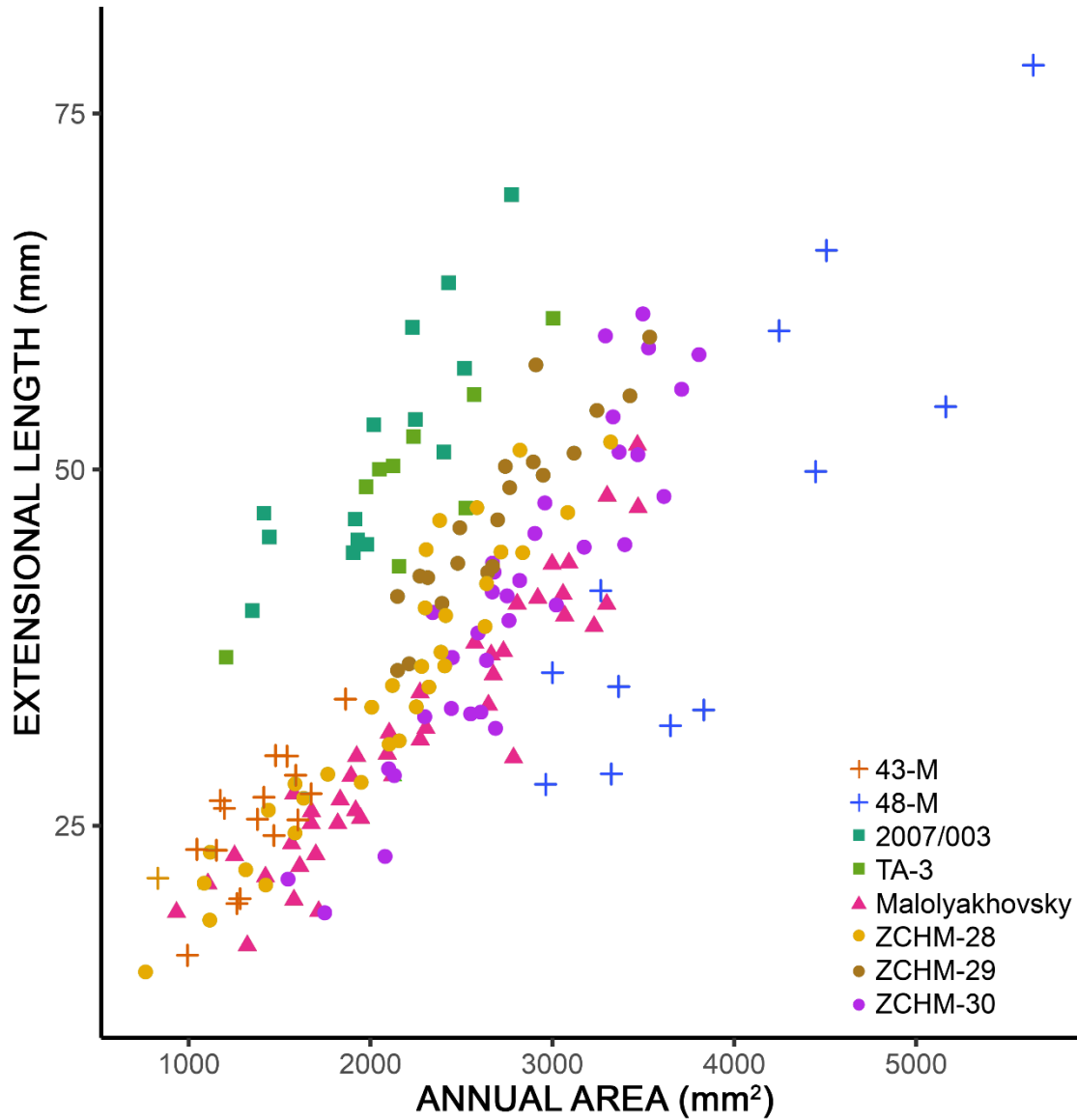
Figure 5.22. Contour plot showing the generalized additive model for annual area measurements on extensional length and appositional thickness for all female specimens within the study. Note that there is relatively little change in area with increase in apposition (without a change in extension), while increase in extension results in greatly increased area.
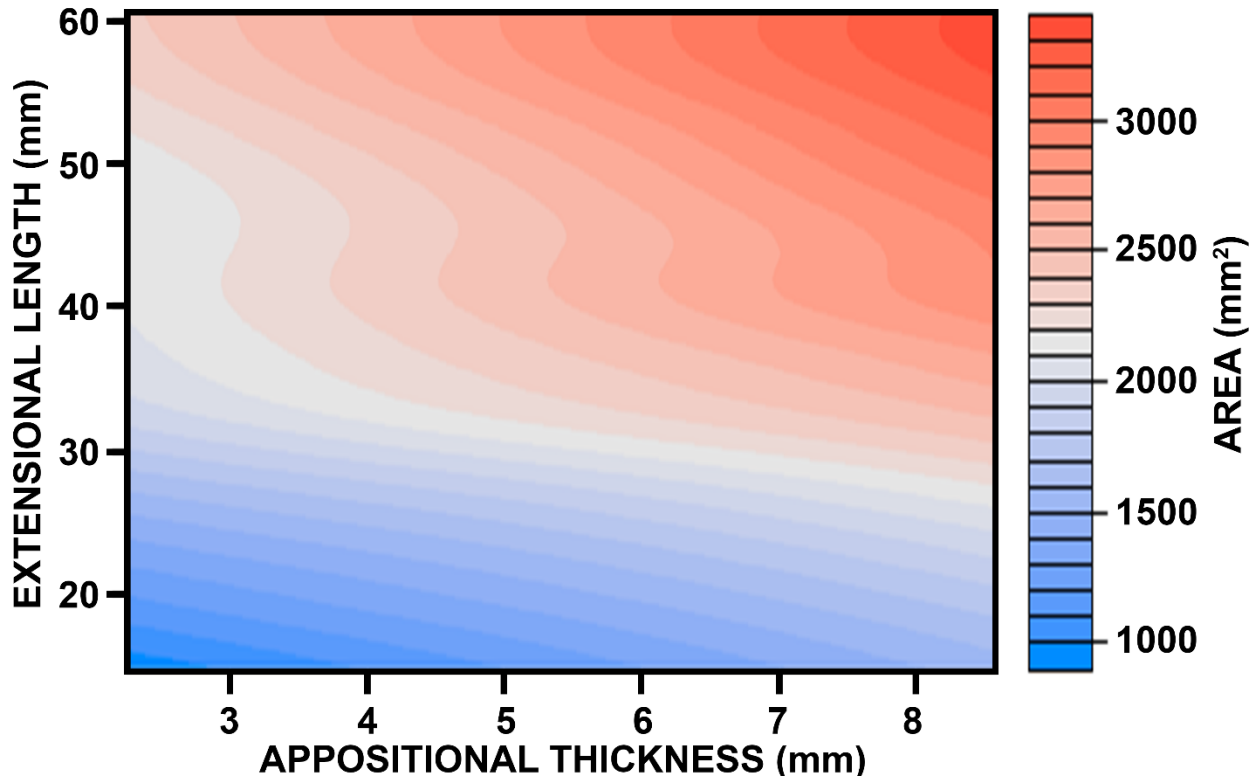
Figure 5.23. Life history hypotheses applied to the pattern of annual extensional length measurements taken from ZCHM-46. Vertical dashed line marks the age of maturation at the end of the pattern of year-to-year increase in extension rate and the onset of the secondary pattern. We interpret each undulation within the secondary pattern as reflecting the signal of a calving interval with conception (C) at the peak of the undulation and birth (B) following approximately 22 months later. Completion of weaning (W) is interpreted to occur just before the birth of a subsequent calf based on observations for modern elephants. Numbers in subscript correspond to individual calves in order from first conception. The dagger at year 45 denotes that this was the year of death for this individual.
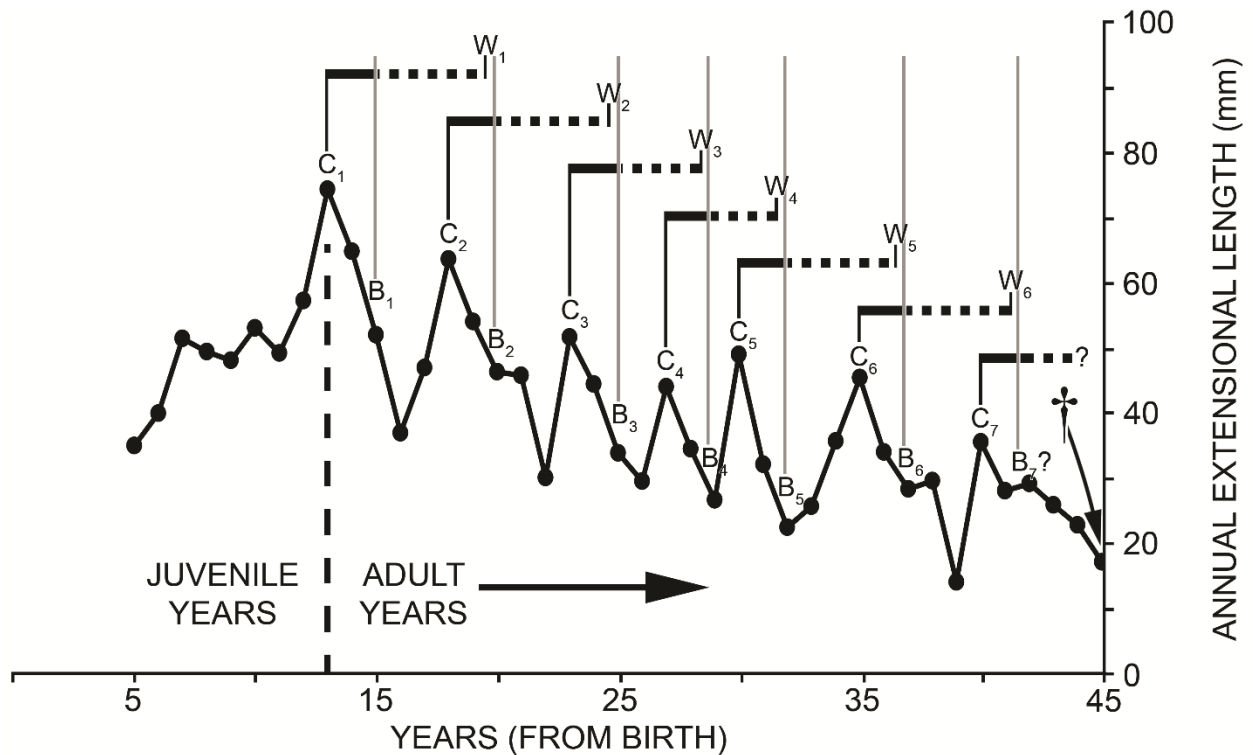
Figure 5.24. Average calving interval for each Pleistocene-age female studied plotted chronologically. Geologic ages for each specimen are from calibrated radiocarbon years before present. Specimens plotted at the far left of the graph are individuals that yielded "infinite" radiocarbon ages. Circles denote specimens from Chukotka, squares are specimens from the Taymyr Peninsula, and triangles represent specimens from the New Siberian Islands.
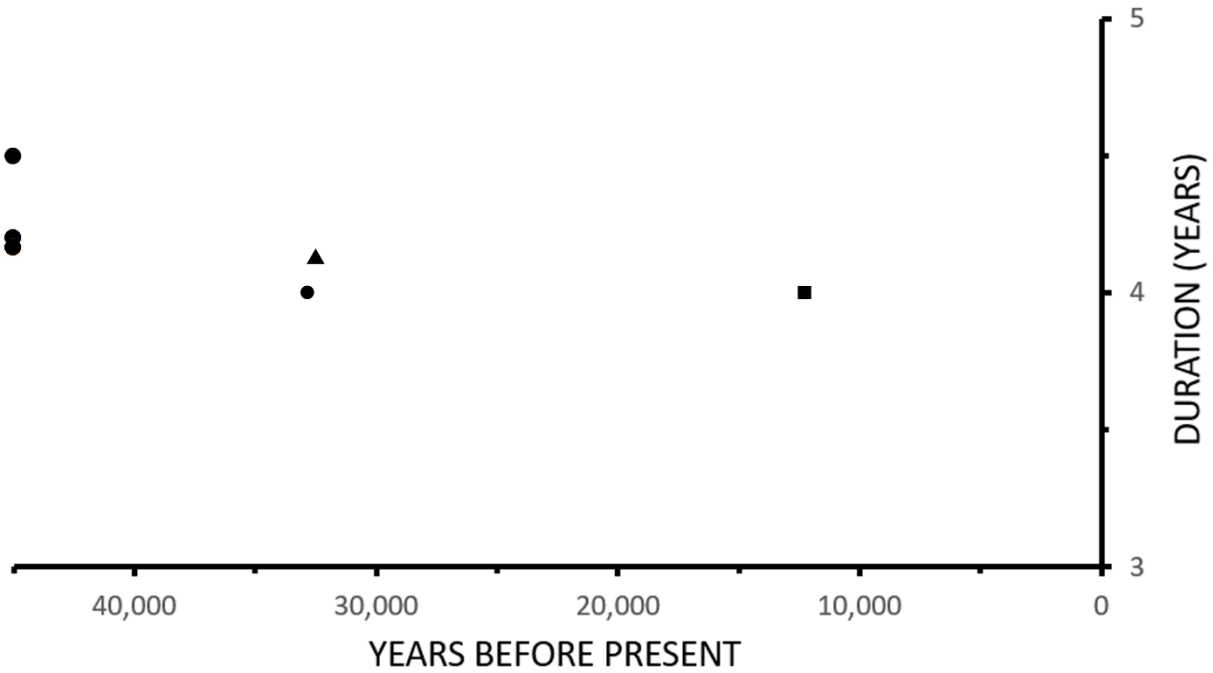
CHAPTER 6

Conclusion

As paleontologists we have the task of recovering what is mostly lost and long-forgotten. While neontologists read from the nearly immaculate final page of an eons-old epic hoping to understand the state of its surviving characters, paleontologists take the scattered words and phrases within the vast breadth of remaining tattered pages and piece together the story of how those characters came to be, as well as what was left behind along the way. Those of us who choose to browse this library of history written down within stratigraphic sequences must come to terms with the knowledge that many pages in the story have either vanished or were never even recorded, lost due to erosional forces, non-deposition, or taphonomic filters. As such, it must appear to an outsider that our endeavors to understand the details of past life border on absurdity or, at a minimum, are so restrictive in their scope as to be inconsequential. But this perspective is relatively narrow-minded. Although the nature of our material deprives us of the luxury of direct observations of behavior or of organismal interactions, it forces us to develop more creative approaches to inferring the nature of the lives of the dead.

Reflecting on the studies that comprise this dissertation, I feel fortunate to stand at the crossroads between the good fortune of having access to such detailed records

of past life and the inordinate creativity (though not always my own) required to interpret them. Proboscidean tusks, with their high-resolution records of growth that can potentially span the interval from before birth until death, represent a pristine page of text hidden among the fragmented chapters in the tome of life that is the fossil record. However, these unspoiled passages are written in a foreign dialect, which we are still only learning to read, but when translated may provide key information for understanding the story of the relatively recent past. It is my hope that the research summarized here has further deciphered the meaning of some of these verses written in the layers of proboscidean tusk dentin.

My research has utilized and expanded upon the methods and techniques that have been developed to analyze the structural and compositional increments in proboscidean tusks over the past two decades by multiple researchers (Fisher, 1996; 2001, 2009; Fox, 2000; Fisher et al., 2003, 2008, 2014; Fisher and Fox, 2007; Rountrey et al., 2012; Cherney, 2016). The finer-scale analyses conducted in Chapters 2 – 4 suggest that X-ray attenuation features observed in microCT scans of proboscidean tusks form on a consistent, periodic basis. In temperate- and high-latitude mammoth taxa, these features are a repeated sequence of low-attenuation dentin gradually transitioning to higher attenuation before abruptly transitioning back to low attenuation and repeating the sequence. Using thin section and stable isotope analyses, we determined that this density cycle represents a year of tusk growth and were able to attribute the abrupt transition from high to low attenuation as the signal of the seasonal change from winter to spring. Mammoths at lower latitudes (e.g., southern California) show CT features of similar duration, but the pattern is, perhaps unsurprisingly, more

muddied (Chapter 2). These findings agree with those of similar analyses conducted concurrently by Cherney (2016). Although this annual pattern of density change is found consistently in all mammoth taxa studied (and has also been documented in mastodons), a pattern of different periodicity (semi-annual) was found in a South American gomphothere (Chapter 3). This finding suggests that more work needs to be done in assessing the taxonomic (and/or geographic) distribution of CT density features within proboscidean tusks. Regardless, the revelation of periodically-forming X-ray attenuation features within tusks may prove revolutionary to the study of proboscidean life histories.

Aside from the clear benefits of being a non-destructive type of analysis, microCT scans can unlock multiple decades of growth history from a single individual with relative speed and ease. Chapter 5 showed that such scans of whole tusks from Siberian woolly mammoths allow us to document aspects of reproductive life history and ontogeny. Juvenile individuals show a year-to-year increase in growth rates while adults show an overall declining trend. Furthermore, adult female woolly mammoths all record a 3-to-6 year pattern of growth characterized by a year-to-year decrease in annual area (and extension) followed by a multi-year increase in annual area, which persists throughout life. This pattern has been identified as the signal for calving, which allows for detailed study of the timing and duration of reproduction in woolly mammoths. The onset of this undulating pattern and the change from increasing to decreasing trend in year-to-year growth rates marks the age of maturation (i.e., year of first conception) in females. Detailed records of life history from a single individual of an extinct organism, such as these, are essentially unheard-of in the fossil record and can provide a wealth

of information on past life. However, perhaps just as importantly, these records of life history can provide valuable tests for cause of extinction.

As discussed in Chapters 4 and 5, the timing and duration of different aspects of life history are expected to behave predictably under the pressure of different agents of extinction. Therefore, documenting changes in life history before and during an extinction event could provide a test for the overall cause. In the case of the end-Pleistocene extinction, the two main hypothesized causes of extinction (climate change and human hunting) are expected to have an antithetical effect on age of maturation and calving interval. Based on studies of multiple vertebrate taxa, age of maturation is expected to be earlier when hunting pressure dominates and later when climate change dominates as a source of ecological stress. Calving interval should also change under these pressures with shorter calving intervals expected under a hunting-induced extinction and longer calving intervals expected due to negative consequences of climate change. Chapter 5 documents a small decline in both age of maturation and calving interval toward the end of the Pleistocene, supporting the hunting-hypothesis, but our dataset is admittedly quite limited in size. However, studies of weaning ages in Siberian woolly mammoths by Cherney (2016) and ages of maturation in Great Lakes Region mastodons by Fisher (2009) have both revealed similar results. These congruent findings across multiple aspects of life history, regions, and taxa suggest that this pattern is in fact real and indicative of the effects of some external pressure. This pattern begins to paint a picture of a population of animals at the end of the Pleistocene that were apparently thriving as individuals despite their impending disappearance. Though further analyses of other proboscidean populations across the world are

needed to understand the complete story of the end-Pleistocene extinction, it appears

that at least in northern Siberia, these large herbivores may have met their end at the

hands of human hunters.

REFERENCES

Cherney, M.D., 2016. Records of Growth and Weaning in Fossil Proboscidean Tusks as Tests of Pleistocene Extinction Mechanisms.

Fisher, D.C., 1996. Extinction of proboscideans in North America. In: Shoshani, J., Tassy, P. (Eds.), The Proboscidea: Evolution and palaeoecology of elephants and their relatives. Oxford University Press, Oxford, pp 296–315.

Fisher, D.C., 2001. Season of death, growth rates, and life history of North American mammoths. In: West, D.L. (Ed.), Mammoth site studies: Proceedings of the first international conference on mammoth site studies. Publications in Anthropology vol. 22, University of Kansas, Lawrence, pp. 121–135.

Fisher, D.C., 2009. Paleobiology and extinction of proboscideans in the Great Lakes region of North America. In: Haynes, G. (Ed.), American megafaunal extinctions at the end of the Pleistocene, Springer, New York, pp. 55–75.

Fisher, D.C., Beld, S.G., Rountrey, A.N., 2008. Tusk record of the North Java mastodon. In: Allmon, W.D., Nester, P.L. (Eds.). Mastodon paleobiology, taphonomy, and paleoenvironment in the late Pleistocene of New York State: Studies on the Hyde Park, Chemung, and Java sites. Palaeontographica Americana vol 61, pp. 417-463.

Fisher, D.C., Cherney, M.D., Newton, C., Rountrey, A.N., Calamari, Z.T., Stucky, R.K., Lucking, C., Petrie, L., 2014. Taxonomic overview and tusk growth analyses of Ziegler Reservoir proboscideans. Quaternary Research 82, 518-532.

Fisher, D.C., Fox, D.L., 2007. Season of death of the Dent mammoths: Distinguishing single from multiple mortality events. In: Brunswig, R.H., Pitblado, B.L. (Eds.). Frontiers in Colorado Paleoindian archaeology: From the Dent site to the Rocky Mountains. University Press of Colorado, Boulder, Colorado, pp. 123–153.

Fisher, D.C., Fox, D.L., Agenbroad, L.D., 2003. Tusk growth rate and season of death of *Mammuthus columbi* from Hot Springs, South Dakota, USA. In: Reumer, J.W.F., De Vos, J., Mol, D. (Eds.), Advances in mammoth research (Proceedings of the Second International Mammoth Conference, Rotterdam, May 16–20 1999) vol. 9, Deinsea, pp. 117–133.

Fox, D.L., 2000. Growth increments in *Gomphotherium* tusks and implications for late Miocene climate change in North America. Palaeogeography, Palaeoclimatology, Palaeoecology 156, 327–348.

Rountrey, A.N., Fisher, D.C., Tikhonov, A.N., Kosintsev, P.A., Lazarev, P.A., Boeskorov, G., Buigues, B., 2012. Early tooth development, gestation, and season of birth in mammoths. Quaternary International 255, 196-205.